STATUS OF THESIS

Title of thesis	SYNTHESIS, CHARACTERIZATION AND EVALUATION OF SURFACTANTS DERIVED FROM NATURAL OILS FOR EOR APPLICATIONS

I MUHAMMAD MUSHTAQ

hereby allow my thesis to be placed at the Information Resource Center (IRC) of Universiti Teknologi PETRONAS (UTP) with the following conditions:

1. The thesis becomes the property of UTP
2. The IRC of UTP may make copies of the thesis for academic purposes only.
3. This thesis is classified as

☐ Confidential

☑ Non-confidential

If this thesis is confidential, please state the reason:

_____

The contents of the thesis will remain confidential for ____ years.

Remarks on disclosure:

_____

_____

Signature of Author

Permanent address:
House No. D15, Nargis Road,
Central Park, Wah Cantt,
Pakistan.

Date : 27-12-12

Endorsed by

Signature of Supervisor

Assoc. Prof. Dr. Isa M Tan

DR. ISA MOHD TAN
Associate Professor
Fundamental & Applied Sciences Department
Universiti Teknologi PETRONAS, PERAK

Date: 27-12-12

UNIVERSITI TEKNOLOGI PETRONAS

SYNTHESIS, CHARACTERIZATION AND EVALUATION OF SURFACTANTS DERIVED FROM NATURAL OILS FOR EOR APPLICATIONS

by

MUHAMMAD MUSHTAQ

The undersigned certify that they have read, and recommend to the Postgraduate Studies Programme for acceptance this thesis for the fulfillment of the requirements for the degree stated.

Signature: _____

Main Supervisor: Assoc. Prof. Dr. Isa M Tan

Signature: _____

Co-Supervisor: Dr. Lukman Ismail

Signature: _____

Head of Department: Assoc. Prof. Dr. Mohd Azmi Bustam

Date: _____

SYNTHESIS, CHARACTERIZATION AND EVALUATION OF SURFACTANTS DERIVED FROM NATURAL OILS FOR EOR APPLICATIONS

by

MUHAMMAD MUSHTAQ

A Thesis

Submitted to the Centre of Graduate Studies

as a Requirement for the Degree of

DOCTOR OF PHILOSOPHY

CHEMICAL ENGINEERING DEPARTMENT

UNIVERSITI TEKNOLOGI PETRONAS

BANDAR SERI ISKANDAR,

PERAK

DECEMBER 2012

DECLARATION OF THESIS

Title of thesis	SYNTHESIS, CHARACTERIZATION AND EVALUATION OF SURFACTANTS DERIVED FROM NATURAL OILS FOR EOR APPLICATIONS

I MUHAMMAD MUSHTAQ

hereby declare that the thesis is based on my original work except for quotations and citations which have been duly acknowledged. I also declare that it has not been previously or concurrently submitted for any other degree at UTP or other institutions.

Witnessed by

Signature of Author

Signature of Supervisor

Permanent address:
House No. D15, Nargis Road,
Central Park, Wah Cantt,
Pakistan.

Assoc. Prof. Dr. Isa M Tan

Date : 27-12-12

Date : 27-12-12

SYNTHESIS, CHARACTERIZATION AND EVALUATION OF SURFACTANTS DERIVED FROM NATURAL OILS FOR EOR APPLICATIONS

by

MUHAMMAD MUSHTAQ

A Thesis

Submitted to the Centre of Graduate Studies

as a Requirement for the Degree of

DOCTOR OF PHILOSOPHY

CHEMICAL ENGINEERING DEPARTMENT

UNIVERSITI TEKNOLOGI PETRONAS

BANDAR SERI ISKANDAR,

PERAK

DECEMBER 2012

DECLARATION OF THESIS

Title of thesis	SYNTHESIS, CHARACTERIZATION AND EVALUATION OF SURFACTANTS DERIVED FROM NATURAL OILS FOR EOR APPLICATIONS

I MUHAMMAD MUSHTAQ

hereby declare that the thesis is based on my original work except for quotations and citations which have been duly acknowledged. I also declare that it has not been previously or concurrently submitted for any other degree at UTP or other institutions.

Witnessed by

Signature of Author

Signature of Supervisor

Permanent address:
House No. D15, Nargis Road,
Central Park, Wah Cantt,
Pakistan.

Assoc. Prof. Dr. Isa M Tan

Date :

Date :

DEDICATION

To my family for their love and prayers

ACKNOWLEDGEMENTS

No amount of my thanks and gratitude will be enough for Allah the Almighty for giving me strength and help to accomplish this work and all my endeavors.

I would like to express my utmost gratitude to my supervisor Dr. Isa M Tan for his seasoned guidance and advice throughout my research. He not only gave me the freedom to think and explore on my own, but also supported me with immeasurable time and guidance when my steps faltered. His unwavering faith and confidence in my abilities and in me is what has shaped me to be the person I am today.

I am also deeply indebted to my co-supervisors Dr. Cecelia Devi, Dr. Lukman Ismail and field supervisor Dr. Nadeem for their guidance and supervision. They were more than generous with their expertise and precious time.

I would like to thank Professor Birol Demiral, Professor Mustafa Onur and Professor Mariyamni Awang for their help and support during the work in the EOR Centre. I am also thankful to the members of the EOR Centre for their excellent help.

Much appreciation is expressed to all my friends for their companionship. Special thanks to Sagir, Rehan, Arsalan, Susan and Saeed Majidaei for their help, friendship and encouragement.

My heartiest thanks go to my parents, brothers and sisters for their unconditional love and prayers. They have always supported me with their best. My life and academics would not be the same without their help, encouragement and support.

Finally, my sincerest gratitude goes to my beloved wife, Dr. Rukhsana, for her love, constant understanding and help which will always be treasured. I am indebted to my wife and our sons Ali and Hashim for their sacrifices and patience.

ABSTRACT

Enhanced oil recovery methods are directed towards the recovery of residual oil from a reservoir. Surfactants have been gaining prominence as a main chemical for EOR methods. Natural oils, owing to their naturally long hydrocarbon chains, possess remarkable potential to be used as raw materials for the development of surfactants.

The oleic acid methyl esters obtained from Jatropha oil and high oleic acid methyl esters were modified by the attachment of nine different alkoxy groups (derived from alcohols) and these were successfully converted to 18 types of sulfate and sulfonate based anionic surfactants. The high FFA value of Jatropha oil was suppressed to as low as 1 % by employing an indigenously developed silica based catalyst. The synthesized methyl esters were epoxidized by optimizing the epoxidation process by using the RSM technique utilizing a central composite rotatable design. The DOE successfully optimized the yield and dramatically shortened the reaction time. The obtained oxirane ring was then opened up using nine different alcohols thereby attaching them as alkoxy chains on the oleic acid methyl ester parent chain. Sulfation of the -OH groups located *trans* to the alkoxy groups yielded nine sulfate type surfactants. For the synthesis of sulfonate surfactants, the -OH group was protected by the acetylation reaction before sulfonation by an SO_3-air mixture in a falling film reactor, hence producing nine sulfonate based surfactants. The sulfate and sulfonate surfactants were obtained in high yields. All end products and precursors were characterized by GC-FID, GC-MS, FT-IR and NMR techniques.

The synthesized surfactants were evaluated employing fluid-fluid compatibility studies including temperature, salinity and hardness tolerance, and phase behavior tests. Sulfate surfactants were found relatively more tolerant towards salinity compared to sulfonate surfactants with the same hydrocarbon structure. Sulfonates, on the other hand, were found to possess a more superior temperature stability compared

to the sulfate counterparts. All sulfonate and sulfate surfactants were found to generate microemulsion readily. The solubilization parameters, however, were the highest in the case of the sulfonate surfactant with the *n*-decoxy side chain. This surfactant effectively lowered the IFT between the Dulang crude and brine down to 0.008 mN / m.

The coreflood experiments demonstrated that the in-house developed sulfate surfactants were good at the temperature of 60 °C generating up to 90 % oil recovery. The sulfonates were superior surfactants than sulfate due to their high thermal stability and delivered 96 % of the trapped oil recovery in the case of the 10-Acetoxy-9-decoxy-2-sulfo-octadecanoic acid methyl ester.

ABSTRAK

Kaedah-kaedah perolehan minyak tertingkat (EOR) tertumpu ke arah perolehan sisa minyak daripada takungan. Surfaktan telah semakin menonjol sebagai bahan kimia utama bagi kaedah EOR. Minyak semula jadi yang terdiri daripada rantaian hidrokarbon yang panjang mempunyai potensi yang luar biasa untuk diketengahkan sebagai bahan mentah untuk pembangunan surfaktan.

Kami telah mengubahsuai ester metil asid oleik yang diperolehi dari minyak Jatropha dan juga yang diperoleh dari lampiran sembilan kumpulan alkoksi yang berbeza (terhasil dari alkohol). Melaluinya, 18 jenis surfaktan anionik dari kumpulan sulfat dan sulfonat berjaya dihasilkan. Nilai FFA yang tinggi oleh minyak Jatropha telah berjaya diturunkan ke paras 1 % dengan menggunakan pemangkin berasaskan silika asli. Ester metil yang terhasil telah diepoksidakan dengan mengoptimumkan proses pengepoksidaan melalui teknik RSM yang mempunyai reka bentuk pusat berputar komposit. Penggunaan DOE telah berjaya mengoptimumkan hasil dan telah secara mendadak memendekkan masa tindak balas. Cincin oxirane yang terhasil kemudiannya dibuka dengan menggunakan sembilan jenis alkohol yang berbeza sekali gus melampirkan mereka sebagai rantaian alkoksi pada rantaian induk metil ester asid oleik. Pensulfatan kumpulan OH terletak secara trans kepada kumpulan alkoksi menghasilkan sembilan jenis surfaktan sulfat. Untuk sintesis surfaktan sulfonat, kumpulan OH dilindungi oleh tindak balas asetik sebelum disulfonat oleh campuran SO_3-udara dalam reaktor filem jatuh, seterusnya menghasilkan sembilan surfaktan berasaskan sulfonat. Surfaktan sulfat dan sulfonat diperolehi dalam hasil yang tinggi. Semua produk akhir dan prekursor telah dicirikan menggunakan teknik-teknik GC-FID, GC-MS, FT-IR dan NMR.

Surfaktan yang disintesis telah dinilai menggunakan kajian keserasian bendalir cecair termasuk ujian-ujian toleransi suhu, kemasinan dan kekerasan dan kelakuan fasa.

Dengan struktur hidrokarbon yang sama, surfaktan sulfat didapati lebih toleran terhadap kemasinan berbanding surfaktan sulfonat. Surfaktan sulfonat pula didapati mempunyai kestabilan suhu yang lebih tinggi berbanding dengan kumpulan sulfat. Semua surfaktan sulfonat dan sulfat didapati dapat menjana mikroemulsi dengan mudah. Namun demikian, parameter keterlarutan adalah tertinggi dalam kes surfaktan sulfonat dengan rantaian sampingan n-decoxy. Surfaktan ini berkesan menurunkan tegangan antaramuka antara minyak mentah Dulang dan air garam ke 0.008 mN / m.

Eksperimen banjiran teras menunjukkan bahawa sulfat surfaktan yang dibangunkan mempunyai prestasi yang baik pada suhu 60 °C, dengan perolehan minyak sebanyak 90 %. Surfaktan sulfonat mempunyai prestasi yang lebih baik daripada sulfat kerana faktor kestabilan haba yang tinggi dan berjaya memperoleh 96 % daripada minyak yang terperangkap dengan menggunakan sulfonat jenis rantaian sampingan 10-Acetoxy-9-decoxy-2-sulfo-octadecanoic acid methyl ester

TABLE OF CONTENT

LIST OF FIGURES

LIST OF TABLES

LIST OF ABBREVIATIONS

ACS	American Chemical Society
ANOVA	Analysis of Variance
AOCS	American Oil Chemists Society
AOS	Alpha Olefin Sulfonate
API	American Petroleum Institute
ASP	Alkaline Surfactant Polymer
ASTM	American Society for Testing Materials
BET	Brunauer-Emmet-Teller
bpd	Barrels per day
CCRD	Central Composite Rotatable Design
CMC	Critical micelle concentration
CMC	Critical micelle concentration
CV	Coefficient of variance
CWAG	Chemical Water Alternating Gas
D	Darcy
d	Diameter
DOE	Design of experiments
DW	Deionized water
Ea	Activation energy
EACN	Equivalent Alkane Carbon Number
EDX	Energy-dispersive X-ray spectroscopy
EO	Ethylene oxide
EOR	Enhanced Oil Recovery
FAME	Fatty acid methyl ester
FAWAG	Foam Assisted Water Alternating Gas
FESEM	Field Emission Scanning Electron Microscopy
FFA	Free Fatty Acids
FFR	Falling Film Reactor
ft	Foot

FT-IR	Fourier Transform Infra-Red Spectroscopy
GC	Gas Chromatography
GC-FID	Gas chromatography Flam Ionization Detector
GC-MS	Gas chromatography mass spectroscopy
HATR	Horizontal Attenuated Total Reflectance
HC	Hybrid catalyst
HLB	Hydrophile-Lipophile Balance
HOAME	High Oleic Acid Methyl Ester
HPAM	Partially Hydrolyzed Poly Acrylamide
iBA	Iso butyl alcohol
IEA	International Energy Agency
IFT	Interfacial Tension
IOS	Internal Olefin Sulfonate
IV	Iodine Value
IW	Injection Water
k	permeability
K	Kelvin
k	Rate constant
L	Length
m	milli
M	Mobility ratio
MES	Methyl ester sulfonate
min	Minutes
MW	Molecular weight
Nc	Capillary number
NMR	Nuclear Magnetic Resonance Spectroscopy
O/W	Oil in water
OFAT	One Factor at A Time
-OH	Hydroxyl
OH^{-1}	Hydroxide
OOIP	Original Oil in Place
P	Pressure

p	Probability
Pc	Capillary pressure
PAM	Polyacrylamide
PEG	Poly ethylene glycol
PMT	Potentiometric mass titration
PO	Propylene oxide
PPG	Poly propylene glycol
ppm	Parts per million
psi	Pounds per square inch
PZC	Point of zero charge
Q	Flow rate
R	Gas constant
r^2	Correlation coefficient
RI	Refractive Index
rpm	Revolutions per minute
RSM	Response Surface Methodology
sBA	Secondary butyl alcohol
s	Seconds
S_o	Oil saturation
S_{oi}	Initial oil saturation
S_{or}	Residual oil saturation
S_w	Water saturation
SP	Solubilization parameter
SSA	Silica sulfuric acid
SSB	Silica supported BF_3
TDS	Total dissolved solids
V	Volume
W/O	Water in oil
WAG	Water Alternating Gas
WAT	Wax Appearance Temperature
WOR	Water to oil ratio
Wt.	Weight

XPS	X-ray photoelectron spectroscopy
XRD	X-ray Diffraction spectroscopy
XRF	X-ray florescence spectroscopy
Greek symbols	
μ	viscosity
ν	Interstitial velocity
ρ	Density
σ	Interfacial Tension
Φ	Packing factor
ϕ	Porosity
θ	Contact angle
ω	Rotation rate
Δ	Differential

CHAPTER 1

INTRODUCTION

This chapter provides the general background, motivation of the research, research objectives and scope of this study. The organization of the thesis and chapter summary are also presented.

1.1 Background and Motivation

Enormous urban and industrial developments in recent years have resulted in high demands for energy. According to the International Energy Agency (IEA), world oil demand in 2012 was 89 million barrels per day (bpd). Moreover, it has been predicted that the oil demand will surpass 91.4 million bpd towards the end of 2013 [1]. This ever increasing demand for oil has directed many researchers to find ways to maximize the oil recovery from existing resources as new discoveries of onshore oil fields are scarce. Commonly used oil recovery methods are pressure depletion (primary recovery) and water flooding (secondary recovery). It is believed that after water flooding, two thirds of the original oil in place (OOIP) remains unswept and trapped in the reservoirs. On an average, primary and secondary recovery methods can only produce less that 50 % OOIP. Several production methods have been proposed and are being applied for the recovery of the trapped oil; this is called the tertiary oil recovery. The tertiary oil recovery is commonly termed the Enhanced Oil Recovery (EOR) [2]. In Malaysia, as of 2003, out of 20.1 billion barrels of estimated oil in place, 12.7 billion barrels of oil (63.2 %) is still trapped [3]. It has also been pointed out that the chemical methods are one of the most favorable methods of EOR for Malaysian oil fields [3, 4]. It is estimated that an additional one billion barrels of

oil can be achieved from Malaysian oil fields by EOR methods [3].These chemical methods use surfactants as the major constituent in oil recovery slugs for interfacial tension (IFT) reduction, wettability alteration in straight chemical flooding and as a mobility control agent in water alternating gas (WAG) or foam assisted WAG (FAWAG) processes. Surfactants are unique molecules with a water soluble part (head) and an oil soluble part (tail). Surfactants are not only present in consumer products (such as shampoos, soaps and detergents) but are also one of the most important classes of industrial chemicals. According to a market research study by Ceresana Research, the surfactant market revenue was over US$28 billion in 2011 and it will be more than US$41 billion in 2018 with an average growth rate of 4.5 % [5]. Anionic surfactants, which are about 70-75 % of the total surfactants produced worldwide, with a world demand of 6.5 million tons in 2010 [5, 6], are also the main class of surfactants used for chemical EOR applications for sandstone reservoirs.

1.2 Surfactants and Enhanced Oil Recovery

Anionic surfactants with sulfate or sulfonate head groups are the most commonly employed surfactants for chemical EOR applications. From foam generation to IFT reduction, surfactants can play pivotal roles for enhancing the oil recovery. Major mechanisms involved in the surfactant's enhanced oil recovery for EOR applications include IFT reduction and wettability alteration. It is a fact that the main reason of oil being trapped in a porous medium is the high IFT (about 20-30 mN / m) between the oil and water [7]. Therefore, by reducing IFT between the oil and water, surfactants can help in the recovery of trapped oil from a reservoir.

Surfactants act on a water-oil interface and due to their unique chemical structure they orient themselves at the interface in such a way to generate low IFT. In this way, surfactants can produce emulsions and microemulsions of oil and water. A microemulsion is a thermodynamically stable emulsion with biscontinuous oil and water phases. Due to both the oil and water phases being "joined" together in one phase, microemulsions have ultra-low IFT with oil as well as with water. This

remarkable capability of microemulsions is used to mobilize the trapped oil from a reservoir.

Surfactants are generally produced from petroleum fractions. These petroleum based surfactants are usually considered as a potential threat to the environment due to the benzene rings and long hydrocarbon chains. Moreover, their price is mostly dependent on the crude oil price, and hence generally remains high. Natural oils are renewable resources which are considered as strong alternatives to petroleum fractions for surfactant synthesis. The long fatty acid carbon chains are naturally designed "tails" for a surfactant molecule. In addition, the degree of unsaturation in the structures (from oleic and linoleic acids) makes them attractive when attachment of different functional groups is desired.

1.3 Problem Statement

A surfactant molecule has two components: a long hydrocarbon chain (tail) and a hydrophilic head. Long and straight chains for surfactant molecules can be obtained from natural oils. As natural oils are triglyceride esters, transesterification is required to separate the fatty acids from a glyceride linkage by forming alkyl esters. Transesterification reaction for the oils with high levels of free fatty acids (FFAs) is not considered feasible. Acidic catalysts are usually used for the esterification of FFAs. Efficiencies of these catalysts are low, especially in the presence of high FFA contents in natural oils. Therefore, studies to develop new catalysts for the FFA esterification are needed.

The surfactants' performance of the IFT reduction and wettability alteration depends on their structure. Microemulsions of oil and water can only be formed under certain circumstances. The structure of a surfactant is one of the major parameters (including brine salinity, crude oil, hydrocarbon chain length, temperature etc.) which play an important role in the microemulsion formation. A small chain length usually makes a surfactant more water soluble and more tolerant towards salinity and hardness. However, the smaller chain length reduces the oil-water emulsification, and

hence results in low oil-water solubilization. A chain with a moderate length, usually containing 16-18 carbon atoms, is hence, required. Other associated problems with straight chain surfactants are their packing behavior and long term thermal stability. Long straight chains can result in tight, ordered packing and layers which can elevate the viscosity of the microemulsions. To overcome these predications, surfactant tail groups with branched chains are suggested. Commonly available natural oils do not contain fatty acids with branches. Therefore, branches or side chains need to be inserted into the backbone of the fatty esters.

The attachment of side chains to the backbone of a surfactant tail is important to enhance the surfactant efficiency. Unsaturated fatty acids such as oleic and linoleic acid from natural oils can be used as a precursor to the side chains' attachments. These fatty acids can be epoxidized and subsequently alkoxylated with alcohols of different chain lengths. Attachments of chains as ether linkages pose a major problem when the molecules are subsequently sulfonated. Every attachment achieved by the alkoxylation reaction generates a hydroxyl group (-OH) at the opposite position of the ether linkage. This -OH group must be protected by some suitable protecting agent before a sulfonation process is performed. If kept unprotected, the hydroxyl group readily reacts with the sulfonating agent (SO_3 gas or chlorosulfonic acid) and produces sulfate as the -OH group is more reactive than the hydrogen atom at the alpha position.

The next stage of synthesis is the sulfonation process which is to attach the sulfonate "head" group to the surfactant "tail". This process can be conducted in a Falling Film Reactor (FFR). Sulfonation is an exothermic and slow reaction. A very aggressive chemical, such as sulfur trioxide or chlorosulfonic acid is required to conduct the sulfonation and sulfation, respectively. Control of the reaction temperature as well as the reactants' feed in the reactor is difficult and complicated.

In conclusion, the major challenges involved in the synthesis of suitable surfactants from natural oils can be summarized as:

- To enhance the efficiency of esterification reaction of FFA. One way to achieve this is to develop a new high efficiency catalyst for a successful esterification of FFA.

- The epoxidation of methyl esters commonly takes a long time. There is an urgent need to optimize the reaction time and other reaction parameters.

- The successful attachment of side chains on the methyl esters backbone is desired utilizing a short reaction time at a low temperature and with a relatively lower amount of alcohols.

- The sulfation of hydroxyl group at the *trans* position to the side chain will require methods which can successfully convert the hydroxyl group into the sulfate group.

- The sulfonation at the α-position of the methyl esters in the presence of a side chain requires the protection of the OH group by some effective method. After the protection, the sulfonation at the α-position is desired to be accomplished with high conversion efficiencies.

1.4 Research Objectives

The present research was conducted with the following objectives:

- To synthesize and characterize the surfactants from the natural oils and their derivatives.

- To evaluate the surfactants for EOR applications by performing phase behavior experiments and IFT measurements for the identification of the best surfactant structures with which the oil/water solubilization parameter becomes more than 10 and/or the IFT between the oil and water are typically lowered down to 1×10^{-1} to 1×10^{-3} mN / m.

- To evaluate the surfactants for actual oil recovery by using core flood experiments.

1.5 Scope of Research

This research involves the synthesis of surfactants and the evaluation of the synthesized surfactants in terms of enhanced oil recovery.

The synthesis of surfactants from natural oils is a multi-step process. The natural oils are triglycerides, and hence need to be transesterified to methyl esters. Transesterification reaction is usually performed by using a base catalyzed transesterification reaction. Although base catalysts are efficient and the reaction is fast and complete, there is a stringent requirement of FFA levels below 1 % for natural oil. This value of FFA is normally very high (higher than 30 %) in some oils. The lowering of FFA requires acidic catalysts which are not very efficient at higher FFA contents. Therefore, methods for the lowering of FFA values using high efficiency catalysts, and thus the development of new catalysts, needs to be established.

The attachment of side chains to the methyl esters requires the epoxidation of the double bonds as the first step. The epoxidation reaction is highly sensitive to hydrogen peroxide, formic acid, reaction temperature and reaction time. The effects of these factors on the epoxidation yield and the optimization of the reaction for a maximum yield is extremely important. Therefore, an optimization study of the epoxidation reaction for a maximum yield has been performed.

The opening of the oxirane ring by a suitable precursor requires catalysts and in the presence of excess reactants. The removal of excess reactants is usually difficult, requiring distillation or chromatographic separations. Therefore, performing the oxirane opening reaction with a suitable catalyst using stoichiometric amounts of reagents requires a detailed investigation.

Sulfonation and sulfation reactions are the concluding reactions in surfactant synthesis. Both reactions require aggressive chemicals such as sulfur trioxide and chlorosulfonic acid. Due to the highly reactive nature of these chemicals, the control of the reaction parameters, such as the reaction temperature, is essential. Furthermore, before the sulfonation reaction, any hydroxyl groups attached to the methyl ester molecule should be protected. Therefore, the initial protection of the hydroxyl groups with a suitable protecting agent, and later the sulfonation of methyl esters need to be ascertained. State of the art spectroscopic techniques, i.e., NMR, GC-MS and FTIR are employed for the structural confirmation and elucidation.

The second part concerns the surfactants' evaluation. The evaluation of surfactants for EOR applications involves a multistep procedure. In the first step, the synthesized surfactants are evaluated for compatibility with other allied chemicals, such as alkali and polymers. Thermal stability is evaluated in the next step. Salinity and hardness tolerance are also important factors in the evaluation of surfactants for a particular EOR application. The surfactant samples which pass the above cited tests and evaluations are then subjected to the phase behavior tests. The generation of a microemulsion and the effect of varying the salinity on the different types of microemulsions are studied in the phase behavior tests. In addition, solubilization parameters for the oil and water are also noted and surfactants which demonstrate high values of the solubilization parameter (particularly >10) are selected for further study. High solubilization values are the direct estimates of very low IFT attainment between the oil and water interface. The selected surfactants formulations are also evaluated by spinning drop and pendant drop tensiometers for their capability to lower IFT between the oil and water. In the final step, core flood studies are performed to assess the surfactant performance.

1.6 Research Methodology

This research consists of two parts. The first part focusses on the synthesis and characterization of surfactants from natural oils and their derivatives. The second part describes the evaluation of the synthesized surfactants for chemical EOR applications.

All the raw materials, precursors and products were analyzed by GC-MS, GC-FID, FT-IR and NMR spectroscopy techniques. Several AOCS and ASTM standards methods were used to evaluate different qualities and properties.

The evaluation of the surfactants was performed using the compatibility tests with brine and polymer solutions. The surfactants which were stable under the test conditions with other test fluids were subjected to the phase behavior tests. Microemulsion formation with crude oil and solubilization ratios were established. The surfactants with a solubilization parameter of more than 10 were selected for further evaluation through the core flood tests.

1.7 Organization of Thesis

This thesis has been organized into six chapters including this introduction chapter.

Chapter 2 describes the extensive and critical literature review related to this subject. It also includes the basic concepts and descriptions for enhanced oil recovery and surfactant synthesis. The detailed historical background of the surfactants involvement in the chemical EOR applications, surfactant synthesis and their evaluation is also presented.

Chapter 3 presents the details of the methods used for the synthesis and evaluation of the surfactants. The particulars of the raw materials, synthesis schemes, and characterization and evaluation procedures of the products are discussed here.

Chapter 4 discusses the results of the synthesis of the surfactants. The results regarding the effects of different parameters on the synthesis processes and the analysis of the products are described in detail.

Chapter 5 investigates the properties of the synthesized surfactants for the evaluation purposes. The detailed performance of the compatibility tests, phase behavior tests, adsorption studies and core flood studies are presented here.

Finally, Chapter 6 is devoted to the conclusions of this research. This chapter presents a summary of the thesis and recommendations for future work.

1.8 Chapter Summary

In this chapter, the introduction to this research has been presented. The increasing demand for oil in the world and the importance of the EOR methods for oil recovery have been discussed. The potential impacts of EOR on oil production, particularly for Malaysian oil fields, have been presented. Details regarding the scope of research, methodology involved, problem statement and research objectives have been described. In addition, the organization of the thesis chapters has also been provided.

CHAPTER 2

THEORY AND BACKGROUND

This chapter provides the theory and literature review of the surfactant synthesis, EOR process and surfactant evaluation. Surfactants, their types and historical role in EOR applications are presented in the first few sections. In later sections, the EOR process, the basic concepts and the fundamentals of reservoir properties relating to the EOR process are defined and explained. In addition a detailed account of the surfactant design, synthesis processes, and reaction mechanisms involved in the synthesis and the applications of surfactants is also presented. Surfactant evaluation procedures and protocols are presented towards the closing sections of the chapter. In the end, the chapter summary and conclusions will also be provided.

2.1 What are the Surfactants?

Surfactants are 'surface active agents' and are organic compounds containing at least one lyophilic (solvent-loving) and at least one lyophobic (solvent-fearing) group in the same molecule [6]. When the solvent is water, the terms hydrophobic and hydrophilic are used for solvent-fearing and solvent-loving groups, respectively. Usually the polar group is termed as 'head' and the long non-polar chain is known as 'tail'. The hydrophilic group is polar in nature and is soluble in water while the hydrophobic group is non-polar and is water insoluble. The hydrophobic (or lipophilic) group is soluble in non-polar phases. Due to this unique ability of having two different groups available in the same molecule, surfactants act on the interface of two immiscible phases (e.g., water and oil) and lower the Interfacial Tension (IFT) between these two phases. During this IFT lowering process, the hydrophilic part of

the surfactants remains in the water while the hydrophobic part tries to remain in the oil making more contact between the two phases and causes the IFT to reduce. This interfacial tension is called surface tension when air (or gas) is the in the non-polar phase.The ability of surfactants to act on the interface makes them unique in the chemical industry and therefore, the surfactants play a major role in many industrial and household applications. They are used in domestic and industrial processes for cleaning, wetting, dispersion, emulsification, foaming and antifoaming applications. Numerous industrial and household chemical formulations use surfactants as detergents, soaps, shampoos, inks, paints, adhesives, herbicides, firefighting chemicals, leak detectors and as active agents for enhanced oil recovery (EOR) applications. Due to these multifarious applications, surfactants capture a remarkable portion of the chemical market. Anionic surfactants are the major players in the surfactant market and their global demand in 2010 was 6.5 million tons [8].

2.1.1 Types of Surfactants

Depending on the charge present on their head in solutions, surfactants are divided into four types: anionic, cationic, non-ionic and amphoteric surfactants.

2.1.2 Anionic Surfactants

Anionic surfactants are the most important and widely employed class of surfactants in most of the industrial, household and EOR applications. In aqueous solutions, the head of these surfactants acquires a negative charge. The head groups such as sulfonates, sulfates, phosphates and carboxylates are famous examples from this class of surfactants (Figure 2.1).

Internal Olefin Sulfonate (IOS) and Alpha Olefin Sulfonate (AOS) are commonly used in EOR applications. IOS's are made from the sulfonation of internal olefins (typically $C_{16} \sim C_{22}$ cut). The products obtained are usually a blend of hydroxy alkane sulfonates and alkene sulfonates as shown in the Figure 2.2. Careful control of the reaction conditions gives the desired product. The sulfonate head group is considered

more stable in high temperature environments than the sulfate group. In recent years, anionic surfactants from green and renewable resources such as natural oils have also been given importance due to their environmentally friendly impacts.

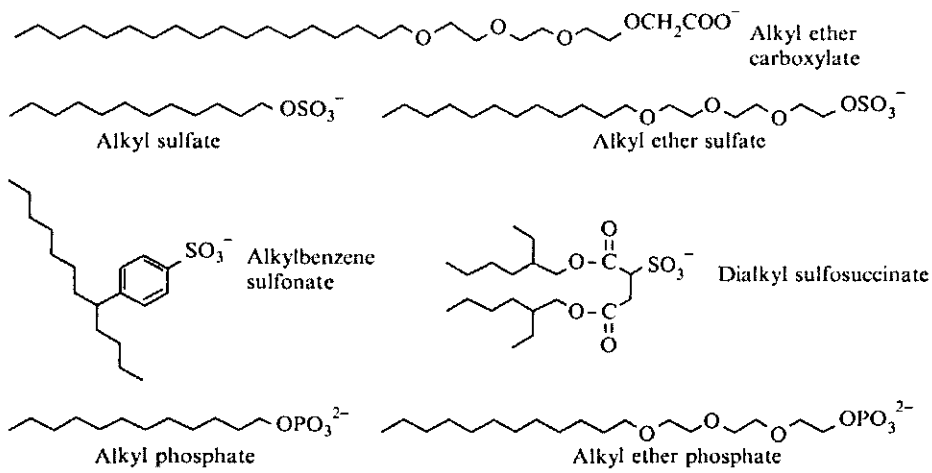

Figure 2.1: Structures of some anionic surfactants [9]

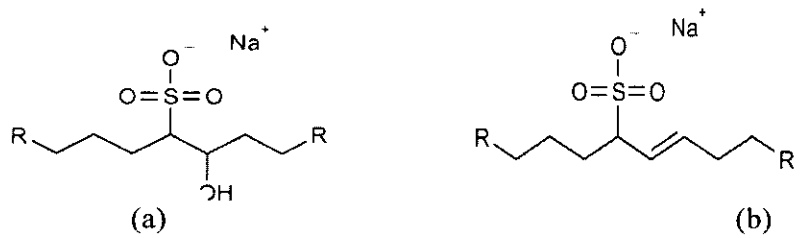

Figure 2.2: Hydroxy alkane sulfonate (a) and alkene sulfonate (b)

Usually these surfactants have been employed for industrial applications such as laundry and cutting oils due to the simple and straight carbon chains derived from the natural oils. The availability of techniques for the alteration of chain length and branching is making them one of the very important groups having great potential for high impact applications such as EOR.

2.1.3 Cationic Surfactants

These surfactants have a positive charge on the head when dissolved in water. Important examples include ammonium salts of fatty acids, simple fatty amine salts

(alkyl amine salts), fatty diamine salts and di-ester amine quaternary salts, as shown in Figure 2.3 [5].

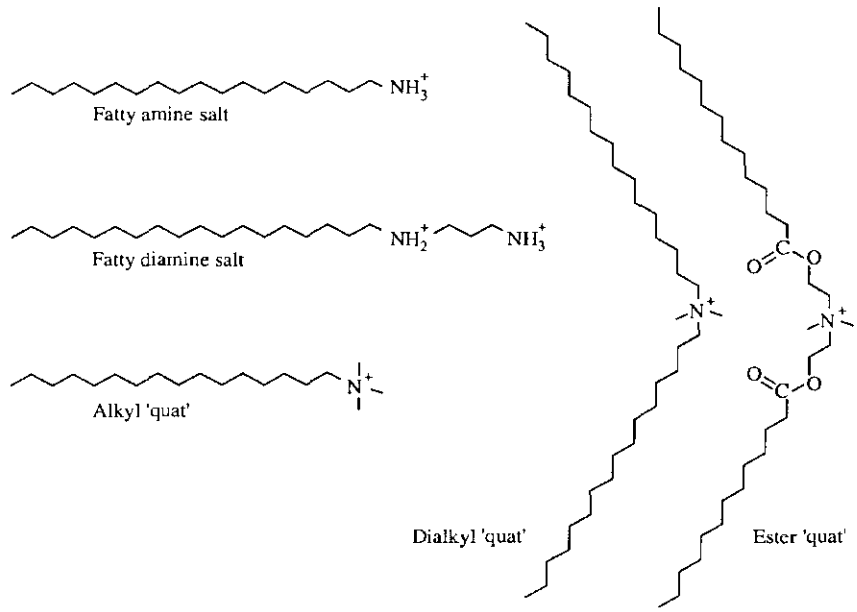

Figure 2.3: Structures of some cationic surfactants[9]

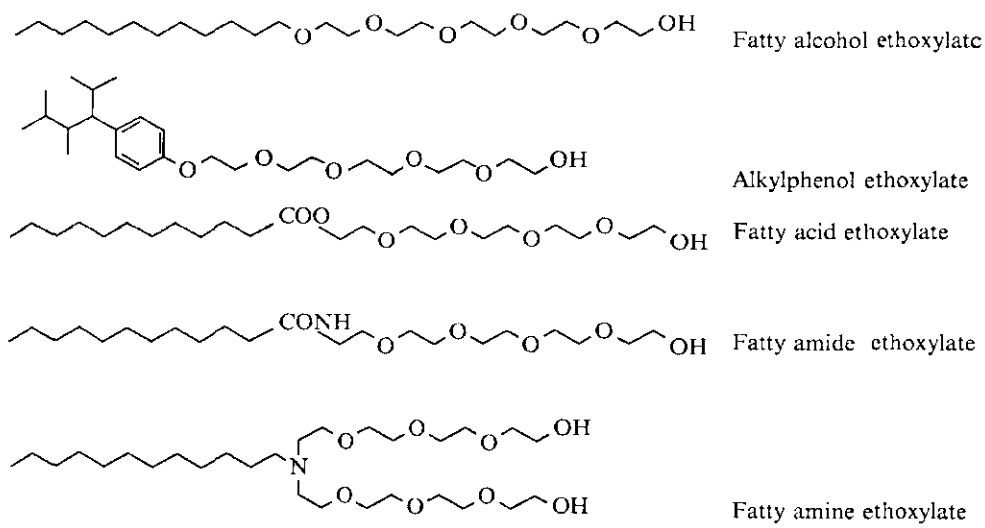

Figure 2.4: Structures of some non-ionic surfactants[9]

2.1.4 Non-ionic Surfactants

These surfactant molecules are neutral, without any charge on the head while in solutions. Poly ethoxylated alcohols, poly propoxylated alcohols and alkyl phenol ethoxylates are representative examples of this group as shown in Figure 2.4.

2.1.5 Amphoteric Surfactants

The charge on the head is dependent on the pH of the solution of the surfactant. For example in Betaines, when the pH is less than 7, the charge on the head will be positive due to the formation of quaternary ammonium ions. When the pH is more than 7, the charge will be negative as now the acid will be converted into salt, which after dissolution will result in a negative charge as shown in Figure 2.5.

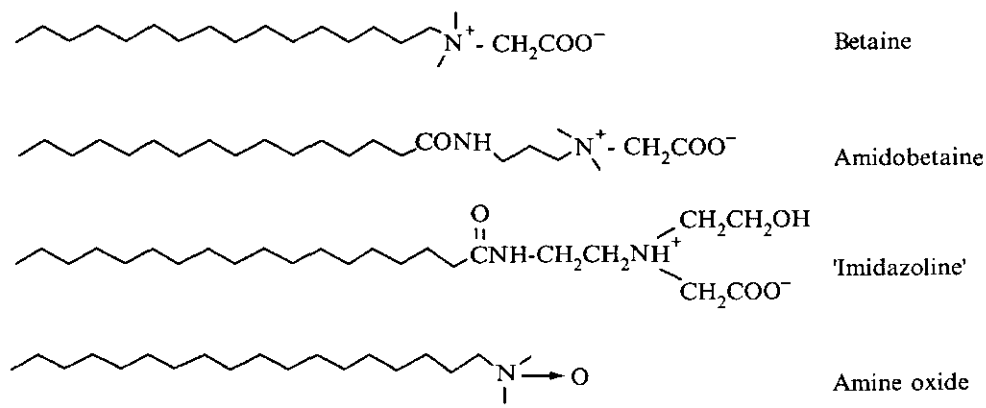

Figure 2.5: Structures of some amphoteric surfactants [9]

2.2 Surfactants in Solution

When surfactants are mixed in an aqueous solution, they tend to be adsorbed between the air-water interfaces. If their concentration is increased continually in the solution, then the surfactant molecules start assembling into well-organized structures, called micelles. Micelles are dynamic structures which form and break in microsecond speed [10].The minimum concentration required to start micelle formation is called Critical Micelle Concentration (CMC), which is one of the very important properties of a

surfactant. Many of the solution's properties change after the CMC has been achieved (Figure 2.7). If oil is also present along with the water-surfactant solution, emulsions can be formed. When water is the continuous phase (water is larger in proportion than oil), surfactants encapsulate the oil droplet in the micelle by making a core with their non-polar tails while their polar heads remain in the water making an outer shell thereby forming an oil in water (o/w) emulsion. When the continuous phase is oil (oil is larger in proportion than water), the micelles are formed in such a way that the heads make an inner core around the polar water droplet and the tails make the shell in the oil phase, thereby making a water in oil (w/o) emulsion. These micelles are called reverse micelles (Figure 2.6 -b).

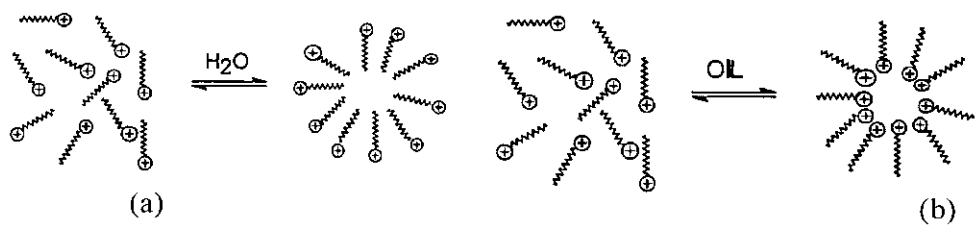

Figure 2.6: Formation of micelle (a) and reverse micelle (b) [10]

CMC is a specific property of a surfactant and it is an important parameter which affects the properties of a solution. Many physical properties of surfactant solutions are dependent on CMC.

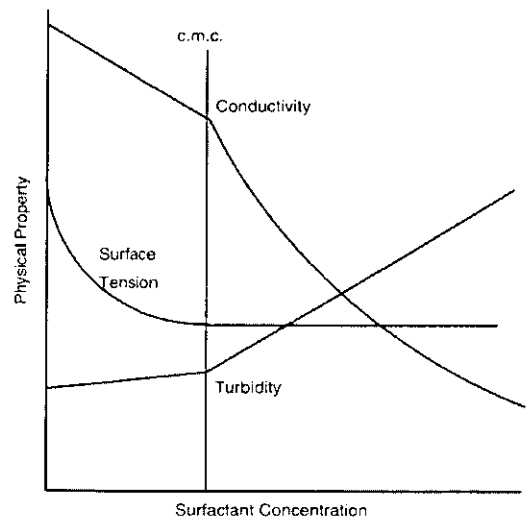

Figure 2.7: Some important indicators of micelle formation [11]

As presented in Figure 2.7, the conductance of the surfactant solution decreases linearly and this trend becomes nonlinear after the CMC. The surface tension also decreases and after the CMC is reached, it becomes constant. Turbidity increased by increasing the surfactant concentration and an abrupt high turbidity formation was detected after achieving the CMC. One important parameter relating to CMC is the Krafft point. It is the minimum temperature required for the micelle formation. The solubilities of the surfactants show a strong increase above the Krafft point [12]. Below the Krafft point, there will not be any micellization and hence no CMC. The Krafft point can be roughly equivalent to the melting point of the hydrocarbon tail of the surfactants [13]

2.3 Enhanced Oil Recovery (EOR)

Enhanced Oil Recovery (EOR) can be defined as the process of oil recovery which is achieved by injecting chemicals originally not native to the reservoir [14]. It is the process of choice after "primary recovery" of oil (achieved by utilizing the inherent energy of the reservoir such as high pressure) and "secondary recovery" (conducted by water injection). EOR methods can be broadly classified according to the types of injectants: thermal, gas and chemical methods. A detailed classification of the EOR methods is shown in Figure 2.8. Thermal methods include steam flooding, hot water injection, in-situ combustion etc. The thermal methods are considered suitable for heavy oils. The gas methods involve the injection of a gas such as CO_2 and nitrogen, the choice usually depends upon the availability of the gas. Gas injection can further be in the form of WAG (water alternating gas), FAWAG (Foam Assisted WAG) or CWAG (Chemical WAG). Chemical methods include injection of alkali, surfactant, polymer and alkaline/surfactant/polymer floods etc. Although thermal and gas injection methods are currently producing much of the EOR production worldwide, chemical methods have also been considered as having a promising future [15]. Chemical methods usually aim to lower the IFT between oil and water, wettability alteration and mobility control for a better sweep of the oil from the reservoir. Surfactants play a major role in IFT reduction and wettability alteration processes. This research work's focus was chemical EOR by utilizing surfactants; therefore,

future discussion will primarily be focused on the aspects of chemical EOR and surfactants.

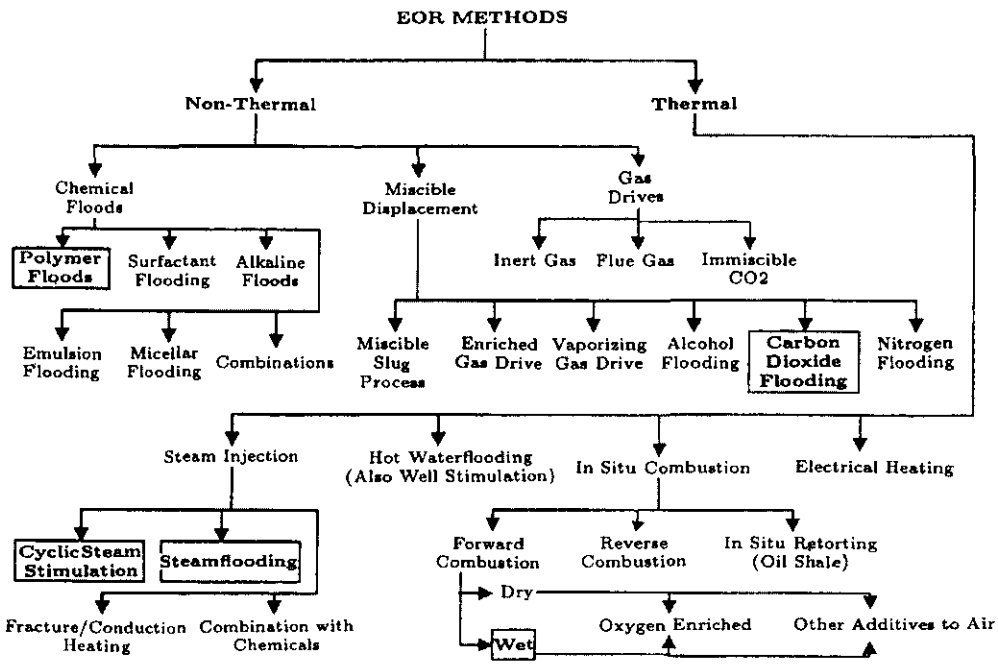

Figure 2.8 General classification of EOR methods [15]

2.4 Surfactants in EOR Applications

Application of surfactants in EOR applications is not new and the injection of surfactants for oil recovery can be dated back to the 1920's [16]. As the reaction process was not well understood at that time and chemicals were also expensive, further development in surfactant flooding was not widely reported in the literature. In the 1960's surfactants started to be produced in large quantities, industrially, and this influenced their possible usage in miscible floods [17]. An early report on a miscible micellar flood was published in 1968 by Davis and Jones [18]. They reported the findings of the micellar flood which contained large amounts of a petroleum sulfonate based surfactant mixed with water and oil. Later on, surfactant flooding was further discussed by Healy and Reed who published their work on the designing and understanding of microemulsions and micellar systems in EOR processes [19-22]. In their studies, ortho xylene sulfonic acid and other sulfonates were employed for

producing microemulsions. Petroleum sulfonate mixtures were studied by several researchers to investigate the correlation between interfacial tension and oil displacement [23]. As a new EOR method, alkaline/surfactant/polymer (ASP) flooding was developed by Shell in the early 1980's [24]. This technique gained importance due to the favorable effect of alkali on acidic components of crude oil to enhance the surfactant action by making in-situ surfactants. The introduction of alpha olefinic sulfonates and internal olefin sulfonates in surfactant slug formulations lowered the IFT between oil and brine to 10^{-3} mN/m, and ASP became an interesting technique. These surfactants are still good workhorses of the EOR industry and are usually used with alcohol alkoxy sulfates. Alcohol alkoxy sulfates have the ability to lower the IFT between oil and brine, and it provides a good tolerance against the high salinity. These surfactants have long alkyl chains, poly ethylene glycol or poly propylene glycol as connecting units and then a sulfate as the head. This combination of an anionic and non-ionic surfactant component in a single molecule has been extensively studied [25, 26]. In the 1980's there were several studies on the effect of surfactant structures on IFT reduction [27], microemulsion displacement systems [28], the effect of IFT on relative oil/water permeabilities [29], the role and measurement of interfacial forces during immiscible displacement [30], the role of surfactant structures on oil/water solubilisation [31-33], and the phase behavior of a surfactant, oil and brine system for oil recovery [28, 34-37].

The current development of surfactants for EOR applications focuses on the development of extended surfactants for ultra-low IFT [38]. These surfactants are alcohol alkoxy sulfates possessing different hydrocarbon chain lengths, and EO and PO groups. Recently, high molecular weight internal olefin sulfonates (IOS) have been studied for their performance in high temperatures and high viscosity oils [39]. The alkoxylates from Guerbet alcohols were also employed for the laboratory studies and reported to be important for EOR applications due to their bulky hydrophobic part and relatively economical starting raw materials [40]. Surfactants for high salinity and high temperature conditions were proposed by Maura, Hirasaki and Miller (2012) [41]. These alkoxyglycidylether sulfonates were found to be good for high temperature, high salinity conditions. Alkoxy carboxylate surfactants were also shown to be prominent against a high temperature (100 °C) and a high salinity of 57000 ppm

concentration [42]. More recently, Julian Barnes *et al.* (2012) proposed controlled hydrophobe branching to match the crude oil composition. They investigated mixtures of IOS and alcohol propoxy sulfates to assess the relationship between hydrophobe bulk and crude oil microemulsion viscosity. It was proposed that a good sampling practice was essential for obtaining good results. Moreover, it was also presented that the matching of the hydrophobic part of the surfactant with the oil Equivalent Alkane Carbon Number (EACN) can be a helpful tool for obtaining the optimum surfactant formulations [43].

Methyl ester sulfonates are famous laundry detergents [44-47]. These have been given importance in recent years due to their superior performance and biodegradability, which is an important factor in the chemical industry due to environmental issues by surfactants based on petroleum fractions [45, 48]. Although this class of surfactants are being used in almost every consumer product requiring surfactants, it is surprising that very little work has been done on the possibility of their use in the EOR process. The only available reference was from the work of Marc Baviere and colleagues [49] in 1991. In this study, several tests were performed to evaluate the performance of MES. The phase behavior was investigated against dodecane in the presence of brine, alcohol and surfactant at a 1 wt. % concentration. Thermal stability was evaluated at different temperatures (50 – 100 °C) in sealed test tubes having pH ranges from acidic to basic (buffered solutions, pH 3, 7 and 11). Adsorption studies on Kaolinite were also performed at different temperatures. It was concluded that the interfacial efficiency was satisfactory over a wide range of temperatures and salinity. The solubilization power was more when long chain surfactants were used. The stability was found good at neutral pH even at high temperatures; however, hydrolysis was worse at high temperatures exceeding 50 °C and pH on acidic and basic range extremes. The surfactant adsorption was found to be higher in high salinity and especially in the presence of calcium cations [49]. From this study, it can be concluded that these surfactants have great potential to be used as EOR surfactants and suitable modifications of the backbone with pendant chains consisting of several CH_2 groups can impart further desirable properties.

2.5 Factors and Parameters Affecting Chemical EOR

EOR focuses on the trapped oil in porous media. Mobilization of this oil can only be facilitated by altering some factors by injecting fluids and thereby altering the intimate properties of oil and brine and to some extent reservoir rock. A better understanding of the trapping mechanism of oil is important in this context. The trapped oil exists as stuck, immobile oil droplets due to the high capillary forces between water and oil droplets. This mechanism is discussed in detail in the following section. In addition some key concepts involved in defining EOR mechanisms such as IFT, capillary number, capillary pressure, permeability and wettability are also discussed.

2.5.1 Oil Trap Mechanism in Porous Media

Water flooding, as seen in the secondary oil recovery method, is not successful beyond a certain extent due to the oil trapped in the porous media. Oil can be trapped in fine capillaries in the form of disconnected ganglia. Capillary trapping of oil may be of two types, namely the snap-off process and the bypass process [9].

In the snap-off process, the oil is trapped in the wider parts of the pores, which possess a larger ratio between the pore body and the pore throat akin to a bottle. As the wetting phase is water, it forms a layer around the non-wetting phase, the oil. The thin water layer gradually thickens in the throat and forces oil strands to break down near the pore throats thus making the oil drops separated from each other, surrounded by water.

The by-pass process is actually caused by the relative competition between the flow of oil and water in the pores of different sizes. The flow is faster in larger channels. The capillary forces will draw the displacing phase (water) into the smaller, narrow pores due to stronger interaction of water with the capillaries than the oil. Therefore, water is driven into the smaller pores, and at low injection rates, due to a lower viscosity than oil, the water becomes lodged in the smaller pores by capillary action. Oil, on the other hand, gets trapped in the larger pores and the water keeps on

by-passing the oil by flowing through the smaller capillary. These processes are shown in Figure 2.9 [9].

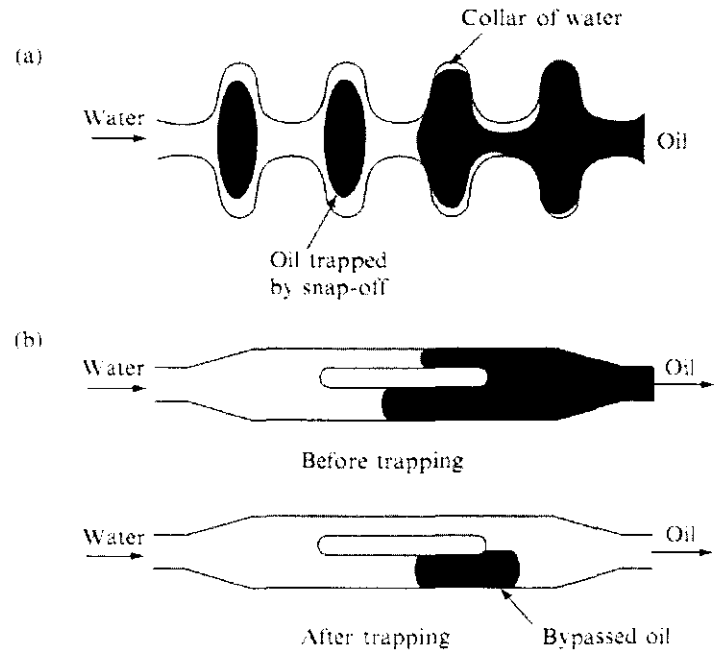

Figure 2.9: Oil trapping mechanisms: a) snap-off and, b) by-passing [9].

2.5.2 Interfacial Tension (IFT)

IFT is caused by the difference in the cohesive forces of molecules within one phase and the adhesive forces of dissimilar molecules at the interface. IFT is the force per unit length parallel to the interface between two phases such as oil and water. It is the excess free energy per unit area and is reported in dynes/cm or mN / m. The IFT between crude oil and water is normally in the range of 20 ~ 30 mN / m [7]. Due to the high IFT the oil and water behave like two immiscible phases and the water alone is unable to drive off the oil trapped in the pores. For EOR applications, it is generally implied that the IFT value should be decreased to 10^{-3} mN / m, which can be achieved by using surfactants [7]. When the IFT is reduced between the oil and water, these phases become more "alike" and hence a near miscibility condition can be achieved. The two near miscible phases can progress through the porous medium together, and hence the improved oil recovery is achieved.

2.5.3 Capillary Number (Nc)

The recovery of any remaining oil in the reservoir after water flooding depends upon the ratio of the two forces, namely viscous forces trying to displace the oil, and the capillary forces holding/ trapping the oil in the pores. The relationship between these two forces is defined by the Capillary Number (N_c), which is a dimensionless quantity, as defined in Equation 2.1 [50].

$$\frac{F_v}{F_c} = \frac{v\mu_w}{\sigma_{ow}\cos\theta} \tag{2.1}$$

where F_v and F_c are the viscous and capillary forces, respectively, v is the interstitial velocity, μ_w is the viscosity of the water (displacing fluid), σ_{ow} is the oil-water IFT and θ is the contact angle between oil and water. It is measured through the more dense fluid.

The Capillary Number can also be expressed without using the θ term (Equation 2.2): $N_C = \frac{v\mu_w}{\sigma_{ow}}$ (2.2)

where *Nc* is the capillary number and other variables are as defined above. A more generalized expression for the capillary number can be expressed as in Equation 2.3:

$$N_c = \frac{\Delta p}{\sigma b_c} \tag{2.3}$$

where Δp is the pressure drop along the capillary, σ is the IFT between the oil and water and b_c is the minimum width of the capillary at the constriction.

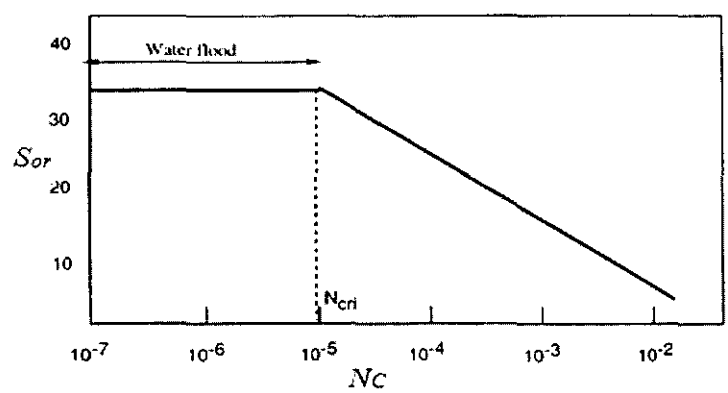

Figure 2.10 Capillary desaturation curve for a nonwetting phase [12]

The residual oil saturation S_{or} (i.e., the remaining oil) becomes constant and does not reduce further below a specific value of N_c, (typically in the range of $10^{-4} \sim 10^{-5}$). In a water flood, the N_c values are even below this level, typically 10^{-7}, and therefore, not very successful at reducing S_{or}. Above a critical N_c value, the residual oil saturation decreases almost linearly with the log N_c. The capillary number which corresponds to the break in the desaturation curve is called the critical capillary number, N_{cri}, [12] as shown in Figure 2.10. Therefore, a high value for the N_c, such as 10^{-2} to 10^{-1} is essential in order to reduce the residual oil saturation S_{or}, and hence for a high recovery of oil (Figure 2.11).

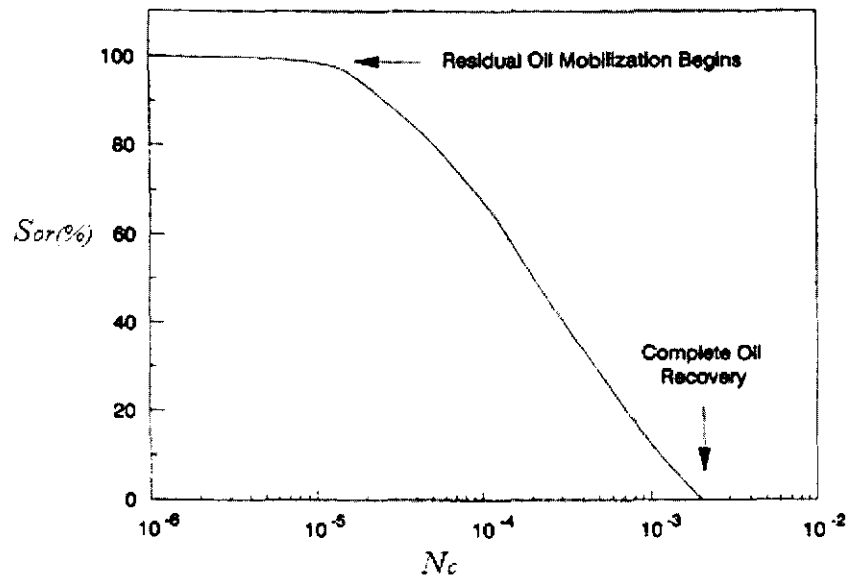

Figure 2.11: Capillary number correlation with percent of oil recovery [51]

Considering Equation (2.1), it is evident that the N_c can be increased by (a) increasing the viscous forces, the numerator, i.e., the velocity and viscosity of the water flood ,(b) decreasing the IFT and (c) a combination of both of (a) and (b). Increasing viscous forces is not practical due to the very high pressure involved which may result in reservoir damage. The other alternative choice is through the manipulation of the capillary force. This capillary force is actually the IFT between the oil and water and it can be decreased to achieve the high N_c value desired. For a water wet rock, it can be calculated that an IFT of at least in the order of 10^{-3}mN/m is required for a good oil recovery (Figure 2.11) [9].

2.5.4 Wettability

Wettability refers to the preference of one fluid to spread over or adhere to the solid surface in the presence of other immiscible fluids[52]. In a typical reservoir, wettability is mainly dependent on the chemical composition of the rock, composition of the fluids such as water and oil mixture, the initial water saturation and the reservoir temperature. It is one of the most important properties of the reservoir and is crucial to understanding the physical and chemical interactions between rock / water, rock / oil and water / oil under given reservoir conditions [53].

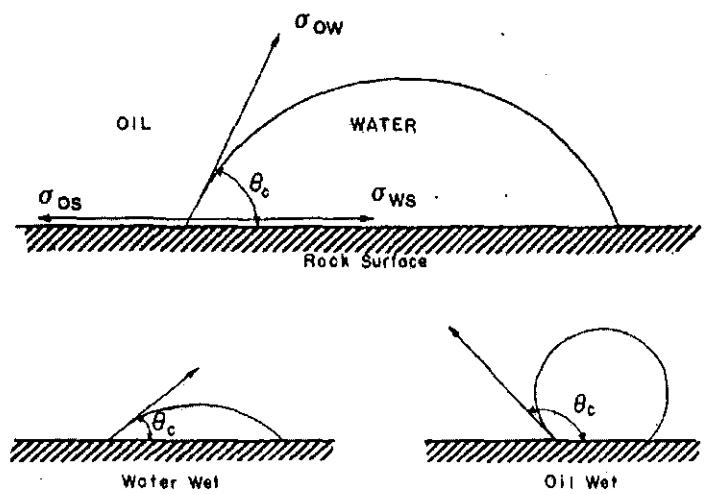

Figure 2.12: Contact angles defining the wettability of an oil/rock/water system [54]

Wettability can be determined by many methods but two methods, the Amott test and the USBM (US Bureau of Mines) test, both employing the displacement behavior of rock/brine/oil, are generally used [55]. Both tests are derived from the capillary pressure phenomena [56]. The contact angle is also used for wettability determination as shown in Figure 2.12. It is based on the wetting properties of a fluid towards the surface and is usually measured through the denser liquid phase, which is commonly the brine. Generally for an oil/water system, wettability can be defined according to the contact angle; if the contact angle is 0°-75°, the rock is water wet; if 75°-115 °, it is intermediate and with an angle of 115°-180°, the rock will be oil wet [57].

According to Figure 2.12, the surface energies can be interpreted by Young's equation (Equation 2.4):

$$\sigma_{ow}\cos\theta = \sigma_{os} - \sigma_{ws} \quad (2.4)$$

where σ_{ow} is the IFT between oil and water, σ_{os} is the IFT between oil and solid, σ_{ws} is the IFT between water and solid, and θ is the contact angle (the angle of the water/oil/solid contact line). The contact angle is measured through the water [54].

2.5.5 Capillary Pressure

If oil and water are placed together on a surface, a curved interface is formed between the oil and water. The contact angle which is measured through the water defines the wettability of the system, as seen in the previous section. As the interface is curved, the pressure is abruptly increased across the interface to balance the huge difference in the IFT forces. This high pressure is called the capillary pressure[58]. Therefore, capillary pressure is defined as the pressure difference between the pressures in the wetting and non-wetting phases at the interface. Two immiscible phases which are at equilibrium in a porous medium possess a distribution of forces defined by the capillary forces, which depend on the diameter of the pore and the IFT between the phases. The magnitude can be determined by the Young-Laplace equation [59], as presented in Equation 2.5

$$P_c = P_{nw} - P_w = \frac{2\sigma}{r_m} \quad (2.5)$$

where P_c is the capillary pressure, P_{nw} is the pressure of the non-wetting phase, P_w is the pressure of the wetting phase, σ is the interfacial tension and r_m is the mean diameter of the pore (capillary).

2.5.6 Permeability

Permeability (k) is the measure of the ease with which fluids can flow through the porous media at a given pressure gradient. Permeability depends on the pore size, shape and interconnection of the pore network. It is measured in Darcies (D) but commonly expressed in millidarcies (mD) due to its low values. Generally, a system with a value of k <1 mD is considered as poor permeability while 1~10 mD is fair

,10~50mD is moderate and 50~250 mD is considered as good permeability. Any value higher than 250 mD is usually regarded as very good permeability [60].

Flow rate has a direct relationship with permeability, as shown by Darcy's law (Equation 2.6):

$$q = -\frac{kA}{\mu}\frac{dp}{dx} \tag{2.6}$$

where q is the flow rate, k is the permeability, A is the area, μ is the viscosity, P is the pressure, and x is the length of the capillary.

Permeability is further divided into three forms: absolute, effective and relative permeability. Absolute permeability is the measurement of the permeability conducted when a single phase or fluid is in the rock. Effective permeability is the ability to preferentially flow or transmit a particular fluid through the rock when other immiscible fluids are also present in the reservoir. The relative permeability is the ratio of the effective permeability of a particular fluid at a particular saturation to the absolute permeability of that fluid at total saturation. Hence, if a single fluid is present in a rock, its relative permeability will be 1 [61].

2.6 EOR Mechanism

The overall efficiency of an oil recovery process can be defined on the basis of the total oil recovered from the amount initially present in the reservoir. This is defined in Equation 2.7.

$$E = \frac{R_{cumu}}{OOIP} = \frac{\text{Amount of oil recovered}}{\text{Amount of oil originally in place}} \tag{2.7}$$

where E is the overall efficiency and R_{cumu} is the cumulative recovery.

The main mechanisms for EOR methods are increasing the capillary number and providing a 'favorable' (M < 1.0) mobility ratio between the displacing and the displaced phases. The capillary number which is the ratio of the viscous to the capillary forces is defined in Equation 2.1 in section 2.6.3.

The mobility ratio, M, is defined as the ratio of the mobility of the displacing fluid to that of the displaced fluid as seen in Equation 2.8 [62].

$$M = \frac{\left(\frac{k}{\mu}\right)_a}{\left(\frac{k}{\mu}\right)_b} \tag{2.8}$$

where subscript a is for the displacing phase and subscript b is for the displaced phase. k is the relative or effective permeability, and μ is the viscosity of the respective phase.

The overall efficiency of any EOR process (i.e., the oil recovered by the process divided by the oil in place at the start of the process) depends on both the microscopic and macroscopic sweep efficiencies [50].

$$E = E_D \times E_V \tag{2.9}$$

where E is the overall efficiency, E_D is the microscopic displacement efficiency and E_V is the macroscopic (volumetric) sweep efficiency (both E_D and E_V are expressed in fractions).The macroscopic displacement efficiency relates to the effectiveness of the displacing fluid in contacting the reservoir in a volumetric level. E_V is a measure of "how effectively the displacing fluid sweeps out the volume of a reservoir, both areally and vertically".

The microscopic displacement is the displacement process occurring at the pore level. It will be useful to determine the amount of oil that was mobilized and how much was left trapped. Therefore, E_D is the measure of the effectiveness of the displacing fluid in mobilizing the oil in those places in a reservoir where the fluid actually contacted the oil. E_D is defined in terms of residual oil saturation, S_{or}, as shown in Equation 2.10

$$E_D = \frac{S_{oi} - S_{or}}{S_{oi}} \tag{2.10}$$

where S_{oi} is the initial oil saturation and S_{or} is the residual oil saturation (i.e., the saturation after the recovery process). The oil saturation, S_o, itself is defined as:

$$S_o = \frac{\text{Volume of oil in the rock, } V_o}{\text{Total pore volume of the rock, } V_p} \quad (2.11)$$

The volumetric sweep efficiency can be defined as:

$$E_V = E_{AS} \times E_{VS} \quad (2.12)$$

where E_{AS}: areal sweep efficiency and E_{VS}: vertical sweep efficiency.

E_V is a measure of the reservoir volume contacted by displacing the volume, composite of areal sweep (E_{AS}) and vertical sweep (E_{VS}). It is mostly affected by mobility ratio (M) and reservoir heterogeneity. E_D is a measure of how well the displacing fluid mobilizes the residual oil once the fluid has contacted the oil. It depends on many factors such as IFT, wettability etc. [50].

2.7 Role of Surfactants in Recovering Trapped Oil

After water flooding, the remaining oil left in the reservoir is immobile as it is bypassed by water (Figure 2.13). This phenomenon is common in capillaries of an uneven diameter. However, oil flow in normal capillaries which have an even diameter throughout the length is not very difficult. In a normal water flood process, the oil is mobilized by viscous flow of water only, without using much force, as explained in the following example. If oil is in a capillary of uniform diameter, the ΔP can be calculated using the following relationship as shown in Equation 2.13.

$$\Delta P = P_o - P_w = \frac{2\sigma}{r} \quad (2.13)$$

where P_o and P_w are the pressures of oil and water, respectively, σ is the interfacial tension between the oil and water and 2/r is the interfacial curvature. By inserting typical values of r = 10 μm ($10 \times 1 \times 10^{-6}$ m) and σ = 30mN / m, ΔP can be calculated as 6 kPa (0.87 psi). The oil can be mobilized by applying any pressure greater than 0.87 psi. However, if the capillary has a non-uniform diameter, the oil becomes trapped in it and remains immobile by using merely 0.87 psi.

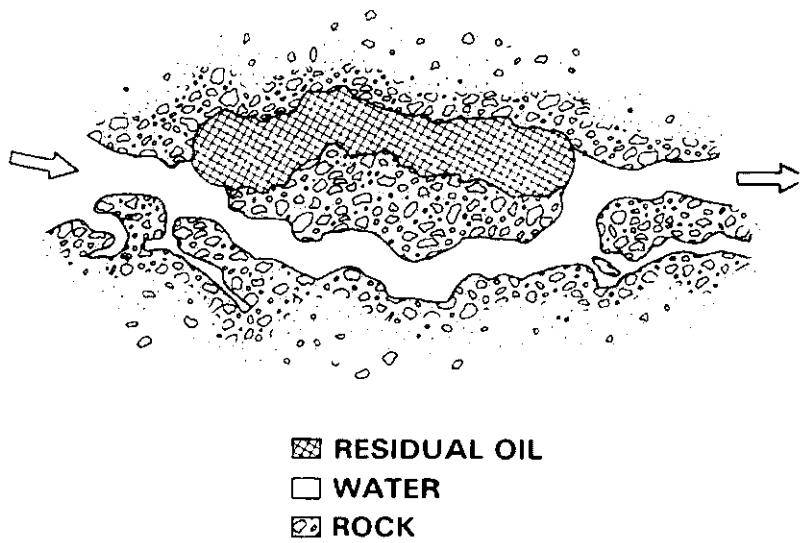

Figure 2.13: An approximate configuration of a trapped oil ganglion with water by-passing [63]

If the example of a capillary is considered which has a bottle like structure with a smaller pore side diameter of 10 μm and a large side diameter of 100 μm, (Figure 2.14) with the length of the oil trapped on both sides as 50 μm, then by using the following relationship, the pressure gradient, $\frac{\Delta P}{\Delta X}$, can be calculated as shown in Equation 2.14:

$$\frac{\Delta P}{\Delta X} = \frac{P_{o2} - P_{o1}}{\Delta X} = \frac{2\sigma}{\Delta X}\left[\frac{1}{R_2} - \frac{1}{R_1}\right] \tag{2.14}$$

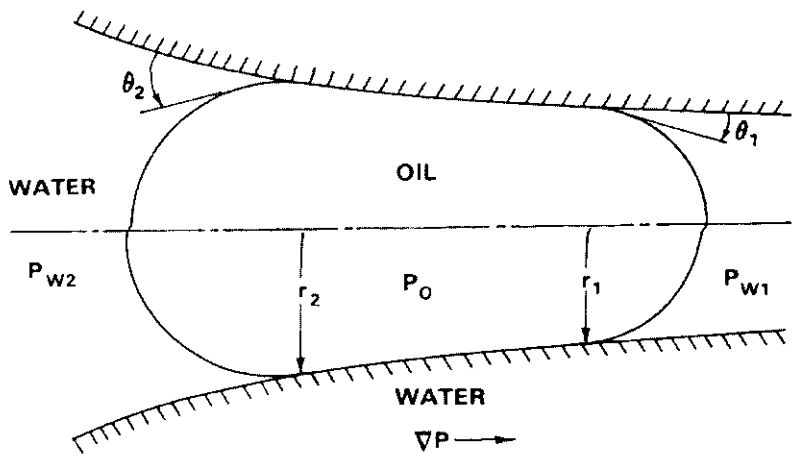

Figure 2.14: Model of an oil ganglion trapped by capillarity and a pore constriction [63]

$\frac{\Delta P}{\Delta X} = 10^7$Pa/m or 3500 psi / ft. This is a huge pressure to apply to move the oil and is not practically applicable as in typical reservoirs the pressure applied is in the vicinity of 1psi / ft.

From Equation 2.14, it is obvious that pore diameters cannot be varied and the only parameter which can be varied is σ (IFT). If the interfacial tension, σ, in this example is replaced by a typical number of 10^{-3} mN / m, the required pressure gradient is reduced to 0.175 psi / ft. This situation demonstrates the fundamental importance of reducing IFT. The only way to reduce the IFT down to this level is by the use of surfactants.

Traditionally, surfactants have been used in EOR primarily for reducing the IFT between oil and water, and wettability alteration. These are used alone or with other allied chemicals such as alkali and polymer in AS, SP and ASP processes. The main functions attributed to surfactants in the ASP process are IFT reduction, typically down to 10^{-3} mN / m and wettability alteration. More recently, however, surfactants have also been used for EOR in foam generation[64] and for making worm-like micelles having viscoelastic properties for mobility control [65, 66]. However, their major role in EOR is considered as IFT reducing agents. In this context, the injected surfactant slug must achieve an ultralow IFT with oil to mobilize it in a continuous phase with water by making microemulsions. Furthermore, this low IFT condition should be maintained throughout the process so that the mobilized oil should not be trapped back in the capillaries [67]. It is well understood that the formation of microemulsion at an ultra-low IFT is the key process in surfactant flooding [68]. As the microemulsion is the product of oil, water and brine, the phase behavior of the surfactants, water and oil, is of fundamental importance. Therefore, phase behavior studies are discussed in detail in the following sections.

2.8 Phase Behavior of Surfactants, Oil and Brine

A microemulsion is a mixture of water, oil and a surfactant. Sometimes the system also has a co-surfactant and co-solvent along with the surfactants. The co-surfactants

are used to enhance the solubilization ratio of the oil and water. These are typically long chain alcohols or sometimes the long chain alcohol propoxy sulfates. Co-solvents are short chain (C_3~C_5) alcohols such as isobutyl alcohol (iBA) and secondary butyl alcohol (sBA). These are added to the system to shorten the equilibration times. They are also used to reduce the microemulsion viscosity and gel formation [69]. The phase behavior study is the simplest method to screen the surfactants for the selected reservoir and fluid. Winsor in 1954 described the phase behavior of microemulsions [70]. Based on his study, it was found that different factors such as types of surfactants, co-surfactants, co-solvents, salinity, temperature and crude oil composition etc. are involved in the phase behavior of a microemulsion system. For a particular microemulsion system, the salinity is the most important parameter of the phase behavior [71]. Figure 2.15 [72] shows ternary phase diagrams for different types of microemulsion systems that were identified by Winsor.

The ternary diagram is a convenient way to describe the phase behavior and the effect of electrolytes [73]. In a particular system of a fixed surfactant concentration, selected crude oil and varying salinity, the phase behavior of a microemulsion can be classified into three different classes, Winsor type I or lower-phase microemulsion, Winsor type II or upper phase microemulsion and Winsor type III or middle phase microemulsion. In literature, some authors use type II(-) for Winsor type I, type II(+) for Winsor type II and type III for Winsor type III [72].

Winsor type I microemulsion is an oil-in-water microemulsion that coexists with nearly pure excess oil (two phases only). Here, all of the water and a portion of the oil have been solubilized. This type of microemulsion is also called a "lower phase" microemulsion. If the salinities are increased to a higher value, the type II microemulsion (water-in-oil) will be generated in which the microemulsion coexists with the excess water phase. This type is also called an "upper phase" microemulsion because the microemulsion is lighter than the water, and hence resides above the water phase. Here a portion of the water has been solubilized by the surfactant and all of the oil is solubilized. At intermediate salinities, three phases are present instead of only two phases. A type III microemulsion (bicontinuous microemulsion) is formed in equilibrium with both excess oil and brine. As the density of the microemulsion is

intermediate between the oil and water, it will form the middle phase with the excess oil above and the excess water below. Therefore, this kind of microemulsion is also called a "middle phase" microemulsion.

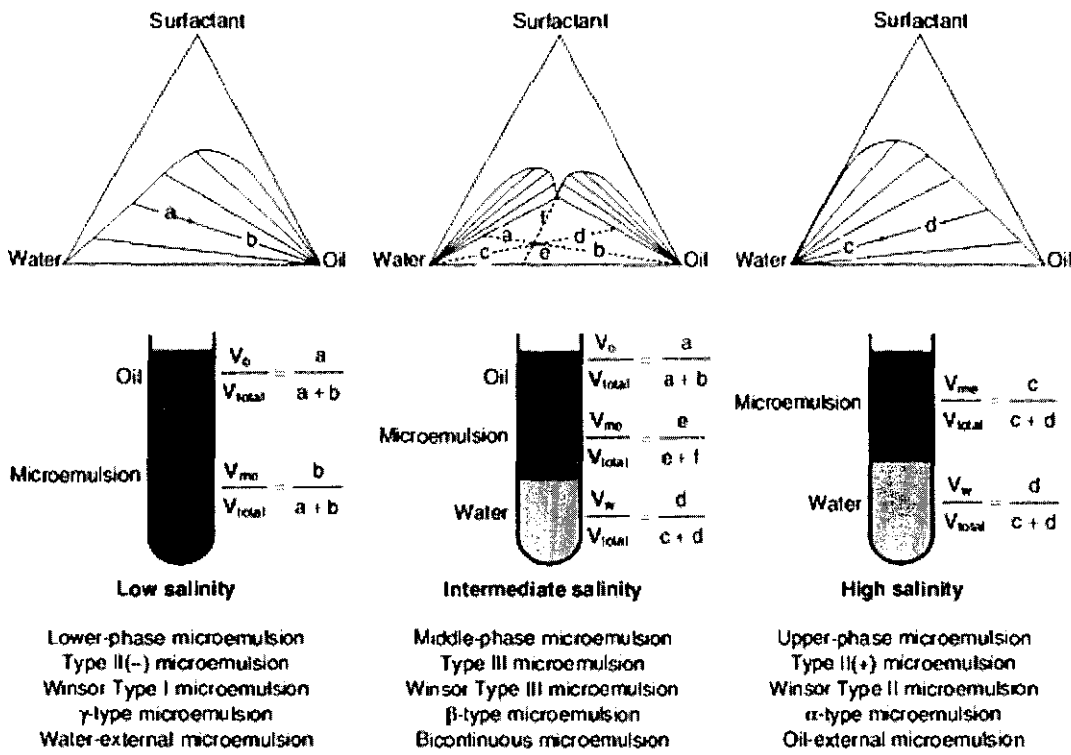

Figure 2.15: Phase behavior and types of microemulsions relating to a varying amount of salinity [72]

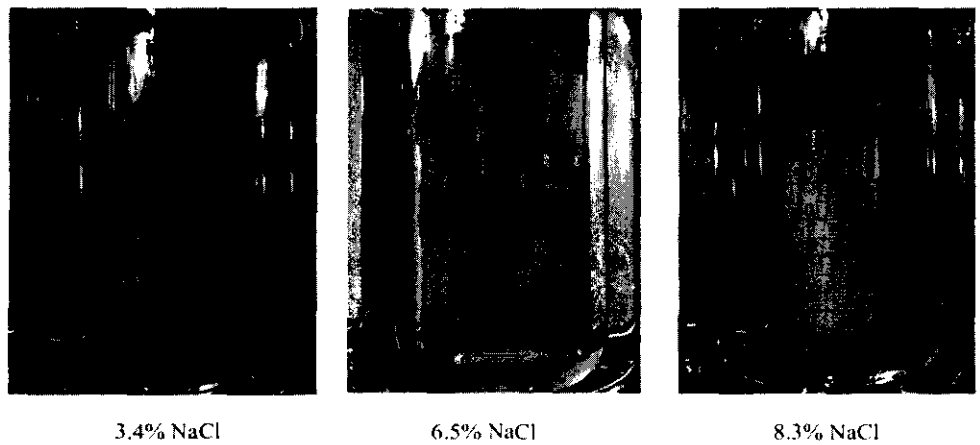

Figure 2.16: Effect of salinity on the microemulsion phase behavior [26]

Because of the ultra-low interfacial tension between the microemulsion type III and crude oil, and also with the aqueous phase, this type of microemulsion is of great interest in the EOR process. Figures 2.15 and 2.16 show typical examples of how the microemulsion type changes with salinity.

2.8.1 IFT and the Solubilization Ratio of Oil and Brine

The relative amounts of oil and water solubilized with each other (to form a middle phase microemulsion) are correlated with the IFT between the oil and the water. If the IFT is low, more oil and water will be solubilized and a bigger middle phase of the microemulsion will be formed. The solubilization ratio for oil (water) is defined as the ratio of the solubilized oil (water) volume to the surfactant volume in the microemulsion phase [72]. These ratios are also called solubilization parameters (SPs) and can be calculated as follows:

$$SP_{oil} = \frac{V_o}{V_s} = \frac{Volume \text{ of oil in microemulsion phase}}{Volume \text{ of surfactant in microemulsion phase}} \tag{2.15}$$

$$SP_{water} = \frac{V_w}{V_s} = \frac{Volume \text{ of water in microemulsion phase}}{Volume \text{ of surfactant in microemulsion phase}} \tag{2.16}$$

As the solubility of the oil in the water is decreased with an increase in the salinity, the solubilization parameter for the oil, $SP_{oil} = \frac{V_o}{V_s}$, increases, while the solubilization parameter for the water, $SP_{water} = \frac{V_w}{V_s}$, decreases as the salinity increases (Figure 2.17 b).

At the optimum salinity for both, the SP_{oil} and SP_{water} are equal and the minimum value of IFT is observed. This relationship is shown in Figure 2.17 (a). The γ_{mo} is the microemulsion-oil IFT and γ_{mw} is the IFT between the microemulsion and the water. Healy in 1976 first developed an empirical correlation between the phase behavior and IFT [71, 73]. Later on, Huh also reported a model for the determination of IFT

from solubilization parameters. He proposed [74] an empirical relationship between the solubilization ratio and IFT as shown in Equation 2.17:

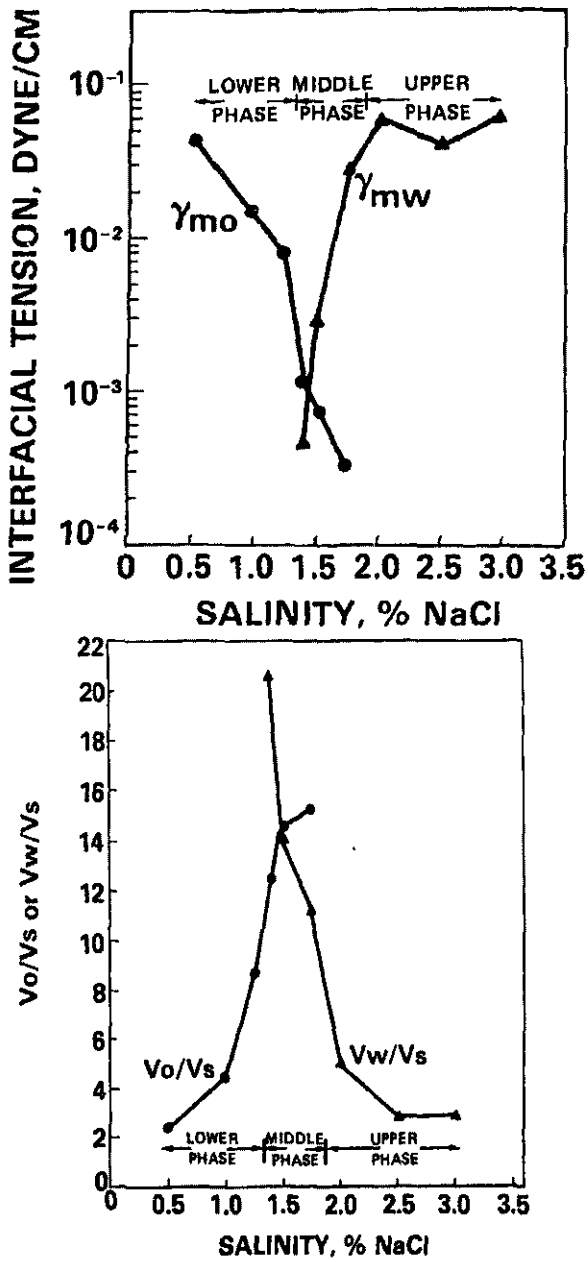

Figure 2.17: IFT and solubilization parameter versus salinity [73]

$$\sigma = \frac{C}{(V_i / V_s)^2} \tag{2.17}$$

where σ is the interfacial tension, V_i is the water or oil solubilised in the microemulsion and V_s is the volume of the surfactant. The constant C has been assigned a value of 0.3 which is a good approximation for most crude oils and microemulsions.

Glinsmann experimentally validated this relationship [75]. From the Huh Equation, it can be calculated that a solubilization ratio of > 10 is required for an IFT of ~10^{-3} mN / m. It is common to have solubilization ratios in the range of 15-25 with good surfactant solutions [76]. This correlation for the assessment of IFT is important as the IFT measurement by using instrumental techniques is time consuming and more difficult than the phase behavior observations. Sometimes it is almost impossible to measure the IFT between some crude oil and its lower phase microemulsion. Due to these reasons, it is believed that by using the phase behavior observation and the measurements of the solubilization ratios, it is much simpler and faster to estimate the IFT of the oil/water/microemulsion system, especially for surfactant screening [77, 78]. However, it is always beneficial to measure the IFT by using instrumental techniques after a good formulation has identified by the phase behavior study.

2.8.2 Static and Dynamic Adsorption

Anionic surfactant molecules are negatively charged in an aqueous solution. If the solid interface is positively charged, severe adsorption can occur. The adsorption is highly undesirable due to the resultant loss of availability of the surfactant for its intended functions such as the lowering of IFT or foam generation [17]. The static adsorption test is carried out on a crushed core which has a very high surface area as compared to a consolidated core, and hence represents the worst case scenario due to very high adsorption [79]. For measurement of static adsorption, a solution of a known concentration of the surfactant is stirred well with the solid crushed core sample at the required temperature and pH, and kept in an oven for several days at the required temperature. After a specific time interval, the sample from the aqueous phase is drawn and analyzed for the available amount of surfactant by using a suitable analytical technique such as titration, chromatography, RI or UV-Visible spectrophotometry. Surface tension measurements of the aqueous solution before and after the adsorption test can also be used [80].The adsorption is calculated by noting the difference in the surfactant concentration before and after the contact with the core sample. It is generally presented in mg / g (mg surfactant per gram of rock sample). The dynamic adsorption test is performed by using the core flood system. The surfactant solution is passed through the core sample underspecified conditions. The

core is saturated with formation brine first, and then the aqueous solution of the surfactant containing a non-absorbing tracer such as NaCl or KCl is passed through the core by using an injection pump. The concentration of the surfactant, after it comes out of the core, is estimated by using any suitable method and is corrected with the help of the tracer concentration difference [81]. In another technique, the increasing amounts of surfactant slugs are passed through the core until the exiting concentration of the surfactant becomes equal to the injecting surfactant concentration. After this step, the surfactant is removed from the core by using a solvent such as ethanol, methanol or chloroform. The amount of the surfactant removed from the core is estimated by using any standard technique as presented above.

2.8.3 Trapped Oil Mobilization and Recovery

As the trapped oil is held in place due to capillary forces and the high IFT between the oil and the water, the surfactant drive is used to recover the oil. The surfactant slug and alkali generate a microemulsion during their first contact with oil. The microemulsion has a very low IFT with both oil and water, and hence can effectively mobilize the contacted oil to oil bank. The chasing slug is usually a polymer solution having a relatively high viscosity than brine. This high viscosity improves the macroscopic sweep efficiency and pushes the oil bank forward towards the production well.

2.9 Structure-Performance Relationship of Surfactants

The performance of a surfactant molecule in terms of lowering the IFT between the oil and the water is a function of its molecular structure. Both the head and tail groups in a surfactant molecule have a large influence on their performance in solutions. In the following sections a brief account of the structure-performance relationship is provided.

2.9.1 Head Groups

Anionic surfactants are the most common candidates for EOR applications. Among these, the sulfonates and sulfates are mostly used [82]. Cationic surfactants are not employed on sandstone reservoirs due to severe adsorption on negatively charged rock surfaces. The non-ionic surfactants suffer from chromatographic separation and selective adsorption on the reservoir rock [83, 84]. However, they are being employed together with the anionic surfactants for better salt tolerance and their ability to lower the viscosity of the microemulsion [85].

In the anionic surfactants, sulfonates are given special importance due to their thermal stability at elevated temperatures (~130 °C) [39]. Petroleum sulfonates are good surfactants for EOR applications but their limited solubility in hard water requires blending with ethoxylated sulfonates in varying proportions [86]. The latter are better towards hard water (salinity) tolerance [37]. Traditionally, the surfactants containing the sulfates as heads are considered not very stable at high temperatures and low pH conditions due to the hydrolytic problems of the sulfate groups at temperatures exceeding 60 °C [87]. However, at lower temperature conditions, the sulfates can be used to substitute the sulfonate. Moreover, sulfates are found to be more tolerant to the divalent cations compared to the sulfonate surfactants [14]. Recently, the high temperature tolerance of sulfate groups has also been revised and reported by Adkins *et al.* [88], and it has been proposed that the sulfate group in the alkyl ether sulfates is tolerant to high temperatures (85 °C and 100 °C) and has an improved endurance from 1.6 years to several years provided that the pH of the solution is in the range of 10-11.

2.9.2 Tail Groups

The surfactants tail is the hydrophobic part of the molecule and is mostly composed of long hydrocarbon chains. It is a well-established fact that the oil solubilization ratio increases if the hydrocarbon chain length or bulk increases. This also enhances the hydrophobic nature of the overall structure, which results in a low solubility in water and leads to a low salt tolerance [89, 90]. These relationships are shown in Figure

2.18. It can be observed that the solubilization parameter is very high with IOS 20-24 (20-24 -CH_2 groups) as compared to IOS 15-18 (15-18 -CH_2 groups). However, the salt tolerance (optimal salinity) is reversed, the short chain IOS is more stable in high salinity environment as compared to its long chain counterparts [25].

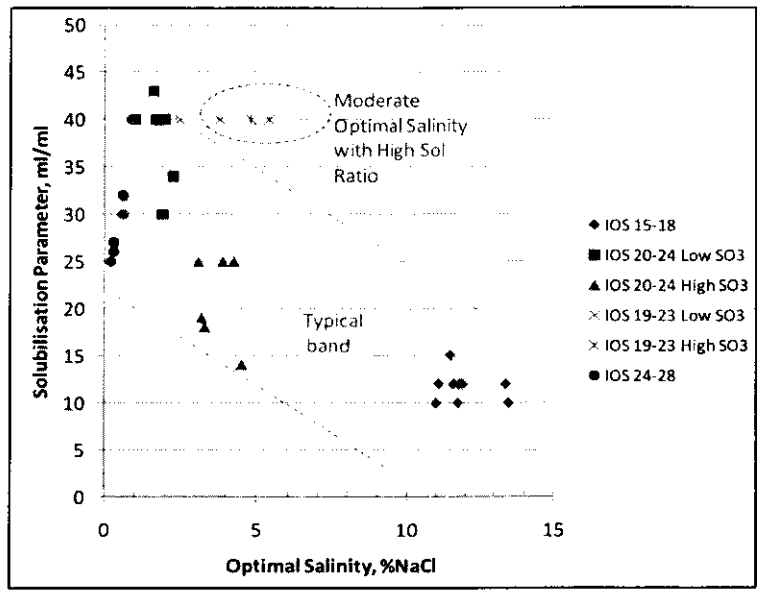

Figure 2.18: Relationship between optimal salinity and solubilization parameter as a function of chain length in IOS surfactants [25]

Therefore, the required bulk of the chains and length depends on the applications for which the surfactants are designed and a balance known as HLB is desired for the required properties of the solubilization of the oil versus water solubility and salinity tolerance of the surfactant [24]. Straight chain surfactants such as alpha olefin sulfonates and sulfates are common surfactants with single chains of $-CH_2-$ groups of varying chain lengths [91]. As discussed above, an increase in chain length renders the surfactant less tolerant towards salinity. Another problem associated with the single, long chain surfactants is their formation into high viscosity microemulsions, ordered arrays and layered structures which can cause problems in mobilization [39]. To overcome these problems branching in the tail is introduced which can resist the formation of these organized structures which lead to gels and liquid crystals [26]. In addition, branching also helps in lowering the viscosity of the microemulsion phase due to the aforementioned reason [92].

2.9.3 Linking Groups in Surfactants

Recently, there have been studies considering the possibility of EOR slugs that are deprived of alcohols as co-surfactants / solvents [37]. In this context, many surfactant structures containing polyethylene and polypropylene glycol groups (PEG and PPG, respectively) between the head and tail are emerging and being extensively tested [86]. As these PEG and PPG are water soluble, these groups are expected to further enhance the water soluble nature of the head groups. It is considered that these groups can produce a less viscous microemulsion without having a co-solvent [93]. Moreover, surfactants containing these groups are more salinity tolerant and are soluble in high concentrations of total dissolved solids (TDS) [17]. It has also been reported that these groups, when present between the head and tail, lower the optimum salinity and increases the calcium tolerance [94].

2.9.4 Hydrophile-Lipophile Balance (HLB)

The HLB concept given by Griffin [95] as a tool for the characterization of surfactants has been discussed widely in literature [96, 97]. This approach defines the ability of a surfactant to make water in oil (W/O) or oil in water (O/W) emulsions. A high HLB means the surfactant is more soluble in water and consequently will generate O/W emulsions. On the other hand, surfactants having a low HLB will be more soluble in oil and will preferably make W/O emulsions. Due to the relative solubility in oil or water phase, the salinity of the system has a marked effect on the emulsification process. Therefore, for a high salinity environment, a high HLB surfactant will perform better and vice versa because a high HLB surfactant is more soluble in water and its solubility performance will be less affected by the presence of salinity.

Griffin's method of HLB determination involves the incorporation of the molecular weight of the hydrophile and lipophile portions of the surfactant, by the following relationship as shown in Equation (2.18):

$$\mathrm{HLB} = \frac{20 MW_{H}}{MW} \tag{2.18}$$

Where MW_H is the molecular weight of the hydrophilic moiety and MW is the total

molecular weight of the surfactant. An arbitrary scale of 0-20 has been defined for these values, a value of 0 defines the completely hydrophobic compound and a value of 20 refers to a completely hydrophilic compound. The following guidelines have been given relating the properties and the HLB of surfactants (Table 2.1) [2].

Table 2.1: Classification of surfactants according to their HLB values

HLB value	Surfactant
0-3	Antifoaming agent
4-7	W/O emulsifier
7-9	Wetting agent
8-18	O/W emulsifier
13-15	Detergent
10-18	Hydrophobe

As the HLB concept has not been clearly defined on a quantitative basis [97], a notable contribution to this concept was given by Davies [98] in 1957. The strong point of his theory was to assign different values to the different chemical groups according to their emulsification strength. The relation given by Davies is shown in Equation 2.19:

$$\mathrm{HLB} = \sum(\text{hydrophilic group numbers}) - n(\text{group number per } CH_2 \text{ group}) + 7 \quad (2.19)$$

The values for the different groups demonstrated by this model, match closely to the experimentally achieved values. This approach, however, is not suitable for very high molecular weight groups and an upper value of 20 is the limit. Moreover, ethylene oxide has been given the hydrophilic nature while propylene oxide has been defined as having the hydrophobic nature. Some represented values of the groups are shown in Table 2.2.

2.9.5 The R-ratio

As the surfactants possess interactions with both oil and water, Winsor [99] provided the R-ratio as a quantitative approach to demonstrate the mutual interactions of a

surfactant, oil and water system. In a system containing oil, water and surfactants, the interfacial layer contains hydrophobic tails (L), hydrophobic heads (H), oil and water. If the interaction of the surfactant molecules is strong with oil, the surfactants will be soluble in oil. This interaction (A_{CO}) will comprise the interaction of the oil with the surfactant heads (A_{HCO}) and the surfactant tails (A_{LCO}). So, A_{CO} can be defined as:

$$A_{CO} = A_{LCO} + A_{HCO} \tag{2.20}$$

Likewise, if the surfactant has more interaction with water, it will solubilize in water easily and the interaction A_{CW} will be defined as:

$$A_{CW} = A_{LCW} + A_{HCW} \tag{2.21}$$

Table 2.2: HLB group numbers [98]

Hydrophilic groups	Group number
$-SO_4.Na^+$	38.7
$-COO.K^+$	21.1
$-COO.Na^+$	19.1
N(tertiary amine)	9.4
Ester (free)	2.4
-COOH	2.1
Hydroxy group (free)	1.9
-O-	1.3
Lipophilic groups	
-CH-	
$-CH_2-$	
CH_3-	-0.475
=CH-	
Derived groups	
$-(CH_2-CH_2-O)-$	+0.33
$-(CH_2-CH_2-CH_2-O)-$	-0.15

As the lipophilic tails are oriented in oil only, A_{HCO} can be neglected in Equation 2.20. Likewise, hydrophilic heads are only present in the water phase; therefore, A_{LCW} can be neglected in Equation 2.21. The overall surfactant affinity to oil or water can be defined as in Equation 2.22:

$$R = \frac{A_{CO}}{A_{CW}} \tag{2.22}$$

Equation 2.22 does not take into account any repulsive interaction among the surfactant heads, surfactant tails, water molecules and oil molecules.

To show a more realistic approach, Bourrel and Schechter [100] redefined R by considering repulsions between the oil molecules (A_{oo}), between the water molecules (A_{ww}), between the tails (A_{ll}) and between the surfactant heads (A_{hh}) as shown in Equation 2.23:

$$R = \frac{A_{CO} - A_{oo} - A_{ll}}{A_{CW} - A_{ww} - A_{hh}} \tag{2.23}$$

According to Equation 2.23, if R<1, the relative miscibility of a surfactant with water will be increased or with oil will be decreased. Consequently, if R>1, the relative miscibility with oil is increased and with water will be decreased. In cases where R<<1, the emulsion type will be Winsor type I, i.e., O/W emulsion. For the R>>1, the emulsion will be of type II (W/O). For the value R=1, the Winsor type III emulsion will be formed.

2.9.6 The Packing Factor

Wang *et al.* [101] presented their approach explaining various types of emulsions formed by defining the dependence on the size of the head and the tail in surfactants. They defined a property of emulsions called the Packing parameter as given in Equation 2.24:

$$\Phi = \frac{V}{a_o L_c} \tag{2.24}$$

Where V is the volume occupied by the tail (hydrophobic group) in the micellar core, a_o is the cross-sectional area occupied by the head in the micellar zone and L_c is the

length of the tail in a surfactant molecule. These characteristics are defined in Figure 2.19.

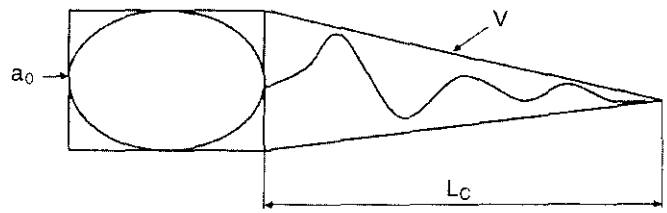

Figure 2.19: The parameters defined for the packing factor, adopted from Sheng J.[2]

The packing factors and the type of emulsion are shown in Table 2.3.

Table 2.3: Packing factors for aggregate structures [2]

Packing parameter	Micelles and emulsions
<0.33	Spherical, ellipsoidal micelles
0.33 – 0.5	Rod-like micelles
0.5 – 1.0	Vesicles, bilayers
1.0	Planner bilayers (minimum IFT)
>1.0	Reverse micelles (small head and large tail)

Figure 2.20 further explains the packing of the surfactant in a micelle. The surfactant structure must meet the size criteria to be fitted in the spherical micellar shape.

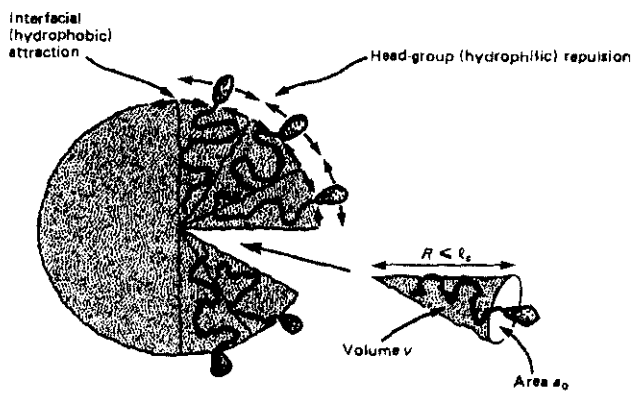

Figure 2.20: Packing of the surfactant in a micelle, explanation of the packing parameters [102]

2.10 Synthesis of Surfactants

Surfactants have two structural components: head and tail. The head, as discussed earlier in section 2.10.1 is mostly anionic in nature. An anionic head may be sulfate or sulfonate, the latter is considered as being more important due to its relatively higher thermal stability than that of the former. Both sulfate and sulfonate are industrially prepared from the reaction of SO_3 with the alkyl chain. The tail can be derived from petroleum fractions or from natural oil derivatives. Petroleum based products have been extensively used in the past decades. As petroleum is the major energy source, its usage as a precursor of chemicals has been discouraged [103]. In addition, the petroleum based products are considered as a direct threat to the environment due to their toxic nature and non-biodegradability [104] . In this context, it is essential that the long chain hydrocarbon be obtained from sources such as natural oils which are environmentally friendly and renewable [105, 106].

Natural oils are important commodities due to their major usage as food. Products obtained from natural oils have been given prime importance in recent years due to the depletion of petroleum reservoirs and environmentally related problems posed by petroleum derived products [107]. The plant oils are eminent due to their usage in food and technical applications which are not restricted to soaps only but are expanded to value added products such as polymers, resins, biodiesel, cutting oils, high-tech surfactants, lubricating oils and nano-composites to count a few [7, 108-110]. Therefore, natural oils are being studied extensively for their possible usage as the precursor of chemicals [111-113] and surfactants [114-116]. Although many surfactant types can be produced from natural oils, our focus will be on methyl ester sulfonates and sulfates, which are presented in a detailed manner in the following sections.

2.10.1 Synthesis of Methyl Ester Sulfonates from Natural Oils

Methyl Ester Sulfonates (MES) or α-sulfonated methyl esters are synthesized from natural oils. The general structure is given in Figure 2.21.

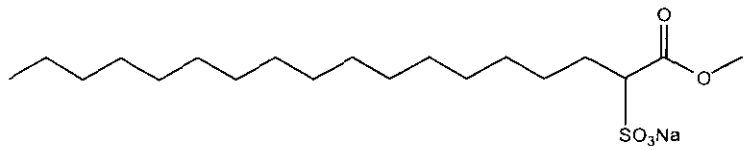

Figure 2.21: General structure of methyl ester sulfonate

MES was known in the early 1950's but was not given any importance due to the unavailability of the appropriate process for its synthesis on a commercial scale. The generally proposed route involves the sulfonation of fatty acids and subsequent esterification with methanol. The process gained importance in the late 50's to early 60's and several other synthetic routes and strategies were proposed in the literature during the 1960's [117-119]. The main difficulty in the preparation using methyl esters was the relatively less active α-hydrogen in the methyl esters in comparison to that in the fatty acids [120]. Therefore, a more vigorous and strong sulfonation agent was required. The availability of SO_3 for the industrial process in the 1960's solved the problem of the industrial manufacturing process. Liquefied SO_3 and chlorosulfonic acid were employed for lab scale synthesis of MES and were not used for industrial setups due to the highly aggressive nature of the reactants and the reaction control challenges [121].

2.11 Synthesis Route

Methyl ester sulfonates are synthesised by the sulfonation of fatty acid methyl esters. These fatty acid methyl esters are derived from the natural oils by the reaction of methanol in the presence of a catalyst. Glycerine is produced as a by-product [103]. Methyl esters sulfonates are obtained by the reaction of SO_3 gas with methyl esters. The detailed process is discussed in later sections.

2.11.1 Natural Oils

All natural oils are triglycerides of fatty acids. The composition of fatty acids varies according to the type of oil. Common fatty acids in natural oils include Palmitic acid (C16:0), Oleic acid (C18:1), Linoleic acid (C18:2) and Stearic acid (C18:0) [106].

2.11.2 *Jatropha* Oil

As the major use of natural oils is still for food, there has been a considerable search for oils which are inedible and are, therefore, not a direct threat to the food market when they are used in bulk for synthesis purposes. *Jatropha curcas* is one of those industrially significant oils which are consumed in huge amounts for technical purposes rather than food crops, due to its non-edible properties. It is inedible due to the presence of toxic substances and it has no competition with the food or feed markets [122]. In recent years, it has been extensively investigated for bio-diesel synthesis [123-131]. Its oil content is reasonably high, reported to be 40 to 50 % w/w [123]. The fatty acid composition of *Jatropha oil* is given in Table 2.4. Complete information of the oil profile is required for the design of the chemical reactions such as epoxidation, alkoxylation and sulfonation steps. A profile analysis is usually performed by using GC-MS, after the transesterification reaction as the oil sample should be converted into its methyl esters for GC-MS analysis. The AOCS official method Ce1–62 (09) is used for the composition of fatty acid methyl esters. For this analysis, a method employed by Smith [132] can also be used.

Due to its inedible nature, *Jatropha curcas* oil has attracted many researchers for its usage as a technical oil. From its composition containing over 75 % unsaturated fatty acids, it can successfully be used as the raw material for surfactants and other value-added products [103]. Unsaturated fatty acids have double bonds in the structure. These unsaturated sites, due to the π bonds, are easily used for the attachment of different groups. The iodine value (IV) is the direct measure of the unsaturation present in methyl esters and oils.

This quantity is required for designing the experiment for the epoxidation reaction. AOCS official method Cd1–25 (93) [133] is used for the determination of IV. A method based on ^{13}C and ^{1}H NMR is also available [134].

Table 2.4: Fatty acid Composition of *Jatropha oil*[a]

Fatty Acid	Content % (mass basis)
Palmitic acid (16:0)	16.6 ± 0.02
Palmitoleic acid (16:1)	1.1 ± 0.01
Stearic acid (18:0)	6.9 ± 0.03
Oleic acid (18:1)	40.2 ± 0.01
Linoleic acid (18:2)	35.2 ± 0.01

[a]Adopted from Rao [135]

2.12 Synthesis of Methyl Ester Sulfonates

Synthesis of MES from natural oils consists of three main steps:

(i) Transesterification, (ii) Modification of the backbone carbon chain, (epoxidation and subsequent alkoxylation) and (iii) Sulfonation [118]. Every major step in turn consists of several intermediate or smaller steps to complete the process.

2.12.1 Transesterification

Natural oils are triglycerides of different fatty acids. Replacement of glycerol with a different alcohol is called transesterification. Methanol (due to its low market price) is mostly used for transesterification to obtain methyl esters of fatty acids. The reaction is shown as in Figure 2.22. Although different types of catalysts such as acids, bases, enzymes and heterogeneous catalysts have been studied for transesterification reactions, the most effective and economical are found to be the acids and bases. The bases are most successful, and NaOH or KOH as methanolic solutions are employed in the concentration range of 0.4 -2 % w / w of oil [136]. Alkali alkoxides such as sodium methoxide are also extensively used. A basic catalyst is about 4000 times faster than the acidic catalyst and its conversion is usually >95 % [137]. Lipase based enzymes have also been used for the transesterification reaction but these are

expensive and difficult to apply at the industrial level [138]. The oil must be dried before the transesterification reaction to avoid any soap formation. Karl Fischer's titration is used for the determination of moisture content according to the AOCS official method Ca2e–84 (09) [133]. Moisture content should be lower than 0.10 % for a successful transesterification reaction. The subsequent alkoxylation reaction requires the moisture content to be very low or absent altogether.

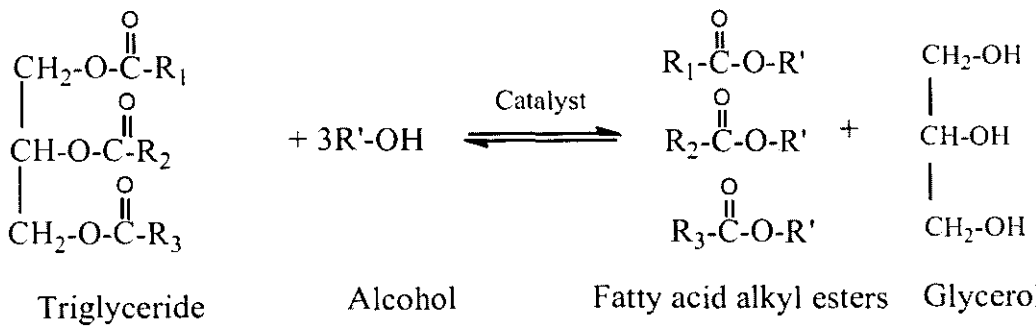

Figure 2.22: Schematic of the transesterification process [138]

The transesterification reaction, therefore, is almost always catalyzed by basic catalysts such as NaOH, KOH or sodium / potassium methoxide. Completion of this reaction is very important and there should not be any mono, di or tri-glycerides present in the product. In addition, there must not be any free glycerol present. This analysis is performed by using GC-FID according to ASTM D6584-00. A relatively straight forward analysis can be performed by taking the ^{1}H NMR spectra and looking for glyceride peaks at 4.09-4.34 ppm [139].

2.12.1.1 Transesterification Reaction and a High FFA Value

Despite the base catalysts being more efficient and effective in transesterification, they are nevertheless not used if the free fatty acid (FFA) value of oil is more than 1 % [129]. The FFA (Free Fatty Acid) content should be kept low for a successful transesterification reaction. The FFA content must be lower than 1 % for the success of a base catalyzed transesterification. If it is more than 1 %, both acid and base catalyzed transesterification reaction steps are required [8, 9].

The FFA content is determined by using the AOCS Official Method Ca5a–40 (09) [133, 140]. This method requires a sample of the oil dissolved in neutralized isopropanol and titrated against the standard 0.1M NaOH to the phenolphthalein end point. With a high value of FFA, the conventional base catalysed transesterification reaction provides a low yield due to the undesired side reaction of generating soaps. As these soaps are surfactants in nature, therefore, washing with water leads to strong emulsified products which pose difficulties in the separation of the product from the bulk reactants. Due to this difficulty, a good cleaner product with a high yield is scarcely obtained. Owing to this reason, it is generally suggested that the FFA value of the feedstock should be less than 0.5-1.0 % for the base catalysed transesterification reaction [141, 142]. The effect of a high FFA value on methyl esters conversion was also discussed by Naik *et al.* [143]. The findings are depicted in Figure 2.23. It can be observed that a high FFA value drastically reduces the methyl esters production and the conversion becomes less than 10 % when the FFA value is higher than 5 %. As pointed out earlier, cheap feedstock generally have very high FFA values, sometimes reaching up to 30 % [144], therefore, a two-step approach is mostly used for the esterification of oil. In the first, the FFA value is reduced to less than 1 % by using an acid catalyst and in the second step, the base catalysed transesterification is launched [145]. As methanol is not very reactive with fatty acids at normal process conditions, generally acid catalysts are employed for the esterification reaction.

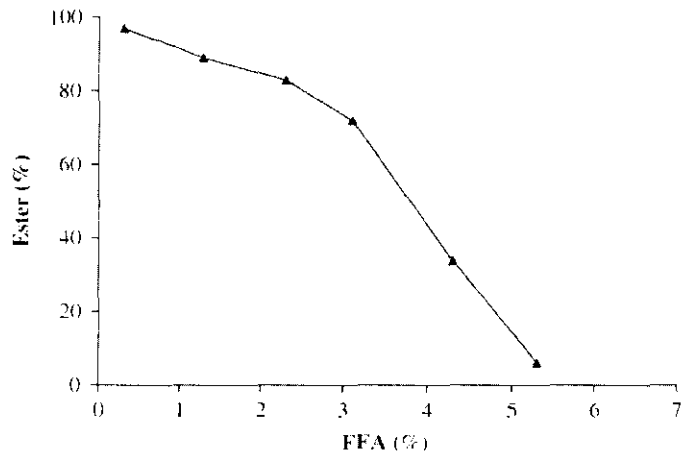

Figure 2.23: Effect of the FFA value on the yield of esters (%) [143]

For the catalysis of the esterification reaction, Bronsted acids such as sulfuric acid, hydrochloric acid and phosphoric acid and Lewis acids such as BF_3 and $TiCl_4$ are usually employed. However, sulfuric acid is the most commonly used catalyst. Despite its good conversion, its use is not without problems. A common hurdle is its native acidic nature which severely hampers its ease of application. A low efficiency at lower temperatures and darkening of the color of the product at higher temperatures are common impairments of sulfuric acid usage. In addition, the removal of liquid catalysts from a bulk product requires several washing steps [146]. To overcome these challenges, enzymes [147] and supercritical methanol [148] have also been attempted but the longer reaction times for the former and the high pressure involved in the latter make them unattractive. Several heterogeneous catalysts have been proposed for oils containing high FFA values. Hen *et al.* (2007) [149] reported the synthesis of a series of mesoporous sulfated silica-zirconia catalysts and their catalytic activity in the esterification of palmitic acid and lauric acid with methanol. The maximum conversions for lauric acid and palmitic acid were found to be 87.4 and 89.2 % respectively after a 6h reaction time at 68 °C. Chung and co-workers [150] described the synthesis of zeolite based catalysts for FFA removal from waste cooking oil and a conversion of FFA up to 80 % at 60 °C was achieved. In their later study, [151] 10 % oleic acid in soybean oil was used to investigate the catalytic ability of zeolite based catalysts. About an 80 % conversion of oleic acid to methyl esters was reported. Kiss and co-workers [152] used a dodecanoic acid esterification reaction with methanol and other alcohols by using a sulfated zirconia catalyst. A reaction using a 1wt. % catalyst of alcohol: acid ratio of 3:1 at 140 °C gave 80 % conversion. Mbaraka et al. [153] reported the synthesis and application of organosulfonic acid – functionalized mesoporous silicas for the esterification of palmitic acid in soybean oil. The conversion of acid to methyl esters was about 82-85 % at 85 °C. A preparation and application of a solid acid catalyst from a glucose-starch mixture was also reported [154]. It was shown that the catalyst produced 90 % conversion to methyl esters after a 12h reaction time.

As BF_3 and sulfate group based catalysts are found to be effective in many esterification reactions, it is appropriate to consider new catalyst candidates for this reaction. In heterogeneous catalysts for organic synthesis, silica supported BF_3 has

been reported by Wilson and Clark [155]. It was reported that the catalyst had a very strong Lewis acid (BF_3) as well as some strong Bronsted acid sites. Another catalyst, silica sulfuric acid, [156] has also been used in several studies as a catalyst having strong Lewis acid – Bronsted acid sites. This catalyst has not been used widely for the esterification reaction catalysis and only one study [157] was reported, employing waste cooking oil with an FFA value of 3.57 %. The FFA was reduced to 1 % (90 % efficiency) at 60 °C with a 1.5 wt. % catalyst. A reaction time of 30 minutes was employed. This catalyst has not been tried to catalyse the esterification reaction of oil with a very high FFA value. It is expected to exhibit superior catalyst performance for FFA reduction.

2.12.2 Modifications in a Backbone Carbon Chain

Oleic and linoleic acids are the most abundant unsaturated fatty acids found in the *Jatropha curcas* oil. The double bonds present at positions 9 (oleic) and 9,12 (linoleic) acids are the most favorable sites to attach functional groups for structure alteration in the chain [132]. A simple route involves the epoxidation of the acid or ester and then attachment of the functional moiety by opening up the oxirane ring in the presence of a suitable catalyst [158]. In the following sections, these two chemical processes are discussed in detail.

2.12.2.1 Epoxidation

Epoxidation reaction in natural oils and alkyl esters has gained prominence in recent years due to its multifarious usage in many industrial synthetic processes. As natural products are being extensively used in recent years due to the depletion of petroleum reserves and environmental concerns [159], the epoxidation reaction is gaining more importance as a reaction route in natural oils, fatty acid methyl esters and related oleo chemical conversions [160]. Products such as polymers, resins, biodiesel, cutting oils, high-tech surfactants, lubricating oils and nano-composites benefit from the epoxidation reaction [161-163] .

A schematic of the epoxidation reaction is depicted in Fig.2.24. Peroxy acid is required as the oxygen carrier for this reaction and traditionally an organic acid such as acetic or formic is used with hydrogen peroxide to generate peroxy acid [164]. The peroxy acid can be employed as a separate reagent or can be synthesized in-situ, but the most common method involves an in-situ generation of peroxy acid. Nevertheless many heterogeneous catalysts and enzymes were also suggested and employed to augment the effects of organic acids and hydrogen peroxide to enhance the yield. It was also found that peroxy formic acid was more efficient than peroxy acetic acid [164, 165].

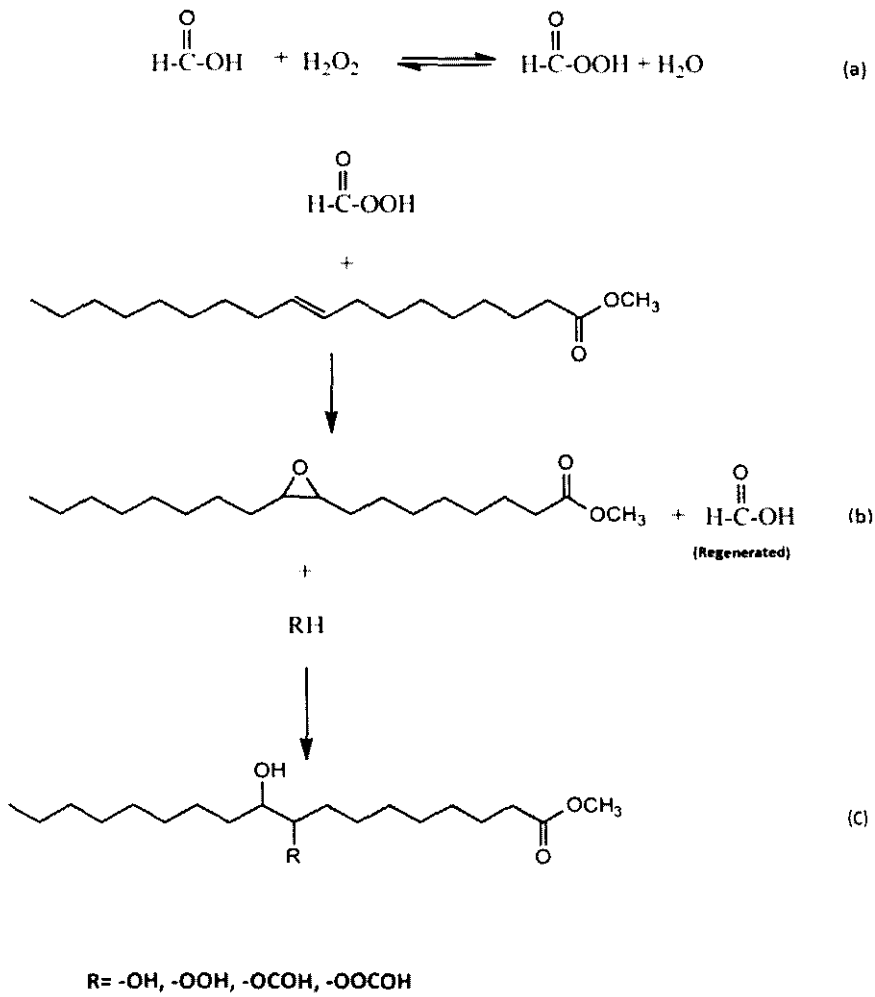

Figure 2.24: (a) *In-situ* generation of peroxy formic acid, (b) epoxidation of oleic acid methyl ester, (c) degradation of the oxirane ring [166, 167]

As shown in Figure 2.24, in the course of the epoxidation reaction, an epoxidized product can undergo a premature ring opening reaction which is highly undesirable. This ring opening reaction has been investigated extensively and various studies have been reported on the kinetics of the ring opening reaction [111, 168]. The ring opening reaction is associated with the presence of hydrogen peroxide and formic acid at elevated reaction temperatures [166]. To overcome this hindrance, some researchers have tried organic solvents such as benzene and toluene. For example, Goud *et al.* [165, 169] used organic acids and hydrogen peroxide with ion exchange resins for the epoxidation reaction in the presence and absence of toluene as a solvent. The solvent has been found to be beneficial in minimizing the ring opening reaction. However, it has been demonstrated by several researches, by conducting kinetic studies, that although the rate of the opening of the oxiranes can been reduced in the presence of a solvent, the conversion efficiency has been compromised [107].

Another reaction parameter, the reaction temperature, is also an important parameter in this reaction. Campanella *et al.* [167] studied the effect of high temperatures and it was shown that an increase in the temperature during the course of the reaction was found to be detrimental for the epoxidation reaction as the ring opening process was facilitated at higher temperatures. Therefore, a careful control of the amount of reactants and the reaction temperature is vital for achieving a high yield of epoxidation.

After the epoxidation reaction, a quantitative determination of the oxirane oxygen is required. The AOCS official method Cd 9–57 (09) is used for this determination [133]. NMR based methods are also available and are discussed elsewhere [170]. During the epoxidation process, the oxirane ring can be opened by a reaction with water (from 30 % H_2O_2) in the presence of the formic acid being used as catalyst. To prevent this reaction, temperature control is vital [107, 108]. However, this unavoidable reaction usually takes place and to quantitatively determine the amount of hydroxy groups, the Hydroxyl Value is determined by using the AOCS official method Tx1a–66 (09) and Cd4–40 (99) [133].

2.12.2.2 Alkoxylation

The alteration in the main carbon backbone of fatty esters and acids by attaching different moieties such as alkyl chain, alkyl ester, fatty acid or alkyl ether has been studied by many researchers [171]. A schematic of the alkoxylation reaction is presented in Figure 2.25. Historically, Swern *et al.* in 1948 [172] discussed the synthesis of hydroxy ethers from epoxy stearic acid using several alcohols. A large excess of alcohols was mixed with the epoxy stearate and the mixture was cooled down to 30 °C. Catalytic amounts of sulfuric acid were used drop by drop while shaking the mixture by hand. Then the mixture was heated on a steam bath for 2 hours and the products were separated by vacuum distillation after neutralization of catalyst by an equivalent amount of sodium bicarbonate. The products were purified by re-crystallization in cold acetone. Depending upon the alcohol used, the reported yield was 40 – 85 %.

Moser *et al.* [173] synthesized the iso propyl oleate from oleic acid and isopropanol. Epoxidation of this ester was accomplished by employing performic acid generated in-situ at a 95 % yield. A series of α-hydroxy ethers were synthesized by employing ten different alcohols. As the catalyst, 10 mol % sulfuric acid was used at room temperature for rather long reaction times of 24 to 240 hours depending on the alcohol type.

After the completion of the reaction, the reactants were mixed in hexanes and treated with sodium bicarbonate to neutralize the sulfuric acid. After several washes, the products were dried and purified by vacuum distillation especially for those cases which employed an alcohol of more than a C_6 chain. ^{1}H NMR, ^{13}C NMR and FT-IR were employed for analysis.

In the extension of their work on the aforementioned research, Moser *et al.* synthesized several esters by employing different alcohols. The epoxidation and subsequent alkoxylation was achieved to afford both homogenous and heterogeneous head and ether groups. Sulfuric acid was used as the catalyst in a 10 mol % concentration at room temperature for 24 to 240 hours. A higher reaction temperature of 60°C was employed for the synthesis of the homogenous ether and ester groups and

it was observed that a temperature greater than 60 °C resulted in unwanted side reactions. The ^{1}H NMR, ^{13}C NMR and FT-IR were used for analysis [174, 175].

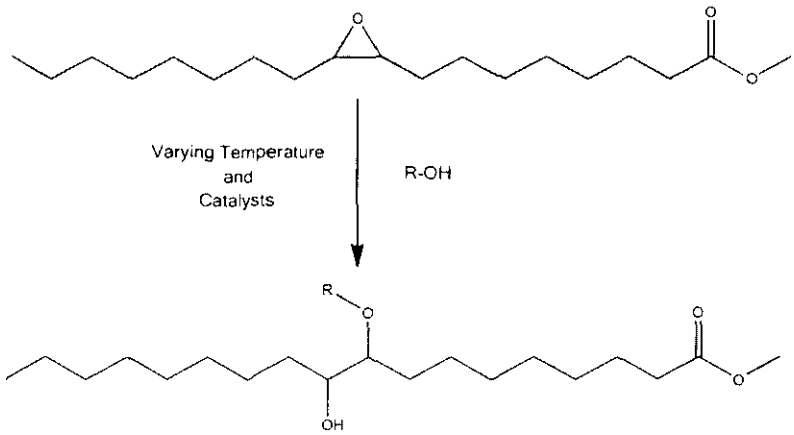

Figure 2.25: Schematic of the Alkoxylation reaction

In recent biodiesel investigations, Smith *et al.* [132] employed the transesterification of canola oil with methanol, ethanol and butanol. The epoxidation of unsaturated fatty esters was performed at 60 °C for 6 hours by employing per acetic acid or per formic acid generated in-situ. For the alkoxylation catalyst, 2.5 mole % sulfuric acid was employed while alcohols were used in a molar ratio of 14:1 with ester. The reaction temperature was 60 °C for 1 hour. The products were washed to remove residual alcohol and the catalyst, and then dried over sodium sulfate. GC –FID and GC-MS were employed for the analysis of the alkyl ester and alkoxy alkyl esters, respectively. Further research by the same group focused on the synthesis of butyl biodiesel and its butoxylation reaction [158]. In recent work, butyl biodiesel from canola oil was synthesized and epoxidized. Its alkoxylation with several alcohols ranging from methanol to *n*-octanol and 2-ethylhexanol was attempted. GC-MS was used for the analysis [171].

Instead of alcohols, polymers such as poly ethylene glycol (PEG) can also be attached on the backbone of methyl esters. However, the attachment of PEG to fatty acid backbones has not been widely studied. Only one study, reported by Hedman *et al.* (2003) [114] describes the attachment of different molecular weight polymers to tall fatty oil methyl esters. Three PEG, named PEG 350, PEG 550 and PEG 750 (numerals are the molecular weights) were attached on the backbone of the oleic acid

methyl ester. Epoxidation of the tall fatty ester was accomplished by using the Ishii-Venturello Catalyst and H_2O_2. The catalyst was prepared from tungstenic acid. GC and NMR were employed for the analysis of the epoxide. The attachment of PEG was achieved by the help of the BF_3 catalyst. A very good yield (98 %) was obtained. FT-IR and ^1H NMR were used to characterize the product.

2.12.3 Sulfonation and Sulfation

The sulfonation and sulfation reaction attaches the head to the alkyl moiety to form a surfactant. Sulfonation of fatty acid methyl esters has been studied extensively [118, 120, 121 and 176]. A schematic of the reaction is shown in Figure 2.26. The traditional route for the synthesis of MES involves the sulfonation of fatty acids, and subsequently the esterification of the sulfonated fatty acids to obtain α-sulfonated methyl esters. This route was laborious and was not very successful. Smith and Stirton [118] first described the sulfonation of alkyl palmitates and stearates by using a 2.4 molar ratio of liquid SO_3 as the sulfonating agent at 0 °C. The yield was reported as 70-80 %. Later on, a notable review from Stein and Baumann [120] described the comprehensive coverage of sulfonation methods and problems associated with the sulfonation reaction. They studied sulfonation by using different apparatus for different production levels of sulfonate generation, employing lab scale apparatus, a pilot plant and an industrial scale plant. For the lab scale studies, they employed a falling film reactor of a capacity of 600 g / hr, by using a mixture of SO_3-air in the volume ratio of 5 % SO_3 in air. For the pilot and industrial plants, a Chemithon Cascade apparatus was used, with a capacity of 45 kg / hr and 800 kg / hr, respectively. Bleaching and neutralization of sulfonates were also discussed in detail. They concluded that a temperature of 70-90 °C was optimum for the sulfonation process. At lower temperatures, the sulfonation was found to be incomplete and at higher temperatures, a dark colored product was obtained. It was also described that a large excess of SO_3 was required to accomplish more than 95 % sulfonation. A 30 mole % SO_3 was required for the lab scale falling film reactor and 10-20 mole % SO_3 was needed for the Chemithon plant. For the bleaching, it was reported that a 2 % H_2O_2 by weight of sulfonated fatty esters would be optimum. For the neutralization

process, it was emphasized that the temperature must not be in excess of 45 °C and the pH should remain between 7.5 and 9. The optimum concentration of NaOH should be chosen so that the resultant slurry of MES should be around 40 wt. %.

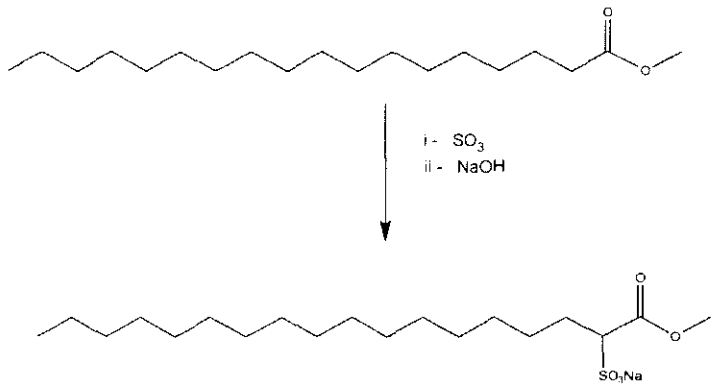

Figure 2.26: Schematic of sulfonation and the subsequent neutralization reaction

In another detailed study of the sulfonation of higher molecular weight FAMEs (up to a 20 carbon chain), Kapur *et al.* (1978) [121] described the sulfonation process for the lab and industrial setups. The findings included the percentage of SO_3 gas in air, its molar ratio to methyl ester, temperature, bleaching and neutralizations which were similar to the ones described by Stein and Baumann [120]. In addition to the experimental study, they also described the prevailing manufacturing techniques and explained different sulfonation processes including Ballestra's, Stepan, Allied and Chemithon processes.

Besides SO_3, chlorosulfonic acid has also been used for sulfonation purposes. Most importantly, alcohols were sulfonated to produce the respective sulfates. The typical reaction is shown in Figure 2.27. In sulfonates, the carbon atom of the alkyl group is directly bonded to the sulfur atom of the sulfonate (C-S linkage), while in sulfates, the oxygen atom is bonded with the sulfur atom (C-O-S linkage). Therefore, alcohols always form sulfates when reacted with the sulfonating agents and in this case, the sulfonation reaction can also be termed as a sulfation reaction. Sosis and Dringoli [177] reported the sulfation of C12-C16 linear fatty alcohols with the reaction of chlorosulfonic acid. The sulfation reaction was performed at a normal temperature, while chlorosulfonic acid was introduced under the surface of the alcohol solution. An air stream was used to remove the HCl gas produced during the

course of the reaction. A mole ratio of 0.95 (alcohol: acid) was used at temperatures between 25 to 30°C. The reaction was reported to be 95-96 % complete (unreacted alcohol ~ 4.1 – 4.3 %).

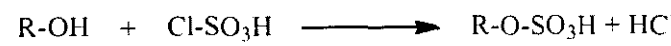

Figure 2.27: Sulfonation of alcohol with chlorosulfonic acid

The use of chlorosulfonic acid has also been discussed in detail by Cremlyn, RJ. [178]. It is described that the aliphatic carboxylic acid with at least six carbon atoms and their derivatives such as chlorides, anhydrides, nitriles or esters can be sulfonated by using chlorosulfonic acid, in an inert solvent such as CCl_4 or $CHCl_3$ at reflux temperatures [179].

2.12.3.1 Mechanism of Sulfonation

Several mechanisms of sulfonation were reviewed and discussed by Kapur *et al.* (1978) [121]. Smith and Stirton [118] discussed the case of long chain fatty esters and SO_3, describing that the reaction consisted of two steps, as shown in Figure 2.28. In the first step, a complex between sulfur trioxide and saturated fatty acid methyl ester is formed. This complex activates the α-hydrogen, which is then attacked by another molecule of SO_3. In the second step, the rearrangement of this intermediate occurs at an elevated temperature and the first molecule of SO_3 is lost prior to neutralization. The mechanism is shown in Figure 2.28.

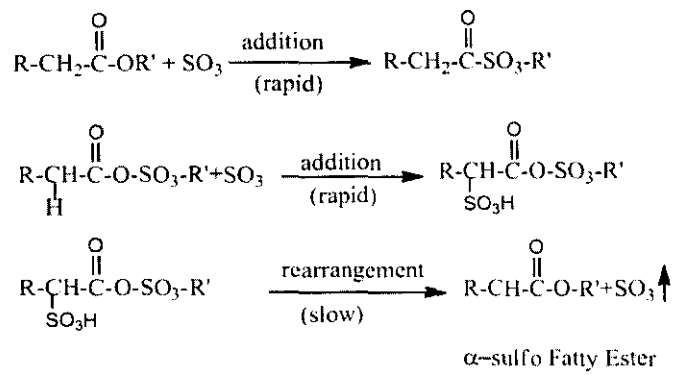

Figure 2.28: Mechanism of sulfonation according to Smith and Stirton [118]

Stein and Bauman [120] proposed a slightly different mechanism. According to them, in the first step, SO_3 reacts with the carbonyl oxygen in the fast reaction step forming an adduct. This attachment of SO_3 with carbonyl oxygen activates the α-hydrogen and the *same* SO_3 molecule attacks α-hydrogen in a rearrangement step, which is a relatively slower step, as shown in Figure 2.29.

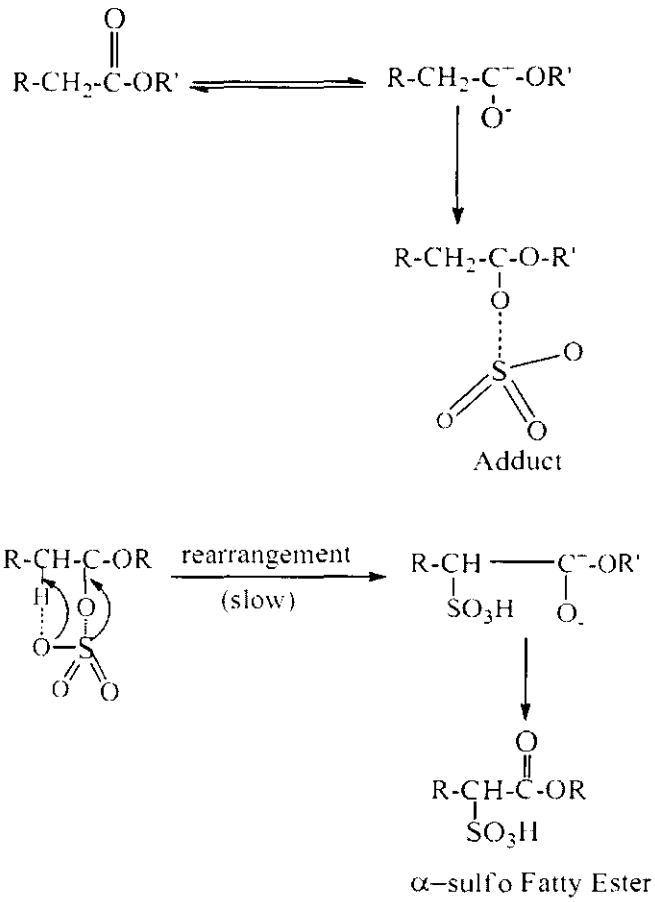

Figure 2.29: Mechanism of sulfonation according to Stein and Baumann [120]

Later Nagayama *et al.* (1978) of the Lion Corporation Japan [121] further refined and confirmed the mechanism by using the NMR technique. They concluded that in the first step, SO_3 reacts with carbonyl oxygen at a low temperature, which activates the α-hydrogen, and then the second molecule of SO_3 attaches at α- position to give an intermediate. Now, if the neutralization is performed immediately, a di-salt is formed, i.e., the ester group is broken and the sodium salt of the fatty acid is produced. If the neutralization reaction is delayed, the desired MES is formed. The mechanism is shown in Figure 2.30.

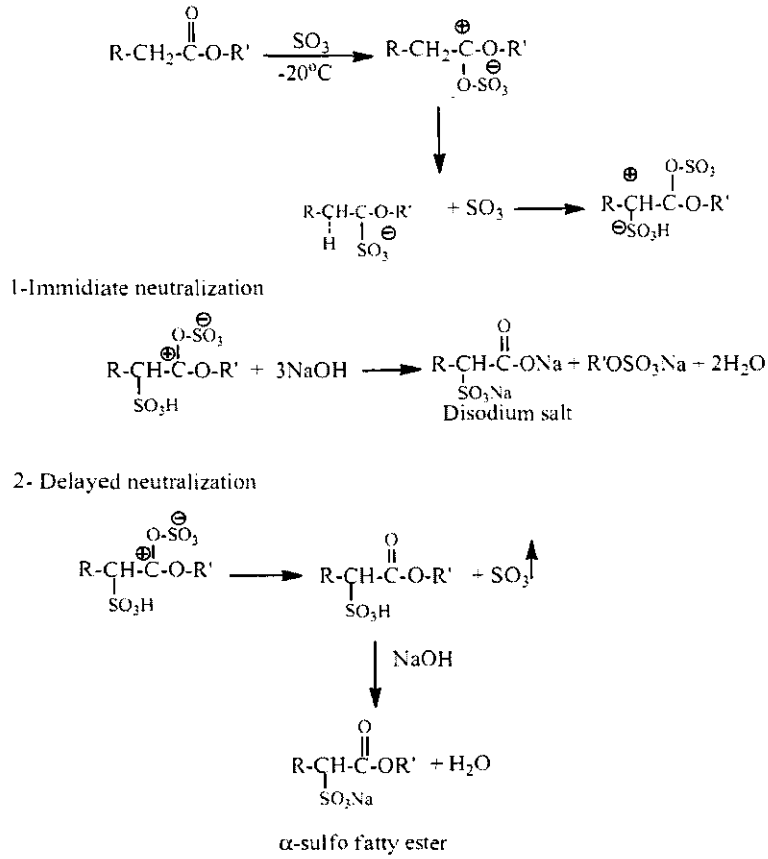

Figure 2.30: Mechanism of sulfonation according to Nagayama *et al.* [121]

Sulfation and sulfonation processes are not efficient up to 100 % and some unreacted material known as neutral oil as fatty acid or fatty ester is present in the product. It is determined by extraction of the ethanol/water solution at pH ~ 3 using petroleum ether. The extract is titrated against a standard alkali to determine the fatty acid content and the ester value can be determined by the difference [180].The sulfation and sulfonation processes are monitored by using the NMR and FT-IR techniques. Several aspects of the structural chemistry of the surfactants can be revealed by employing NMR as the analytical tool. Both proton (^{1}H NMR) and carbon-13 (^{13}C NMR) can be used to identify the availability / position of unsaturated sites, sulfate (-C-O-S) linkage, sulfonate (-C-S-O) linkage, fatty acid (C-OH), Ester (C-O-R), ether (-C-O-C), alcohol (-C-OH) and ester alcohol type [181].

Fourier Transform Infra-Red spectroscopy (FT-IR) is a powerful technique used for the identification of functional groups. It is helpful to identify several functional groups present in surfactants such as sulfonate, sulfate, fatty acid, ester, ether and

alcohol. In addition, it is sensitive towards moisture and can readily be used to detect the presence of moisture in a sample [181].

For the evaluation of active matter, the two phase titration method is widely used for MES surfactants. It was originally proposed by Holness and Stone [181] and has now become the standard test method, as presented by ASTM D3049-89 (2009) [182].

2.13 Design of Experiments

The statistical design of an experiment (DOE) is an efficient procedure for planning experiments so that the data obtained can be analyzed to yield valid and objective conclusions [183]. In a common experiment or process, many factors are involved which can affect the yield. Typically these factors are tested one by one, holding other factors constant. This approach is called the One-Factor-at-a-Time (OFAT). This approach becomes inefficient when different factors need to be tested simultaneously. Moreover, when a detailed study is required, the OFAT approach usually suggests a large number of experiments to be performed and yet the results remain incomplete and meaningless due to the inability of this approach to test more than one variable at the same time. To overcome these issues and problems, a statistical design of the experiments is used in industries, extensively. An experimental design has the following components which are divided into inputs and outputs to the process. The inputs and outputs for the process can be grouped according to factors, levels and response as follows:

2.13.1 Factors

Factors are inputs to the process. These are classified as controllable and uncontrollable variables. The controllable variables are parameters such as reaction temperature, reaction time, pressure, moles of ingredients etc. The uncontrollable factors are random statistical errors which can be controlled to some extent by randomization and blocking.

2.13.2 Levels

Levels are the settings for each factor. These include temperature, pressure and reaction duration settings. Most of the time, the levels are defined in a range, e.g., 30 – 300 °C temperature range etc.

2.13.3 Response

Response is the output of the experiment. The output may be conversion efficiency in percent, color, molecular weight etc. Response is dependent on the factors and the required response may obtained by manipulating the factor settings.

2.13.4 Process Models for DOE

For fitting the experimental data, the most common models take either a linear form or a quadratic form.

2.13.5 Linear Model

If two factors X_1 and X_2 are considered, the linear model can be written as in Equation 2.25:

$$Y = \beta_0 + \beta_1 X_1 + \beta_2 X_2 + \beta_{12} X_1 X_2 + E \qquad (2.25)$$

Where Y is the response (e.g., % conversion) for the given levels of the main factors X_1 and X_2. The term X_1X_2 represents the possible interaction effect between X_1 and X_2. The constant β_0 is the response of Y when both main effects for the factors are zero.

If the case of three factors, X_1, X_2 and X_3 are considered which is more complicated than a two factor case, Y can be calculated as:

$$Y = \beta_0 + \beta_1 X_1 + \beta_2 X_2 + \beta_3 X_3 + \beta_{12} X_1 X_2 + \beta_{13} X_1 X_3 + \beta_{23} X_2 X_3 + \beta_{123} X_1 X_2 X_3 + E \qquad (2.26)$$

Where E is the experimental error and the three terms with a single X (i.e., X_1, X_2 and X_3) are the main effects. In addition, there are 3 two-way interaction terms (i.e., X_1X_2, X_1X_3 and X_2X_3) and 1 three-way interaction term (i.e., $X_1X_2X_3$). This three way interaction term is usually omitted for simplicity and is negligible in most cases. All unknown β parameters are estimated after collecting and analyzing the experimental data and the coefficients of the "X" terms are tested to estimate which terms are significantly different from 0.

2.13.6 Quadratic Model

A quadratic model (second-order) does not include the three-way interaction term but adds three more terms to the linear model, as shown in Equation 2.27:

$$\beta_{11}X_1^2 + \beta_{22}X_2^2 + \beta_{33}X_3^2 \qquad (2.27)$$

The quadratic model is mostly and typically used in response surface experimental designs. Usually in a quadratic model, many interactions are possible but these are not included in the model due to the insignificant effects represented by them.

2.14 Process Optimization Study Using the Design of the Experiments

There is a growing interest in the statistical design of the experiments for chemical engineering processes. As discussed above, these experimental designs are performed based on the empirical relationships in terms of a mathematical model. These relationships may be between one or more measured output responses and a number of input variables [184]. As the traditional methods of optimization can only involve the changing of one independent variable while fixing the others at a certain level, these are not very efficient [185]. Due to time and cost constraints, the experiment design techniques were developed to allow for the maximum process information with the minimum number of experiments, hence saving both time and cost [186]. In the statistical design of experiments, Response Surface Methodology (RSM) is the

technique which is widely used for the process optimization purposes [187-189]. The details of RSM are discussed in the following sections.

2.14.1 Response Surface Methodology (RSM)

In the statistical design of experiments, the Response Surface Methodology (RSM) is a collection of statistical and mathematical tools. It was introduced by Box and Wilson in 1951 [190]. Since then, it has been widely used for the modeling and analysis of the situations in which the response of interest (i.e., the response) is affected by many process variables [191]. For example, production of a certain gas is directly dependent on the process pressure (p) and temperature (t). The different combinations of pressure and temperature for this process can affect the yield in different ways. Hence, yield (y) can be regarded as the function of pressure and temperature and can be expressed as in Equation 2.28:

$$y = f(p,t) + e \tag{2.28}$$

In Equation 2.28, e is the experimental error which can be due to measurement error or from random errors. The p and t can behave as independent variables with individual effects as well as interactive effects on y.

For the development of an approximation for response function f, linear or quadratic models are developed. If the response can be defined by a linear function of independent variables, then the function may be a first order model, as shown in Equation 2.25 for two independent variables. If there are interactions involved and the effect is not linear (a curvature is involved in the response surface), a higher order polynomial is used. For example, for two variables, a second order model can be applied, as presented in Equation 2.26. The experimental design is used to collect the data and after collection, the method of least squares is used to determine the parameters in the polynomials. The fitted surface is used to perform the response surface analysis.

As the response surface methodology (RSM) is being used in the optimization of industrial processes [192], it will, therefore, be used for the optimization of the epoxidation process for this work.

2.14.2 Response Surface Designs

Statistical approaches are commonly used in experimental designs to optimize and relate several parameters simultaneously. Generally, these approaches are full factorial, partial factorial and response surface designs. A full factorial design requires at least three levels of individual variables to provide the response model. This technique gives a high number of experiments to execute to get the optimization of the desired responses. The second technique, partial factorial design, gives fewer experiments than the full factorial design. Nevertheless, this technique is applicable in cases where some of the process variables are already known to show no effect [193]. The central composite rotatable design gives more information than the three factorial design, requires less experimental runs as compared to the full factorial design and has shown considerably good optimization to most of the steady state process [194].

2.14.3 Model Fitting and Statistical Analysis

In order to test the significance of the experimental data for a particular model, test for regression model, the individual model coefficients and lack of fit are performed in the analysis of the variance (ANOVA) [195]. The ANOVA provides statistical results that enable researchers to evaluate the suitability of the models [196].

In general, the significance of the model can be checked using factors that can be ranked based on the *F*-value or *P*-value (also known Prob. > *F*). The larger the magnitude of the *F*-value and correspondingly, the smaller the *P*-value, the more significant is the corresponding coefficient. The *P*-values are used as a tool to check the significance of each of the coefficients. For a confidence level of 95 % of the variability of the responses, the *P*-value should be less than 0.05. For lack of fit, the *F*-values higher than 0.05 show the insignificance which is desirable for a particular model to be fit.

Similarly, the approach of the significance and insignificance of individual variables and the interaction of two or more variables for a particular response can also be explained based on the *P*-values [197]. The interaction of two or more variables can also be explained by 2D or 3D graphs. The 2D graph is also known as contour [186].

The precision of the regression model is checked by the coefficient of the determination coefficient (R^2). However, R^2 increases as the number of variables increases, so Adj-R^2 is introduced as an additional variable in the model. The high values of these two coefficients show a good correlation among the independent variables [197].

2.14.4 Optimization of the Epoxidation Process by RSM

RSM has been applied in many process optimizations like biodiesel production, adsorption processes, synthesis of oleo chemicals and catalyst development [187]. However, there are scarce reports on the optimization of epoxidation of oils and alkyl esters [188, 189]. Therefore, a study which presents the application of RSM for the optimization of epoxidation reaction parameters of methyl esters along with their role and significance in the reaction would be justified. A 2^4 full-factorial Central Composite Rotatable Design (CCRD) for four independent variables (hydrogen peroxide / C=C mole ratio, formic acid / C=C mole ratio, reaction temperature and reaction time) can be used to investigate their effects on the yield of the epoxidized product. The optimization conditions obtained by the model can be applied to obtain the maximum yield of the product.

2.15 Evaluation of Surfactants for EOR Applications

Surfactants are evaluated for their suitability and performance for a particular application by different methods. A surfactant should be compatible with the reservoir fluids under reservoir conditions. In addition, it should be thermally stable and should be tolerant towards brine salinity and hardness. The performance of surfactants is usually evaluated by the phase behavior test which allows one to find out about the IFT of a surfactant solution against oil as well as the solubilization ratio, microemulsion viscosity and stability. The IFT of a surfactant and oil is also determined by the help of a spinning drop tensiometer. To confirm the surfactant performance in terms of oil recovery, coreflood tests are performed. In these tests, the surfactant solution is injected in the reservoir core sample under reservoir conditions

imitating the conditions of trapped oil in a real reservoir. The produced oil is measured and the pressure variability is studied to assess the suitability of the surfactant for an EOR application. In the following sections these evaluation procedures are described briefly.

2.15.1 Thermal Stability and Compatibility with Reservoir Fluids

This is one of the most important tests for the suitability of surfactants in a formulation. In a typical test, a relatively more concentrated aqueous solution of the surfactant is mixed with injection water / brine (IW), polymer and alkali in a sealed tube or pipette and subjected to the reservoir temperature conditions. The sample is observed for any cloudiness or precipitation over a specified period of time (Figure 2.31). A clear aqueous layer, without any cloudiness or turbidity passes the surfactants in this important test [26, 198].

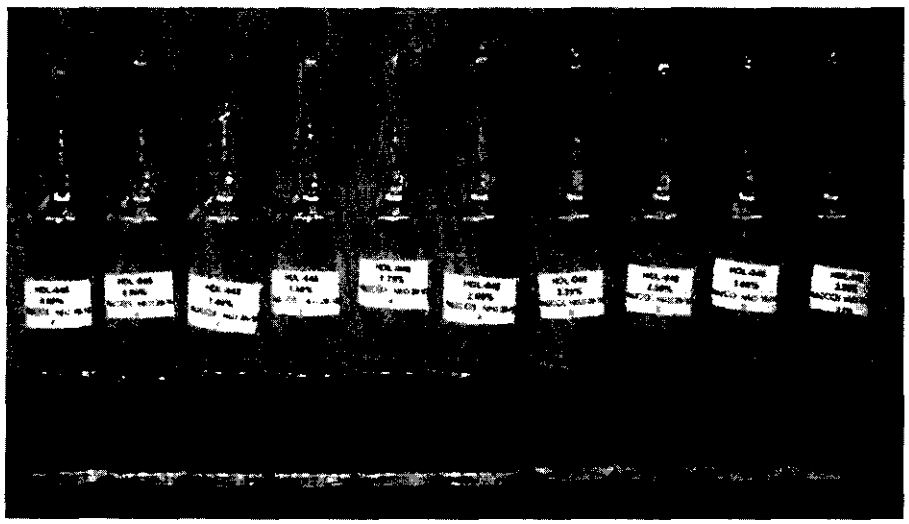

Figure 2.31 Aqueous stability test [2]

2.15.2 Phase Behavior Test

The phase behavior test is applied to evaluate the microemulsion generation and effects of salinity on the formed microemulsion. In a typical salinity scan an

increasing amount of salinity is added serially while the surfactant concentration and oil / water amount is fixed. A real salinity scan is shown in Figure 2.32. The equilibration temperature, equilibration time, requirement of co-surfactants and effects of alkali are also monitored [69, 199].

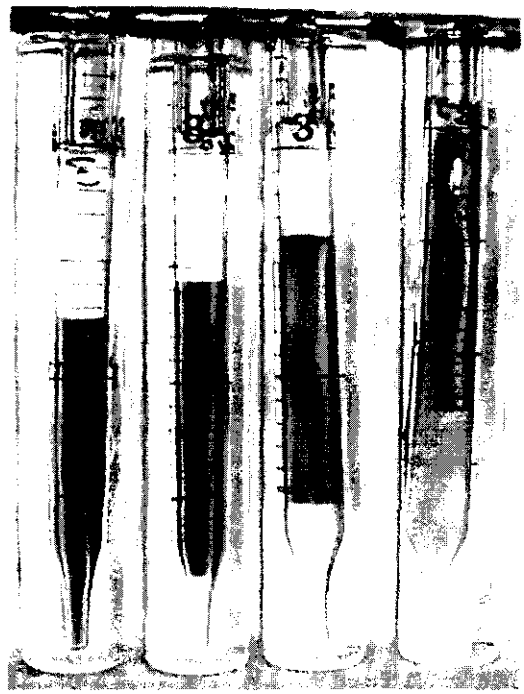

Figure 2.32: Typical phase behavior test results, salinity increases from left to right [77]

2.15.3 IFT Test with Spinning Drop Tensiometer

The spinning drop apparatus is frequently used to measure the IFT in an ultra-low range. As shown in Figure 2.33, two immiscible fluids, i.e., a surfactant solution and oil, are placed in a capillary tube, which can rotate at a specified speed. Fluid A is the less dense fluid (such as oil), while fluid B is the more dense fluid (such as brine or surfactant aqueous solution). The capillary is rotated at a specified rotational speed until the oil drop becomes elongated to a length almost four times its diameter, due to centrifugal forces. The configuration of the drop is determined by the balance of the centrifugal force and interfacial tension force.

The centrifugal force elongates the drop, while the IFT suppresses this elongation to minimize the interfacial area by forming a perfectly spherical drop. For a cylindrical drop whose length is at least four times greater than its radius, the following expression (Equation 2.29) is often used to calculate IFT:

$$\sigma = \frac{\Delta\rho\omega^2 r^3}{4} \tag{2.29}$$

where σi: Interfacial tension (Nm^{-1}), $\Delta\rho$: Density difference of the two fluids (kg/m^3) ω: Rotation rate, (rad/s) and r: Radius of the less dense drop (m).

Sometimes, the measurement of IFT on a spinning drop tensiometer is not reproducible due to the dispersion of produced soaps and emulsions. It is suggested by Zhang *et al.* (2006) [200] that the samples of the oil and surfactant solution should be rotated for 24 hours prior to the determination of IFT. Then both phases should be separated and placed in the respective rotating tubes for another 12 hours. Any sedimentation present should be separated and after that the samples are ready for IFT measurement using the spinning drop tensiometer.

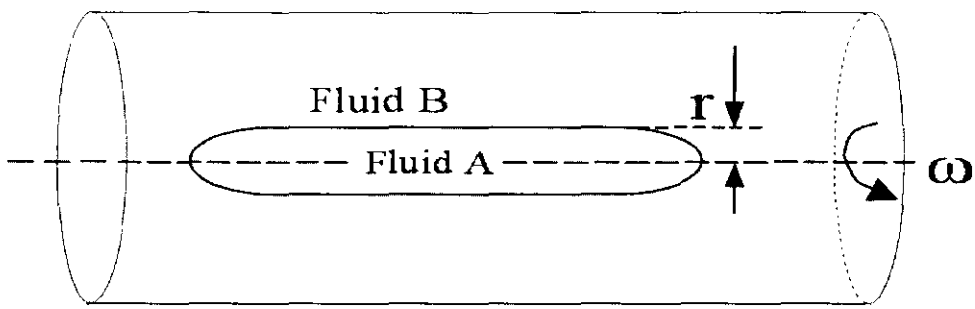

Figure 2.33: Schematic of the spinning drop method [201]

2.15.4 Core flood Tests

A formulation which has good solubilization and aqueous stability in the phase behavior can be selected for a core flood experiment. Brine, oil, and water flooding experiments are then performed to obtain the core parameters, and to prepare the core at the residual oil saturation for the actual flood process [77].

Core flood equipment consists of an injection pump, a core holder, an oven to heat the core, pressure and temperature gauges to record pressure and temperature, a separator to separate oil, gas and brine. In addition, the equipment has back pressure regulators and pressure safety valves to ensure the maintenance of the required pressure in the system.

For a typical coreflood experiment, first, the core is selected by specifying its type, size and permeability. The selected core is cleaned, dried well, evacuated and weighed. The weight is recorded. Then, the known composition brine is prepared and the core is dipped in the brine for at least 3 days for the brine saturation step. The saturated core is weighed again to estimate the porosity. The prepared core is then placed in the core holder for the displacement experiments. Oil is injected in the core until the oil cut becomes 100 % to attain the original oil in place (OOIP) condition. The oil removes the brine in the core and the recovered brine volume is used to calculate the oil and water saturations. The next step is the displacement of the oil by water flooding and the production data are used to determine the water and residual oil saturations. At this stage, the core represents the typical condition of the reservoir rock after the water flooding (secondary recovery) and is ready to be operated for the tertiary oil recovery (EOR) experiment by using the ASP, SP or WAG process. Chemical slugs are then injected in the core to displace the remaining oil. The production data are utilized to evaluate the incremental oil recovery and fluid saturation [50]. The results from a core flood experiment are usually utilized to evaluate many important parameters such as relative permeability, capillary pressure, recovery factor, resistance factor and residual resistance factor for the polymer injection and mobility reduction factor for foam flooding.

2.16 Chapter Summary

The structure and chemistry of surfactants and their role in EOR applications has been clearly manifested. It has also been shown by defining and explaining the reservoir properties and trapped oil mechanisms that the surfactants are extremely important in EOR applications. Moreover, a historical overview of surfactants' usage for EOR methods has also revealed that new types and modified structures of surfactants are a constant need for better oil recovery. During the literature review discussion of EOR surfactants, it has been pointed out that there is an obvious research need and gap for methyl ester sulfate and sulfonate type surfactants. Their excellent structure performance relationship augmented with the modifications capabilities in the structure suggests that these surfactants may play a significant role in EOR applications.

CHAPTER 3

MATERIALS AND METHODS

This chapter covers the research procedure, which includes the methods of synthesis, characterization and evaluation of the surfactants. Specifications of the raw materials, chemicals and all allied materials used in the research such as crude oil, brine and core samples are presented in the first portion of the chapter. The comprehensive procedures and schemes of the surfactant synthesis are presented in the second part of this chapter. The third and last part of this chapter is dedicated to the description of the analyses and evaluation procedures for the synthesized surfactants. In the end, a chapter summary is also provided.

3.1 Research Methodology

This research work is divided into two parts. The first part covers the synthesis of the surfactants and the second part discusses the evaluation of the synthesized surfactants for EOR applications.

For the synthesis of the surfactants, *Jatropha curcas* oil and high oleic acid methyl ester (HOAME) were used. The process flow chart is shown in Figure 3.1. A high percentage of FFA was present in the *Jatropha oil.* The FFA was esterified to methyl esters by using an ingeniously developed solid phase catalyst. Kinetics studies of the esterification reaction were also performed to understand the reaction mechanism under the influence of the developed solid catalyst. The treated oil with less than 1 % FFA was transesterified with methanol by using a sodium methoxide catalyst. The obtained methyl esters were epoxidized by using H_2O_2 and formic acid. The synthesis process was optimized for the maximum yield by using the response

surface methodology (RSM). The oxirane ring of the epoxidized methyl esters was opened catalytically in the presence of BF_3 by using nine different alcohols, namely, ethanol, *n*- propanol, isopropanol, *n*- butanol, iso- butanol, hexanol, octanol, decanol and dodecanol. These alcohols were attached on the main fatty acid chain by an ether linkage. As a result of this process, a hydroxyl (-OH) group was also obtained on the *trans* side of the ether attachment. For the synthesis of the sulfate surfactants, these *trans* -OH groups were converted to sulfate groups by reacting with chlorosulfonic acid. For the synthesis of the sulfonate surfactants, the -OH groups were protected by using acetyl groups obtained from acetic anhydride. After this step, the resultant product was sulfonated in a falling film reactor to obtain α-sulfo fatty acid methyl esters with alkoxy groups attached as a side chain. The produced surfactants were purified and analyzed for the purity. Different analytical techniques including GC-FID, GC-MS, FT-IR, ^{1}H NMR and ^{13}C NMR, and volumetric analyses were used for the analysis and characterization of the products and raw materials.

The evaluation of the surfactants started with the thermal stability test of the surfactant solution under high salinity, pH and temperature conditions. This test defined the maximum salinity, temperature and pH tolerance for a given surfactant solution at a specified concentration. The next step was to evaluate the phase behavior of the surfactant solution mixed with brine, alkali, co-solvent and crude oil. The solubilization values for the oil and water were obtained and IFT was calculated based on the Chun Huh equation. The spinning drop tensiometer was also employed to determine the IFT value of the selected mixtures of oil and surfactant / brine solutions. The core flood tests were performed to evaluate the performance of the surfactants in terms of enhanced oil recovery. The surfactants adsorption on Berea sandstone cores was investigated by using batch adsorption test in the presence of specific amounts of alkali, salinity and temperature. To evaluate the findings of the adsorption of the surfactants onto the sandstone cores, different tests of the cores, such as chemical composition, surface charge density and point of zero charge were performed and the results were evaluated. Different analytical techniques such as Refractive index, XRF, FESEM, BET surface area analysis and potentiometric titration of the surfactants were used for the evaluation of the surfactants for EOR applications.

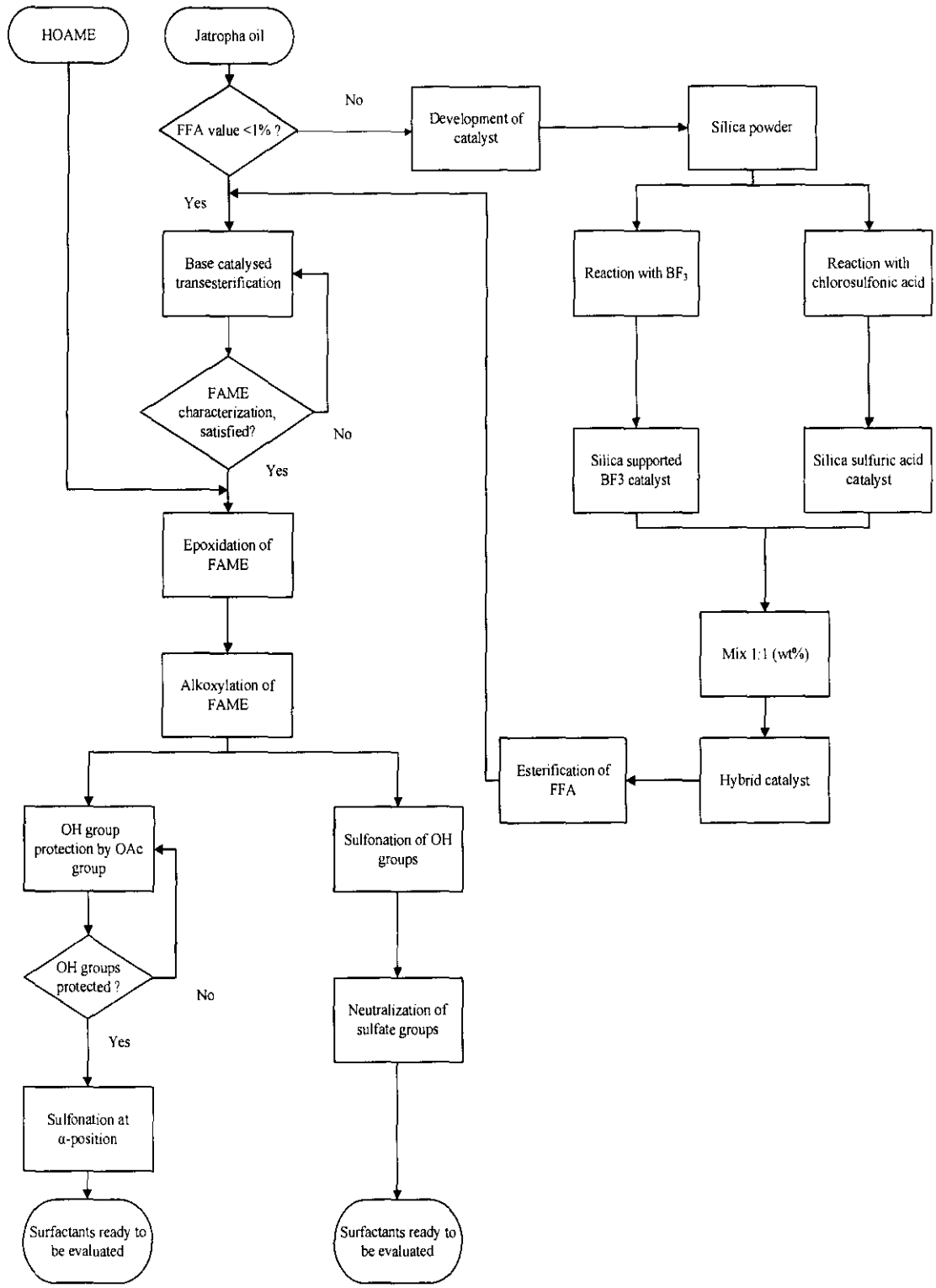

Figure 3.1: Process flow of the synthesis of the surfactants from *Jatropha oil* and HOAME

3.2 Raw Materials and Chemicals

Jatropha oil and high oleic acid methyl esters (HOAME) were the raw materials used for the synthesis of the surfactants.

3.2.1 *Jatropha oil* and High Oleic Acid Methyl Ester

The Jatropha oil was procured from BATC Development Bhd., Malaysia and the HOAME was obtained from SOLTEQ Sdn. Bhd. Malaysia. Some properties of *Jatropha oil* and HOAME as provided by the suppliers are presented in Table 3.1.

Table 3.1: Properties of Jatropha curcas oil and high oleic acid methyl esters

Property	*Jatropha oil*	High oleic acid methyl ester
Color	Yellowish brown	Light yellow
Moisture	~0.5 %	0.01 %
FFA	6.64 % as oleic acid	N/A
Foreign matter	Absent	Absent
Sediments	Absent	Absent
State	Liquid	Liquid

Jatropha oil and HOAME were used after drying by heating at 105°C for 30 minutes and the subsequent cooling and filtration was performed by using Whatman© No.1 filter paper.

3.2.2 Chemicals and Reagents

All chemicals used in this research were at least ACS purification grade. The chemicals were obtained from different sources. The details are presented in Table 3.2.

Table 3.2: List of chemicals used in research

Name	Specifications / purity	Supplier
Methanol, , Ethanol, *n*-propanol, propa*n*-2-ol, *n*-butanol, buta*n*-2-ol, *n*-hexanol, *n*-octanol, *n*-decanol, Oleum (20 % SO_3)	ACS grade	Fisher scientific/ Acros chemicals Belgium
sodium sulfate, silica, hydrogen peroxide (30 % solution), acetic anhydride, acetic acid, 0.004M Hyamine , *n*-hexane, potassium dichromate, starch indicator, HBr in acetic acid, mixed indicator, acetone, silica gel.	Analytical grade	Fisher scientific Malaysia
Boron trifluoride - diethyl etherate complex (50 % BF_3), Acetic acid, sodium bicarbonate, chloroform, Hydrochloric acid, Formic acid and chlorosulfonic acid, Wijs solution, cyclohexane, sodium thiosulfate.	Analytical grade	Merck chemicals, Germany
Hexanes, anhydrous sodium sulfate, sodium chloride, Sodium hydroxide, potassium hydroxide , sulfuric acid	ACS grade	J.T. Baker, USA.

3.2.3 Crude Oil and Brine

The injection water used for the Dulang oil field was used as the brine throughout the research work. It was donated by PETRONAS Research Sdn. Bhd. The properties of

the brine are presented in Table 3.3. Synthetic brine was also used in this study. The required amounts of salts were dissolved in deionized water to obtain the required concentration of ions. For the phase behavior studies, a NaCl solution (0.5 to 10 wt. %) in deionized water was also employed.

Table 3.3: Properties of the brine

Test	Results
Density (g / cc)	1.0229
Conductivity (μS/cm)	46608
TDS	30.745
Salinity	30.78
pH	8.05
Ion	Concentration (ppm)
Na	10590
Mg	1217
Ca	328.9
K	324.6
Sr	4.259
Fe	<0.07
Ba	<0.003
$(HCO_3)^{-1}$	163
$(CO_3)^{-2}$	Not Detected
$(OH)^{-1}$	Not Detected
$(Cl)^{-1}$	18899
$(SO_4)^{-2}$	2600

3.2.4 Core Samples

Berea sandstone core samples were obtained from Cleveland Quarries, Ohio, USA. For the adsorption studies, a portion of each core sample was crushed into powder. The properties of the Berea core samples, as provided by the supplier are presented in Table 3.4.

Table 3.4: Properties of the Berea core samples

Property	Core #1	Core #2	Core #3	Core #4
Length (cm)	7.69	7.73	7.59	7.76
Diameter (cm)	3.78	3.78	3.83	3.84
Porosity	0.187	0.187	0.246	0.219
Mass (g)	183	184	196	188

3.2.5 Polymer

Partially hydrolyzed poly acrylamide (HPAM), with a degree of hydrolysis of 30 %, was obtained from SNF, Floerger, France, with the trade name FLOPAAM 3330S and was used as the polymer. The molecular weight of the polymer was 8 million Daltons.

3.2.6 Synthesis of the Surfactants

The synthesis of the surfactants was comprised of five steps, as shown in Figure 3.2. The first step was the reduction in the FFA value (conversion of fatty acid to methyl esters) by using a silica based catalyst, and thereby, the development of a new catalyst for this purpose. The transesterification of the treated oil was performed in the second step. As HOAME are already methyl esters, the esterification and transesterification step was not required; so, these methyl esters entered to the third step directly as shown in Figure 3.2. In the third step, the epoxidized methyl esters were prepared from the methyl esters. The fourth step involved the attachment of side chains to the methyl esters by the alkoxylation process with alcohols. For the final step, the obtained methyl esters with the attached side chains were divided into two portions. The first portion was used for the sulfation reaction to produce the sulfate surfactants. The second portion underwent the process of hydroxyl protection by the acetylation

and was subsequently sulfonated to produce the sulfonated surfactants. All of the synthesis steps are discussed in detail in the following sections.

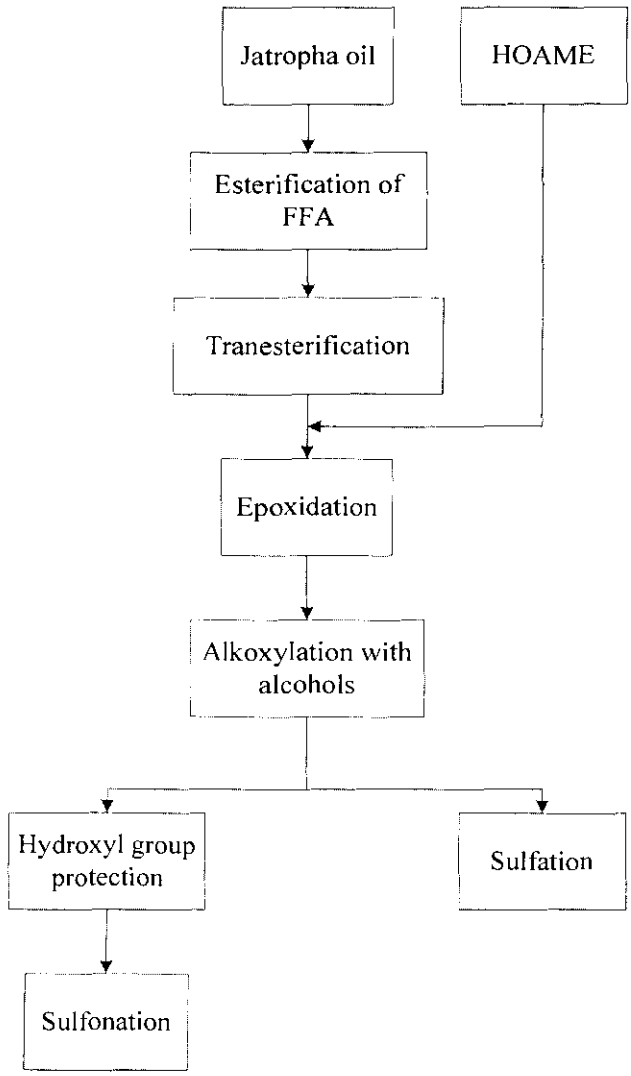

Figure 3.2: Simplified block diagram of the synthesis process

3.2.7 Characterization Techniques

Several techniques were employed for the characterization of the raw materials, precursor and synthesis products. The techniques and procedures used for the individual analysis are presented with the synthesis procedure where applicable. However, common techniques such as NMR, FT-IR and GC-MS and some analytical

tests (for oils and their derivatives) such as the FFA value, Iodine value, Hydroxyl value, Oxirane oxygen are described in the following sections.

3.2.7.1 FT-IR Spectroscopic Analysis

The FT-IR spectra were recorded with the Perkin Elmer Spectrum One FT-IR spectrometer equipped with a ZnSe 45° HATR assembly. A thin layer of the sample was applied on the ZnSe plate and the scan process was conducted. An average of 30 scans was used with a spectral resolution of 4 cm^{-1}over a range of 4000 - 600 cm^{-1}. Air was used to calculate the background spectrum.

3.2.7.2 NMR Analysis

The ^{1}H NMR spectra were taken on a Bruker Ultrashield 400 at 400 MHz. Chloroform-d and D_2O were used as the solvent depending upon the sample type. The ^{13}C NMR spectra were obtained by using the same instrument at a frequency of 100 MHz.

3.2.7.3 GC Analysis

Gas chromatography (GC) was used to analyze the composition of the different samples. Two detectors, namely, the flame ionization detector (FID) and mass spectrometric detector (MS) were employed. The GC equipment used with FID was the Shimadzu GC 2010 system with a fitted FID-2010. The GC system used with MS was the Agilent 7890A GC System coupled with the Agilent 5975C inert XL EI / CI MSD with a Triple-Axis Detector. The capillary column used for both systems was BP5, 30 m × 250 μm × 0.25 μm. The oven temperature program was as follows: 3 min at 100 °C, 25 °C / minute to 170 °C, 2 °C / minute to 230 °C, and 20 °C / minute to 250 °C, and was maintained at 250 °C for 10 minutes [202]. Helium was used as the carrier gas with a flow rate of 0.5 mL / minute and enough time was given for the elution of all of the peaks.

3.2.7.4 Density

The density of natural oil, crude oil and brine was determined by the Anton Par DM40 density meter. The capillary tube was cleaned well with acetone, water and acetone in sequence to remove all contaminations of organic or inorganic types. The system was calibrated by both deionized water and dried air at the temperature of the test before the measurement of the density for the sample. For the density measurements, the sample was injected carefully by using a syringe to avoid any air bubble formation. After the sample was injected successfully, the instrument attained the set temperature for the analysis and then the density was measured and displayed.

3.2.7.5 Refractive Index

The samples were analyzed for the refractive index on the Mettler Toledo RM40 refractometer. The cell was cleaned well with water and acetone and a few drops of the sample were placed in the measuring cell. The sample was automatically heated by the instrument to the test temperature and the reflective index was measured and reported.

3.2.7.6 Moisture Analysis

The moisture analysis was performed by using the Karl Fischer titration method, conducted on a Metrohm 831 KF Coulometer with a diaphragm generator electrode. A small amount (about 0.1 g) of the sample was used to determine the moisture content.

3.2.7.7 FFA Value

The *Jatropha oil* was analyzed for the FFA value according to the AOCS Official Method Ca 5a-40 [133]. In the first step, two drops of 0.1 % phenolphthalein indicator solution were added to the 75 mL ethyl alcohol (95 %) and then it was neutralized with the standard 0.1N NaOH to a faint but persistent pink color. Then a

sample weight of 7.05 ± 0.0.05 g was transferred into the Erlenmeyer flask containing 75 mL of hot pre neutralized ethyl alcohol. After swirling, the sample was titrated against the standard 0.25 M NaOH solution until the pink color of the same intensity appeared as that of the neutralized alcohol before the addition of the sample. The calculations were made on the basis of oleic acid, as shown in Equation 3.1:

$$\text{FFA as oleic acid, \%} = \frac{\text{mL of alkali} \times \text{N} \times 28.2}{\text{mass, g of sample}} \tag{3.1}$$

Where N is the normality of the standard NaOH solution.

3.2.7.8 Iodine Value

The iodine value was determined according to the AOCS Official Method Cd 1d-92. In an iodine flask, 0.130 g of the sample (dried) was weighed. Then, 15mL of a cyclohexane - acetic acid reagent were transferred in the flask and the sample was dissolved in it. Then 25 mL of Wijs solution were transferred in the flask and the stopper was placed immediately and the time was noted. A blank sample in an iodine flask was also prepared in the same manner but without the sample in it. Both flasks were immediately transferred to the dark for 1 hour at room temperature. After one hour, both flasks were removed and 20 mL of KI solution was added followed by 100 mL of distilled water. The solution in both flasks was titrated against the standard sodium thiosulfate with the addition of the starch indicator towards the end of titration. The iodine value was calculated according to Equation 3.2.

$$\text{Iodine value} = \frac{(B-S) \times N \times 12.69}{W} \tag{3.2}$$

where B is the volume of the titrant, mL (for blank); S is the volume of the titrant, mL (for sample); N is the normality of the $Na_2S_2O_3$ solution and W is the weight of the sample, g.

3.2.7.9 Oxirane Oxygen

The epoxidation progress was monitored by the AOCS Official Method Cd 9-57 [133]. For this estimation of oxirane oxygen, a 0.3-0.5 g sample was weighed into a 50

mL titration flask which contained 10 mL of glacial acetic acid, with a stopper with a hole for the tip of the burette. Then, 0.1 mL of crystal violet indicator solution was introduced and rapid stirring was started. The solution was titrated with 0.1 N HBr solution to a blue-green end point which persisted for 30 seconds. Calculations were performed according to Equation 3.3.

$$\text{Oxirane oxygen},\% = \frac{\text{mL HBr to titrate sample} \times N \times 1.60}{\text{mass of sample,g}} \qquad (3.3)$$

where N is the normality of the HBr solution. Further quantification was achieved by GC-MS as described above under the methyl esters profile analysis. Enough time was given at 250°C to elute all of the necessary peaks.

3.2.7.10 Hydroxyl Value

During the epoxidation process, as an undesired side reaction, the oxirane ring may open and yield hydroxyl groups (-OH groups) on either side of the oxirane carbon. The extent of this side reaction could be estimated by analyzing the sample for the hydroxyl value. The hydroxyl value was defined as the mg of the potassium hydroxide equivalent to the hydroxyl content of 1 g of the sample. The AOCS Official Method Tx 1a-66 [133] was used for the analysis. In an Erlenmeyer flask, weighed 5 g of the sample and 5 mL of a pyridine-acetic anhydrite reagent (3 volumes of pyridine and 1volume of acetic anhydrite) were added and the contents were thoroughly mixed together. The flask was stoppered tightly and saved undisturbed for 24 hours. A second flask with the same amounts of the reagent but without any sample was also prepared and sealed and saved for 24 hours as a blank. Another portion from the sample was taken and its acid value according to the AOCS Method Te 2a-64 (APPENDIX A) was measured [133]. After 24 hours, 10 mL of water were added to both the sample and the blank flasks and 10 mL of pyridine were also added. The flasks were stoppered and shaken well to mix the contents. Both flasks were kept for 30 minutes with occasional shakings. After 30 minutes, 25 mL of *n*-butyl alcohol were added to both the sample and the blank flasks and 1mL of phenolphthalein indicator was added and titrated with a 0.5N alcoholic KOH solution to a faint pink end point. Calculations were made as shown in Equations 3.4 and 3.5.

$$\text{Hydroxyl value} = \left[\frac{(B-S)\times N\times 56.1}{W}\right] + [\text{Acid value}] \quad (3.4)$$

$$\%\ \text{OH} = \frac{\text{Hydroxyl value}}{32.98} \quad (3.5)$$

where B is mL of KOH used for the blank, S is mL of KOH used for the sample, and W is the weight of the sample.

3.3 Synthesis of Methyl Esters

Due to the high FFA value of *Jatropha oil*, the synthesis of the methyl esters was achieved by a two step esterification reaction. In the first step, the high FFA value was reduced by esterification and in the second step, the base catalyzed transesterification reaction was conducted. A new silica based catalyst was developed in this study for the acid catalyzed esterification reaction.

3.4 Development of the Catalyst for the Esterification of Free Fatty Acids

Silica was used as the support for the catalyst. A detailed process flow diagram is presented in Figure 3.1. Three types of catalysts, namely, silica supported BF_3 catalyst, silica sulfuric acid catalyst and hybrid catalyst were prepared and evaluated for efficiency. The synthesis process is discussed in the following sections.

3.4.1 Preparation of Silica Supported-BF_3 Catalyst

Silica supported-BF_3 (SSB) was prepared according to Wilson and Clark [155]. Silica was dried at 300 °C for 24 hours and then cooled in a desiccator. Under dried conditions, in a three-neck flask, 10 g of silica was mixed with100 mL of ethanol and then 40 mmol of boron trifluoride - diethyl etherate complex was added. The mixture was stirred at room temperature for 2 hours. The slurry was dried slowly in the rotary

evaporator under vacuum at 50°C. The dried catalyst was stored in a stoppered glass bottle.

3.4.2 Preparation of the Silica Sulfuric Acid Catalyst

The silica sulfuric acid (SSA) catalyst was prepared according to Khalifi *et al.* [156]. In a three-neck flask, 60 g of silica was transferred, and 23.3 g of chlorosulfonic acid was added drop by drop in the course of 30 minutes. A mild nitrogen stream was applied to remove the hydrogen chloride gas produced during the reaction. The product was agitated to facilitate the reaction and the removal of HCl gas. When the reaction was completed, (HCl gas ceased to come out), the silica powder became homogenous with a dried appearance once again, and no lumps of silica with chlorosulfonic acid were observed. The obtained product (76 g) was stored in a stoppered bottle.

3.4.3 Preparation of the Hybrid Catalyst

An amount of SSA and SSB was mixed in a 1:1 (weight ratio) of both catalysts to make the hybrid catalyst (HC). The dried catalyst was an off-white powder without any sign of wetness or vapors. The product was stored in a stoppered glass bottle.

3.4.4 Preparation of the Synthetic Jatropha Oil with High FFA

The neat *Jatropha oil* had an FFA value of 6.64 % (as oleic acid). A series of samples was prepared with varying values of FFA to evaluate the performance of the synthesized silica based catalysts. For this purpose, a portion of the oil was converted to its fatty acids by saponification with NaOH and subsequent treatment with sulfuric acid.

In a 1000 mL beaker, 50 g of oil was transferred. The mixture was heated to 70°C with a constant stirring. Then, 50 mL of a 40 % NaOH solution was added slowly and the mixture was kept under stirring and heating for 1 hour to complete the saponification reaction. A viscous light yellow material was obtained when the

saponification was completed. The soaps were treated with a 10 % sulfuric acid solution with constant stirring at 70 °C. Fatty acids immediately appeared as an oily mass floating on the water. Addition of sulfuric acid was continued until the pH was acidic. The fatty acids were separated and washed with hot distilled water to remove the sulfuric acid until a neutral pH was obtained. The fatty acids were dried at 105°C in a beaker on a hot plate. The *Jatropha oil* was spiked with different amounts of fatty acids to obtain FFA values of 9.25, 15.47, 27.85, 35.01 and 45.64 % with corresponding acid values of 18.41, 30.79, 55.42, 69.67 and 90.88 mg KOH / g of oil, respectively. In addition, the neat oil with the FFA value of 6.64 % (acid value 13.21 mg KOH /g of oil) was also used in this study. The five prepared varieties of the *Jatropha oil* were analyzed for their FFA values. In addition, the FT-IR analysis of the samples was also conducted.

3.4.5 Acid Catalyzed Esterification Reaction

In a 300 mL three neck round bottom flask equipped with a magnetic stirrer bar, coil condenser and thermometer (Figure 3.3A), 50 g of filtered and dried *Jatropha oil* were transferred and heated to the required temperature (30 – 65 °C) with stirring at a fixed speed of 600 rpm. In a 250 mL beaker, the required amount of methanol (1-20 moles with respect to FFA moles of oil) and the catalyst (0.5 – 3.0 wt. %) were mixed and heated to the required temperature (30 – 65 °C). Then, the methanol-catalyst mixture was transferred to the oil bearing flask and stirring was continued for 30 – 180 minutes. Then, the mixture was transferred to a separatory funnel to separate the methanol and oil – methyl esters. After 30 minutes, the two layers were separated and the oil-FAME layer was washed with warm (55 °C) water until the washings were a neutral pH. The treated oil was dried over anhydrous sodium sulfate.

3.4.5.1 Kinetics Studies of the Acid Catalyzed Esterification Reaction

The kinetics of the acid catalyzed esterification reaction was also studied. The esterification reaction was performed by using optimized reaction conditions. A series of experiments at 30, 40, 50, 60 and 65 °C was conducted. Samples were drawn at

specific intervals (30, 50, 80 and 100 minutes) and washed with hot water until the pH of the washings was neutral. The samples were dissolved in hexanes and dried on anhydrous sodium sulfate and the solvent was removed by evaporation at 70°C and 30 mbar pressure. The dried samples were analyzed for the FFA value (section 3.2.7.7) and FT-IR spectroscopy (section 3.2.7.1). The obtained results were interpreted for kinetics and the energy of the activation calculations.

3.4.5.2 Conversion efficiency of the catalyst

The FFA value was determined by the AOCS Official Method Ca 5a-40, as described in detail in section 3.2.7.7. The conversion of FFA was calculated by the expression shown in Equation 3.6:

$$FFA\ conversion = \frac{FFA_i - FFA_t}{FFA_i} \times 100 \qquad (3.6)$$

3.4.6 Base Catalyzed Transesterification of Oil

For the base catalyzed esterification, the treated oil (by hybrid catalyst) with an FFA value less than 1 % was used. In a 300 mL three neck round bottom flask equipped with a magnetic stirrer bar, coil condenser and thermometer, 50 g (0.06 moles) of filtered and dried *Jatropha oil* were transferred and heated to the required temperature of 60°C with stirring at a fixed speed of 1000 rpm. In a 250 mL beaker, 12 g of methanol (6 moles with respect to the moles of oil) and 0.25 g of the sodium methoxide catalyst (0.5 wt. %) were mixed and heated to 60 °C (Figure 3.3 A). Then, the methanol-catalyst mixture was transferred to the oil bearing flask and stirring was continued. The reaction was continued for 60 minutes at 65 °C. The mixture was transferred to a 500 mL separatory funnel (Figure 3.3 B) and kept undisturbed for 2 hours. After that, the lower dark glycerin - water layer was separated and a golden yellow layer (Figure 3.3 B) of methyl esters was washed with warm (55 °C) water until the washings were a neutral pH. The esters were dried over anhydrous sodium sulfate and weighed to determine the methyl ester yield by using Equation 3.7.

$$\text{Yield of methyl esters (\%)} = \frac{\text{Weight of methyl esters}}{\text{Weight of Oil}} \times 100 \quad (3.7)$$

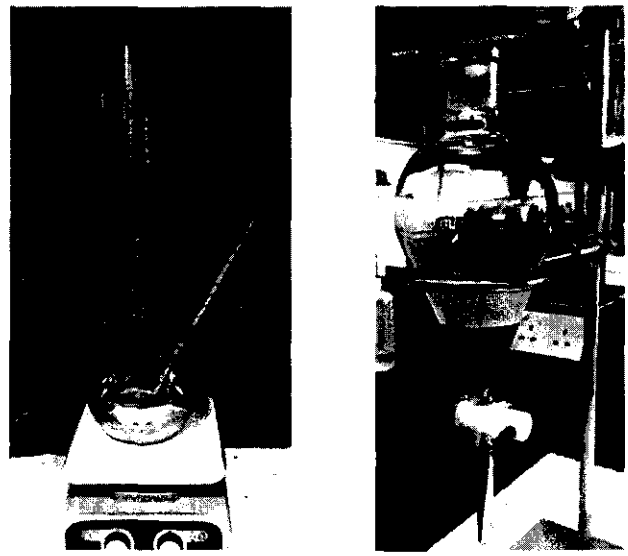

(A) (B)

Figure 3.3: Esterification of *Jatropha oil*: (A) esterification reaction, (B) separation of glycerin and methyl esters

3.5 Epoxidation of Fatty Acid Methyl Esters

The epoxidation of the synthesized fatty acid methyl esters was conducted by using peroxy formic acid generated in-situ by the reaction of hydrogen peroxide and formic acid.

To investigate the effects of the reaction parameters on the yield and to optimize the reaction conditions for the maximum yield, the design of the experiment by using the response surface methodology (RSM) was used. The methodology is discussed in the following sections.

3.5.1 Experimental Design

Four variables, i.e., hydrogen peroxide / C=C methyl esters molar ratio (H_2O_2 moles), Formic acid / C=C methyl esters molar ratio (formic acid moles), reaction temperature and reaction time were selected as the reaction variables and the epoxidation yield

was designated as the response factor. Design Expert software version 8.0.7.1 from Stat-Ease Inc. Minneapolis, USA was used for the experimental design and to analyze the statistical data.

The ranges of the designed reaction variables comprised for 1 mole of C=C were as follow: hydrogen peroxide (0.5 – 4 moles), formic acid (0.20 – 2.0 moles), reaction temperature (25 – 85 °C) and reaction time (30 – 360 minutes). All experiments were conducted at a fixed stirring speed of 1500 rpm which was found to be the optimum in the authors' lab. The range and levels for each parameter with its respective symbol are shown in Table 3.5.

The full factorial CCRD for four independent variables at five levels proposed 30 runs of the experiment by using the following relation (Equation 3.8):

$$2^k + 2k + 6 \qquad (3.8)$$

Where k is the number of independent variables which were four in this experiment. The experiment design contained eight axial points, sixteen factorial points and six center points. The centre points were the replications of trials for the estimation of the experimental error. The detailed table (Table B1) is presented in APPENDIX B.

The epoxidation yield (%) was taken as the response variable, defined by the following expression (Equation 3.9):

$$\text{Epoxidation Yeild (\%)} = \frac{O_{\exp}}{O_{theo}} \times 100 \qquad (3.9)$$

Where O_{exp} and O_{theo} were the experimental and theoretical oxirane oxygen (%), respectively.

Table 3.5: Range and levels of the reaction parameters for CCRD

Variable	Symbol	Coded variable level				
		Lowest	Low	Centre	High	Highest
		-2	-1	0	1	2
H_2O_2/C=C (mole ratio)	X_1	0.5	1.375	2.25	3.125	4.0
Formic acid/C=C (mole ratio)	X_2	0.20	0.65	1.1	1.55	2.0
Temperature (°C)	X_3	25	40	55	70	85
Reaction time (minutes)	X_4	30	112.5	195	277.50	360

With an iodine value of 101.3 g I_2 / 100 g of methyl esters, the theoretical oxirane oxygen for methyl esters was calculated to be 6.0 % by using the expression presented in Equation (3.10) [108].

$$O_{theo} = \left[\frac{(IV/253.8)}{\left[100 + (IV/253.8)16\right]} \right] \times 16 \times 100 \qquad (3.10)$$

where IV was the Iodine value (g I_2 / 100g methyl esters).

3.5.2 Epoxidation Process

The epoxidation reaction was conducted at a selected temperature for a specific reaction time by utilizing the peroxy formic acid generated in-situ when the hydrogen peroxide reacted with the formic acid. The reaction was accomplished in a 1000 mL three neck round bottom flask equipped with a magnetic stirrer placed in a temperature controlled bath on a hotplate/stirrer assembly. The mixture of methyl esters and formic acid was stirred continuously at a fixed speed of 1500 rpm, the required amount of hydrogen peroxide was added drop wise in the course of 30-45 minutes at room temperature. The mixture was gradually heated to the required temperature and kept at a constant temperature for the selected reaction time.

Later on, the mixture was transferred to a separating funnel and the aqueous layer was drained, immediately. The product was washed with a saturated sodium bicarbonate solution, distilled water and a saturated sodium chloride solution in sequence. After water removal, the product was diluted in hexanes and dried over anhydrous sodium sulfate. The hexanes were removed by vacuum distillation.

3.5.3 Kinetics Studies of the Epoxidation Reaction

The kinetics studies of the epoxidation process were also performed. Optimized reaction conditions for H_2O_2 and formic acid were used. A series of experiments at 30,40,50,60 and 70 °C was conducted. Samples were drawn at specific intervals (30, 50, 80 and 100 minutes) and washed with saturated $NaHCO_3$ until the pH of the

washings was slightly basic. Then, the samples were washed with water to remove the $NaHCO_3$ remnants. In the last step, the sample was dried over anhydrous sodium sulfate.

3.5.4 Analysis of the Epoxidized Methyl Esters

The quality of the product was assessed by determination of the oxirane oxygen (section 3.2.7.9). Further quantification was achieved by GC-MS as described under the methyl esters profile analysis. Enough time was given at 250°C to elute all of the necessary peaks. The hydroxyl value was determined for the assessment of the extent of the ring opening reaction. The method is described in the section 3.2.7.10. The fatty ester profile was determined by GC-MS while the spectroscopic analyses include FT-IR and NMR analyses.

3.6 Alkoxylation of the Epoxidized Methyl Esters

The reaction of alcohol with epoxidized methyl esters results in the opening of the oxirane ring and the attaching of alcohol by the ether linkage. In this research, nine different alcohols having varying chain lengths as well as straight chain and branched chain characters, were used to obtain the side chains. These alcohols included methanol, *n*-propanol, iso-propanol, *n*-butanol, iso-butanol, *n*-hexanol, *n*-octanol, *n*-decanol and *n*-dodecanol.

3.6.1 Alkoxy Side Chain Attachment

The oxirane ring opening and the attachment of the alkoxy groups were achieved by the method reported by Hedman [114] with some modifications. In this method, BF_3 was used as the catalyst. The catalyst was mixed in alcohol and the epoxidized methyl esters were slowly mixed in the catalyst-alcohol mixture. The order of mixing was important and was strictly followed.

In a well dried apparatus and absolutely dried conditions, alcohol (0.1 moles) was charged into a 100 mL three neck flask at room temperature with continuous stirring.

BF_3 - diethyl etherate complex (0.5 wt. % BF_3 of alcohol used) was injected into the alcohol beneath the surface to avoid the loss of BF_3. Epoxidized methyl esters (0.095 moles) were added drop wise into the flask over the course of 30 minutes. The mixture was heated to 45-50 °C for 30 - 45 minutes with continuous stirring. Then, the product was cooled to room temperature. Approximately 30 mL of hexanes and 10 g of sodium bicarbonate were added into the flask and the contents were stirred for 5 minutes before filtering through a filter paper to remove the catalyst residues. Litmus paper was used to assess the pH of the mixture, and hence confirm the absence or presence of catalyst remnants. The solvent and residual alcohol was removed by distillation at 70 °C and at 30 mbar pressure.

3.6.2 Removal of the Excess Alcohol

Although a small excess of alcohol was used to minimize the free excess alcohol in the reaction mixture, the excess amount of alcohol was also removed. Small chain alcohols (ethanol, propanol, and iso-propanol) which were soluble in the water were removed by repeated water washings. The process of cleaning was continued until the washings became clear and verification was done on FT-IR.

Butanol, iso-butanol, hexanol, octanol, decanol and do-decanol were removed by using the steam distillation process. In a three neck flask, 30 g of the mixture were loaded and heated to 80°C. In another two neck flask, steam was generated and passed through the mixture. The condensate was monitored for any remnants of alcohol and the process was stopped when it became clear.

3.6.3 Analysis and Characterization of the Epoxidized FAME

The product was analyzed for its purity and structure by using the GC-MS profile analysis, FT-IR spectroscopy, NMR spectroscopy and titrimetric analysis for oxirane oxygen contents. In addition, the distillate of the steam distillation process which contained the removed alcohols was also analyzed to observe the possible carry-over of methyl esters.

3.7 Sulfonation and Sulfation of the Modified Fatty Acid Methyl Esters

For the synthesis of the surfactants, attachment of a head group was achieved by the sulfonation or sulfation of the product. Two groups of surfactants were synthesized, namely, sulfate and sulfonates from the modified (side chains attached) fatty acid methyl esters. The sulfate head group was attached on the 10^{th} carbon atom containing the -OH group. The sulfonation of the -OH results in the O-S bond and it was performed by using chlorosulfonic acid. The sulfonation reaction was carried out to attach the sulfonate group at the alpha position. As there was an -OH group present at the *trans*-position of the ether linkage, SO_3 gas would react first with the -OH to produce the sulfate. To overcome this issue, it was necessary to protect the -OH group by acetylation. The details of the synthesis process are presented in the next sections.

3.7.1 Sulfation of the Modified Fatty Acid Methyl Esters (Unprotected -OH Groups)

This process was conducted in absolutely dry conditions. In a 300 mL three neck flask with condenser, dry tube (DRIERITE®) and a thermometer, 16.0 g of methyl esters and 50 mL of chloroform were transferred. The solution was cooled to 5 °C in an ice bath and with strong stirring; 13.18 g of chlorosulfonic acid which was pre-cooled to 3 °C in 50 mL of chloroform, and transferred in the course of 20 minutes. The temperature was maintained at 0 to 5 °C. The HCl gas was removed by applying a mild vacuum. The mixture was stirred for 30 minutes at 0-5 °C and after that, the ice bath was removed and the mixture was slowly heated to 60 °C in 45 minutes. The temperature was maintained at 63 – 65 °C to reflux for one hour. Then, the mixture was cooled to 0 °C and neutralized to pH 6 - 6.5 with 20 % w/v methanolic sodium hydroxide. The mixture was dried at 70 °C and 30 mbar pressure for 30 minutes to obtain a semisolid brown mass.

3.7.1.1 Removal of the Neutral Oil and the Purification of the Product

The unreacted methyl esters, known as neutral oil were removed by extraction at a low pH. The product was dissolved in 50 mL of water and the pH was maintained at

3-4 with 1 M H_2SO_4, transferred to a 500 mL separatory funnel. The neutral oil was extracted with 90 mL of *n*-hexane (3 × 30 mL). After the evaporation of the hexane, the neutral oil was obtained as brown oil. The aqueous layer was mixed with 30 mL of HCl (10.5 M), shaken well and extracted with 60 mL of diethyl ether (4 ×15 mL). The combined layers were evaporated under vacuum and the ether was collected for recycling.

3.7.1.2 Analysis and Characterization of the Product

The sulfated alkoxy methyl esters were analyzed for active matter, pH, FT-IR and NMR spectroscopic analysis. The analytical techniques are discussed in section 3.8 "Analysis of the Synthesized Surfactants".

3.7.2 Sulfonation of the Modified Fatty Acid Methyl Ester (Protected -OH Groups)

For the sulfonation reaction, the -OH groups were protected by the acylation reaction. The sulfonation of the acetylated product was conducted in the Falling Film Reactor (FFR). Details of the process are given in the following sections.

3.7.2.1 Protection of the -OH Groups

For the acetylation of the -OH groups, the method reported by Matinez-Pascual *et al.* [158] was used with minor modifications. In a three neck flask, alkoxylated methyl esters (0.2 moles) were mixed with 50 mL of ethylene chloride. Then, a stoichiometric amount of acetic anhydrite (according to the -OH groups present) was introduced. In the next step, 0.5 ~ 1.0 mL of BF_3-etherate complex was introduced under the surface of the solution with the help of a fine-tipped glass pipette. The solution was stirred for 10 seconds and then poured into ice water and further stirred for 20 minutes. The organic layer was extracted with the hexanes and washed three times with water. Then, it was washed with 10 % aqueous $NaHCO_3$ until the washings were mildly basic. In the last washing step, the organic layer was washed with water

to remove the bicarbonate. The product was dissolved in hexanes and dried over anhydrous sodium sulfate. The solvent was evaporated to afford the acetylated product ready to be sulfonated.

3.7.2.2 Analysis and Characterization

The product was analyzed for the hydroxyl value by the AOCS Official Method Tx 1a-66 [133] as described in section 3.2.7.10. This method determined the left over, unreacted -OH groups which were not converted to acetyl groups by the acetylation reaction. The conversion efficiency of the acetylation reaction can be determined by using Equation 3.11:

$$\text{Conversion efficiency (\%)} = \frac{\text{-OH value after acetylation}}{\text{-OH value before acetylation}} \times 100 \qquad (3.11)$$

FT-IR analysis of the product was performed to confirm the acetyl group attachment.

The NMR analysis was performed on the Bruker Ultrashield 400 at 400 MHz and 100 MHz to determine the ^{1}H NMR and ^{13}C NMR spectra, respectively. The solvent used was chloroform-d. ^{1}H NMR was used to confirm the absence of a proton signal from the -OH group while ^{13}C NMR was used to confirm the appearance of a signal from the carbonyl carbon of acetyl group.

3.7.2.3 Sulfonation in the Falling Film Reactor

A photograph of the Falling Film Reactor used in this study is shown in Figure 3.4 and a schematic diagram is presented in Figure 3.5. The heart of the falling film reactor is a vertical glass tube. The SO_3 gas, diluted with air entered from the top along with the fatty acid methyl esters. The FAME came in the form of a thin film. The sulfonation reaction occured on the sides of the tube with the thin film of FAME. Oleum, heated to 150°C was used for the generation of SO_3 gas.

For the sulfonation reaction, the temperature of reactor (falling film) was set at 85 °C and the air flow was set at 11g/min. When the steady flow of SO_3 was maintained, the methyl esters were heated to 90 °C and introduced at a flow rate of 3 g / min. For the required amount of SO_3 gas, the oleum flow rate was set at 2.30 g /min (1.6 mol / mol of methyl esters). The color of the product in the falling film tube was changed to light brown. The product produced in the first 10 minutes of the reaction was discarded. The product produced in the next 10 minutes was collected in a beaker and then heated in a water bath to 85 °C for 30 minutes to allow the intermediates formed in the previous steps to fully form the surfactants. The product was neutralized by the aqueous NaOH (20 %) solution to a pH of 6.5.

A B

Figure 3.4: Falling Film Reactor (A) and control panel (B).

Figure 3.5: Schematic of Falling Film Reactor

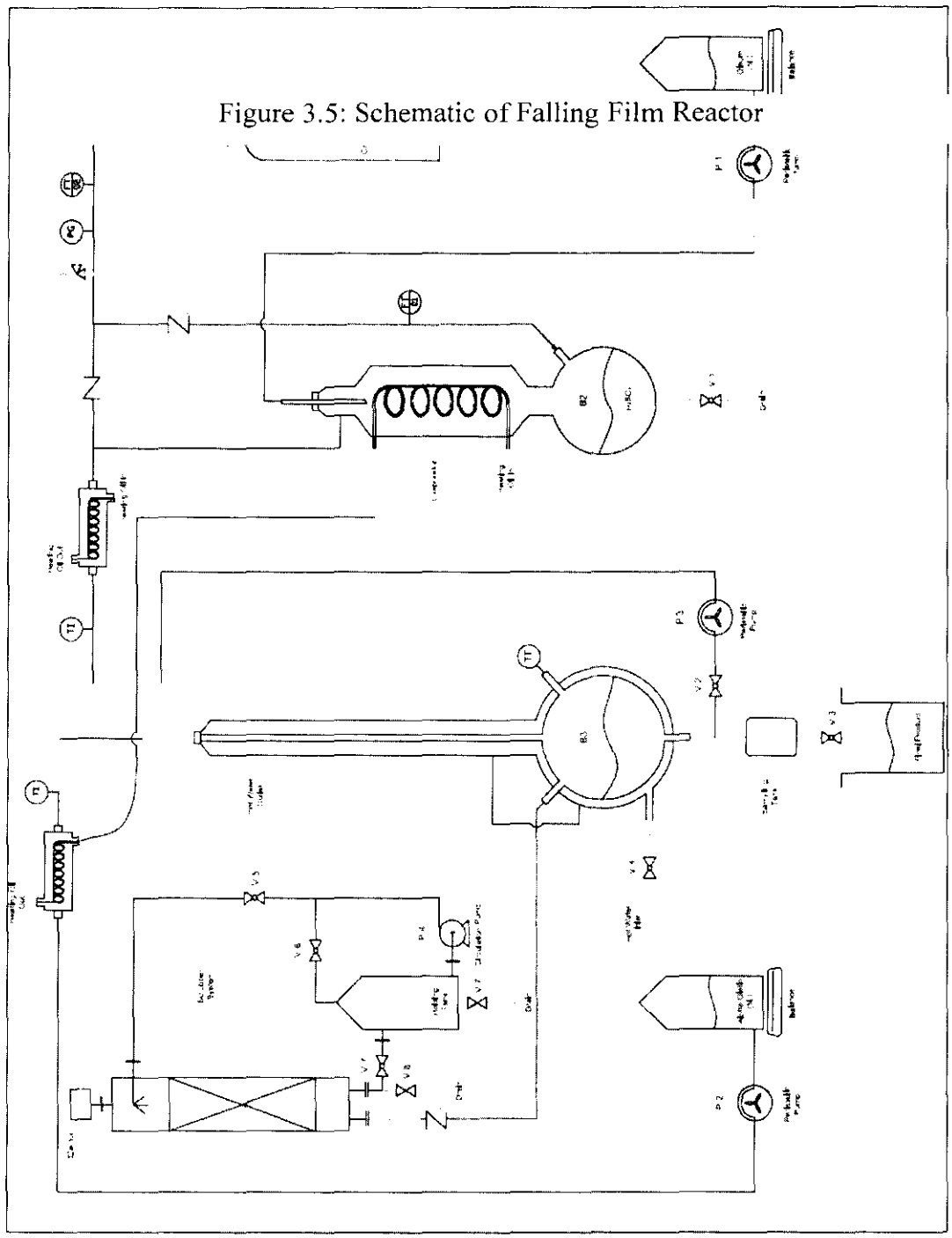

3.8 Analysis of the Synthesized Surfactants

The description of methods used for the analysis of the surfactants is presented in the following sections.

3.8.1 Active Matter (Weight %)

The synthesized sulfated and sulfonated surfactants were analyzed and characterized by using the ASTM Standard Test Method D4251-89. Metrohm auto titrator Titrando 888 with a 20 mL burette was used for this test. The electrode system consisted of a Metrohm electrode for the anionic surfactants (Ionic Surfactant) and a Metrohm Ag/AgCl reference electrode. The standard Hyamine 1622 solution (0.004 N) was used as the titrant. The data were manipulated with Metrohm software tiamo^{TM} version 2.3.

For the analysis, 1 g of the surfactant was dissolved in distilled water to make 100 mL of solution. From this solution, 10 mL were transferred in a 150 mL tall form beaker. The sample was made acidic to a pH ~3 by adding a few drops of 0.5 M H_2SO_4. Then, 5 mL of methanol were added and the sample beaker was placed on a Metrohm stirrer plate 804. Stirring was started and after two minutes, the titration was commenced. The end point was detected by the software and the system automatically, and the results were calculated by using the following expression (Equation 3.12).

$$\text{Anionic active matter, \%w} = \frac{V \times N \times M}{10 \times W} \qquad (3.12)$$

where V is the volume of the Hyamine used, N is the normality of Hyamine, M is the molecular weight of the surfactant and W is the weight of the sample used.

3.8.2 FT-IR and NMR Spectroscopic Analyses

The powdered sample was used to conduct the FT-IR spectroscopic analysis. In about 1 g of KBr, 100 mg of the sample was mixed and both were grounded well in an agate mortar with an agate pestle. The well ground mixture was transferred into the stainless steel mount for making pellets on a hydraulic hand-press. The clear and transparent pellet was mounted on the cell plate of the Perkin Elmer Spectrum One FT-IR spectrometer and the analysis was conducted. An average of 30 scans was used with a spectral resolution of4 cm^{-1} over the range of 4000 - 400 cm^{-1}. Air was used to calculate the background spectrum.

The NMR analysis was performed on the Bruker Ultrashield 400 at 400 MHz and 100 MHz to determine the ^{1}H NMR and ^{13}C NMR spectra, respectively. The solvent used was D_2O. For sulfated surfactants, the ^{1}HNMR spectra were used to confirm the removal of H from the -OH groups and the appearance of a signal from the proton of the HSO_4 group. In sulfonated surfactants, ^{13}C NMR was used to confirm the appearance of the peak from the C-S bond from the sulfonate group.

3.8.3 Evaluation of the Surfactants

The synthesised surfactants were evaluated for their performance as surfactants. A number of tests were performed and are discussed in the following sections.

3.8.4 Critical Micelle Concentration (CMC)

CMC of the surfactants was measured by the conductance measurements. The conductance measurements were performed at 23°C. The surfactant solutions were prepared in ultra-pure water and kept in the lab for 3 hours to attain the lab temperature of 23 °C. A Trans Instrument bench top conductometer model BC3020 was used to measure the conductance of the solution. The electrode was washed with ultra-pure water after each measurement and rinsed with a portion of the sample solution twice before conducting the measurement. A plot of the conductance against the concentration was used to calculate the CMC.

3.8.5 Refractive Index

A refractive index of the series of the surfactant solutions having varying concentrations was conducted at 30 °C. A Mettler-Toledo RM40 refractometer was used for the measurements. The sample was placed in the cell and the temperature was set at 30 °C by the instrument, automatically.

3.8.6 High Temperature Tolerance Test

In six test tubes with screw caps, 1 wt. % solution of the surfactant in distilled water was transferred. The test tubes were placed in the ovens at 50, 60, 70, 80, 90 and 100 °C. The samples were inspected every day for any precipitation, phase separation or cloudiness. If the solution was found clear, the solution was recorded as stable at that temperature.

3.8.7 Salinity Tolerance Test

In this test, 1 wt. % of the surfactants solutions were tested for the salinity tolerance of 35000 ppm TDS (Dulang injection water, will be called IW). The surfactant solution was made in IW and transferred in screw capped test tubes. The solution was inspected for any cloudiness or precipitation; if this occurred, the sample was regarded as intolerant against the salinity. Those solutions which were clear at room temperature were transferred to the ovens at the specified temperatures as listed in the previous section. Clear solutions at a particular temperature were regarded as tolerant at that temperature and salinity.

3.8.8 Compatibility with Polymer and Alkali

The surfactants were also evaluated for their tolerance against alkali and polymers. The same procedure, as noted in earlier sections was used. Partially hydrolysed polyacrylamide (HPAM) as the polymer and sodium metaborate for the alkali was used for the evaluation of the surfactant compatibility against these chemicals. Any precipitation or cloudiness in the solution indicated the instability for that condition.

3.8.9 Interfacial Tension (IFT) and Surface Tension Measurements

The surfactant solutions were tested for surface activity with the IFT measurements against Dulang crude oil and the surface tension against air.

3.8.9.1 IFT measurement with a Spinning Drop Tensiometer

The measurement of IFT was conducted on a spinning drop tensiometer. A Dataphysics model SVT20 was used for the IFT measurement. The density of the oil and brine was measured before the IFT measurement. For the brine sample, the refractive index was also determined. The capillary of the tensiometer was filled with brine with care to avoid any air bubbles. The rotation of the capillary was started at 500 rpm. After that, the oil was taken in a fine needle syringe and only one oil drop was injected into the rotating capillary. Then, the speed of the capillary was increased to 4000~4500 rpm or more until the drop became elongated (cylindrical in shape with a length four times that of the diameter). Initial readings were noted for IFT and the capillary was kept on rotating until the equilibrium conditions were achieved and then the IFT value was noted.

3.8.9.2 Surface Tension with a Pendant Drop Tensiometer

A pendant drop tensiometer from Vinci (France) was used for the determination of the surface tension of the aqueous solutions of the surfactants. The sample was loaded in the sample syringe and the temperature of the "needle" was maintained at the required temperature. The camera was set to have a sharp picture of the end of the needle. With the help of a syringe, a drop was made hanging from the needle and its picture was analyzed by the system software to calculate the respective angles for the determination of the surface tension.

3.8.10 Phase Behavior Test

The phase behavior test was used for two purposes: to find the optimum salinity (salinity scan) and to find the minimum IFT attained at the optimum salinity by using

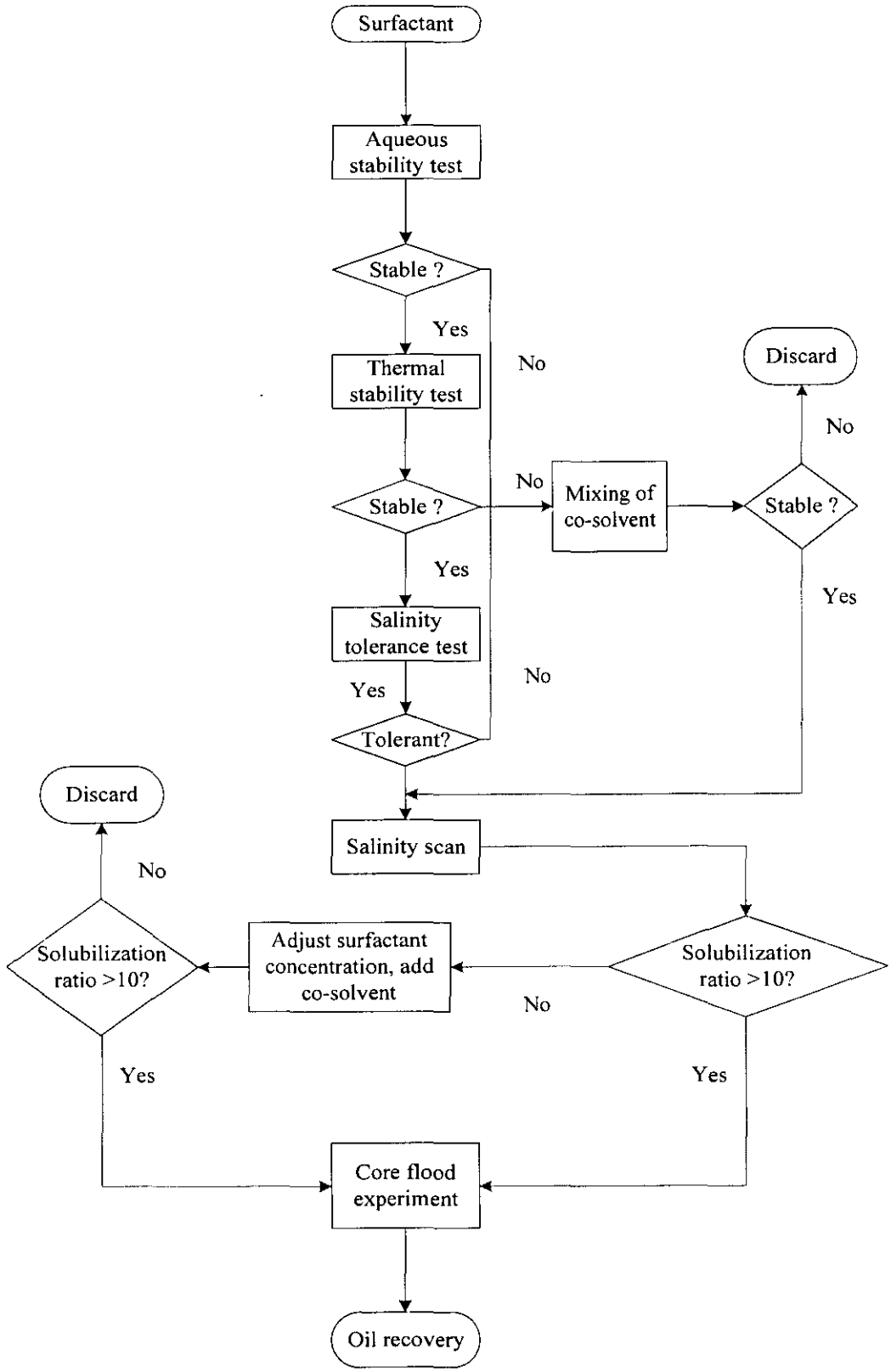

Figure 3.4: Flow chart of the phase behavior test

the solubilization ratios method. A detailed flow chart of the phase behavior test is given in Figure 3.4. For a typical phase behavior test, a 2 % surfactant concentration was used. The surfactant solution containing the selected amount of alkali and co-solvent was transferred into several pipettes which were previously sealed from the lower tip. Then, varying amounts of the salinity solution were introduced. Then, an equal volume of crude oil was transferred into the pipettes to attain the condition of equal WOR (water to oil ratio) and the upper ends of the pipettes were sealed with a flame. All pipettes were shaken well to mix the phases and then placed in the oven at a specific temperature. The pipettes were visually inspected for the formation of any microemulsion, viscous phases or macro emulsion etc.

In case of a middle phase microemulsion, the oil and water solubilisation parameters were noted. The solubilization parameters were calculated by using Equations 3.13 and 3.14.

$$SP_{oil} = \frac{V_o}{V_s} = \frac{\text{Volume of oil in microemulsion phase}}{\text{Volume of surfactant in microemulsion phase}} \tag{3.13}$$

$$SP_{water} = \frac{V_w}{V_s} = \frac{\text{Volume of water in microemulsion phase}}{\text{Volume of surfactant in microemulsion phase}} \tag{3.14}$$

where V_o and V_w were the volume of the oil and water solubilized in the microemulsion phase, noted from the volume difference on the pipette, V_s was the volume (or the mass) of the surfactant used.

The IFT was calculated by using the following expression (Equation 3.15):

$$\sigma = \frac{C}{(V_i/V_s)^2} \tag{3.15}$$

Where σ was the interfacial tension, V_i was the water or oil solubilised in the microemulsion and V_S was the volume of the surfactant. The constant C was assigned to a value of 0.3.

3.8.11 Static Adsorption Test

The static adsorption of the surfactant was studied by using 1 g of the crushed core sample in 20 mL of the surfactant solution containing a specific amount of surfactant, alkali and salinity. The mixtures were agitated for 24 hours on a horizontal shaker at 25°C. Then, the mixtures were centrifuged at 3000 rpm for 30 minutes and the supernatant was filtered through a syringe filter of 0.45 μm. The filtrate was analyzed for the surfactant concentration by titration against the standard Hyamine 1622 solution on the Metrohm auto titrator. The titration method used was essentially the same as described in section 3.8.1. For the adsorption calculations, a difference in the surfactant's concentration before and after its contact with the core sample (Equation 3.16) was calculated to record the amount of surfactant adsorbed (mg/g) on the crushed core samples.

$$q_e = (C_0 - C_e)\frac{V}{W} \tag{3.16}$$

where q_e was the equilibrium adsorption of the surfactant (mg/g), C_0 and C_e were the initial and final concentrations of the surfactant solutions (mg/L), respectively, V was the volume of the solution (L) and W was the weight of the core sample (g).

3.9 Core Flood Tests

The core flood analysis is actually a multiple analyses scheme. The analysis can be divided into two parts. In the first part, the determination of the core properties such as porosity, permeability and grain density were investigated. In the second part, the actual displacement experiment to evaluate the oil displacement efficiency of the surfactants was conducted. Details of the core flood tests are presented in the following sections.

3.9.1 Fluid Preparation

The fluids include crude oil, brine, alkali and polymer solutions. All aqueous solutions were prepared in deionized water.

3.9.1.1 Oil Samples

The oil sample was filtered at a temperature higher than the wax appearance temperature (WAT) or cloud point of the oil (50 °C). The filtration process removed the solid particles (either sand or other mechanical particles) from the oil phase without changing the oil properties.

3.9.1.2 Brine and Alkali Solutions

The brine and alkali solutions were prepared by dissolving the required amounts of the chemicals in deionized water.

3.9.1.3 Polymer Solution

The polymer solution was prepared in deionized water or brine according to the requirements. The polymer stock solution was made and then diluted, accordingly, when required. For the stock solution preparation, the required amount of polymer powder was added slowly while constantly stirring the deionized water. The polymer was added to the shoulder of the vortex slowly, care was exercised to avoid the appearance of lumps and agglomerations. The solution was kept stirring at a low rpm for 24 hours to avoid any gel formation. The prepared solution was filtered through a filter paper to determine its consistency and homogeneity. The filtration ratio was measured using the following Equation (3.17):

$$\text{Filtration ratio} = \frac{\Delta t_{180} - \Delta t_{160}}{\Delta t_{40} - \Delta t_{20}} \tag{3.17}$$

Where Δt was the time interval and 180, 120, 40 and 20 were the milliliters of the polymer solution collected after that particular time. A filtration ratio less than 1.2 was considered good for a consistent polymer solution.

3.9.2 Core Sample Treatment

To calculate the area of the core plug, its length and diameter were measured and then the core plug was weighed to record its dry weight. In the next step, the core plug was evacuated for 2-3 hours to remove the air from the pores. Then, the core was saturated by dipping in the formation brine; during this process, the vacuum process was continued for half an hour. When it was assured that the core was fully saturated with the formation brine, it was removed from the container and rolled over to a brine-saturated filter paper to remove the surface water/brine. The core was weighed again and the porosity and pore volume were calculated.

3.9.3 Core Flood Procedure

The core flooding procedure includes the brine flooding, oil flooding, brine flooding and then chemical flooding or ASP flooding. The processes were conducted in sequence. For the sulfate surfactant, the core flood test was conducted at 60°C and for the sulfonate surfactants, it was performed at 95°C. Tests were conducted at a flow rate of 2-4 mL min^{-1} and at a low pressure (80-120 psi). The following sections provide the description of each process.

3.9.3.1 Measurement of Viscosity

The measurement of the viscosity of the crude oil, brine and polymer solution was an important test. The viscosity was measured on the OFITE M-1100 HPHT viscometer at a specific temperature and different shear rates. The viscometer used a bob-and-cup fixture. The range of the shear rates which could be applied on the instrument was 0.01 s^{-1} - 1000 s^{-1}. The viscometer was equipped with ORCADA software for the data interpretation and plotting.

3.9.3.2 Water (brine) Flooding

The brine flooding was conducted to determine the absolute brine permeability. The brine was injected at a flow rate of 2-4 mL min^{-1} until the pressure drop became

constant and the pressure stabilized. The absolute brine permeability was calculated from the pressure drop behavior.

3.9.3.3 Oil Flooding

The oil flooding was conducted after the water flooding. The pre filtered oil was injected at a constant pressure (80-120 psi) and selected temperature (60 or 95 °C). About 1.5 pore volume of the oil was injected. The fluids were collected in the graduated cylinders to measure the quantities. The oil flooding was continued until the water cut was less than 1 % and the pressure stabilized. The pressure drop data was used to calculate the oil permeability. The amount of displaced brine was noted to calculate the saturated oil in the core by the mass balance. The initial oil saturation, residual water saturation, effective oil permeability and relative oil permeability were also calculated.

3.9.3.4 Water (brine) Flooding

After the oil flooding, the water (brine) flooding was conducted. The water flooding was conducted at a low and constant flow rate of 0.4-0.45 mL min^{-1}. The water flood was continued until the oil cut was less than 1 % and the pressure became constant. About 1.5 pore volume of water was injected to achieve the residual oil saturation. The residual oil saturation was calculated by noting the volume of effluents collected in the graduated cylinders. The effective water permeability and relative water permeability was calculated by the pressure drop across the core plug.

3.9.3.5 ASP (chemical) Flooding

After the water flooding, the chemical flood was injected. The alkali, surfactant and polymer were injected in a single slug and the polymer slug was injected as the polymer drive. The chemical flooding was conducted to evaluate the performance of the surfactant by noting the recovery of the residual oil as the enhanced oil recovery process. Typically, 0.3 to 0.5 PV of the ASP slug was injected at a flow rate of 0.4-0.5

mL min^{-1}. After the ASP slug, 1.5 -2.0 PV of the polymer was injected as the polymer drive. The flooding was continued until no emulsion or oil was produced. The effluents were collected in the graduated cylinders to record the amount of produced oil and surfactant adsorption. The residual oil saturation was determined by mass balance calculations. The oil was separated from the brine by heating and subsequent centrifuging at 1000 rpm for 24 hours.

3.9.4 Core Flood Calculations

Many calculations were performed for the core flood experiment. These included the calculations of the pore volume, porosity, effective permeability, phase saturation, fluid mobility, polymer resistance factor, permeability reduction factor and oil recovery. The particulars of the important calculations are presented in the following sections.

3.9.4.1 Pore Volume

The pore volume of the core was calculated by the mass balance. The pore volume was calculated as follows (Equation 3.18):

$$\text{Pore Volume} = V_p = \frac{W_{sat} - W_{dry}}{\rho_{brine}} \qquad (3.18)$$

Where W_{sat} and W_{dry} were saturated and dry weights (g) of the core sample and ρ_{brine} was the density (g / cm^3) of the brine.

3.9.4.2 Bulk Volume and Porosity

The porosity could be calculated by dividing the pore volume with the bulk volume (Equation 3.19):

$$\text{Porosity (\%)} = \sigma = \frac{V_p}{V_{bulk}} = \frac{V_p}{\pi D^2} \times \frac{L}{4} \times 100 \qquad (3.19)$$

Where V_p was the pore volume (cm^3), V_{bulk} was the bulk volume (cm^3), D was the core diameter (cm), and L was the core length (cm).

3.9.4.3 Brine Permeability

The core was flushed with the formation brine at a flow rate of 0.4-0.5 mL min^{-1} until the pressure drop across the core was stabilized. Then, the flow rate was changed and when the pressure drop became steady, the flow rate and pressure drop were recorded. This process was repeated for another flow rate and the pressure drop was recorded for the flow rate. All the flow rates and their respective pressure drop values were recorded and the absolute permeability to the brine was calculated by using Darcy's law (Equation 3.20). The plot between the flow rate and the pressure drop should have yielded a straight line.

$$k_{abs} = \frac{Q\mu_{brine}L}{A\Delta P} = \frac{Q\mu_{brine}L}{\pi D^2 \Delta P} \times \frac{1}{4} \qquad (3.20)$$

where Q was the flow rate (cm^3/h), μ_{brine} was the brine viscosity, L was the length of the core (cm), A was the cross sectional area of the core (cm^2), D was the diameter of the core (cm) and ΔP was the pressure drop (psi).

3.9.4.4 Effective Oil Permeability

The effective oil permeability was calculated from the oil flood data at the residual water saturation. The pressure drop across the core plug was measured. When the pressure was stabilized and the water cut was less than 1 %, the pressure drop was recorded. Darcy's equation (Equation 3.20) was used to calculate the relative permeability.

3.9.4.5 Effective Water Permeability

The effective water permeability was calculated during the water flood at the residual oil saturation. The pressure drop was measured across the core plug. When the oil cut

was less than 1 % and the pressure stabilized, the pressure drop was recorded and used in Darcy's equation (Equation 3.20) to calculate relative permeability.

3.9.4.6 End Point Oil / Water Relative Permeability

The end point relative permeability of both the oil and the water was calculated after running the water flood. The end point oil relative permeability (k^{o}_{ro}) was calculated by dividing the effective oil permeability by the brine permeability (Equation 3.21).

$$k^{o}_{ro} = \frac{k_o}{k_{brine}} \tag{3.21}$$

Endpoint water relative permeability (k^{o}_{rw}) was calculated as shown in Equation 3.22:

$$k^{o}_{rw} = \frac{k_w}{k_{brine}} \tag{3.22}$$

3.9.4.7 Mobility Ratio

The mobility was calculated by noting the viscosities and permeabilities of the oil, chemical slug and polymer drive. The following relation was used to calculate the mobility ratio (Equation 3.23):

3.9.4.8 Initial Oil Saturation

The initial oil saturation was estimated by the oil flood. The oil was injected as described above until the water cut reduced to less than 1 % and the pressure stabilized. The amount of the produced water was equal to the amount of the oil saturated in the core. The initial oil saturation (S_{oi}) was calculated by dividing the volume of the water produced by the pore volume as shown in Equation 3.23.

$$S_{oi} = \frac{V_w}{V_p} \tag{3.23}$$

where V_w and V_p were the volume of the produced water and the pore volume, respectively.

3.9.4.9 Residual Oil Saturation

After the core was saturated with oil, the water flood was conducted (2-4 mL min^{-1}) until the oil cut was less than 1 % and the pressure stabilized. The volume of the oil produced during the water flood was the mobile oil saturation. The residual oil saturation was calculated by using Equation 3.24:

$$S_{orw} = \frac{V_w - V_o}{V_p} \tag{3.24}$$

Where S_{orw} was the residual oil saturation after the water flood, V_w was the volume of the water produced from the oil flood and V_o was the volume of the oil produced from the water flood. The residual oil saturation after the chemical flood (ASP) was the difference between the volume of the oil remaining after the water flood and the volume of the oil produced after the chemical flood. The residual oil saturation after the chemical flood could be calculated by using Equation 3.25.

$$S_{orc} = \frac{S_{orw}\left(V_p - V_o\right)}{V_p} \tag{3.25}$$

Where S_{orc} was the residual oil saturation after the chemical flood, V_o was the volume of the oil produced after the chemical flood, V_p was the pore volume, and S_{ow} was the residual oil saturation after the water flood.

3.9.4.10 Oil Recovery

The oil recovery was calculated after the chemical flood. The oil recovery was calculated by dividing the volume of the oil recovered from the chemical flood by the volume of the residual oil after the water flood as shown in Equation 3.26.

$$\text{Oil Recovery} = \frac{V_{op}}{V_{or}} \tag{3.26}$$

where V_{op} was the total volume of the oil produced and V_{or} was the volume of the residual oil after the water flood.

3.9.5 Crushed Core Sample Properties

The Berea core samples were evaluated for their chemical and physical properties. The samples were ground in a ball mill and their BET surface area was measured. The chemical composition was also evaluated by the XRF analysis. Surface pictures were taken by using FESEM, which also provided the XPS analyses. The point of zero charge of the core samples was also measured.

3.9.5.1 Surface Area

The specific surface area (BET) of the core sample was measured on a Micromeritics ASAP 2020 by the physiosorption of N_2. The N_2 adsorption and desorption isotherms were measured at -196°C. The sample was degased at 160°C for 4 h before the analysis. The specific surface area was measured by using the multipoint Brunauer–Emmet – Teller (BET) method.

3.9.5.2 X-ray Fluorescence (XRF) Analysis

The XRF analysis of the core for the elemental analysis was performed on the Bruker S4 PIONEER X-ray fluorescence Spectrometer. A Ru target at 4 kW power was used.

3.9.5.3 Field Emission Scanning Electron Microscopy (FESEM)

The morphology of the ground core samples was studied by using the FESEM model SUPRA 55VP (Carl Zeiss AG, Germany). The SEM samples were prepared by taking a replica on the ultra-thin gold film. The gold film was deposited by using a low vacuum sputter coater.

3.9.5.4 X-ray Photoelectron Spectroscopy (XPS)

The XPS was used to determine the elemental composition (wt. %) of the core samples. The samples were analyzed by using the Leybold spectrometer using Al K α radiation (1486.6 eV). The instrument was run at the fixed analyser transmission mode at a pass energy of 50eV with a 300W X-ray power source. The samples were mounted onto the indium holder (by pressing) and then introduced in a pre-chamber under a vacuum of 10^{-5} torr. All binding energies were referenced to C 1s at 285 eV. All of the peaks (C 1s, N 1s, O 1s and P 2p) were fitted into several components having the same full width at the half maximum (FWHM).

3.9.6 Point of Zero Charge (PZC) of the Core Samples

The point of zero charge of the core samples was also determined to examine the surface charge properties at varying pH values of the solutions. Three different methods were used to evaluate the PZC. Details of the methods are presented in the following sections.

3.9.6.1 PZC Determination by the Salt Addition Method

The method used was essentially the same used by Mustafa et al. [203]. For the determination of the PZC, the core sample was ground. A solution of 0.01 M NaCl was used as the background electrolyte. It was prepared by using high purity deionized water which was preboiled to remove all of the dissolved gasses. A portion of 40 mL of this solution was apportioned into eleven flasks and the pH was maintained at 2, 3, 4, 5, 6, 7, 8, 9, 10, 11 and 12 by a 0.1 M NaOH or 0.1 M HCl solution. The pH was measured and carefully recorded by using the Metrohm 888 Titrando. Then, 0.2 g of the crushed core sample was added into all of the flasks and continuously shaken well for 24 hours at 25°C. Then, the solutions were removed from the shaker, kept undisturbed for 30 minutes to allow for settling of all of the suspended particles. Then, the final pH values were recorded. The difference between the initial and final pH values (Δ pH) was plotted against the initial pH values. The

PZC value was identified at the pH when Δ pH was zero; that was when the initial pH was equal to the final pH.

3.9.6.2 PZC Determination by the Fast Titration Method

The method described by Farooq et al. [204] was used. A portion of 30 mL salt solution (0.001 M NaCl) was taken in a 100 mL double walled thermo - stated cell equipped with a magnetic stirring bar on a stirrer hot plate. A specific temperature was maintained by circulating the water in the double walled jacket. A 0.2 g crushed core sample was then added into the cell and equilibrated at room temperature (25 °C) for 40 minutes. A portion of 2 mL of 0.1 M HCl was then transferred to the solution and stirred for 20 minutes. The pH value was recorded by using the Metrohm 888 Titrando as the initial pH value. The sample was then titrated against the 0.1 M NaOH solution by adding 0.2 mL portions and recording the pH values after 2 minutes. The surface charge density was determined by using the following expression (Equation 3.27):

$$\sigma_o = \frac{\left\{C_A - C_B + \left[OH^{-1}\right] - \left[H^{+1}\right]\right\}.F}{mS} \qquad (3.27)$$

Where C_A (mol.dm^{-3}) and C_B (mol.dm^{-3}) were the concentrations of the acid and the base added to the sample suspension, [OH^{-1}] and [H^{+1}] were the concentrations of the respective ion and were calculated from the pH values of the solution, F (C.mol^{-1}) was the Faraday constant, m was the mass (g) of the core sample and S (m^2 .g^{-1}) was the specific surface area of the core sample. The titration was also performed with the ionic strength of the 0.01 and 0.1 M NaCl solutions. The PZC was identified at the pH value where the surface charge density, σ_o, was zero.

3.9.6.3 PZC Determination by using the Potentiometric Mass Titration (PMT) Method

The PZC of the core sample was also determined by using the PMT technique [205]. A 1500 ppm Na^+ solution was made in deionized water. Three 100 mL portions of

these solutions were transferred into titration flasks, and the crushed core samples having weights of 0.2, 0.4 and 0.6 g were transferred to the respective flasks. A fourth solution called the blank was also prepared by using the same electrolyte solution but without the addition of the core sample. All four solutions were equilibrated at room temperature under a nitrogen atmosphere for 24 hours. Then, 5 mL of 0.1 M NaOH was transferred to the solution and stirring commenced. After recording the initial pH value, the solution was titrated against the 0.1 M HCl solution using 0.2 mL additions. The pH was recorded after every 30 seconds. The other three samples were titrated in the same way and their titration curves were plotted. The common intersection point between the blank and the sample solutions was identified as the PZC.

3.10 Chapter Summary

This chapter presented the detailed methodology of the research. All chemicals and related materials with specifications have been reported in this chapter. The synthesis of the methyl esters, attachment of the side chains to them and then the synthesis of the surfactants from the methyl esters was described in detail. In addition, detailed schemes of the synthesis method and analysis protocols were also reported.

CHAPTER 4

SYNTHESIS AND CHARACTERIZATION OF SURFACTANTS

The synthesis and characterization of the surfactants is discussed in this chapter. The complete reaction schemes with the necessary process conditions are presented. Characterization of the precursors and the end product by different techniques has also been provided.

4.1 Overview of the Synthesis Process

The surfactants were synthesized from Jatropha oil and high oleic acid methyl esters. The Jatropha oil was converted to methyl esters (**1**) by the transesterification reaction with methanol in the presence of a sodium methoxide catalyst. The obtained methyl esters were epoxidized to epoxidized methyl esters (**2**) by the peroxy formic acid generated in-situ (by the reaction of the formic acid and the hydrogen peroxide). The epoxy ring (oxirane ring) was opened up by using nine different alcohols in the presence of a boron trifluoride catalyst. This process attached the alcohol (as an alkoxy group by an ether linkage to form a side chain) to the methyl ester parent chain at position 9 and generated an –OH group at position 10 (or vice versa) to form nine types of alkoxy-hydroxy methyl esters (**3a – 3i**) depending on the type of alcohol used. For the synthesis of the sulfate surfactants, the 9-alkoxy, 10-hydroxy fatty acid methyl esters were treated with chlorosulfonic acid. The –OH group was converted to sulfate by this reaction. The subsequent neutralization of this product with sodium hydroxide produced nine sulfate based surfactants (**4a-4i**). For the synthesis of the sulfonate based surfactants, the sulfonate group must be attached at the α-position ("2" position). Due to the relatively more reactive nature of the –OH group (at

position 10) than the α-hydrogen (at position 2) the -OH group was protected by the acetylation reaction by using acetic anhydrite to produce acetoxy-alkoxy methyl esters (**5a-5i**). After the protection of the –OH group, a sulfur trioxide gas-air mixture was used to conduct the sulfonation reaction in a falling film reactor. The sulfonated methyl esters (with acetyl and alkoxy groups) were neutralized with sodium hydroxide to obtain nine sulfonate based surfactants (**6a-6i**). The complete reaction scheme is shown in APPENDIX C as Figures C1-C6.

4.2 Synthesis of the Methyl esters From *Jatropha oil*

Jatropha oil was one of the raw materials for the synthesis of the methyl esters. The transesterification reaction is the major reaction for the conversion of *Jatropha oil* to methyl esters. The *Jatropha oil* FFA value was 6.64 %, much higher than the permissible limit of ≤ 1 % for a base catalyzed transesterification reaction; therefore, the transesterification reaction was not feasible. Therefore, a two-step strategy for the production of the methyl esters was employed. In the first step, the oil was treated with methanol in the presence of a silica based catalyst to convert all of the FFAs to methyl esters by the esterification reaction. In the second step, the treated oil was reacted with methanol in the presence of sodium methoxide for the transesterification reaction to produce the methyl esters.

4.2.1 Properties of the *Jatropha oil*

The *Jatropha oil* was examined for its fatty acid composition. The fatty acid composition, determined by the GC-MS analysis, showed the presence of a high proportion of unsaturated fatty acids, i.e., oleic and linoleic acid, which were important for the later synthesis steps. The fatty acid composition of the *Jatropha oil* used in this research was the same, with small variations, as reported in the literature [131, 206]. The fatty acid composition of the *Jatropha oil* is presented in Table 4.1.

Table 4.1: Fatty acid composition of the *Jatropha oil*

Fatty acids	Common acronym	Composition (wt. %)
Palmitic acid	C16:0	13.5
Palmitoleic acid	C16:1	0.9
Stearic acid	C18:0	7.1
Oleic acid	C18:1	44.3
Linoleic acid	C18:2	32.8
Others	--	1.4

The major fatty acids were oleic acid, linoleic acid, palmitic acid and stearic acid.

The neat oil had an FFA value of 6.64 % and an Iodine value of 102.3 mg I_2 / g oil.

4.2.2 Esterification of the Free Fatty Acids of the Jatropha Oil

Esterification reaction of fatty acids with alcohols requires a catalyst to proceed, as shown below (Equation 4.1):

$$R\text{-}COOH + CH_3OH \leftrightarrow R\text{-}COOCH_3 + H_2O \quad (4.1)$$

As the methanol is not soluble in *Jatropha oil* and fatty acids [127], the reaction is heterogeneous in nature. It requires a catalyst, high molar excess of methanol and a high temperature for the forward reaction.

4.2.3 Development of the Catalyst for the Esterification of FFA of Jatropha Oil

Three catalysts were prepared for the esterification of FFA of the *Jatropha oil*. These were a Silica Supported BF_3 (SSB) catalyst, a Silica Sulfuric acid (SSA) catalyst, and a Hybrid catalyst (HB). The *Jatropha oil* with varying amounts of FFA was prepared and the catalysts were used to esterify the free fatty acids. The esterification reaction

was studied in detail and the effects of the different reaction parameters were evaluated. The findings are discussed in the following sections.

4.2.3.1 Effect of the Stirring Speed

The effect of the stirring speed on the FFA conversion is shown in Figure 4.1. It can be observed that a stirring speed beyond 600 rpm does not show any improvement in the FFA conversion. The FFA conversion, however, at 400 rpm is low. It is due to insufficient mixing, and thereby poor mass transfer effects at the low stirring speed. The stirring speed is important in heterogeneous systems for better mixing and facilitation in a mass transfer process. It becomes an important factor at lower reaction temperatures. However, at higher temperatures, particularly near the boiling point of methanol, the boiling can provide sufficient agitation required for the reaction. The optimum stirring speed of 600 rpm found in this research is also supported by several studies showing that a stirring speed beyond 600 rpm has no significant effect on the conversion [150, 153, 207, and 208].Therefore, in this study a fixed stirring speed of 600 rpm was used for all of the experiments.

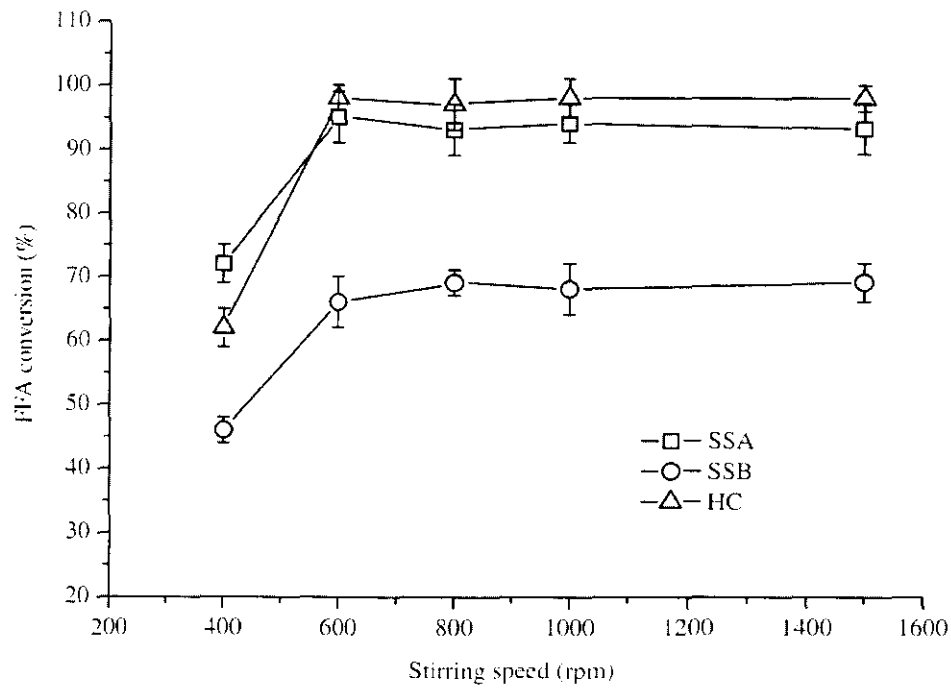

Figure 4.1: Effect of the stirring speed (rpm) on the FFA conversion (%)

4.2.3.2 Effect of the Reaction Temperature

The effect of the temperature on the FFA conversion is shown in Figure 4.2. The esterification reaction is highly dependent on the reaction temperature. At room temperature, the extent of the reaction is low [209], which increases with an increase in temperature. A similar pattern of effect of the reaction temperature was also observed in this study.

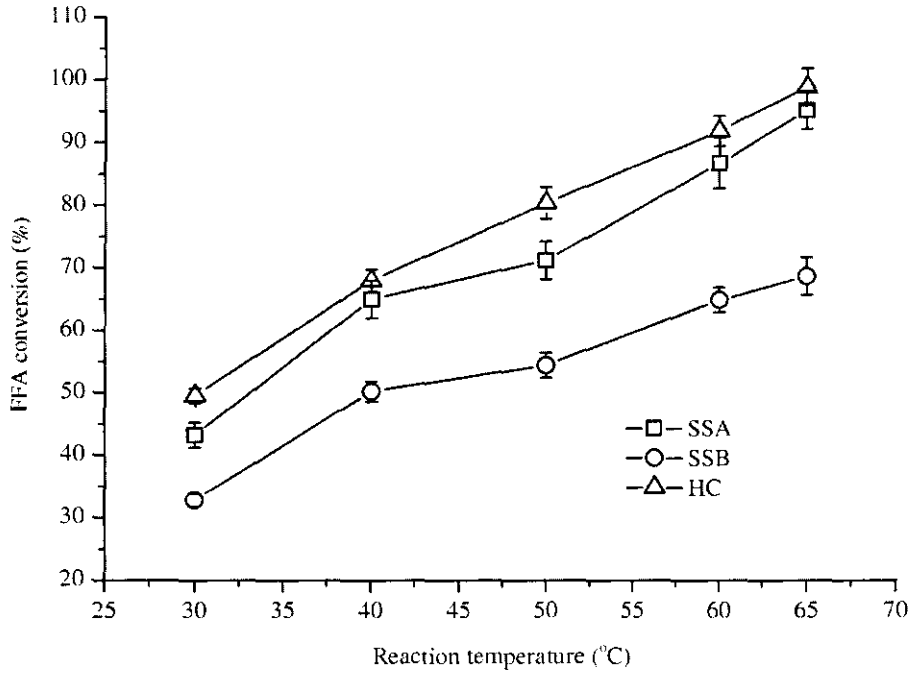

Figure 4.2: Effect of the reaction temperature on the FFA conversion (%)

It can be noted that the reaction rate increased steadily at higher temperatures because the elevated temperature provided sufficient energy for the reaction as well as reduced the viscosity of the oil and FFA, thereby providing better phase mixing. The employed FFA – methanol ratio was 1:20 and the amount of the catalyst used was 1.5 wt. % of oil. It can be observed that the hybrid catalyst (mixture of two catalysts) showed better catalytic activity even at a low reaction temperature. The conversion steadily increased with an increase in the temperature and a 98.2 % FFA conversion was obtained at 65 °C. The effect of the individual catalysts, SSA and SSB, were somewhat lower than that of the hybrid catalyst and a conversion of 92.2 % and 66.4 % was achieved for the SSA and SSB, respectively. The silica supported boron trifluoride was found to possess a lower efficiency compared to the silica sulfuric acid. This could be due to the higher apparent acidity of the SSA. The synergistic

effect of the hybrid catalyst was probably associated with the additive effects between the very strong Lewis acid capability of BF_3 and the superior Brönsted acidity of SO_3.

4.2.3.3 Effect of the Reaction Time

Reaction time is one of the most important factors affecting the esterification reaction. It is also associated with the reaction temperature. At higher temperatures, relatively short reaction times are sufficient for the maximum conversion. The effect of the reaction time with the three heterogeneous catalysts is presented in Figure 4.3.

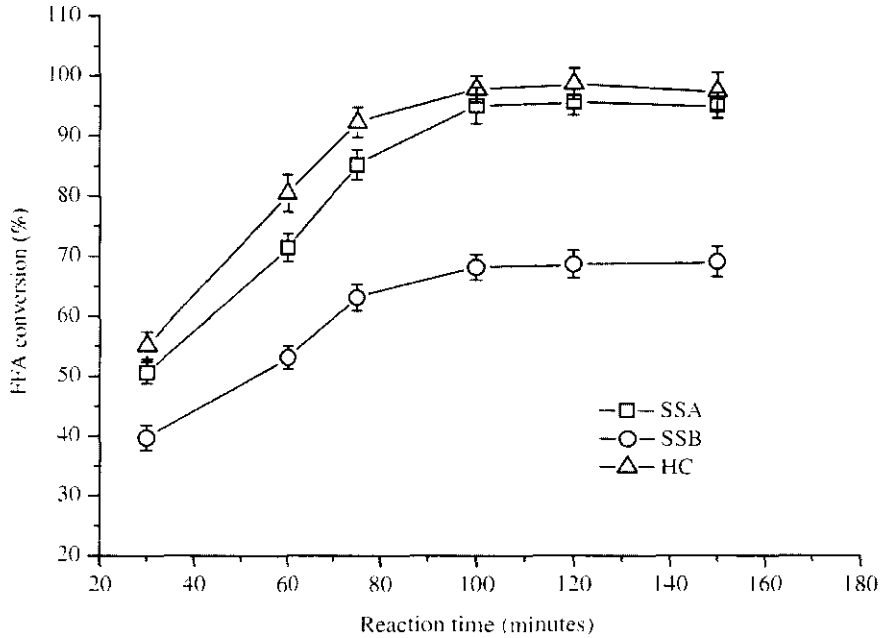

Figure 4.3: Effect of the reaction time on the FFA conversion

The reaction was conducted at 65°C with the FFA – methanol ratio of 1:20. The amount of the catalyst used was 1.5 wt. % of the oil. It was observed that the catalysts did not have a very significant effect on the reaction time and the reaction completed in about 110 minutes for all of the catalyst supported reactions. The reaction completed in 100 minutes for all of the catalysts. HC was superior in the performance and a 98.4 % conversion was achieved. While the SSA converted 90.5 % FFA to FAME, the SSB was found to perform poorly with only 68.7 % FFA converted to FAME in 100 minutes; after which, the reaction became non progressive. The almost same reaction times imply that the catalysts were similar in the surface area due to their preparation from the same support, the silica. The attached BF_3 and sulfuric acid

groups showed the catalytic activities but could not show the fast reaction times when compared to each other.

4.2.3.4 Effect of the Catalyst Amount

The catalyst amount is also an important parameter in an esterification reaction and varying the amount of the catalyst showed a noticeable effect (Figure 4.4). The reaction was studied for the FFA conversion by using 1:20 moles of FFA : methanol, a reaction temperature of 65 °C and a reaction time of 120 minutes. The catalyst amount was varied from 0.5 to 3 wt. % of the oil as shown in Figure 4.4.

The plot shows the maximum conversion (98.21 %) for HC at 2 wt. %, and there was no significant effect found for the amount of the catalyst exceeding 2 %. The SSB and SSA showed a different trend and were lower in performance when compared to the hybrid catalyst even at a 3 wt. % loading. The SSB converted 69.2 % FFA at 3wt. % and the SSA converted 93.6 % FFA at 3 wt. % amount.

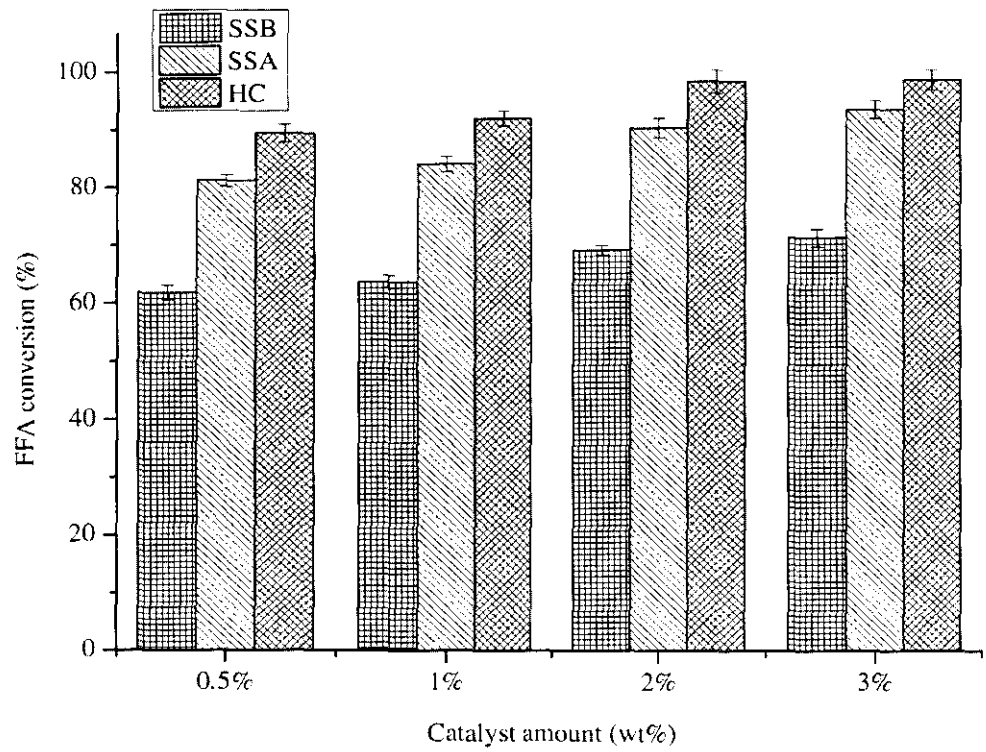

Figure 4.4: Effect of the catalyst amount on the conversion of FFA

4.2.3.5 Effect of the Methanol Molar Ratio to FFA

Methanol is the major reagent in the reaction. As the esterification reaction is a reversible reaction, a high molar excess of methanol is required for driving the reaction to the forward direction.

The effect of the methanol amount is shown in Figure 4.5. A reaction temperature of 65 °C was used with a 1.5 wt. % of the catalyst for a reaction time of 120 minutes. It can be seen from Figure 4.4 that the conversion was very low when a stoichiometric amount of methanol was used and all of the catalysts were almost similar in their efficiency. However, at a higher molar excess, the reaction becomes more efficient and the maximum conversion was achieved at FFA: methanol molar ratio of 1:15. The hybrid catalyst efficiently converted 98.11 % of FFA to methyl esters while the SSA converted 93.3 %. The SSB was lower in performance and a maximum conversion of only 68.8 % was achieved at a 20 molar excess of methanol. It was found that the15:1 mole ratio of methanol : FFA was sufficient for the maximum conversion and any further increase did not show a progressive effect. Therefore, with this catalyst system, a relatively lesser amount of methanol was required whereas in many studies a large excess of methanol was employed, such as 1:50 and 1:60 [10,28].

The role of the high molar excess of the methanol in this context is further discussed in the section 4.2.3.6.

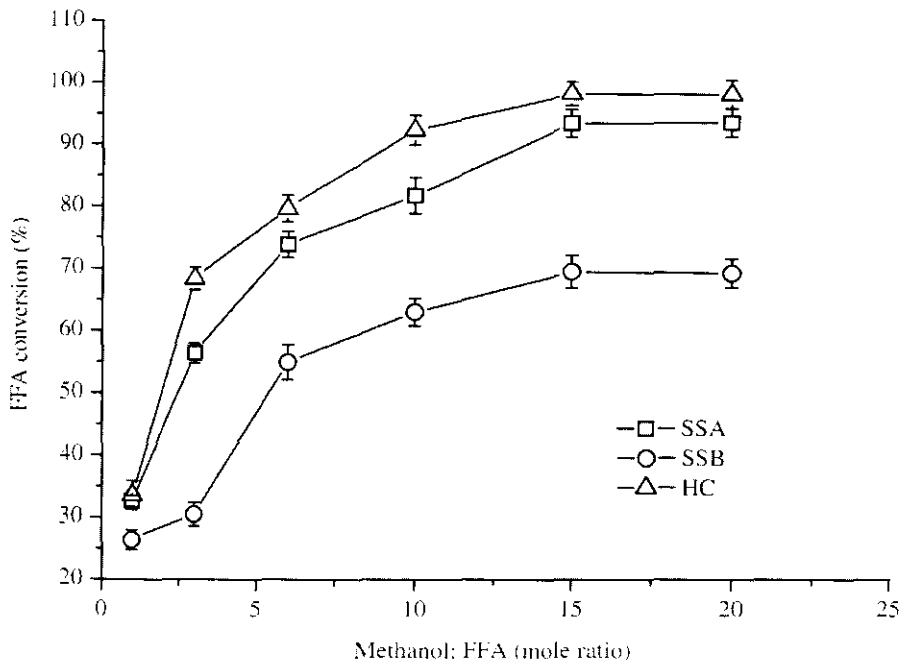

Figure 4.5: Effect of the methanol molar ratio to FFA

4.2.3.6 Effect of the FFA Contents of the Feedstock and the Methanol Amount

The cumulative effect of varying the amount of FFA and methanol was also studied. It was found that the amount of methanol required for the maximum conversion was strongly dependent on the initial FFA value of the oil. At lower FFA values (6.64 and 9.25 %), a relatively lower FFA: methanol molar ratio (1:6) is sufficient but at higher FFA values, a relatively higher molar ratio of methanol is required (1:15 – 1:20). The lower molar excesses of methanol such as 1:10 and 1:6 are not sufficient for the maximum conversion at the FFA values of 35.01 and 45.64 %. This effect for the hybrid catalyst is presented in Figure 4.5. It can be observed that the conversion was the maximum for the molar ratios of 1:15 and 1:20 (FFA: methanol). This requirement of the high amounts of methanol may be attributed to the amount of water produced during the esterification reaction. As methanol and water are mutually soluble, a relatively high amount of methanol is required to be available for a successful reaction. Figure 4.6 also verifies that the hybrid catalyst can successfully be used for oils having varying amounts of FFA.

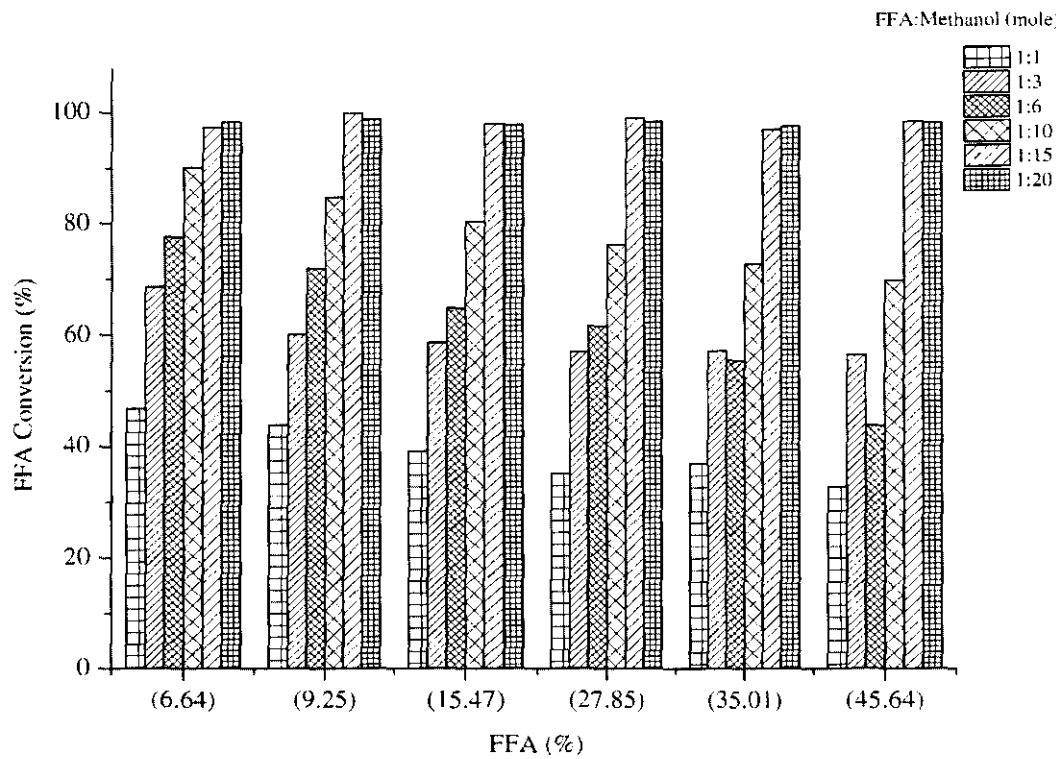

Figure 4.6: Cumulative effect of the initial FFA amount and the methanol / FFA mole ratio on the FFA conversion for the Hybrid Catalyst

4.2.3.7 FT-IR Analysis

The FT-IR spectra were recorded for the neat oil, oil with FFA and methyl ester. The transmittance band for the carbonyl group in fatty acids appeared at 1711 cm^{-1} (band "a" in Figure 4.7) and for the methyl esters (and oils) at 1746 cm^{-1} [210]. In addition, the fatty acids showed a typical broad band around 3100 cm^{-1}(band "b") while in methyl esters (and oils), this band was absent.

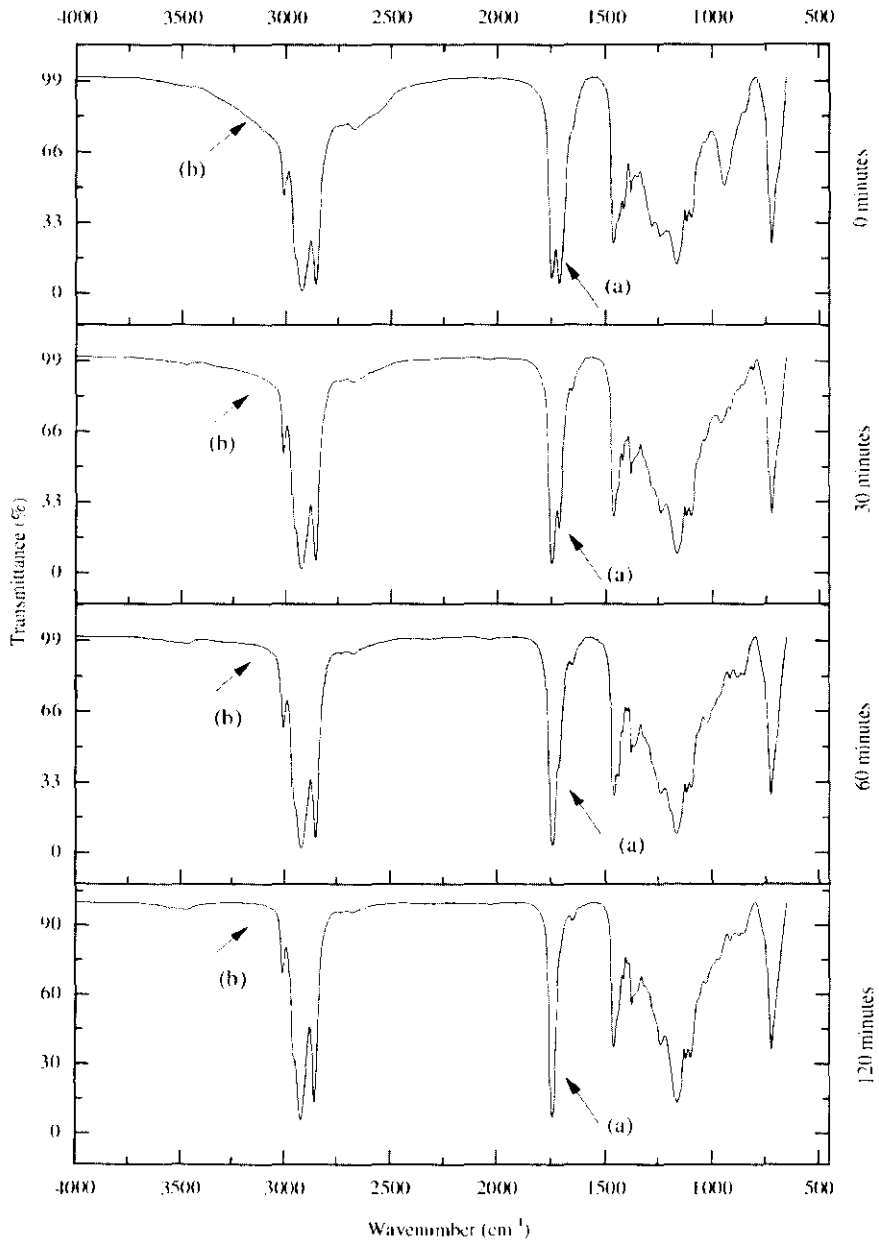

Figure 4.7: FT-IR spectra showing the course of the FFA conversion reaction

These bands were observed during the esterification reaction with the hybrid catalyst. In the course of the reaction, samples were drawn and their FT-IR spectra were recorded after several cleaning steps. As can be observed in Figure 4.7, the bands at 1708 cm^{-1}(a) and 3100 cm^{-1} (b) were distinctly visible when the oil had an FFA value of 45.64 % (reaction time = 0 minutes). However, after 30 minutes, the FFA value was reduced to 15 % and the bands (a and b) at 1708 and 3100 cm-^{1} were reduced in intensity. These bands further decreased in intensity after 60 minutes of reaction time. After 120 minutes of reaction, when the reaction was complete, these bands diminished and the FFA value became less than 1 %. The band at 1742 cm^{-1} was for the ester carbonyl group.

4.2.4 Kinetics Studies

The kinetics studies of the esterification reaction are discussed for the hybrid catalyst. As the reaction rate is dependent on the reaction time and temperature, various experiments at specific reaction temperatures up to 150 minutes were performed.

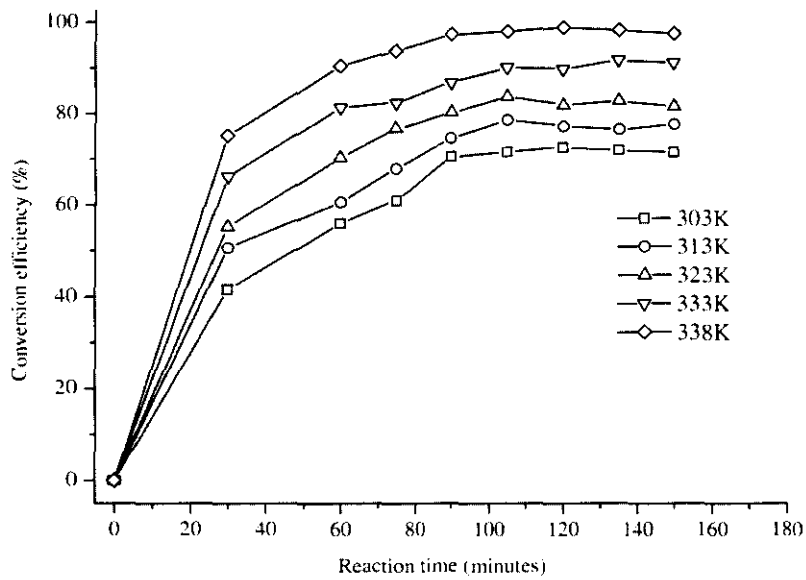

Figure 4.8: Effect of the reaction time at different reaction temperatures on the FFA conversion

It was found that the conversion reached a constant level after 100 minutes of the reaction time. Therefore, a plot of the FFA conversion versus the reaction time is

shown in Figure 4.8. At a high reaction temperature, the reaction rate was noticeably high.

4.2.4.1 Determination of Rate Constant (k)

The data from the plot shown in Figure 4.8 were used to calculate the rate constant (k) by using linear regression (Equation 4.2) [211].

$$\ln \frac{[FFA]_t}{[FFA]_i} = -kt \qquad (4.2)$$

where $[FFA]_i$ and $[FFA]_t$ were the FFA values at the start and at a specific time, respectively. The data are shown in Table 4.2.

Table 4.2: Reaction rate constants at different temperatures

Temperature (K)	Rate constant k (s^{-1})	Correlation coefficient (R^2)
303	1.09×10^{-4}	0.9876
313	1.74×10^{-4}	0.9894
323	2.94×10^{-4}	0.9969
333	4.95×10^{-4}	0.9937
338	7.30×10^{-4}	0.9965

ln $[FFA]_t$ / $[FFA]_i$ and time (seconds) were plotted for all of the temperatures (Figure 4.9) and a linear regression of each curve was used to calculate the value of k. The results are presented in Table 4.2. The high values of the linear correlation coefficient (R^2) indicated that the reaction followed the first order kinetics. The esterification reaction of FFA with a large excess of methanol in the oil was also reported to be of the first order [146, 207 and 211].

4.2.4.2 Determination of the Activation Energy

The activation energy (E_a) was calculated by using the Arrhenius Equation (Equation 4.3):

$$\ln k = \ln A - \left(\frac{E_a}{R}\right) \times \left(\frac{1}{T}\right) \tag{4.3}$$

Where A was the frequency factor, E_a was the activation energy (kJ. mol^{-1}), T was temperature (K), and R was the gas constant (JK^{-1} mol^{-1}).

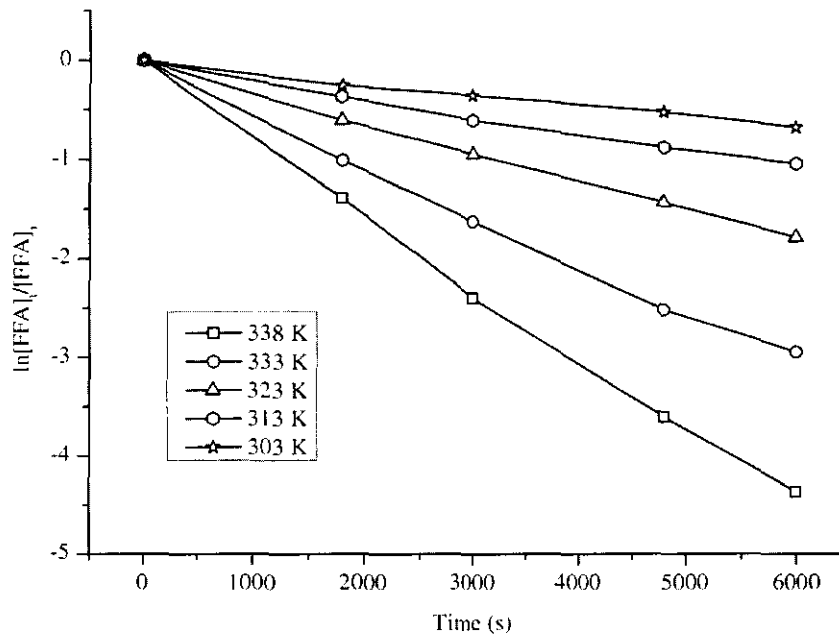

Figure 4.9: Plot between ln [FFA]t / [FFA]i and the reaction time (s)

The plot between ln *k* and 1/T was used to calculate the activation energy (E_a). The plot is shown in Figure 4.10.

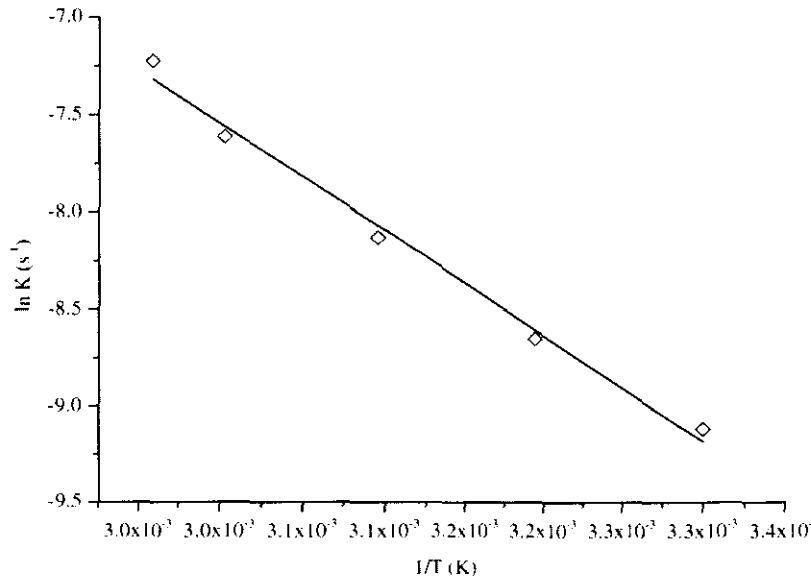

Figure 4.10: Plot between ln k and 1/T (K)

Linear regression of the plot gave the activation energy of the reaction as 45.42 kJ mol^{-1} which was very close to the values (45 kJ mol^{-1} and 51 kJ mol^{-1}) as reported elsewhere [207, 211]. The value of 45 kJ $mol^{-1}$for E_a was reported by using 10 % sulfuric acid as the catalyst and 51 kJ mol^{-1} was reported by using 12-tungustophosphoric acid (1 mol %) as the catalyst for the esterification of the oleic acid [211]. Furthermore, a similar value (46.69 kJ mol^{-1}) of the activation energy was reported by using the $SnCl_2$ catalyst to esterify the oleic acid to a methyl ester in soybean oil [212].

4.2.5 Development of the Catalysts: Findings and Conclusions

In this study, three solid catalysts, namely, silica sulfuric acid (SSA), silica supported boron trifluoride (SSB) and a hybrid catalyst (HC) consisting of a 50-50 mixture of the SSA and SSB, were investigated for the esterification of the high FFA in *Jatropha curcas* oil. It was observed that the catalytic activity of the hybrid catalyst was superior to those of the SSA and SSB alone. There was a strong synergistic effect found in the catalytic activity of the mixed (hybrid) catalyst and an initial FFA value of 45.64 % was 98 % converted to methyl esters. The reaction conditions were optimized for the FFA: methanol mole ratio of 1:15, a reaction temperature of 65 °C and a reaction time of 100 minutes. Furthermore, while using 1.5 wt. % of the hybrid catalyst with the oil samples having FFA values of 6.64 to 45.64, the FFA conversion to methyl esters was more than 98 %.The reaction was found to follow the first order kinetics. The activation energy was calculated to be 45.42 kJ.$mol^{-1}$for 1.5 wt. % of the hybrid catalyst. It has been concluded that the studied hybrid catalyst can be used successfully to esterify FFA to methyl esters in a more efficient way.

4.2.6 Base catalyzed Transesterification

A very small amount of triglycerides can be converted to methyl esters by using an acid catalyst. Therefore, the base catalysed transesterification was performed by using sodium methoxide. It was observed that the pre-treated oil was suitable for the

transesterification reaction and a high conversion of oil to methyl esters, 93.12 %, was achieved.

4.2.6.1 Effect of the Stirring Speed

For investigation of the effect of the stirring speed, a methanol oil mole ratio of 6:1 was used at the reaction temperature of 65 °C and for a reaction time of 60 minutes. The catalyst amount used was 1 wt. % with respect to the oil weight. The results are shown in Figure 4.11. It was found that the reaction efficiency was low at low stirring speeds and became higher at high stirring speeds when the reaction time and temperature were kept constant. It was observed that there was not much improvement in the conversion efficiency when a speed beyond 1000 rpm was used. Therefore, throughout the study, 1000 rpm for the stirring speed was used.

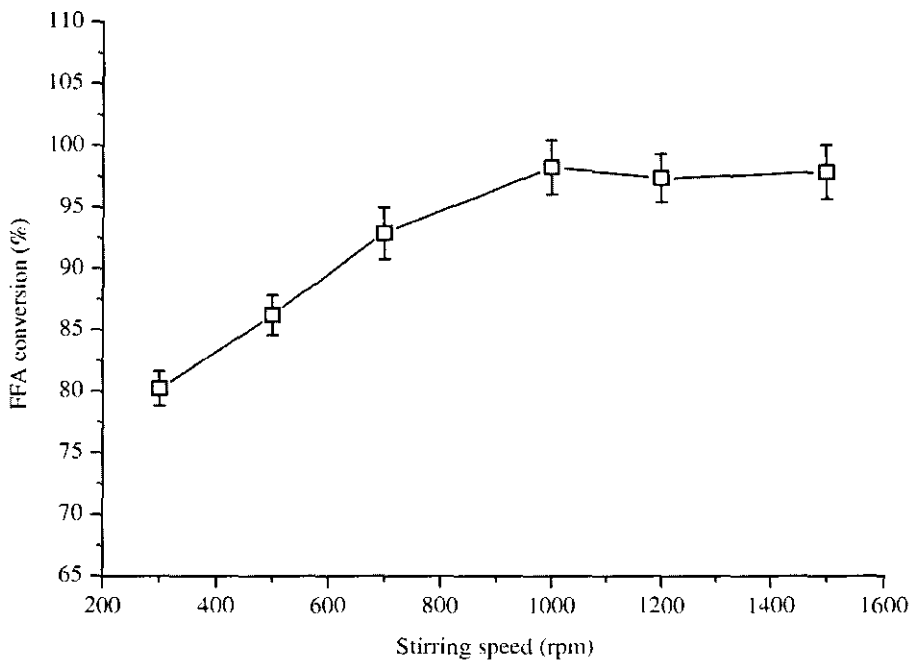

Figure 4.11: Effect of the stirring speed on the methyl ester yield (%)

4.2.6.2 Effect of the Reaction Temperature

The effect of the reaction temperature is directly associated with the reaction time Therefore, a reaction time of 60 minutes was used for all of the investigations with a

fixed stirring speed of 1000 rpm. The findings are presented in Figure 4.12. The yield of the methyl esters was low at 40 and 50°C. It was observed that the maximum yield of methyl esters was obtained at a reaction temperature of 65 °C. A higher reaction temperature was

not possible due to the boiling point of the methanol. For investigation of the effect of the reaction temperature, the methanol-oil mole ratio of 6:1was used with a1 wt. % catalyst with respect to the oil weight. The yield was better at 50 and 60 °C also, but it required longer reaction times.

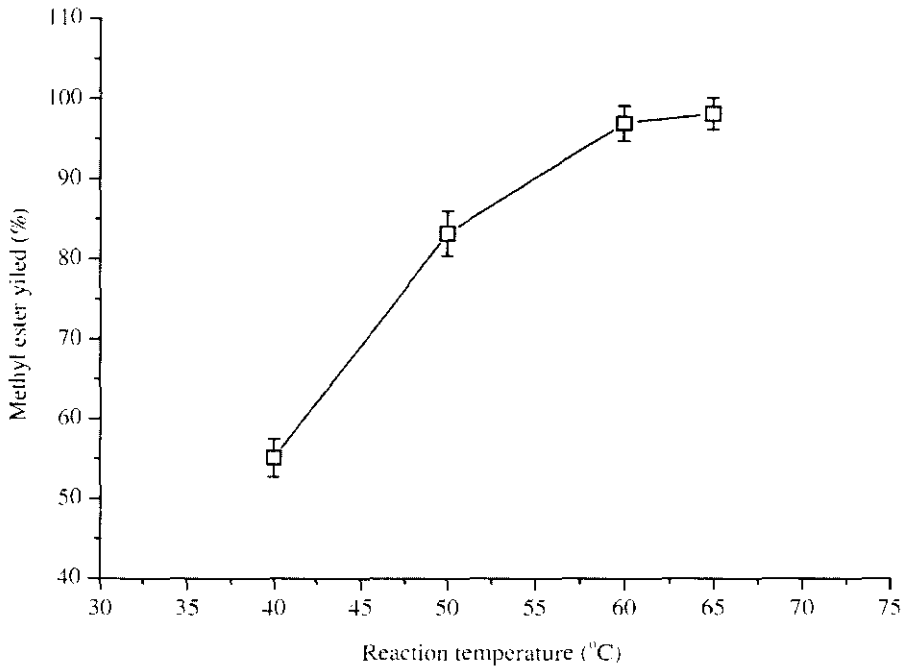

Figure 4.12: Effect of the reaction temperature on the methyl ester yield (%)

4.2.6.3 Effect of the Catalyst Amount

Sodium methoxide was used as the catalyst for this reaction. The catalyst amount is an important factor in a transesterification reaction as there is no reaction without a catalyst in a normal reaction time. Different amounts of catalyst, based on the weight percent (wt. %) of the oil used, were investigated for the conversion efficiency (%) while all other parameters were fixed. The methanol-oil mole ratio of 6:1 was used at the reaction temperature of 65 °C for a reaction time of 60 minutes. The stirring speed

was fixed at 1000 rpm. The results are presented in Figure 4.13. The reaction efficiency became low with a low amount of the catalyst. Consequently, relatively high conversion efficiency was observed with high amounts of the catalyst. However, beyond a 1 wt. % of the catalyst, there was no further improvement in the yield of the methyl esters. Furthermore, the reactants became viscous at higher amounts of the catalyst, and hence the reaction efficiency was lower. In addition, it was also observed that washing of the product was also difficult due to the large amount of emulsions which were difficult to break. From Figure 4.13, it can be noted that a catalyst amount of 1.0 % is optimum. Therefore, a 1.0 wt. % of the sodium methoxide was used throughout the study. Different studies have also reported a similar amount (0.9 -1.0 %) of sodium hydroxide and sodium methoxide [208, 213].

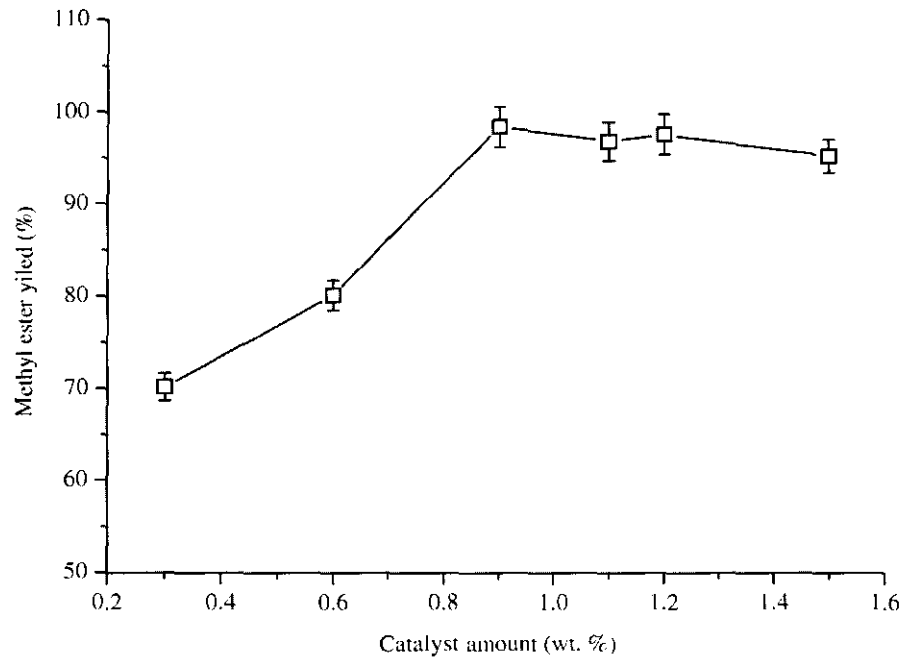

Figure 4.13: Effect of the catalyst amount on the methyl ester yield (%)

4.2.6.4 Effect of the Methanol to Oil Ratio

A stoichiometric amount of methanol for one mole of oil is 3 moles. Increasing the amount of the methanol beyond this limit is not economical. However, if 3 moles of methanol are used, the reaction is usually very slow and never completes due to its reversible nature. This trend was also observed during this reaction. Varying methanol

to oil mole ratios were used to study the effect of the methanol amount on the reaction efficiency. The results are shown in Figure 4.14. The reaction temperature of 65 °C for a reaction time of 60 minutes was used with a fixed stirring speed of 1000 rpm. The catalyst amount used was 1 wt. % with respect to the oil weight. It can be noted that only a 55 % conversion could be achieved by using 3 moles of the methanol. The reaction conversion gradually became better by increasing the amount of methanol. However, any increase in the amount of methanol beyond 6-7 moles did not show any significant effect. Therefore, the optimum amount of methanol was selected as 6 moles per mole of oil. This finding was also according to the results reported in literature [214, 215].

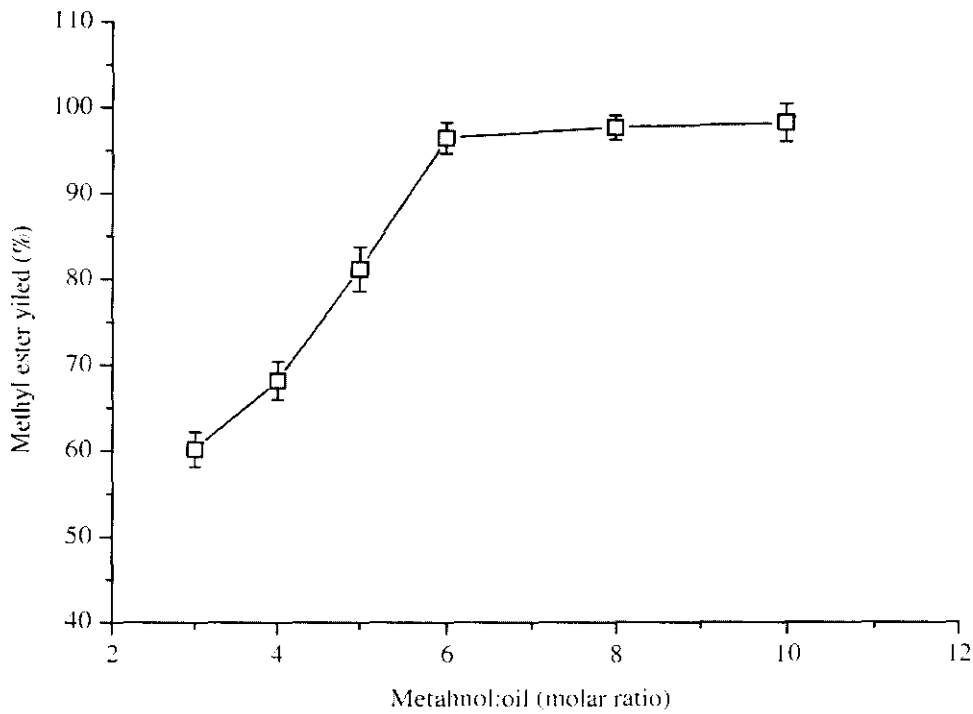

Figure 4.14: Effect of the methanol/oil molar ratio on the methyl ester yield (%)

4.2.6.5 Effect of the Reaction Time

As discussed earlier, reaction time depends upon the reaction temperature. At high a temperature, the reaction was fast. To investigate the effect of the reaction time, a methanol oil mole ratio of 6:1 was used with 1 wt. % of the catalyst. A reaction temperature of 65 °C was used for all of the investigations with a fixed stirring speed

of 1000 rpm. The results are presented in Figure 4.15. It was found that at 65°C, the reaction was completed in 60 minutes. While at 50°C, the reaction was not completed in 60 minutes requiring more time. Therefore, the optimum reaction time was found to be 60 minutes at 65°C.

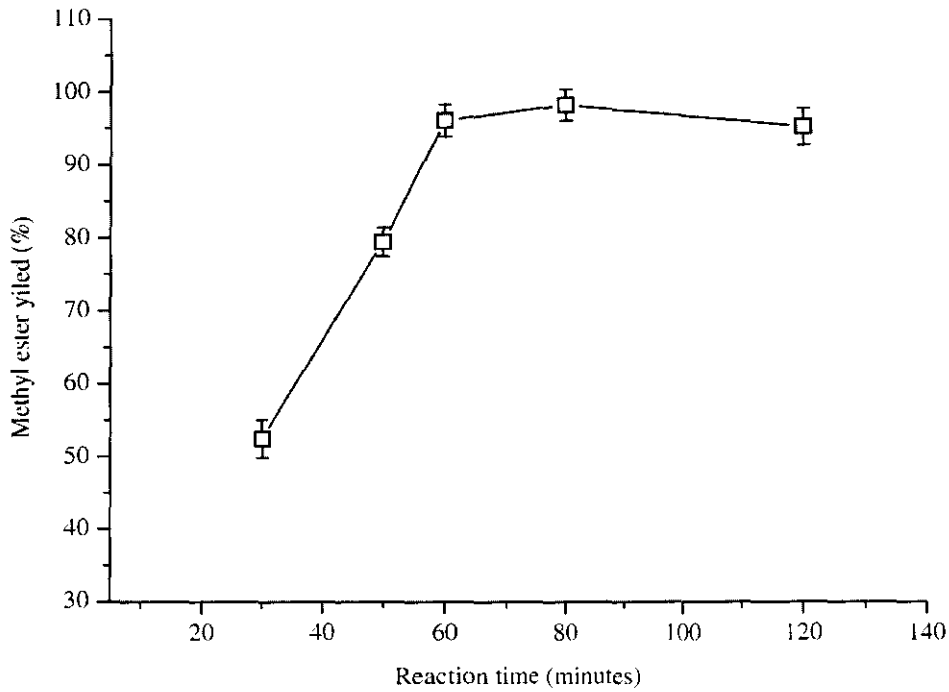

Figure 4.15: Effect of the reaction time on the methyl ester yield (%)

4.2.6.6 Optimum Transesterification of the Reaction Conditions

This study has found that for the base catalyzed transesterification reaction of *Jatropha oil,* a reaction temperature of 65°C is suitable at a stirring speed of 1000 rpm and for a reaction time of 60 minutes. The optimum molar ratio of methanol to oil is six moles and the optimum amount of catalyst is 1 wt. % of the amount of oil used.

4.2.7 Analysis of the Methyl Esters

The obtained methyl esters were analyzed for purity by GC-FID, GC-MS, FT-IR and NMR. The results are presented in the following sections.

4.2.7.1 GC-FID Analysis

Methyl esters were obtained from triglycerides. Traces and remnants of mono, di and triglycerides along with free glycerol were quantitatively determined by using GC-FID. The results are presented in Table 4.3. It can be observed that the amount of total glycerides in all of the three batches was less than 0.01 %, hence the purity of the methyl esters was more than 99 % which is better than the reported studies elsewhere [145].

Table 4.3: Total glycerides (free and bound) examined by GC-FID

Species (μg)	Batch 1	Batch 2	Batch 3
Free glycerol	0.0111	0.0508	0.0422
Mono glycerides	4.2561	2.9642	3.2453
Di glycerides	6.7425	2.4021	6.9495
Tri glycerides	0.3018	0.0136	0.0218
Total glycerides	11.3115	5.4307	10.2588
Sample weight (μg)	1.24E+05	1.17E+05	1.21E+05
Total (wt. %)	0.0091	0.0046	0.0085

4.2.7.2 GC-MS Analysis

A GC-MS analysis was conducted to obtain the fatty acid composition of the methyl esters. It was confirmed that the obtained methyl esters had the same composition as obtained for the characterization of the *Jatropha oil*. The composition of the methyl esters with the retention time of the individual peaks is presented in Table 4.4.

It can be observed that the oleic acid methyl ester was the most abundant ester in the composition with 44.3 % of the total weight of the esters. The second most available ester was linoleic acid with 32.8 % of the total weight. These two unsaturated fatty esters made the *Jatropha oil* methyl esters an important precursor for surfactant synthesis. Due to these two unsaturated methyl esters, the total unsaturated fatty acid contents of the Jatropha methyl esters were 77.1 %. Other fatty esters were saturated,

namely, palmitic acid methyl ester and stearic acid methyl ester, 13.5 % and 7.10 %, respectively.

Table 4.4: Results of the GC-MS analysis

Esters	Retention time	Weight %
Palmitic acid methyl ester	20.080	13.5
Palmitoleic acid methyl ester	23.530	0.9
linoleic acid methyl ester	26.850	32.8
Oleic acid methyl ester	27.140	44.3
Stearic acid methyl ester	27.850	7.10
Others	--	1.4

4.2.7.3 Spectroscopic Analysis

The FT-IR analysis was used to study the functional groups in the product. Despite the fact that the FT-IR spectra of the methyl esters and the natural oil were remarkably similar, yet there were fundamental differences in the range of 1150 to 1250 cm^{-1}. The same effects were found in the synthesized methyl esters also. Three bands at 1169,1195 and 1244 cm^{-1} were found in the methyl esters which were typical for the methyl esters of the natural oils [216]. As the *Jatropha oil* was pretreated, there was no evidence of the presence of the carboxylic acid carbonyl band (1711 cm^{-1}). The carbonyl band from the oil (glyceryl ester) was found at 1746 cm^{-1}. In the methyl esters, however, the carbonyl band (methyl esters) was found at 11742 cm^{-1}.

NMR spectroscopy is a more powerful technique than FT-IR spectroscopy in terms of the structural elucidation of molecules. There are several obvious differences between the spectra of oil and those of methyl esters. In the ^{1}H NMR spectra, glyceryl protons appear at 4.1 and 4.3 ppm in the form of quintets. The presence of these peaks in a spectrum is a confirmed indication of the presence of glycerides [217]. In the methyl esters, these peaks are absent. Therefore, it is a quick test for the presence of glycerides in a sample. A comparison of the ^{1}H NMR spectra of the *Jatropha oil* and methyl esters is shown in Figure 4.16. Further details are presented in Table 4.5.

Table 4.5: FT-IR and NMR data for the Jatropha oil and the Jatropha oil methyl ester

Oil / methyl ester	FT-IR (neat; cm^{-1})	^{1}H NMR (400 MHz, $CDCl_3$)	^{13}C NMR (100 MHz, $CDCl_3$)
Jatropha oil	3007 cm-1(=C-H cis stretch), 2923, 2852 (CH_2 stretch), 1746 (ester C=O), 1654 (-C=C- stretch),1460 (-C-H bend from CH_2, CH_3),1419 (=C-H bend) 1376 (CH_3 sym bend), 1240, 1165, 1118 (ester CO stretch),1099 (C-O stretch), 970 (-HC=CH- bend), 721 (CH_2 rocking).	0.88-0.91 (-C***H***$_3$), 1.32-1.64 (C***H***$_2$), 1.62 (C***H***$_2$-CH_2COOCH_3) 2.06-2.07 (-C***H***$_2$-CH=CH-), 2.29-2.33 (C***H***$_2$$COOCH_3$), 2.81(-CH=CH-C***H***$_2$-CH=CH-), 4.23 (glycerin protons), 5.32 (-C*H*=C*H*-)	14.43-14.46 (-***C***H_3), 23.29-34.37 (***C***H_2), 61.3 (C1, C3 glycerol), 69.7 (C2 glycerol) 129-131 (***C***H=***C***H), and (-***C***H=***C***H-CH_2-***C***H=***C***H-)
Jatropha methyl ester	3006 cm-1(=C-H cis stretch), 2924, 2853(CH_2 stretch), 1742 (ester C=O), 1654 (-C=C-stretch),1459 (-C-H bend from CH_2, CH_3), 1435 (C-H asymm and symm bend of CH_3-COO),1376 (CH_3 sym bend),1361 (-C-H bend), 1244, 1195, 1169 (ester CO stretch),1016 (O-C-C stretch), 722 (CH_2 rocking).	0.89-0.93(-C***H***$_3$),1.33-1.63(C***H***$_2$), 1.63 (C***H***$_2$-CH_2COOCH_3) 2.06-2.07(-C***H***$_2$-CH=CH-), 2.28-2.32 (C***H***$_2$$COOCH_3$) 2.82 (-CH=CH-C***H***$_2$-CH=CH-) 3.62 (C-OO-C***H***$_3$), 5.31 (-C*H*=C*H*-)	14.42-14.45 (-***C***H_3), 23.29-34.37 (***C***H_2), 51.43 (COO***C***H_3), 128-130 (***C***H=***C***H, (-***C***H=***C***H-CH_2-***C***H=***C***H-) 173.97 (-***C***OO-CH_3).

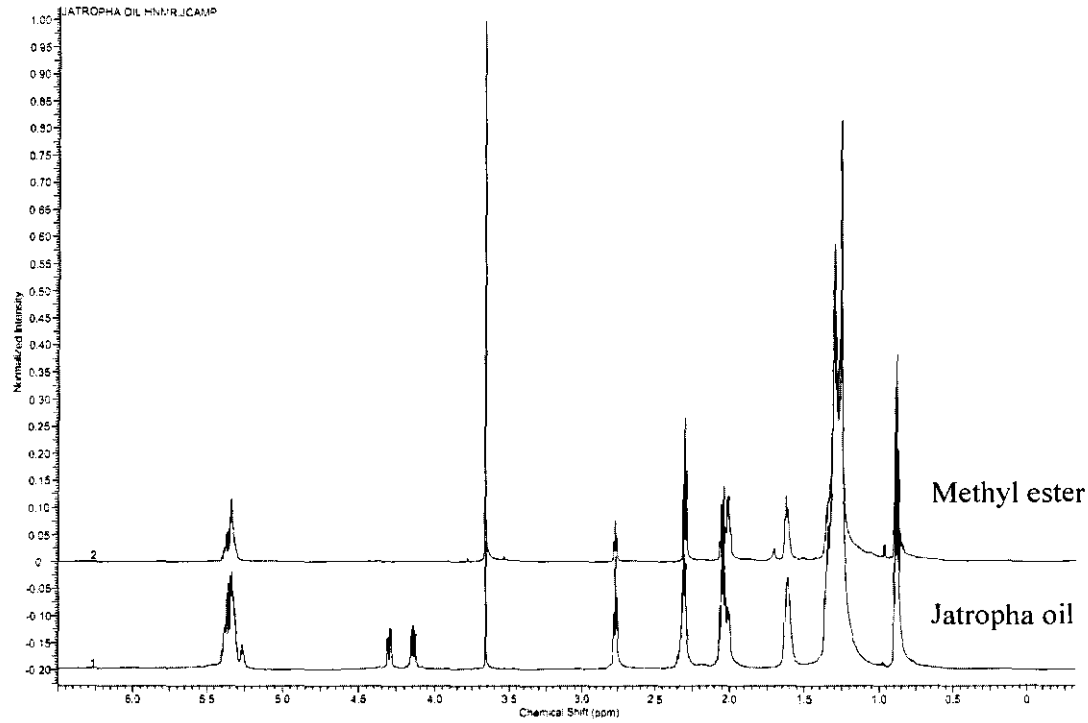

Figure 4.16: Comparison of the 1H NMR spectra of the Jatropha oil and its methyl esters

A few important properties of the obtained methyl esters are presented in Table 4.6.

Table 4.6: Important properties of methyl esters

Property	Value
Fatty ester composition	(wt. %)
Methyl palmitate	13.5
Methyl stearate	7.1
Methyl oleate	44.3
Methyl linoleate	32.8
Iodine Value	101.27 mg I_2 / g
Density (25 °C)	0.9109 g mL^{-1}
Refractive index (25 °C)	1.4689

4.3 Epoxidation of the Methyl Esters

Epoxidized methyl esters were synthesized in the next step. The reaction is shown in Figure 4.17. The reaction is presented for the major unsaturated methyl ester (oleic acid methyl ester **(1)**). In the presence of the hydrogen peroxide and formic acid, the oleic acid methyl ester was converted to the epoxidized methyl ester (methyl 8-(3-heptyloxiran-2-yl) octanoate) **(2)**.

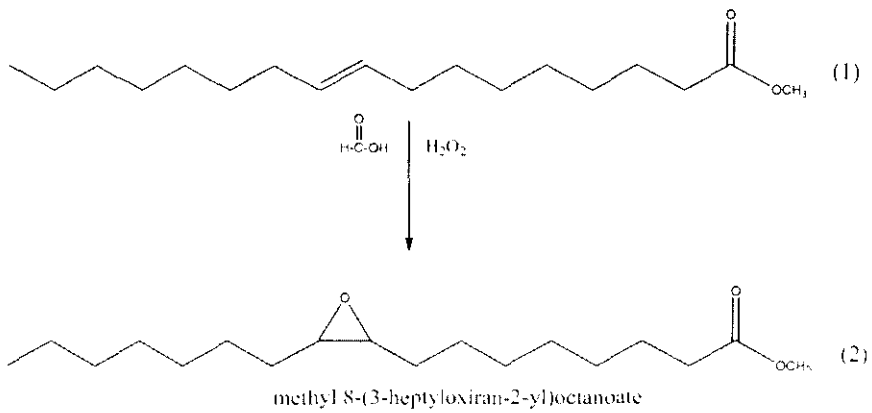

Figure 4.17: Epoxidation reaction of the oleic acid methyl ester

The process of the epoxidation of the methyl esters was optimized by using the response surface methodology (RSM). A total of 30 runs of the experiment were performed according to the scheme calculated by the software. The obtained results are discussed in detail in the following sections.

4.3.1 Optimization of the Epoxidation Reaction Conditions by RSM

Four reaction variables, namely, the hydrogen peroxide concentration, formic acid concentration, temperature and reaction time were studied and evaluated. A set of thirty experiments were performed according to the central composite rotatable design (CCRD). The experimental design with the observed and predicted results for all thirty runs is presented in APPENDIX B as Table B1. The response obtained was correlated with the four independent variables by using a polynomial equation (4.4). The data obtained by CCRD were used to fit an empirical quadratic model and the multiple regression analysis of the experimental data produced the second degree

polynomial equation (in terms of coded factors) for the yield of the epoxidized H-OAME as shown below:

$$y = +72.00 + 11.66X_1 - 2.14X_2 + 9.48X_3 + 8.50X_4 - 0.82X_1X_2 + 4.48X_1X_3 + 1.52X_1X_4 + 1.64X_2X_3 - 2.04X_2X_4 + 1.39X_3X_4 - 5.03X_1^2 - 4.59X_2^2 - 4.82X_3^2 - 4.87X_4^2 \quad (4.4)$$

Here, y is the response factor (Epoxidation yield %) and X_1, X_2, X_3 and X_4 are the coded values of the test variables, i.e., the hydrogen peroxide concentration, formic acid concentration, reaction temperature and reaction time, respectively. The terms X_1X_2, X_1X_3, X_1X_4, X_2X_3, X_2X_4 and X_3X_4 are the first order interaction terms for each paired combination showing the interaction among the pre-defined variables.

The results of the analysis of the variance (ANOVA) for fitting the second-order response surface model by the least-squares method is presented in Table 4.6. A high statistical significance is required for a model to be considered fit for its reliable application. A high significance of the model was indicated by a high F_{model} value of 94.83 at a very low probability of $p < 0.0001$ implying that the model fit was significant with only a 0.01 % chance that the *F model* value of 94.83 could be attributed to noise. In addition, the lack of fit condition for the model was not significant and the fitness of the model was also evaluated by calculating the regression equation and the multiple correlation coefficient, R^2. A high value of R^2 0.9888 indicated that 98.88 % of the response variable (Epoxidation yield) was dependent on the independent variables (X_1, X_2, X_3 and X_4) and only 1.12 % of the total variations were dependent on other variables not defined by the model. Moreover, a high R^2 indicated that this model could be used with reliability to predict the results with good precision. The high reliability of the results from the model was also supported by the low coefficient of the variance (CV = 4.75 %). A low CV indicated a high precision, low scatter and better repeatability in the experimental results. In addition, a high value of the adjusted determination coefficient (Adj. R^2 is 0.9784) also indicated the high significance of the model.

The Normal Plot of Residuals is shown in Figure 4.18 which indicated the normal distribution of the residuals. The points should follow a straight line with a normal acceptable scatter if their distribution is normal. The plot showed that the data distribution was essentially normal.

Table 4.7: Analysis of Variance (ANOVA) for the fitted quadratic polynomial model

Source of variations	Sum of Squares	Degrees of Freedom	Mean Square	*F* Value	*P* Value Probability > *F*
Model	9567.27	14	683.38	94.83	< 0.0001
Hydrogen peroxide / C=C mole ratio (X_1)	3265.03	1	3265.03	453.07	< 0.0001
Formic acid / C=C mole ratio (X_2)	110.12	1	110.12	15.28	0.0014
Temperature (X_3)	2154.80	1	2154.80	299.01	< 0.0001
Reaction time (X_4)	1733.83	1	1733.83	240.60	< 0.0001
X_1X_2	10.84	1	10.84	1.50	0.2389
X_1X_3	321.40	1	321.40	44.60	< 0.0001
X_1X_4	30.72	1	30.72	4.26	0.0567
X_2X_3	692.79	1	692.79	96.14	< 0.0001
X_2X_4	579.00	1	579.00	80.34	< 0.0001
X_3X_4	637.42	1	637.42	88.45	< 0.0001
X_1^2	651.38	1	651.38	90.39	< 0.0001
X_2^2	108.10	15	7.21		
X_3^2	87.52	10	8.75	2.13	0.2095
X_4^2	20.58	5	4.12		
Residual	9675.36	29			
Lack of Fit	9567.27	14	683.38	94.83	< 0.0001
Pure Error	3265.03	1	3265.03	453.07	< 0.0001
Total	110.12	1	110.12	15.28	0.0014

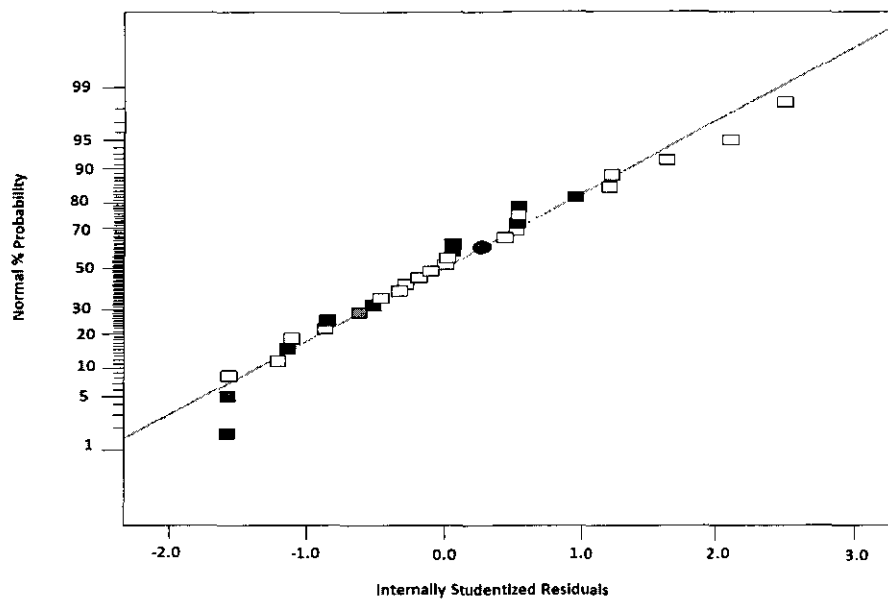

Figure 4.18: Normal plot of residuals

In Figure 4.19, a plot of the actual values against the values predicted by the model is presented. Most of the data points are evenly distributed along the line showing a high value of R^2 (0.9888) and excellent agreement between the experimental results and the model predicted values.

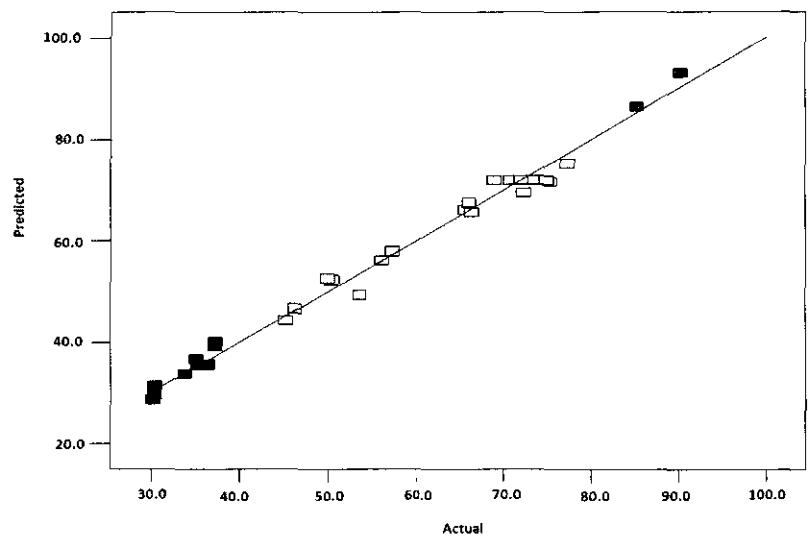

Figure 4.19: Comparison of the actual and predicted values of the response

4.3.2 Effects of the Reaction Parameters

From Table 4.6, individual experimental parameters (X_1, X_2, X_3 and X_4) can be judged for their significance by looking at the corresponding *P*-values. The lower the *P*-values, the higher will be the significance of the corresponding coefficient. In addition, the *P*-values also indicate the strength of the interaction between the cross product of the variables.

Interactions and effects of different variables can be noted by viewing the polynomial model as shown in Equation 4.4. The positive coefficients of X_1 (hydrogen peroxide), X_3 (temperature) and X_4 (time) and for the interaction terms, X_1X_3 (hydrogen peroxide × reaction temperature), X_1X_4 (hydrogen peroxide × time), X_2X_3 (formic acid × reaction temperature), and X_3X_4 (reaction temperature × time) indicated a linear effect of increasing the yield of the epoxidation, while the negative coefficient of X_2 (formic acid), interaction terms, X_1X_2 (hydrogen peroxide × formic acid), X_2X_4 (formic acid × time) and the quadratic terms X_1^2, X_2^2 , X_3^2 and X_4^2 had a negative effect and decreased the yield of the epoxidation.

Moreover, the effect of these parameters on the epoxide yield can be observed by looking at the respective *F*-value and *P*-values shown for each parameter in Table 4.6. The higher the *F*-value (and the lower the *P*-values), the more pronounced will be the effect of the said parameter on the product yield.

The corresponding 2-D contour plots and 3-D response surfaces are graphical representations of the regression equation and can be used to assess the significance of the different parameters for the optimization of the reaction conditions. The contour lines represent the effect of the two parameters on the response variable by using an infinite number of combinations of these variables while keeping the other two variables constant at some specific level. The surface encircled by the smallest ellipse represents the maximum response [218]. Like contour plots, the 3-D response surfaces can also be used for the optimization of the parameters. The 3-D response surfaces of the epoxidation yield (%) predicted from the model are presented in Figures 4.20- 4.25.

Figure 4.20 shows the effects of the hydrogen peroxide formic acid concentrations on the yield. The effect of the varying hydrogen peroxide amount was more significant as

compared to the effect of the changes in the concentration formic acid. This supports the vital role played

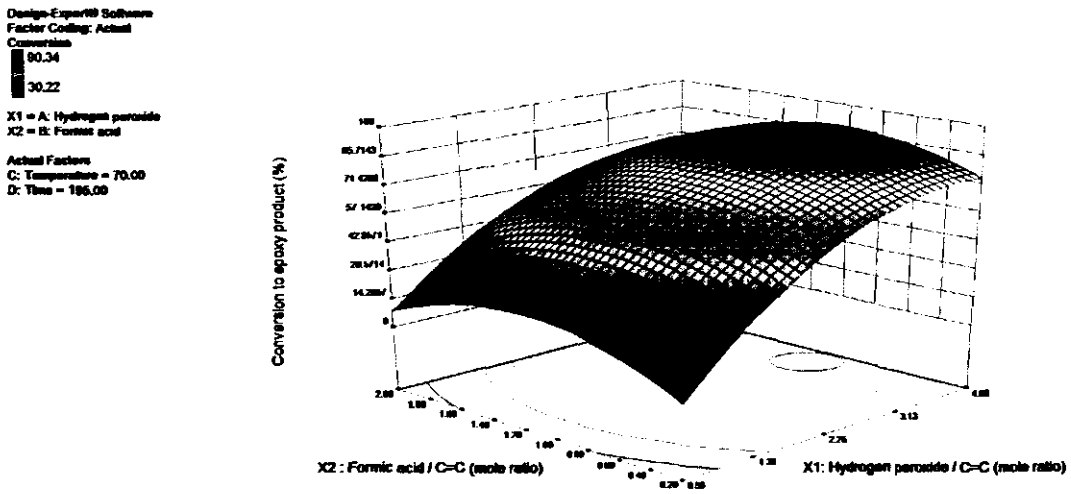

Figure 4.20: Effect of varying the H_2O_2 / C=C mole ratio and formic acid / C=C mole ratio on the response

by the hydrogen peroxide in generating the peroxy formic acid for the oxirane generation while it is opposite the "regenerating" role of the formic acid. Therefore, almost a linear effect in increasing the yield can be observed by increasing the hydrogen peroxide amount while the increase in the formic acid amount is comparatively less important. However, the yield will be very low at very low formic acid amounts and will also decrease at an excessively high concentration due to the oxirane ring opening. The optimum conditions were determined as 3.32 moles of hydrogen peroxide / C=C moles and 0.90 moles of formic acid/C=C moles while the temperature and time were fixed at 70 °C and 264 minutes, respectively.

Figure 4.21 represents the effects of the amount of the formic acid and the reaction time. The effect of the formic acid amount was positive up to a value of about 0.80 – 1.10 moles / C=C moles and after that it became negative. While the reaction temperature had a relatively more significant and positive effect up to about 300 minutes and then it formed formic acid and became non effective. The optimum conditions can be assessed at 1.00 mole of 307.50 minutes reaction time. The hydrogen peroxide and the reaction temperature were fixed at 2.96 moles and 70 °C, respectively.

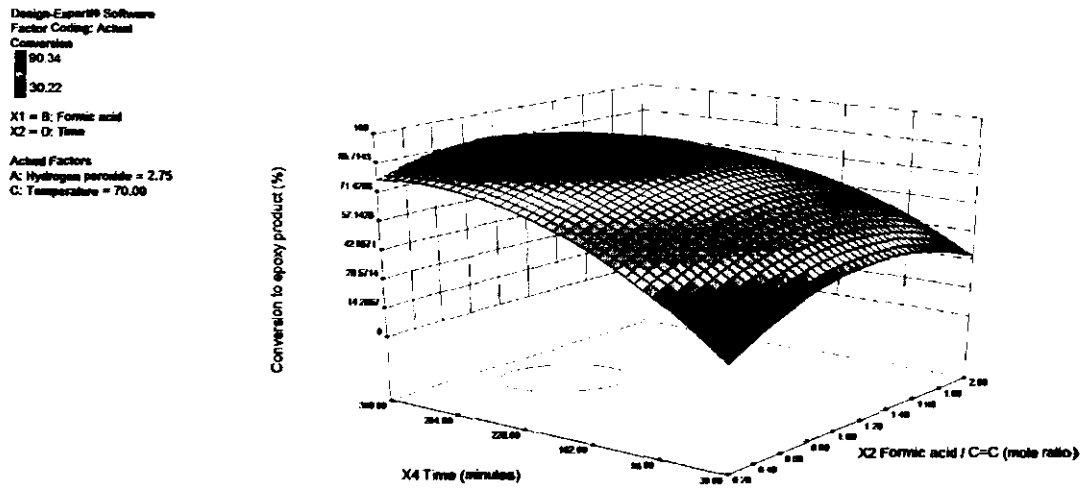

Figure 4.21: Effect of varying the reaction time and the formic acid / C=C mole ratio on the response

In Figure 4.22, the relationship between the amount of hydrogen peroxide / C=C mole ratio and the temperature is shown. The hydrogen peroxide effect was linear over a wide range but the temperature effect was marginally negative at higher values.

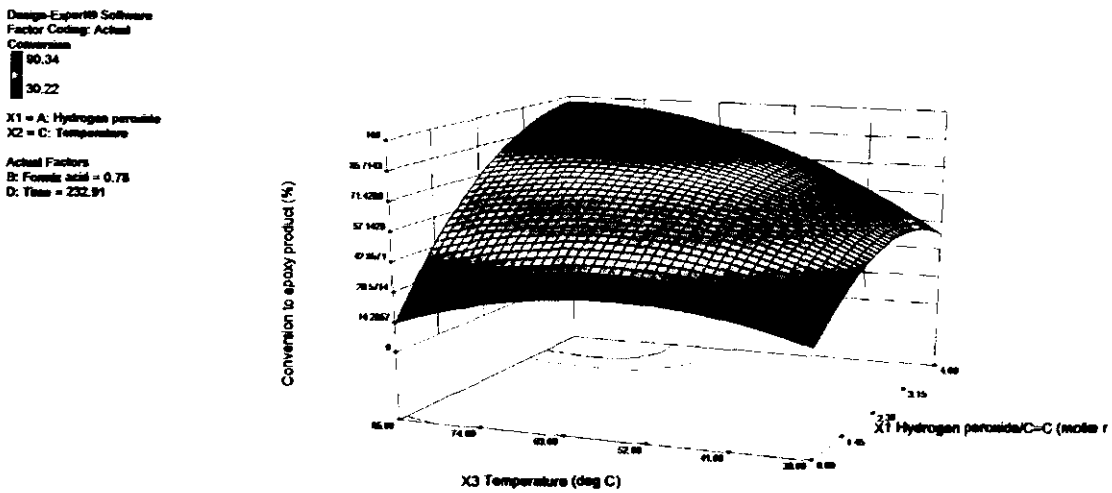

Figure 4.22: Effect of varying the reaction temperature and the H_2O_2 / C=C mole ratio on the response

On the whole, temperature appears to have a more significant effect compared to hydrogen peroxide. The optimum conditions can be assessed at the hydrogen peroxide / C=C mole ratio of 3.88 and a reaction temperature of about 67.5 °C. The reaction

time and formic acid concentration was fixed at 240 minutes and 1.06 moles, respectively.

Figure 4.23 shows the effect of the varying amount of the hydrogen peroxide / C=C mole ratio and the reaction time. Here, the variation in the amount of hydrogen peroxide is relatively more significant than the variation in time. An amount of about 3.81 moles of hydrogen peroxide / C=C moles and 300 minutes for the reaction time can be found to be optimum. The formic acid concentration was fixed at 1 mole / C=C moles and the reaction temperature was fixed at 70°C.

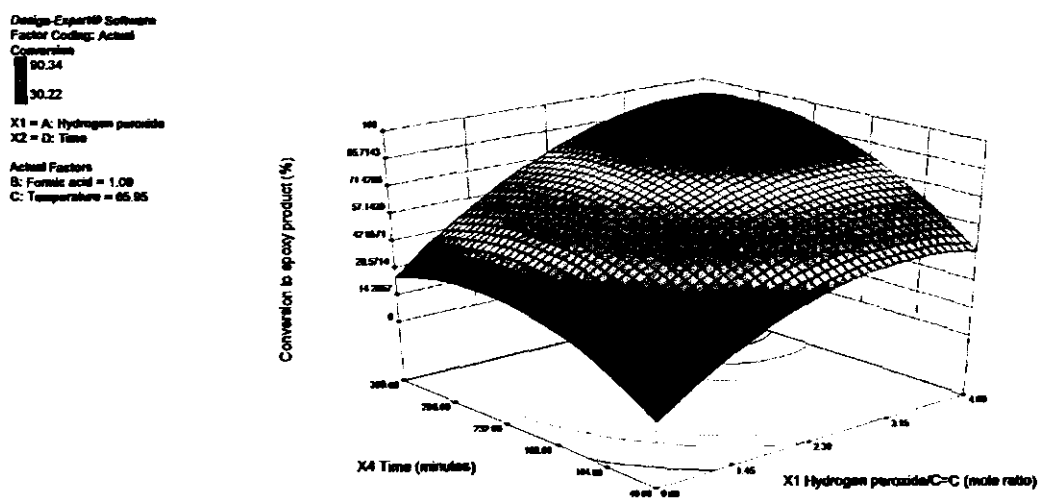

Figure 4.23: Effect of the varying reaction time and the H_2O_2 / C=C mole ratio on the response

Figure 4.24 presents the effect of the varying reaction temperature against the moles of formic acid / C=C moles. The effect of the variation of the reaction temperature was more significant as compared to the relative change in the formic acid amount. This relationship, once again revealed the ability of the regeneration of the formic acid, hence variations in its amount were less effective. However, the temperature showed its effect on the yield by affecting the oxirane generation and the oxirane ring opening reactions. The optimum conditions revealed here were 0.95 moles of formic acid / C=C moles and the temperature of 75.51°C when the hydrogen peroxide concentration and reaction time were fixed at 2.96 moles and 240 minutes, respectively.

Figure 4.25 explains the effect of the varying reaction temperature and reaction time on the response. It is obvious that the effect of the reaction temperature

was more pronounced (more curvature) than that of the reaction time. The reaction temperature, up to about 75°C, had a positive effect and after that, the effect became negative as the oxirane opening reaction commenced. Likewise, at a suitable temperature, the reaction time had a positive effect up to about 250 minutes and after that, it became negative. The optimum temperature and reaction time can be assessed as 72.01 °C and 295 minutes, respectively, while the hydrogen peroxide and formic acid were fixed at 2.96 and 1.00 moles, respectively.

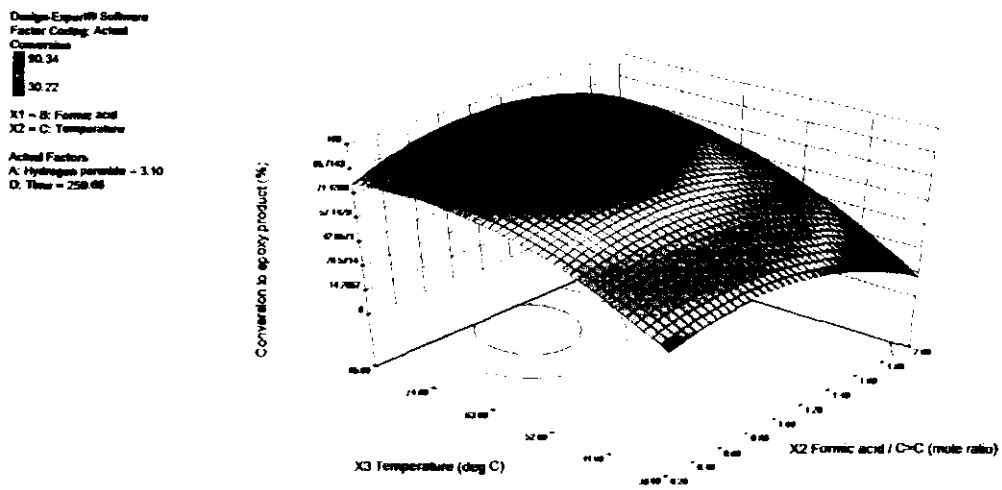

Figure 4.24: Effect of the varying reaction temperature and formic acid / C=C mole ratio on the response

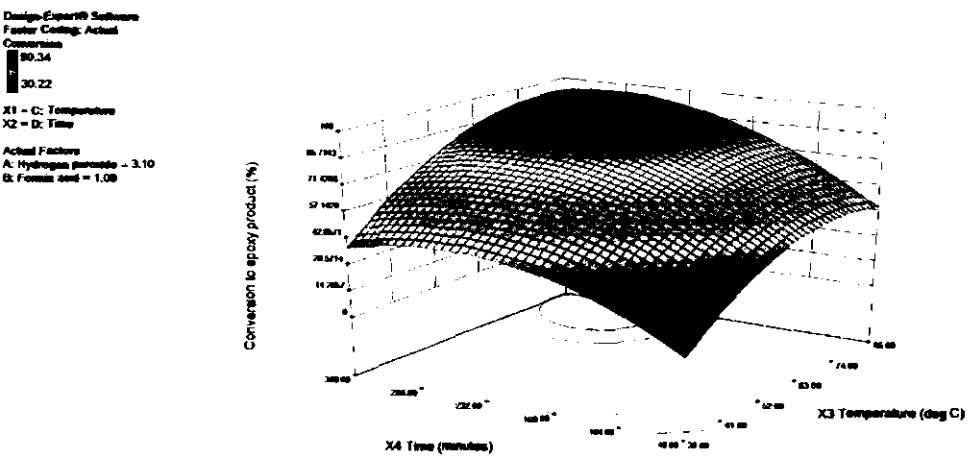

Figure 4.25: Effect of the varying reaction temperature and the reaction time on the response

4.3.2.1 Hydrogen peroxide

The hydrogen peroxide concentration (H_2O_2 / C=C mole ratio) is the most significant first order reaction term. While the role of the hydrogen peroxide is directly associated with formic acid, the latter is not as significant as former. Hydrogen peroxide is the oxidation agent for generating peroxy formic acid. Therefore, hydrogen peroxide and formic acid should be equally significant because peroxy formic acid is the product of the two. However, the concentration of the hydrogen peroxide is more important than that of the formic acid since formic acid can be regenerated from peroxy formic acid after utilizing its oxygen atom. This fact was observed in this study and was also reported by Goud et al. elsewhere [107]. Therefore, for the generation of the peroxy formic acid, the hydrogen peroxide concentration was a more important parameter than the formic acid concentration.

4.3.2.2 Reaction Temperature

The reaction temperature is the second most significant reaction parameter. The first order term of the reaction temperature had a more significant effect on the epoxidation reaction than the reaction time and formic acid concentration. The role of the reaction temperature in this reaction was multifarious: it was important in the generation of the peroxy acid (the sole oxygen carrier), the epoxidation of the double bond, and then in the opening up of the oxirane ring (undesired reaction) in the presence of the formic acid. At low temperatures, the overall epoxidation reaction was very slow (requiring long reaction times) and at a high temperature, the yield became low when the opening of the oxirane ring intensified. Therefore, a careful control of the reaction temperature was highly desired for good epoxidation yields. The effect of the temperature on the epoxide yield was in accordance with the literature reported studies [165, 219 and 220].

4.3.2.3 Reaction Time

Reaction time also has a significant role in the epoxidation reaction. As the ring opening reaction is also associated with the ring generation reaction, prolonged

reaction times promote the former. However, long reaction times at lower temperatures can lead to a high yield of oxirane with the minimum ring opening reaction. The comparatively less significant quadratic term of the reaction time suggests that the effect is almost linear with less curvature effect. Therefore, in some studies, longer reaction times were used for a good product yield but in this study, the reaction was completed in a relatively short reaction time with a high product yield [167].

4.3.2.4 Formic Acid Concentration

The formic acid played a less significant role as compared to the other three reaction parameters. This was mainly due to the regenerating nature of this reactant. Therefore, the concentration effect was relatively less pronounced than that for the hydrogen peroxide. However, in ring opening reactions, the role of formic acid has been presented in literature and the findings in this study were similar [220].

4.3.3 Validation of the RSM Model

The model shown in Equation 4.4 was employed for the optimization of the reaction parameters. The model predicted that the maximum yield of the oxirane at 94.9 % with a standard error of prediction of 1.68 could be obtained by using 3.12 moles of the hydrogen peroxide / C=C moles, 0.96 moles of the formic acid / C=C moles, at the reaction temperature of 70.00 °C for 277.50 minutes of reaction time. The experimental yield by using these optimized conditions was found to be 92.89 % which was significantly higher than the previously reported values. When compared to the results reported in literature [167, 221], there is a marked difference in the formic acid amount used and a relatively higher amount of formic acid used in this study. It may be concluded that a lower amount of formic acid requires a longer reaction time to complete the reaction. When the formic acid is used in higher amount (e.g. 1 mole), a relatively shorter reaction time gives a high conversion, provided that the higher amount of the hydrogen peroxide is used, as explained by the current study.

4.3.4 Characterization of the Epoxidized Methyl Esters

The obtained methyl ester epoxides were characterized by several techniques. The results are presented in Table 4.8.

Table 4.8: Results of the GC-MS results for the oxirane analysis

Species (methyl ester)	Retention time (minutes)	Contents (wt. %)
Palmitic	12.74	13.03
Stearic	16.74	6.97
Oxirane	19.805	1.75
Oxirane	20.10	70.91
Oleic	22.722	1.86
Linoleic	23.258	2.94

The titrimetric analysis was performed according to the AOCS official method Cd 9-57 which delivered the oxirane value of 5.57 %. Therefore, the overall conversion efficiency was found to be 92.89 %. The oxiranes were also analyzed by GC-MS. The details of the peaks with their retention times are presented in Table 4.8. The GC-MS analysis showed that the total oxirane content was 72.66 % (Table 4.8). The conversion efficiency can be calculated as 94.24 %. On the other hand, the amount of the oxirane in terms of total weight % from the titrimetric analysis (AOCS Cd 9-57) was 5.57 % of the oxirane oxygen. The theoretical amount of the oxirane value was 6.0 % (section 3.5.1). Hence, the conversion efficiency in terms of the oxirane oxygen can be calculated as 92.83 %. Therefore, the conversion efficiencies from both the GC-MS and AOCS Official Method Cd 9.57 were 92.89 % and 94.27 % which were fairly close.

4.3.5 FT-IR and NMR Spectroscopic Analysis of the Epoxidized FAME

The FT-IR and NMR data for H-OAME **(1)** and the epoxy methyl esters **(2)** are presented in Table 4.9 with the group assignments; the ^{1}H NMR analysis confirmed [170] the presence of the oxirane ring at 1.5 ppm and 2.84 ppm as shown by peaks A

and B in Fig. 4.26 while the ^{13}C NMR (not shown) showed the oxirane carbons at 56.74 ppm. Unsaturation has completely been vanished as indicated by the absence of the peaks at 2.1 ppm and 5.41 ppm in the ^{1}H NMR spectrum and at 130.59 ppm in the ^{13}C NMR spectrum.

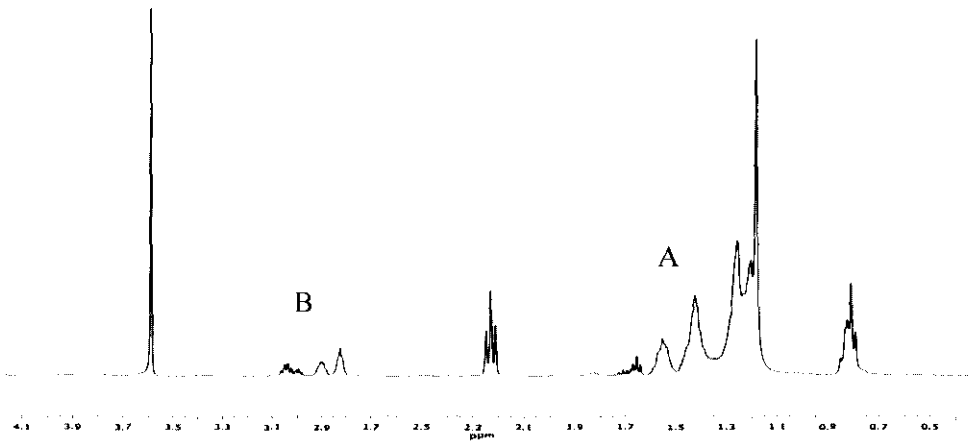

Figure 4.26: ^{1}H NMR spectrum of methyl esters from the Jatropha oil

Table 4.9: FT-IR and NMR data for the epoxidized methyl esters **(1)**

FT-IR (neat; cm^{-1})	^{1}H NMR (400 MHz, $CDCl_3$)	^{13}C NMR (100 MHz, $CDCl_3$)
3468 (OH stretch), 2920 cm^{-1}, 2854 (CH_2 stretch), 1739 (carbonyl stretch), 1459 (CH_2 bend), 1436 (C-H asymm and symm bend of CH_3-COO), 1363 (CH_3 sym bend), 1246, 1196, 1170 (ester CO stretch), 1014 (O-C-C stretch) 846, 827 (C-O-C epoxide stretch) 723 (CH_2 rocking).	0.88-0.94 (-CH3), 1.31-1.53 (CH_2) ,1.49-1.51 (-CH_2-CHOCH-CH_2-) 1.61(CH_2-CH_2COOCH_3) 2.29-2.31 (CH_2COOCH_3) 2.84 (-CHOCH-), 3.62 (C-OO-CH_3),	14.34-14.42 (-***C***H_3), 23.28-34.37 (***C***H_2), 51.43 (COO***C***H_3), 56.74 (-***C***HO***C***H-) 173.94 (-***C***OO-CH_3)

4.3.6 Epoxidation of the Methyl Esters: Findings and Conclusions

RSM based on CCRD was successfully applied for optimization of the reaction parameters for the epoxidation of the methyl esters by using hydrogen peroxide and formic acid. The effects of the hydrogen peroxide / C=C mole ratio, formic acid / C=C mole ratio, reaction temperature and reaction time on the epoxidation reaction yield were also studied for optimization. A polynomial quadratic model was calculated to predict the maximum yield and the optimization of the reaction parameters. The model revealed that the epoxidation yield was more sensitive towards the reaction temperature and the hydrogen peroxide / C=C mole ratio as compared to the formic acid / C=C mole ratio and reaction time. The model was used to optimize the conditions for the maximum epoxidation yield. The optimum conditions predicted were at 3.12 moles of hydrogen peroxide / C=C moles, 0.96 moles of formic acid / C=C moles, reaction temperature of 70.00 °C and 277.50 minutes of reaction time. The predicted yield was 94.90 %. The optimized reaction delivered a 92.89 % yield of the epoxidation for the methyl esters. The current study has suggested a relatively higher amount of formic acid required for a high yield in a short reaction time than the amounts that have appeared in literature. It has also been revealed that the RSM can be successfully utilized to optimize the process conditions and understand the effects and interactions of the reaction parameters for the epoxidation reaction.

4.4 Attachment of Side Chains to the Methyl Esters

The attachment of side chains to the methyl esters will be discussed in this section. It is the third synthesis step of the synthesis of the surfactants, after the transesterification and the epoxidation reaction.

4.4.1 Alkoxylation Reaction

The reaction scheme is shown in Figure 4.27. Alcohols of varying chain lengths were used for the side chain attachments to the epoxidized methyl esters. The oxirane ring of the epoxidized methyl ester was opened by alcohol in the presence of BF_3 as the catalyst. The alcohol was attached with an ether linkage, thereby attaching the

pendent chain structure to the main chain of the methyl ester producing a 9-alkoxy-10-hydroxy-octadecanoic acid methyl ester. An alkoxy molecule depends on the type of alcohol molecule used.

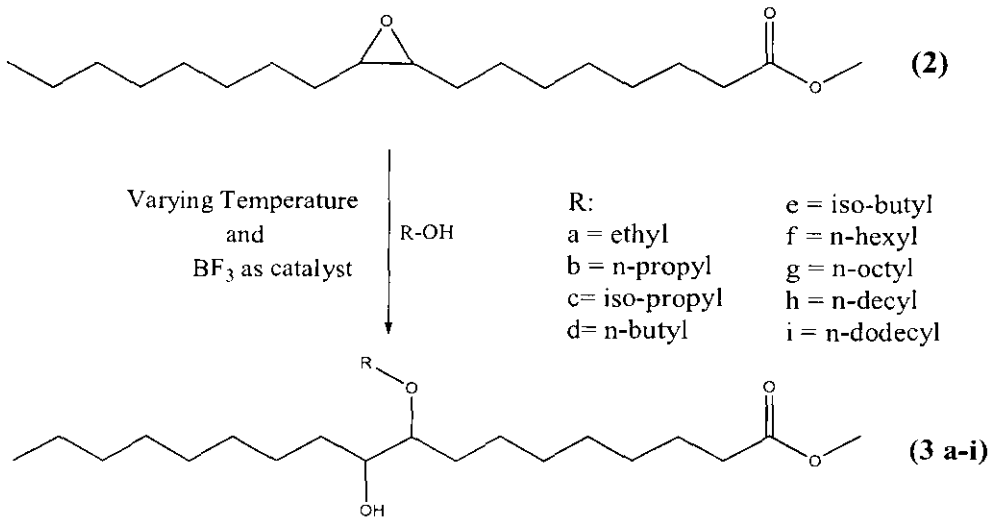

Figure 4.27: Alkoxylation reaction producing a 9-alkoxy-10-hydroxy-octadecanoic acid methyl ester

4.4.1.1 Types of Alcohols used in the Alkoxylation Reaction

Nine alcohols, **R – OH, (R = a –i)** were selected for the attachments of the side chains to the methyl esters. These alcohols included ethanol **(a)**, *n*-propanol **(b)**, iso-propanol**(c)**, *n*-butanol **(d)**, iso-butanol **(e)**, *n*-hexanol **(f)**, *n*-octanol **(g)**, *n*-decanol **(h)** and *n*-dodecanol **(i)**. The selection of the alcohol type was based on the alkyl groups, based on which the alcohols could roughly be divided into: short chain (ethanol, *n*- propanol and *n*-butanol), branched (iso-propanol, iso butanol) and long chain (*n*-hexanol, *n*-octanol, *n*-decanol and *n*-dodecanol) alcohols.

The structures of the alcohols are shown in Table 4.10.

Table 4.10: Types of alcohols used in this study

Alcohol	Structure
ethanol	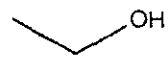
n-propanol	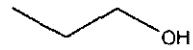
iso-propanol	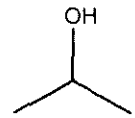
n-butanol	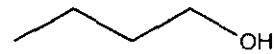
iso-butanol	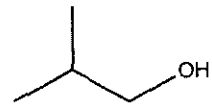
n-hexanol	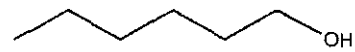
n-octanol	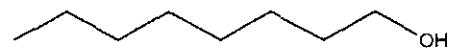
n-decanol	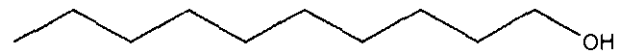
n-dodecanol	

4.4.1.2 Reaction Conditions

The opening of the oxirane ring by alcohols was achieved by using the BF_3-etherate complex [114]. It was ensured that the reactants (alcohols and oxiranes) and the apparatus were meticulously dried before starting the reaction. Dry conditions were maintained throughout the reaction using a $CaCl_2$ dry tube. Moisture, if present in the reagents, would compete for the ring opening with the alcohol molecules. Therefore,

the presence of moisture would result in the formation of a di-hydroxy product. Moreover, water also has a high affinity for BF_3 and a considerable catalyst could be lost in the presence of water by forming other products such as $B(OH)_3$ (boric acid) and HBF_4 (flouroboric acid). Due to the volatile nature of BF_3 gas, the BF_3 solution was injected beneath the surface of the alcohol to minimize the loss of the BF_3 gas.

Table 4.11: Conditions and product yield for the alkoxylation reaction

Alkoxy methyl esters	Reaction conditions		Yield (%)	Exchange of alcohol (%)
	Temperature (°C)	Time (minutes)		
3a	40	30	91.3	0.85
3b	40	30	90.7	0.61
3c	50	45	88.6	1.13
3d	50	45	90.7	1.33
3e	50	45	86.4	0.91
3f	50	45	87.1	0.81
3g	50	45	87.5	1.23
3h	50	45	84.1	1.56
3i	50	45	82.2	1.76

4.4.1.3 Attachment of small chain alcohols

For the ethanol and *n*-propanol, the exothermic reactions maintained the temperatures above 40 °C. External heat was only provided for the last 5 minutes when the temperature reduced to 35 °C. The progress of the reaction was monitored by the oxirane estimation. The oxiranes were fully consumed after 30 minutes of the reaction. The products were analyzed by using GC-MS and a good yield was obtained: 93 and 90 % for the methoxy and *n*-propoxy methyl esters, respectively (Table 4.11). The reaction of the small chain alcohols was essentially completed with good product yields due to less steric hindrance and better mass transfer due to the smaller size of these alcohols. Due to the small hydrophobic chain length, these

alcohol molecules contained a stronger negative charge on the oxygen molecule and the bond between the oxygen and hydrogen was more polar in nature. Therefore, a better reaction in the presence of BF_3 was expected.

4.4.1.4 Attachment of branched and long chain alcohols

For branched chain (iso-propoxy and iso-butoxy) and longer chain (*n*-butoxy, *n*-hexoxy, *n*-octoxy, *n*-decoxy and *n*-dodecoxy) alcohols, a higher temperature (50 °C) and longer reaction time (45 minutes) was required. For these alcohols, a slower addition of the oxiranes was adopted and it was observed that the temperature tended to drop after rising to 35°C. When a drop in temperature was observed, slow heating was commenced until the oxiranes were found to be absent from the mixture. The obtained yield was 82.2 – 91.3 % as reported in Table 4.11.

When the alkoxylation reaction was performed at higher temperatures (≥ 60 °C) in the presence of a catalyst and an excess of alcohol, it was possible that the reactant alcohol could be exchanged with the ester alcohol, hence giving mixed ester groups. In order to overcome this problem, only a slight excess of alcohol was used more than the required stoichiometric amount. In addition, the reaction was performed under milder temperature (40-50 °C) conditions. The extent of the exchanged alcohol was determined by using GC-MS and it was found to be less than 1.76 %, the maximum for *n*-dodecanol (Table 4.11).

A relatively higher reaction temperature (45 °C) and longer reaction time (50 minutes) were required for a complete reaction involving iso-propanol, *n*-butanol, iso-butanol, *n*-hexanol, *n*-octanol, *n*-decanol and *n*-dodecanol. Two factors, namely, the chain length and branching were important in this context. The reaction was slow in cases of branched and long chain alcohols, hence they required more time and heat. This finding of this study was also reported elsewhere [173].

4.4.2 Removal of Excess Alcohol

As these long chain alcohols were not water soluble and had high boiling points, a careful calculation based on the available oxirane oxygen was made and exactly 0.1

moles against 0.095 moles of oxiranes were used. After the reaction was complete, any excess alcohols, if found by the GC-MS analysis, were removed by vacuum distillation and steam distillation. The details are presented in Table 4.12. The steam distillation technique was used for alcohols with longer chains than *n*-butanol. Alcohols with small chains such as ethanol, *n*-propanol and iso-propanol were water soluble, so were easily removed by repeated water washings. However, alcohols with medium chains and long chains were insoluble in water, and therefore, could not be removed by water washings. Steam distillation at normal pressure was used for the removal of these alcohols. The FT-IR spectra were used to verify the completion of the process. It was observed that the alcohols with medium chains such as *n*-butanol, iso-butanol and hexanol were easy to remove with steam distillation. A distillation time of 30-45 minutes was found to be enough for the removal of the last traces of alcohols from the product. However, longer chains, due to their higher boiling points and relatively less solubility in water were difficult to remove. For example, *n*-dodecanol took six hours for the complete removal from the product. Due to the high boiling points of these alcohols, there was a chance that the product may have also been carried out by the steam. For the verification, the removed alcohol was separated from the distillate and dried on anhydrous sodium sulfate.

The FT-IR spectra of "waste" alcohol confirmed that a negligible amount of the product was carried away by the alcohol. The FT-IR spectra for dodecanol are shown in Figure 4.28. From Figure 4.28, it can be noted that the band at 1742 cm^{-1} was due to the ester carbonyl of the product. A relatively small amount of the product was carried away with the dodecanol in the distillate during the steam distillation reaction. This was the alcohol with the longest chain length; therefore, distillates from the other alcohols had an even less amount of product carry-over.

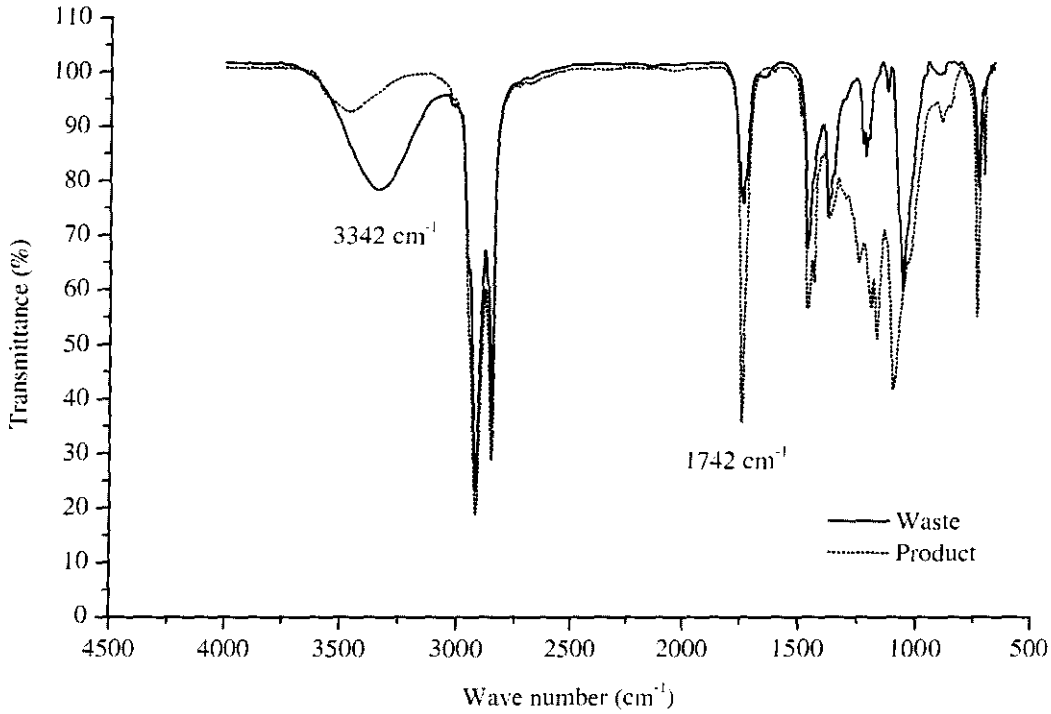

Figure 4.28: FT-IR spectra of the "waste" dodecanol and the product with dodecanol

Table 4.12: Removal of excess alcohols from alcohol attachment products, (W= water washings), (S = Steam distillation)

Product	Alcohol separation technique	Distillation time (minute)
3a	W	N/A
3b	W	N/A
3c	W	N/A
3d	S	45
3e	S	30
3f	S	60
3g	S	120
3h	S	300
3i	S	360

4.4.3 Characterization of the Product

Alkoxy-hydroxy methyl esters were characterized by using the FT-IR and NMR spectroscopy. In addition, the oxirane value was also determined to make sure that there were no remnants of the oxiranes.

4.4.3.1 Oxirane Oxygen

The oxirane group was consumed in the alkoxylation reaction and after the complete reaction, there should not be any oxirane oxygen left in the sample. The analysis (AOCS Official Method Cd 9-57) results showed the complete disappearance of the oxirane group from the methyl esters.

4.4.3.2 FT-IR and NMR Spectroscopic Analyses

In the alkoxylation reaction, the oxirane group vanished and two new groups, namely ether and hydroxy, appeared on the molecule. The -OH group was attached to the opposite side of the ether group, as has already been shown in Figure 4.28. FT-IR spectroscopic analysis confirmed the presence of both groups. The major groups found in the FT-IR spectra are presented in Table 4.13.

The FT-IR bands for the epoxy methyl esters are discussed in detail in section 4.3.4.3.The spectra of the alkoxylated methyl esters are discussed below with the group assignments according to several studies [210, 222-224]. All spectra are also shown in Figures C7-C9 in APPENDIX C.

All of the spectra showed identical bands in the 3450-3470 cm^{-1} region. This was due to the -OH stretch originated from the hydroxyl groups attached at the *trans* position of the ether attachment. A very prominent pair of bands present at 2924 and 2824 cm^{-1} was due to the $-CH_2-$ stretching vibrations. The band representing the carbonyl (C=O) stretching vibrations was located at 1741 cm^{-1}. This important band differentiated the esters from the acids; in case of the later, the band appeared at 1708 cm^{-1}. The typical ester C-O stretching vibration bands for the methyl esters were present at 1245, 1197 and 1170 cm^{-1}. In oleo chemicals, these bands were specifically for the methyl esters,

and hence specified their presence [216]. The most important band which represented the C-O-R linkage, i.e., the ether linkage, typically appears at 1090 cm^{-1}. In all nine attachments, these bands appeared at 1085 -1095 cm^{-1}. The details are shown in Table 4.13. The long methyl ester chain $-CH_2-$ group rocking vibrations appeared at 722 cm^{-1}.

Table 4.13: Appearances of the Hydroxyl and Ether linkage bands in the alkoxy products

Product	-OH band (cm^{-1})	C-O-R band (cm^{-1})
3a	3456	1085
3b	3463	1087
3c	3456	1070
3d	3463	1092
3e	3455	1089
3f	3455	1093
3g	3456	1095
3h	3456	1095
3i	3463	1095

The ^1H NMR and ^{13}C NMR spectra for the alkoxy biodiesel was confirmed according to many studies [139, 170 and 225-229] by the attachments of the alkoxy groups since the peaks for the protons (attached with carbon bearing oxirane) were absent from 1.5 ppm and 2.9 ppm in ^1H NMR. As the opening of the oxirane ring with alcohol produced an –O-R group attached to the 9th carbon and an –OH group attached to the 10th carbon (or vice versa), two new peaks in the range of (3.12 ppm - 3.14 ppm) and (3.58 ppm – 3.62 ppm) appeared in all of the spectra of all of the alcohols. The only exception for the proton attached to the 9th carbon was from the iso-propoxy attachment, which maintained the signals at 2.73 ppm and 2.99 ppm. In ^{13}C NMR, the peaks at 54.54 ppm and 57.02 ppm disappeared. These were from the carbons, 9th and 10th, bearing the oxirane ring. New peaks appeared as the 9th and 10th carbon were presently bearing -OR and -OH groups. For ***C***-O-R, the range of the signal was 83.65 ppm to 83.74 ppm. Only two exceptions were found here: the peak from ***C***-O-R for

the methoxy was at 85.38 ppm and from the iso – propoxy was at 80.91 ppm. All of the peaks for the ***C***-OH carbon from the other alkoxy groups were in the range of 72.49 ppm to 72.81 ppm. The peaks from the O-***C***H_2-R were also important in explaining the attachment of these groups. These are reported in Table 4.14.The details of ^1H and ^{13}C NMR signals are presented in APPENDIX C as Table B2.

Table 4.14: ^{13}C NMR signals for the O-***C***-R carbons

Group	^{13}C NMR signal (ppm)
O-***C***H_2-CH_3	63.33
O-***C***H_2-CH_2-CH_3	72.63
O-***C***$H(CH_3)$-CH_3	70.98
O-***C***H_2-CH_2-CH_2-CH_3	70.74
O-***C***H_2-CH (CH_3)-CH_3	77.94
O-***C***H_2-CH_2-$(CH_2)_3$ -CH_3	71.03
O-***C***H_2-CH_2-$(CH_2)_5$ -CH_3	71.00
O-***C***H_2-CH_2-$(CH_2)_7$ -CH_3	71.10
O-***C***H_2-CH_2-$(CH_2)_9$ -CH_3	71.13

4.5 Synthesis of the Sulfate Surfactants from the Alkoxy-Hydroxy Methyl Esters

Sulfation of the methyl esters with the attached alkoxy chains was conducted by using chlorosulfonic acid. A schematic of the reaction is shown in Figure 4.29. The hydroxyl group at the opposite position was sulfated. The stoichiometric calculations for the reactants were performed on the basis of the available hydroxyl (-OH) groups. Due to the highly reactive nature of chlorosulfonic acid, its slight excess at elevated temperatures can result in unnecessary side reactions. Therefore, the process was optimized for the reaction parameters including the amount of reagents. Residual alcohols from the remnants of the alcohols used for the alkoxylation reaction were analyzed by GC-MS and were compensated for in the stoichiometric calculations.

These alcohols with the hydroxyl values of the samples for all of the precursors are described in Table 4.15.

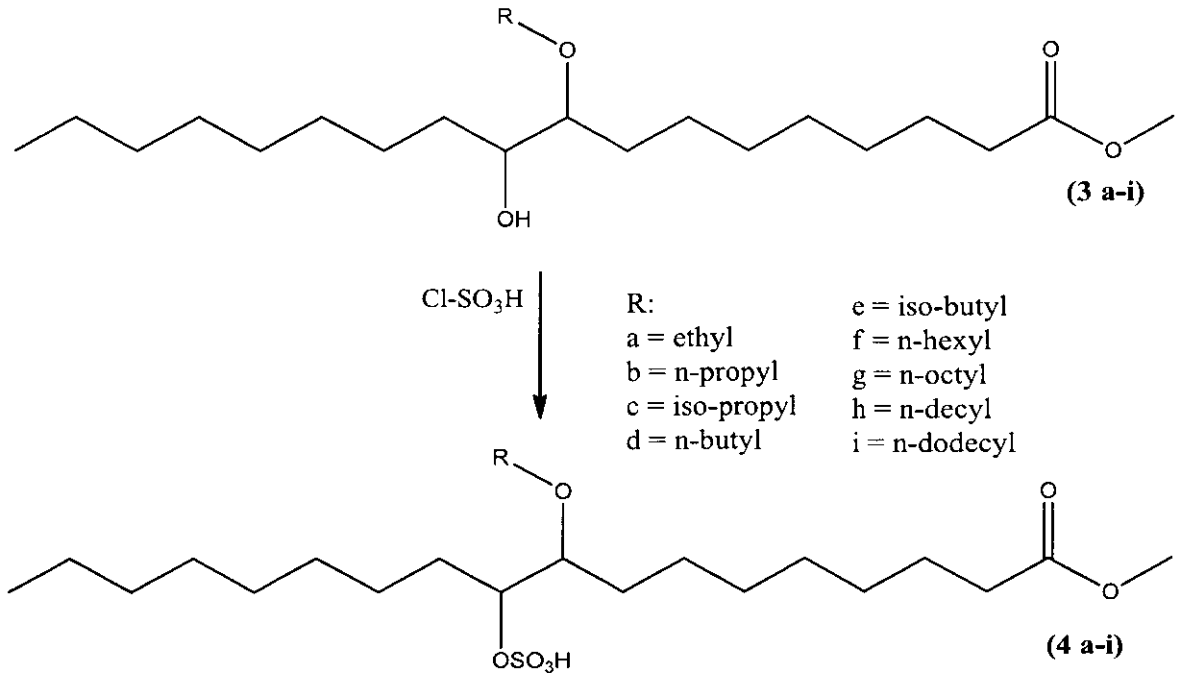

Figure 4.29: Schematic of the sulfation reaction producing a 9-alkoxy-10-sulfooxy octadecanoic acid methyl ester

Table 4.15: Hydroxyl value and residual alcohols in the sulfation precursors

Sample	Hydroxyl Value (mg KOH per g)	Hydroxyl value (%)	Residual alcohol (%)
3a	103.56	3.14	Absent
3b	100.26	3.04	Absent
3c	97.62	2.96	Absent
3d	96.96	2.94	Absent
3e	92.67	2.81	Absent
3f	91.02	2.76	0.16
3g	88.72	2.69	0.21
3h	82.78	2.51	0.25
3i	88.72	2.69	0.33

4.5.1 Optimization of Sulfation Reaction Parameters

The reaction parameters studied for the optimization included the reaction temperature, the reaction time and the molar ratio of the chlorosulfonic acid to -OH groups. These parameters were optimized for the maximum yield of the sulfated product. The product was analyzed by employing the two-phase titration to assess the produced surfactants. The amount of the active present in the sample showed the progress of the reaction during the synthesis process.

4.5.1.1 Effect of the -OH / Chlorosulfonic Acid Mole Ratio

The stoichiometric relation between -OH and chlorosulfonic acid is 1:1 moles. Five different molar ratios of CSA to -OH ranging from 0.50 to 2.0 were investigated. It was, however, noted that a higher amount of CSA was detrimental for the yield as well as for the quality of the product. The results are shown in Figure 4.30.

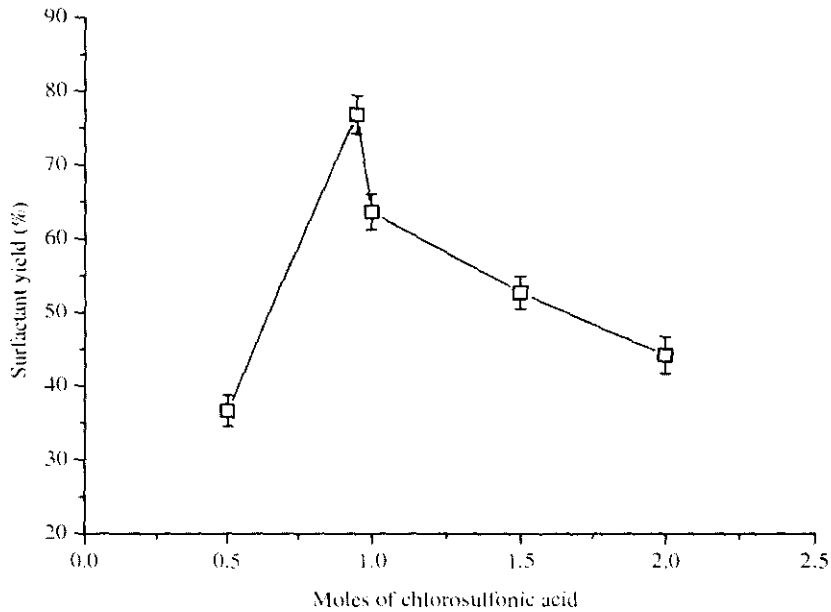

Figure 4.30: Effect of the moles of the chlorosulfonic acid on the surfactant yield (%)

The excess of CSA, as shown in Figure 4.30, led to low yields. Moreover, a thick black mass with an unidentified chemical structure was also obtained at 1.5 and 2.0 molar excesses of CSA. The chlorosulfonic acid, at high excess, produced poly sulfate carboxylates. These moieties were responsible for the dark colored product.

This phenomenon was also reported by Yamada [230]. The optimum conditions for the stoichiometric ratio was found to a 0.95:1 (CSA: OH) mole ratio. The same ratio was also suggested by Sosis [177] who used 0.95 for the sulfation of long chain alcohols.

4.5.1.2 Effect of the Reaction Temperature

Results from the studies on the effect of the reaction temperature are shown in Figure 4.31.The sulfation reaction was started at a very low temperature (5 °C). It was noted that if the reaction was started at room temperature, a vigorous exothermic reaction was the result and the reactants immediately darkened. The viscosity of the reagents became high and the products were difficult to separate at the end of the reaction. Furthermore the overall yield became very low. Those reactions which started at 5 °C were smooth in the course and the product was also lighter in color. When the chlorosulfonic acid was delivered completely to the reaction flask, the temperature of the flask was increased to different temperatures to note the effect of the temperature. It can be noted that a reaction temperature beyond 30 °C was not effective as a low yield was obtained. It was mainly due to the side reactions which occurred due to the reaction of the chlorosulfonic acid and FAME. Therefore, the reaction temperature was set at 30 °C after the addition of the chlorosulfonic acid.

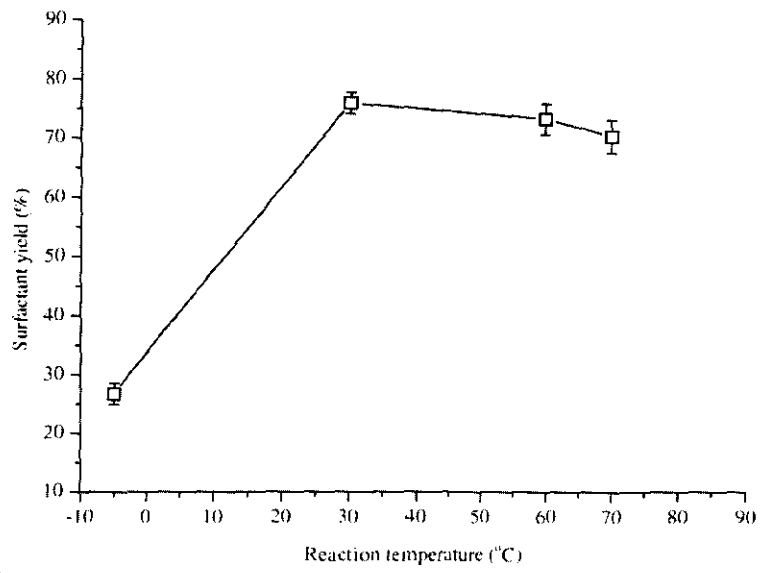

Figure 4.31: Effect of the reaction temperature on the surfactant yield (%)

4.5.1.3 Effect of the Reaction Time

Reaction time is an important factor and it was observed that the product yield was drastically affected if the reaction proceeded for less than 30 minutes. The results are presented in Figure 4.32. However, at 120 minutes the maximum yield was obtained and no notable effect was observed beyond this time. The yield was decreased, although not to too much extent, for an excessively longer reaction time.

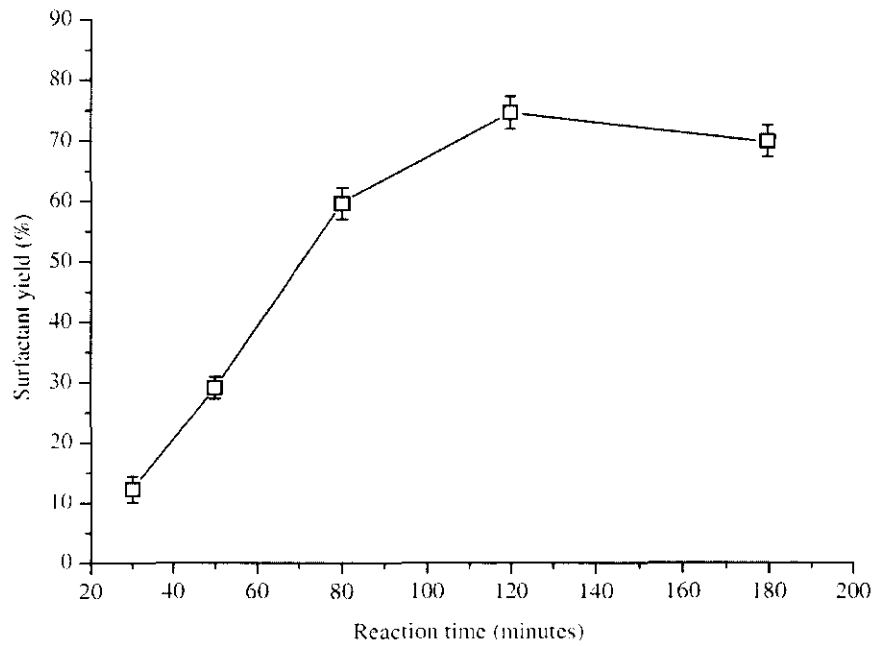

Figure 4.32: Effect of the reaction time on the surfactant yield (%)

4.5.1.4 Optimized Reaction Conditions

The optimized reaction conditions for the sulfation reaction were 0.95 moles of the chlorosulfonic acid against 1 mole of FAME. The reaction time was 120 minutes with a reaction temperature of 30 °C. A reaction proceeded under these conditions afforded the maximum yield. It was, however, found that the sulfation reaction for the FAME molecules having longer alkoxy groups was not very successful and relatively lower yields were obtained. It was due to the steric hindrance, high viscosity and relatively poor mass transfer effects in the case of the bigger molecules.

4.5.1.5 Neutralization of the surfactant

The synthesized surfactants were neutralized by using a 20 % NaOH solution to form the sodium salt. The slurry was kept below 10 °C with vigorous stirring. Addition of the NaOH solution was conducted slowly and stopped at pH 5.5 - 6.5.

4.5.1.6 Yields of the Sulfate Surfactants

The percent yields of the sulfated products are shown in Table 4.16. It can be noted that the products with the attachments of the alcohols with longer chains were not fully sulfated. The viscosity of the reaction mixture with longer side chains was also high as compared to those products with relatively smaller side chains. It may, therefore, be concluded that the high viscosity and large bulk of the molecule were the probable reasons for the low yields of the sulfation for these molecules.

Table 4.16: Yields (%) of the sulfated products (conversion of the -OH groups)

Product	Name	Yield (%)
4a	9-ethoxy-10-sulfooxy octadecanoic acid methyl ester	94.3
4b	9-propoxy-10-sulfooxy octadecanoic acid methyl ester	93.1
4c	9-(3-methyl-propoxy)-10-sulfooxy octadecanoic acid methyl ester	89.2
4d	9-butoxy-10-sulfooxy octadecanoic acid methyl ester	86.6
4e	9-(3-methyl-butoxy)-10-sulfooxy octadecanoic acid methyl ester	90.7
4f	9-hexoxy-10-sulfooxy octadecanoic acid methyl ester	88.6
4g	9-octoxy-10-sulfooxy octadecanoic acid methyl ester	86.3
4h	9-decoxy-10-sulfooxy octadecanoic acid methyl ester	87.3
4i	9-dodecoxy-10-sulfooxy octadecanoic acid methyl ester	85.1

4.6 Characterization of the Sulfate Surfactants

The surfactants were characterized by using FT-IR and NMR techniques.

4.6.1 FT-IR and NMR Spectroscopic Analyses of the Sulfate Surfactants

The band of interest in the FT-IR analysis was from the sulfate group which appeared at ~1250 cm^{-1} (smaller band) and 1212~1215 cm^{-1} (intense band). All of the spectra of the sulfate surfactants showed these bands with almost identical values. The details are presented in Table 4.17.

Table 4.17: Appearance of the sulfate band in the FT-IR spectra and the *C*-O-S ^{13}C NMR peaks from the sulfate surfactants

Product	Sulfate bands (cm-1)	^{13}C NMR (***C***-O-S) bond
4a	1248, 1213	71.23
4b	1250, 1214	72.56
4c	1250, 1216	71.36
4d	1251, 1214	73.02
4e	1249, 1216	73.23
4f	1250, 1214	71.67
4g	1252, 1213	72.87
4h	1248, 1215	71.36
4i	1251, 1212	71.41

Both the ^{1}H NMR and ^{13}C NMR spectra were recorded for the sulfate surfactants. In the ^{1}H NMR spectra, the disappearance of the peaks from O***H*** (~3.11 ppm) was important. The ^{13}C NMR spectra were found more valuable as the appearance of the C-O-S peak from the carbon backbone was clear and strong in the vicinity of 72 ppm. In Table 4.17, the ^{13}C NMR peaks from –***C***-O-S are presented.

4.7 Synthesis of the Sulfonate Surfactants from the Alkoxy-Hydroxy Methyl Esters

Sulfonation at α- position was conducted by using SO_3 gas in a falling film reactor (FFR). Before the sulfonation reaction, the hydroxyl groups at the 10^{th} carbon position were protected by the acetylation reaction. The details are presented in the following sections.

4.7.1 Protection (acetylation) of the Hydroxyl Groups

The schematic of the acetylation reaction is depicted in Figure 4.33. The acetylation reaction was conducted by using acetic anhydride as the acetylating agent. Stoichiometric calculations were performed according to the hydroxyl value of FAME. The reaction was according to Martinez and Pascual [231] and it took less than ten seconds to complete and to produce a 10-Acetoxy-9-alkoxy-octadecanoic acid methyl ester.

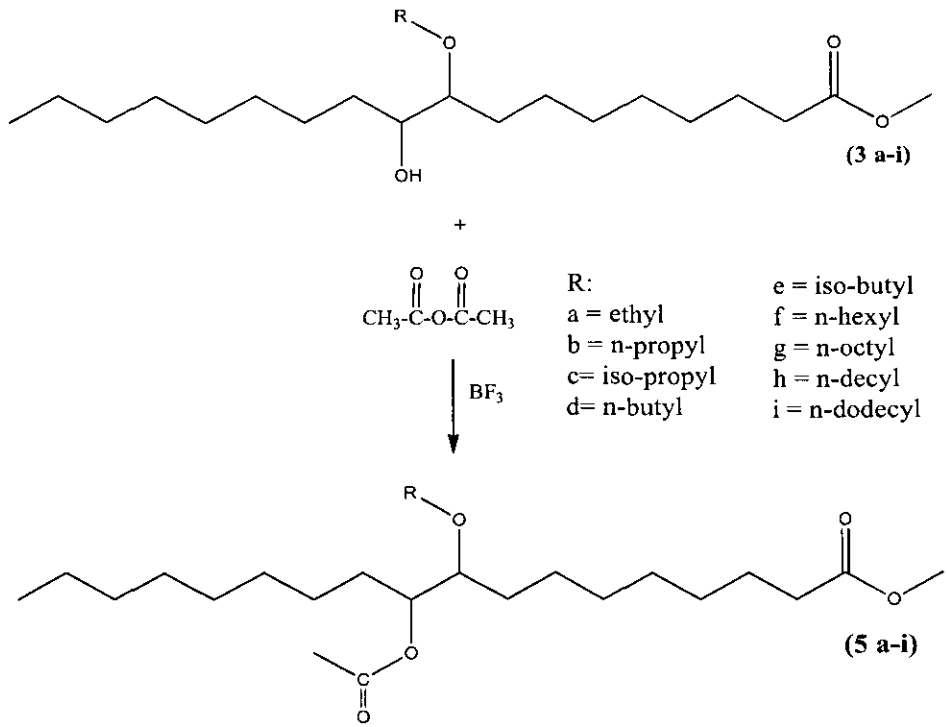

Figure 4.33: Schematic of the acetylation reaction producing a 10-Acetoxy-9-alkoxy-octadecanoic acid methyl ester

The hydroxyl value was determined after the acetylation process to assess the protection of the hydroxyl groups by the acetyl groups. Table 4.18 presents the hydroxyl values (-OH Values) of FAME before and after the acetylation reaction and the conversion efficiency of the reaction. The range of the conversion efficiency 93.4-98.6 %, decreasing with the increase in the size of the alkoxy group attached to the FAME parent chain. For the product yield, when the straight chain groups were compared with the branched chain groups with the same number of carbons, the straight chain bearing molecules showed high conversions, although the difference was not very significant. It can be concluded that the protection of the -OH groups attached to the molecules with the smaller side chains is more efficient and favorable as compared to the molecules with the longer side chains. This can be attributed to the steric hindrance as well as the high viscosity of the FAME molecules with the longer side chains.

Table 4.18: Hydroxyl (-OH) values (mg KOH /g of the sample) of FAME before and after acetylation

Sample	-OH Value before acetylation	-OH Value after acetylation	Conversion efficiency (%)
5a	103.56	1.43	98.6
5b	100.26	1.98	98.0
5c	97.62	2.76	97.7
5d	96.96	2.8 3	97.1
5e	92.67	3.27	96.5
5f	91.02	4.11	95.4
5g	88.72	4.33	95.1
5h	82.78	5.05	93.9
5i	88.72	5.82	93.4

4.7.2 Analysis and Characterization of the Acetylated FAME

A comparison of the FT-IR spectra of the FAME molecule with the butoxy side chain and its acetylated version is shown in Figure 4.34. The bands at 1024.2, 1229.8 and11372.1 cm^{-1} were important. The FT-IR assignments of the bands were according to Stefke et al. [232] and Moses and Frost [233].The band at 1024.2 cm^{-1} was due to C-O vibrations from the acetyl C-O group and the band at 1229.8 cm^{-1} represented the C-O vibrational frequency of the acetyl group. The band at 1372.1 cm^{-1} represented the C-H in the bending vibrations of O-(C=O)-CH_3.The reduced intensity of the -OH band at 3458.6 cm^{-1} was also a confirmed indication that the -OH groups were protected by the acetyl groups.

The details of all of the acetylated product FT-IR spectral vibrations are presented in APPENDIX B as Table B3.

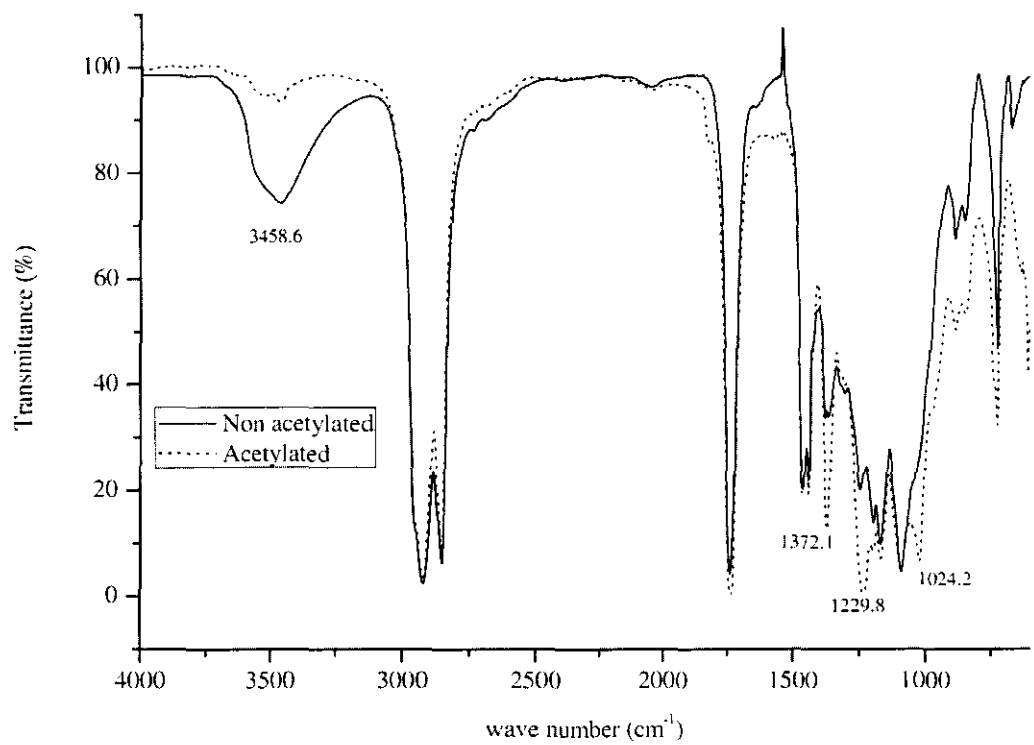

Figure 4.34: Comparison of the FT-IR spectra of the butoxy and acetylated butoxy

The ^{1}H NMR and ^{13}C NMR spectra of the acetylated products were recorded for the confirmation of the acetylation reaction completion. Important peaks in ^{1}H NMR were due to the appearance of acetyl methyl protons. In addition, the absence of peaks of a

proton from the OH group was also an indication that the acetylation reaction was complete. In the ^{13}C NMR spectra, the appearance of the acetyl carbon peak was significant. These important peaks from the ^{1}H NMR and ^{13}C NMR spectra are tabulated in Table 4.19.

Table 4.19: Acetylation reaction, important NMR signals

Compound	^{1}H NMR	^{13}C NMR	
	-C-CO-C***H***$_3$	C-CO-***C***H$_3$	C-***C***O-CH$_3$
5a	2.06	20.32	170.94
5b	2.05	20.29	170.96
5c	2.10	20.32	171.01
5d	2.05	20.34	170.91
5e	2.06	20.45	170.93
5f	2.05	20.31	171.02
5g	2.07	20.42	170.96
5h	2.09	20.32	171.02
5i	2.08	20.43	171.06

4.7.3 Sulfonation of the Acetoxy - Alkoxy Methyl Esters

The sulfonation reaction introduces the carbon-sulfur bond. The sulfonate group in methyl esters attaches at the α-position. The reaction scheme is depicted in Figure 4.35. The sulfonation reaction was conducted in a Falling Film Reactor (FFR). Three fatty acid methyl esters representing all of the nine molecules in terms of the size of attached side chains were selected for the optimization of the sulfonation reaction. These methyl esters included **6a** (10-Acetoxy-9-ethoxy-octadecanoic acid methyl ester), **6e** (10-Acetoxy-9-(3-methyl-butoxy)-octadecanoic acid methyl ester) and **6i** (10-Acetoxy-9-decoxy- octadecanoic acid methyl ester), representing the small side

chain, branched side chain and long side chain attached, respectively. These fatty acid methyl esters were reacted with a mixture of SO_3 gas and air. The reaction temperature and SO_3 concentration (percent of SO_3 in the air) were optimized for the maximum yield of the obtained product (10-Acetoxy-9-alkoxy-2-sulfo-octadecanoic acid methyl ester). The esters with longer side chains had a relatively high viscosity. To overcome the viscosity issue, a little amount of *n*-heptane was used as a diluent. The optimization of the sulfonation reaction is discussed in the following sections.

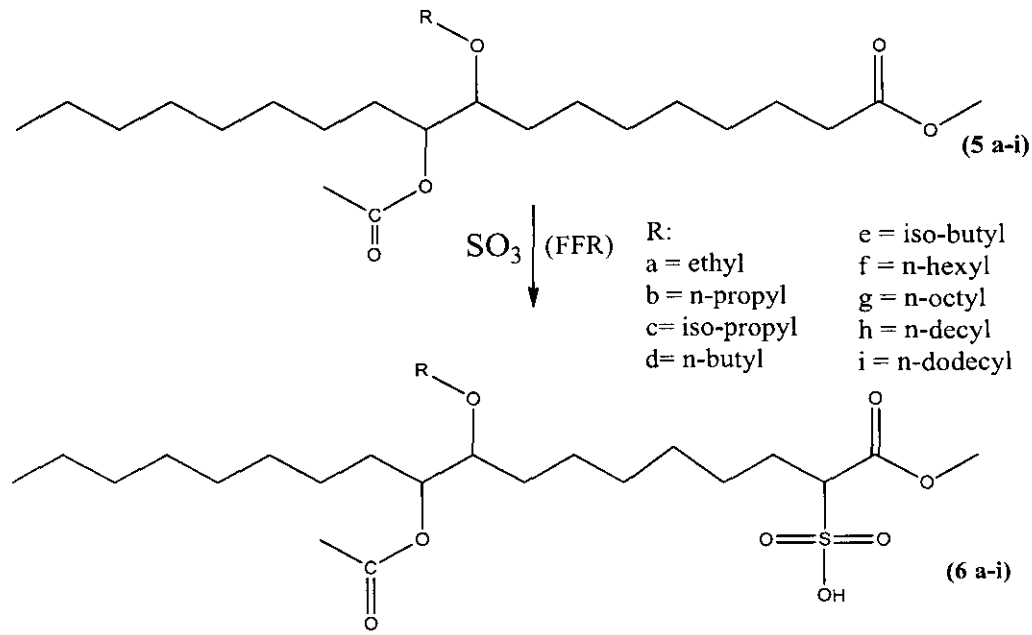

Figure 4.35: Schematic of the sulfonation reaction producing a10-Acetoxy-9-alkoxy-2-sulfo-octadecanoic acid methyl ester

4.7.3.1 Effect of the SO_3-FAME Mole Ratio

The stoichiometric mole ratio of SO_3 with FAME was one. As the reaction was not very efficient due to the difficulty in the removal of the α-hydrogen, a high molar excess of SO_3 was used. The effect of the different SO_3-FAME molar ratios on the efficiency of the reaction is shown in Figure 4.36. It may be observed that the general trend for all types of FAME were similar. However, the longer the chain length was, the lower the yield. This effect could be attributed to the high viscosity of the FAME

with the longer chain attached. The very high molar ratio of SO_3 is not very successful because of the possible side reactions and the production of poly sulfonates. The optimized SO_3-FAME mole ratio was found to be 3:1.

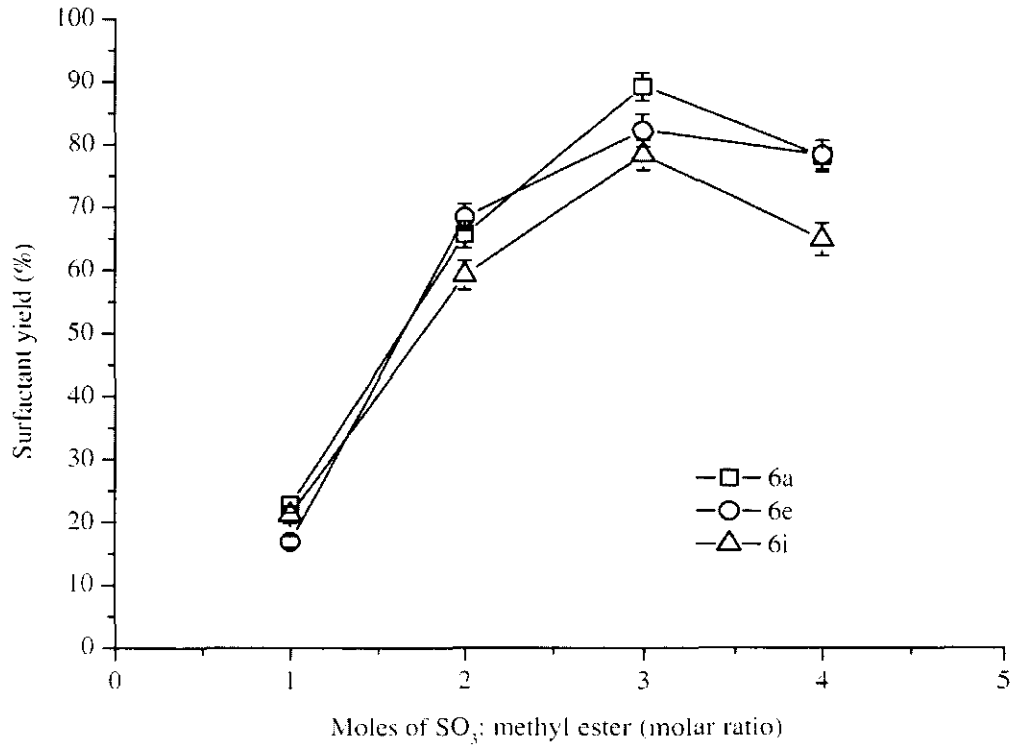

Figure 4.36: Effect of the SO_3-FAME mole ratio on the surfactant yield (%)

4.7.3.2 Effect of the SO_3 Concentration in Air

SO_3 gas is an aggressive reactant and it is usually diluted in air or nitrogen before use. Different concentrations of SO_3 were used for the sulfonation reaction; the findings are depicted in Figure 4.37. The effect of the SO_3 concentration in the air also followed the same trend as shown for the effect of the SO_3-FAME molar ratio. The very high concentration of SO_3 in the air required a very slow flow rate of the SO_3-air mixture to maintain the stoichiometric ratio of SO_3 and FAME. This slow flow rate was found inefficient due to the less efficient mass-transfer effects. Therefore, a 5 % mixture of SO_3-air was found to be optimum for the sulfonation reaction.

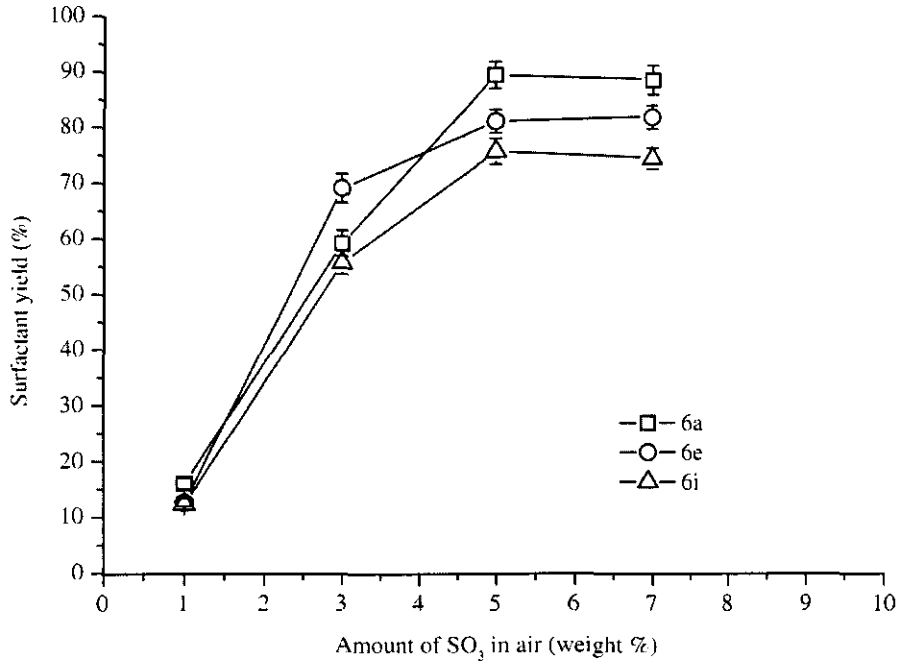

Figure 4.37: Effect of the SO_3 concentration in air on the surfactant yield (%)

4.7.3.3 Effect of the Reaction Temperature

The findings of varying the reaction temperature on the product yield are presented in Figure 4.38.

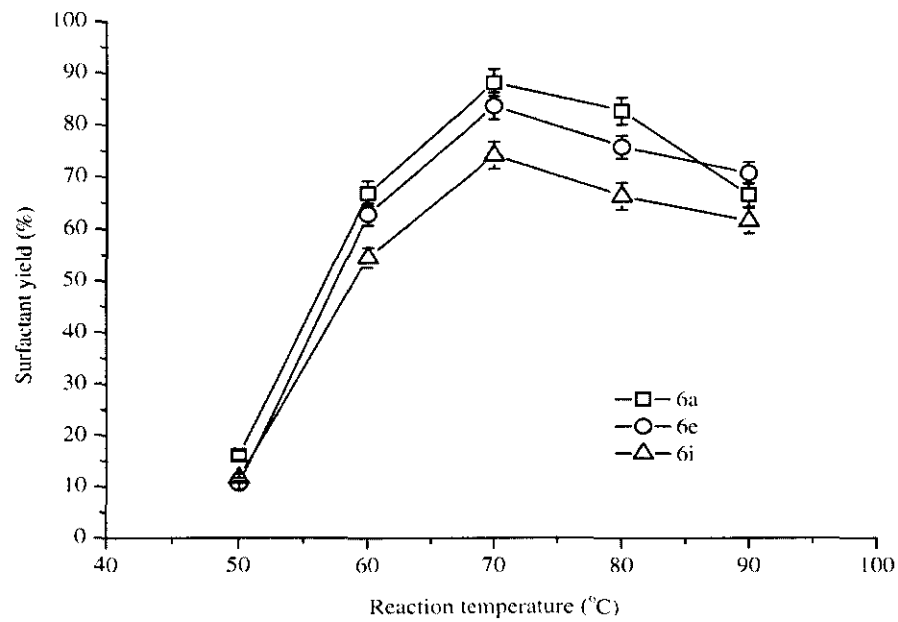

Figure 4.38: Effect of the reaction temperature on the surfactant yield (%)

Sulfonation reaction is an exothermic reaction. The falling film reactor efficiently dissipates the produced heat and controls the reaction progress. If the temperature of FFR is low, the viscosity of the product becomes high, and hence the reaction is disturbed. On the other hand, at a very high temperature, the reaction becomes less efficient due to the excessively high velocity of the SO_3 gas which reduces the contact time with the FAME. Therefore, an optimum temperature was selected for the reaction. As the reaction is exothermic in nature, a very high temperature forces the reaction equilibrium to the left, and hence lowers the yield. The optimized reaction temperature was found to be 70 °C.

4.7.3.4 Optimized Reaction Conditions

The optimized reaction conditions for the sulfonation reactions were noted from the above mentioned experiments. It was found that the optimized SO_3-FAME mole ratio was 3:1 with a 5 % mixture of SO_3-air at a 70 °C reaction temperature.

4.7.4 Bleaching and Neutralization of the Sulfonated FAME

The obtained products were light to dark brown in color. The bleaching was performed with a 10 % H_2O_2 solution. Bleaching was known to oxidize the poly sulfonates and other impurities, and hence reduce the color of the product. After the bleaching, the color of the obtained products was light brown.

Neutralization was conducted after the bleaching process to produce the sodium salt of the surfactants. A sodium hydroxide (20 %) solution was used. The reaction temperature was maintained below 10 °C by using an ice bath. Constant stirring was maintained and the pH was carefully monitored. The color of the product was changed to a lighter brown tint, hence signaling the completion of the neutralization. The reaction was stopped at pH 6-6.5.

4.7.5 Effect of the Side Chain Length on the Yield of the Surfactant

The yield of the sulfonated products is presented in Table 4.20. The yield was lower for the surfactants having long side chains. In addition, it was observed that the molecules with the side chains of iso-propoxy and iso-butoxy groups were difficult to sulfonate.

Table 4.20: Yield of the sulfonate surfactants

Product	Name	Yield (%)
6a	10-Acetoxy-9-ethoxy-2-sulfo-octadecanoic acid methyl ester	87.2
6b	10-Acetoxy-9-propoxy-2-sulfo-octadecanoic acid methyl ester	86.8
6c	10-Acetoxy-9-(3-methyl-propoxy)-octadecanoic acid methyl ester	82.4
6d	10-Acetoxy-9-butoxy-2-sulfo-octadecanoic acid methyl ester	87.6
6e	10-Acetoxy-9-(3-methyl-butoxy)-octadecanoic acid methyl ester	80.7
6f	10-Acetoxy-9-hexoxy-2-sulfo-octadecanoic acid methyl ester	86.2
6g	10-Acetoxy-9-octoxy-2-sulfo-octadecanoic acid methyl ester	85.5
6h	10-Acetoxy-9-decoxy-2-sulfo-octadecanoic acid methyl ester	84.4
6i	10-Acetoxy-9-dodecoxy-2-sulfo-octadecanoic acid methyl ester	81.3

It was probably due to the large bulk of the side chain, and hence contributed to the hindrance in the approaching of the SO_3 molecule at the reaction site. The molecules with the straight side chains showed a reduction in the yield with an increasing chain length. This effect could be attributed to the larger bulk and the associated high viscosity of the molecules. Both factors affected the yield negatively. The longer chain also imparted the high viscosity to FAME. The high viscosity affected the flow rate and a relatively high reaction temperature was required for the reaction. Therefore, both steric hindrance and high viscosity were the main factors affecting the yield of the sulfonation reaction.

4.8 Characterization of the Sulfonate Surfactants

FT-IR and NMR spectroscopic techniques were employed for the characterization of the sulfonate surfactants. Both the sulfonate group and sulfate group appeared in the range of 1205-1210 cm^{-1}. However, it is interesting to note that for the sulfate group, two bands of uneven intensities appeared in the range of 1210-1250 cm^{-1} and in the case of the sulfonate group only a single band appeared around 1205-1210. Hence, for all nine sulfonate surfactant types, all of the bands appeared in the vicinity of 1205 cm^{-1} (Table 4.21).

For the confirmation of the sulfonate group in the sulfonate surfactants, the ^{13}C NMR spectroscopy was used. The signal from the carbon-sulfur bond (–***C***-S-) appeared at 65-67 ppm. The details are presented in Table 4.21. The fundamental difference in the chemistry of the sulfate and sulfonate group was the nature of the attachment. In the sulfate group, the bond was C-O-S and in the sulfonate, it was C-S-O. Therefore, the ^{13}C NMR spectroscopy was able to identify the nature of group attached, whether it was sulfate or sulfonate, based on the ***C***-S signal (sulfonates) which was usually in the vicinity of 65-66 ppm, as compared to the ***C***-O-S signal (sulfates) which appeared in the vicinity of 71-73 ppm.

Table 4.21: FT-IR bands for the sulfonate group, the ^{13}C NMR signals from the - ***C***-S- group of the sulfonate surfactants

Product	FT-IR, Sulfonate bands (cm^{-1})	^{13}C NMR, ***C***-S
6a	1210	66.12
6b	1206	65.24
6c	1208	65.23
6d	1210	66.31
6e	1212	64.65
6f	1206	66.54
6g	1204	65.24
6h	1205	65.72
6i	1209	65.13

4.9 Chapter Summary

The synthesis of the surfactants has been presented in this chapter. The development of a silica based heterogeneous catalyst for the FFA esterification, the esterification of the high FFA of the Jatropha oil by this catalyst, epoxidation reaction optimization by using the RSM technique and the attachment of alkoxy side chains have been discussed in detail. The sulfation and sulfonation reactions of the modified methyl esters were also presented. The characterization of all of the precursors and products has also been provided.

CHAPTER 5

EVALUATION OF THE SURFACTANTS FOR EOR APPLICATIONS

The evaluation of the surfactants by different techniques is discussed in this chapter. Details regarding the phase behavior screening tests and the IFT measurements are provided. Interpretation of the data obtained from the evaluation tests and its usage to design and execute a core flood test for the determination of oil recovery by the selected surfactants is also presented.

5.1 Evaluation of Surfactants

Two types of surfactants were synthesized in this work; the structure of both types is shown in Figure 5.1. The first type, nine surfactants containing sulfate as head groups, were named **4a-4i**. The second type, nine surfactants containing sulfonate as head groups, were called **6a-6i**. Therefore, a total number of eighteen surfactants were synthesized. These surfactants were evaluated for EOR applications by performing several tests. These tests can be divided into two groups. The first group includes the tests which only involve the aqueous solutions of the surfactants interacting with temperature, salinity, alkali and polymer. In the second group, tests involving crude oil and surfactant solutions were performed. These tests included phase behavior tests and IFT measurements between the crude oil and the surfactant solutions. The results and findings of all of the tests and evaluations are discussed in the following sections.

5.2 Aqueous Solution Tests for Solubility, Stability and Compatibility

These tests included the solubility of the surfactants in deionized water (DW) and brine solutions (IW) at room temperature and at high temperatures. In addition, the stable surfactant solutions were then tested for compatibility with alkali and polymer solutions at room temperature. In the final test, the surfactant solution with the alkali and the polymer in the brine solution was tested at two sets of temperatures, at 60 °C and at 90°C. The results of these tests are summarized in Tables 5.1 and 5.2.

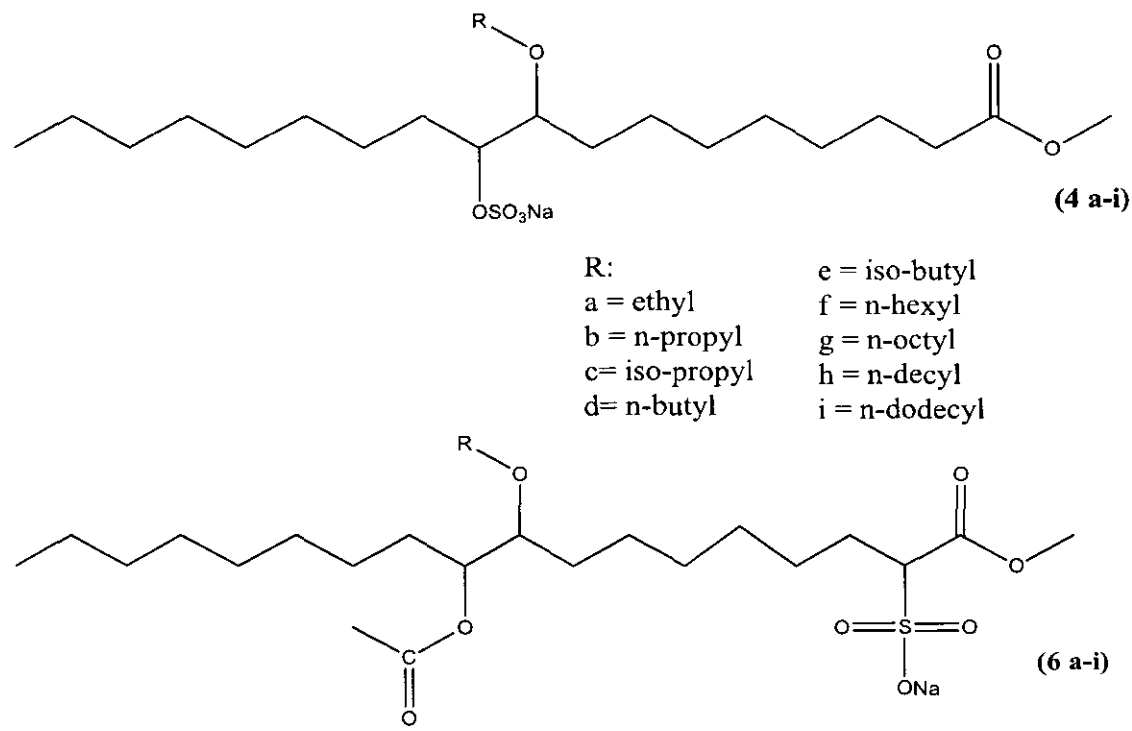

Figure 5.1: General structures of the sodium salts of sulfate (**4a-i**) and sulfonate (**6a-i**) based surfactants

5.2.1 Solubility and Stability in DW and IW

The solubility and stability of the surfactants solution (1 %) was examined in stoppered test tubes.

5.2.1.1 Sulfate Surfactants

The test was performed at room temperature (23 °C) as well as at 60 °C and at 90 °C. From the results summarized in Table 5.1, it can be observed that the sulfate surfactants were soluble in DW up to **4g** (ethoxy, *n*-propoxy, iso-propoxy, *n*-butoxy, iso-butoxy and hexoxy side chains). The samples from **4h-4i** (*n*-decoxy and *n*-dodecoxy side chains) were not soluble completely in deionized water. These insoluble types, however, showed a little different behavior when tested for solubility at 60 °C. The samples from **4a-4e** were readily soluble at 60 °C and the samples **4f** and **4g** were also solubilized after some shaking. The samples **4h** and **4i** were, however, not soluble even at 60 °C with vigorous shaking. The solubility profile of these surfactants can be defined on the basis of the hydrocarbon bulk, which was increasing from **4a** to **4i**. The surfactants with relatively smaller chains (side chains) were readily soluble in DW while with longer chains a higher temperature was needed. However, the surfactants with very long side chains such as –hexyl, *n*-octyl, *n*-decyl and *n*-dodecyl failed to solubilize. High hydrophobic bulk in a molecule reduces its water solubility. Stability in DW at 90 °C was also observed. All of the samples were not stable at 90 °C for more than 24 hours and showed cloudiness in the solutions. It was due to the labile nature of the sulfate group which was not stable at pH values other than 10-10.5 [42].

The compatibility (solubility) in IW was noted at room temperature as well as at 60°C. The samples from **4a-4f** were soluble in IW at 60 °C while **4g-4i** were found insoluble. The insolubility in high salinity environments was also related to the hydrocarbon bulk of the surfactant's tail group. The high hydrophobic nature renders the surfactants less soluble in high salinity environments [43].

All of the sulfate surfactants were compatible with the alkali, polymer and alkali-polymer solutions in IW at 60 °C except **4h** and **4i.** However, no sulfate surfactant was stable in the alkali, polymer and alkali-polymer solutions at 90 °C due to the labile nature of the sulfate group.

5.2.1.2 Sulfonate Surfactants

The solubility and stability studies of the sulfonate surfactants are presented in Table 5.2. At room temperature, all of the surfactants except **6h** and **6i** were found soluble. The long hydrocarbon chains (with n-decoxy and n-decoxy side chains) were the reason for the poor solubility. The solubility and stability at 60 °C in DW was, however, better and all of the sulfonate surfactants were found soluble at this temperature. Moreover, the stability in DW at 90 °C was excellent; all of the surfactants were found to be stable at this temperature.

The stability in IW at 90 °C was also good and only one sulfonate surfactant, **6i**, was found incompatible or insoluble in IW. The solubility of the surfactants with large hydrocarbon chains was usually poor in high salinity environments; this was exhibited by the **6i** surfactant.

All of the sulfonate surfactants were compatible with the alkali, polymer and alkali-polymer solutions in IW at both 60 °C and 90 °C, with only one exception,**6i**, which was found insoluble in IW, and hence incompatible in these tests.

The difference in the chemical nature of the sulfate and sulfonate is important. It can be noted that in the sulfate, there is a –C-O-S (carbon-oxygen-sulfur) bond while in the sulfonate, there is a –C-S (carbon-sulfur) bond. As the carbon sulfur bond is much stronger, the stability of the sulfonates is superior to that of the sulfates. The sulfonate surfactants were, therefore, used at 90 °C while the sulfates were evaluated at 60 °C for further evaluations.

Figure 5.2 shows a photograph of some of the stable and unstable surfactant solutions.

Figure 5.2: Photograph of the test tubes showing some stable (No. 2, 3 and 4 from the left) and some unstable samples

Table 5.1: Solubility and compatibility tests of the surfactants containing sulfate as the head group

Sample ID	Solubility in DW	Stability in DW at 60°C	Stability in DW at 90°C	Compatibility with IW at 60°C	Compatibility with alkali at 60°C	Compatibility with polymer at 60°C	Stability with A/P in IW at 60°C	Stability with A/P in IW at 90°C
4a	√	√	×	√	√	√	√	×
4b	√	√	×	√	√	√	√	×
4c	√	√	×	√	√	√	√	×
4d	√	√	×	√	√	√	√	×
4e	√	√	×	√	√	√	√	×
4f	√	√	×	√	√	√	√	×
4g	√	√	×	√	√	√	√	×
4h	×	√	×	×	×	×	×	×
4i	×	√	×	×	×	×	×	×

Table 5.2: Solubility and compatibility tests of the surfactants containing sulfonate as the head group

Sample ID	Solubility in DW	Stability in DW at 60°C	Stability in DW at 90°C	Compatibility with IW	Compatibility with alkali	Compatibility with polymer	Stability with A/P in IW at 60°C	Stability with A/P in IW at 90°C
6a	√	√	√	√	√	√	√	√
6b	√	√	√	√	√	√	√	√
6c	√	√	√	√	√	√	√	√
6d	√	√	√	√	√	√	√	√
6e	√	√	√	√	√	√	√	√
6f	√	√	√	√	√	√	√	√
6g	√	√	√	√	√	√	√	√
6h	×	√	√	√	√	√	√	√
6i	×	√	√	×	×	×	×	×

5.3 Critical Micelle Concentration (CMC)

The critical micelle concentration of the sulfate and sulfonate surfactants was measured by employing conductivity measurements. As the test was conducted at 25°C in deionized water, not all of the surfactants were found soluble, and hence CMC could not be determined for those which were insoluble in DW at 25°C. The CMC values (mmol / L) for both the sulfate and sulfonate surfactants are presented in Table 5.3. Individual CMC plots (Figures C10 - C23) for each surfactant are presented in APPENDIX C

The CMC values decreased with the increasing chain length of the hydrocarbon tail [6].This trend was observed in this study also. However, there was no uniform trend or behavior found for the surfactants having long chain lengths. The CMC values for the sulfate and sulfonate based surfactants were not similar; sulfonate surfactants possessed lower CMC values. This was probably the attachment of the acetyl group which was absent in the sulfate surfactants.

Table 5.3: CMC values of the sulfate and sulfonate surfactants at 25°C

Product	CMC (mmol / L)	Product	CMC (mmol / L)
4a	1.97	**6a**	0.76
4b	1.02	**6b**	0.485
4c	1.11	**6c**	0.455
4d	0.61	**6d**	0.235
4e	0.72	**6e**	0.195
4f	0.06	**6f**	0.01
4g	0.01	**6g**	0.004

5.4 Phase Behavior Tests

Phase behavior tests were conducted by using the surfactant concentration of 2 %. As a co-solvent, isobutyl alcohol (IBA) was used in concentrations of 4 %. Sodium

metaborate in a 1.5 wt. % concentration was used as the alkali. The water to oil ratio (WOR) was 1 and 2 mL of the surfactants solution used with 2 mL of the crude oil. The test temperature was maintained at 60 °C for the sulfates and 90 °C for the sulfonates. All of the tests were conducted at atmospheric pressure. The sealed pipettes were kept in ovens for at least ten days to achieve equilibrium conditions. The results for the sulfate and sulfonate surfactants are discussed in the following sections. All of the plots of the phase behavior tests are presented in APPENDIX C in the form of Figures C24 - C38.

5.4.1 Sulfate Surfactants

The results of the phase behavior studies for the sulfate surfactants are presented in Table 5.4. Two types of sulfate surfactants, namely **4h** and **4i,** (with *n*-decoxy and *n*-dodecoxy side chain, respectively) were found insoluble in brine even at elevated temperatures. These were not used in further evaluation tests. It can be observed in Table 5.3 that all of the surfactants formed the microemulsion. However, their optimum salinity and solubilization parameter were different from each other. It is obvious that the surfactant molecules with the smaller bulk of the hydrocarbon tail required a high amount of salinity for the middle phase microemulsion. In other words, their "optimum salinity" was high. The solubility in brine was directly related to the hydrocarbon chain bulk. The longer the hydrophobic group in a surfactant, the lower its solubility in the water will be. The situation became worse in the case of the brine as the solubility further decreased in the presence of the salts. This behavior is shown in the Table 5.4 where the optimum salinity for the surfactants having side chains of ethoxy, *n*-propoxy, iso-propoxy, *n*-butoxy and iso-butoxy (**4a** to **4e**) varied from 37000 to 32000 ppm with small variations. While in the case of the surfactants having longer side chains *n*-hexoxy and *n*-octoxy (**4f** and **4g**), the optimum salinity was dramatically decreased to 26000 and 23000 ppm, respectively. It was also observed that these surfactants were not stable in brine containing more than 80000 ppm of NaCl. These findings were according to several published data with different surfactants with varying bulks of hydrocarbon chains [31-33, 39, 69 and 234].

Table 5.4: Phase behavior results of the sulfate surfactants

Product	Microemulsion	Solubilization parameter	Optimum salinity NaCl (ppm)
4a	Yes	9.5	37000
4b	Yes	12	39000
4c	Yes	13	31000
4d	Yes	15	32000
4e	Yes	16.5	32000
4f	Yes	18	26000
4g	Yes	22	23000

The solubilization parameter of the solubilization ratio was an important characteristic of a surfactant for a particular crude oil. A solubilization parameter greater than 10 was sufficient to select the surfactant for the final evaluations because this value was indicative of the ultralow IFT between the oil and the brine. It can be noted from Table 5.4 that the solubilization parameter had a direct relation with the hydrocarbon chain length. The solubilization parameters for the smaller side chain surfactants such as **4a**, **4b** and **4c**, were small, ranging from 9.5 to 13. It was indicative of the fact that although these surfactants were forming microemulsions, they were not suitable for solubilizing a large amount of oil. Therefore, these surfactants should not be considered for core flood evaluations. The surfactants **4d** and **4e** (with *n*-butoxy and iso-butoxy side chains) had relatively higher solubilization parameters (15 and 16.5). The higher solubilization of the oil for the iso-butoxy side chain surfactant as compared to *n*-butoxy side chain surfactant was interesting. It was indicative of the fact that the branched side chains were more important in the solubilization of the oil than the straight side chains. Their solubilization parameter values were high but not high enough to be considered for further evaluations such as for the core flood tests.

The surfactants **4f** and **4g** had the solubilization parameters 18 and 22, respectively. These surfactants were *n*-hexoxy and *n*-octoxy side chain surfactants. Their larger hydrocarbon bulk was the reason for the high solubilization of the crude oil. Furthermore, the high solubilization values indicated the ultra-low interfacial tension (IFT) between the oil and water. These two surfactants were selected for further evaluations in terms of the enhanced oil recovery.

5.4.2 Sulfonate Surfactants

The phase behavior tests for the sulfonate surfactants were conducted in the same conditions used for the sulfate surfactants with the only difference being the temperature. The temperature fixed for the sulfonate surfactants was 90 °C. Only one surfactant, **6i** (with dodecoxy side chain), was found insoluble in the brine even at 90 °C. It was not used in further evaluations. The results of the phase behavior test for the sulfonate surfactants are summarized in Table 5.5. Similar to the sulfate surfactants, the salinity tolerance and solubility in brine solution was directly related to the hydrocarbon bulk of the sulfonate surfactants. The very long side chain surfactants were difficult to dissolve in the solution. It was, however, a supporting fact that there was an effect related to temperature on the solubility present and at 90 °C it was easy to obtain a clear solution for the sulfonates as compared to the sulfates which were used at 60 °C.

The salinity tolerance and optimum salinity profile for the sulfonate surfactants were found similar to those of the sulfate surfactants. The longer side chain surfactants were not very tolerant to high salinity values and surfactant **6h** (with *n*-dodecoxy side chain) was insoluble in a solution containing more than 80000 ppm NaCl.

It is shown in Table 5.5 that the solubilization parameter values for the sulfonate surfactants were slightly higher than for the sulfate surfactants. This observation was possibly due to the higher solubility of the sulfonates than the sulfates in hard water due to the high experiment temperature. The better solubility of any surfactant will

bring enhanced and better contact with the oil, and hence result in higher solubilization of the oil and water together.

The **6h** (with *n*-decoxy side chain) surfactant was found soluble in the brine solution at 90 °C. It showed the highest solubilization value of 25 due to its rather large hydrophobic group. This finding was similar to the studies published in the literature [69, 234 and 235]. Therefore, from the sulfonate surfactants, three surfactants (**6f**, **6g** and **6h**) were selected for further evaluations. These had solubilization parameters with values ranging from 16.5 to 25. Other surfactants (**6a** – **6e**) were found less effective in terms of their oil solubilization ability; their solubilization parameters were in the range of 8 to 16.50. These surfactants were not evaluated for the core flood tests.

Table 5.5: Phase behavior results of the sulfonate surfactants

Product	Microemulsion	Solubilization parameter	Optimum salinity NaCl (ppm)
6a	Yes	8	36000
6b	Yes	10	35000
6c	Yes	13	28000
6d	Yes	15	26000
6e	Yes	16.5	30000
6f	Yes	16.5	26000
6g	Yes	20	25000
6h	Yes	25	24000

5.5 IFT Measurement Results

A total number of five surfactants with a solubilization parameter greater than 9 were selected for the IFT measurements by using the spinning drop tensiometer. The results are presented in Table 5.6.

The variation in IFT values can be noted in Table 5.6. The IFT values were varied according to the solubilization parameter of that surfactant. In this context, surfactant **6h** (with *n*-decoxy side chain) had the least IFT against the crude oil. The solubilization ratio for this surfactant was 25, the highest of all of the surfactants. The highest IFT value was observed with the **6f** surfactant (*n*-hexoxy side chain). The IFT value of 0.025 mN / m was low enough to pass this surfactant for further investigations.

Table 5.6: Summary of IFT test results

Product	Type	IFT (mN / m)
4f	Sulfate	0.021
4g	Sulfate	0.016
6f	Sulfonate	0.025
6g	Sulfonate	0.012
6h	Sulfonate	0.008

The IFT values of all of the surfactants except **6h** were similar, showing the fact that the side chain length below a certain length was not very important for lowering the IFT. Thus, the surfactants with *n*- hexoxy and *n*-octoxy side chains were almost the same in the IFT values. However, **6h** with a longer side chain of ten carbon atoms was found to be ten times stronger in lowering the IFT against the oil.

5.6 Surfactant Adsorption Studies

The static adsorption of the surfactants was studied on the Berea core samples. The surfactant adsorption is mostly dependent on the chemistry of the rock sample. The surface area, surface functional groups and presence of moieties such as silt and other ion exchange groups have a strong influence on the surfactants adsorption. All of the samples were ground into powdered forms for the investigation of the adsorption studies. The surface properties and chemical analyses of the rock samples were performed and are discussed in the following sections.

5.6.1 Surface Area

The surface area of the Berea core was conducted on a surface area analyzer and the results were calculated according to the BET method. The Berea core sample had a relatively high surface area of 24.6879 m^2 / g.

5.6.2 Field Emission Electron Microscopy (FESEM) of the Core Samples

FESEM images were recorded to visualize the surface texture of all of the samples. The results are presented in Figure 5.3.

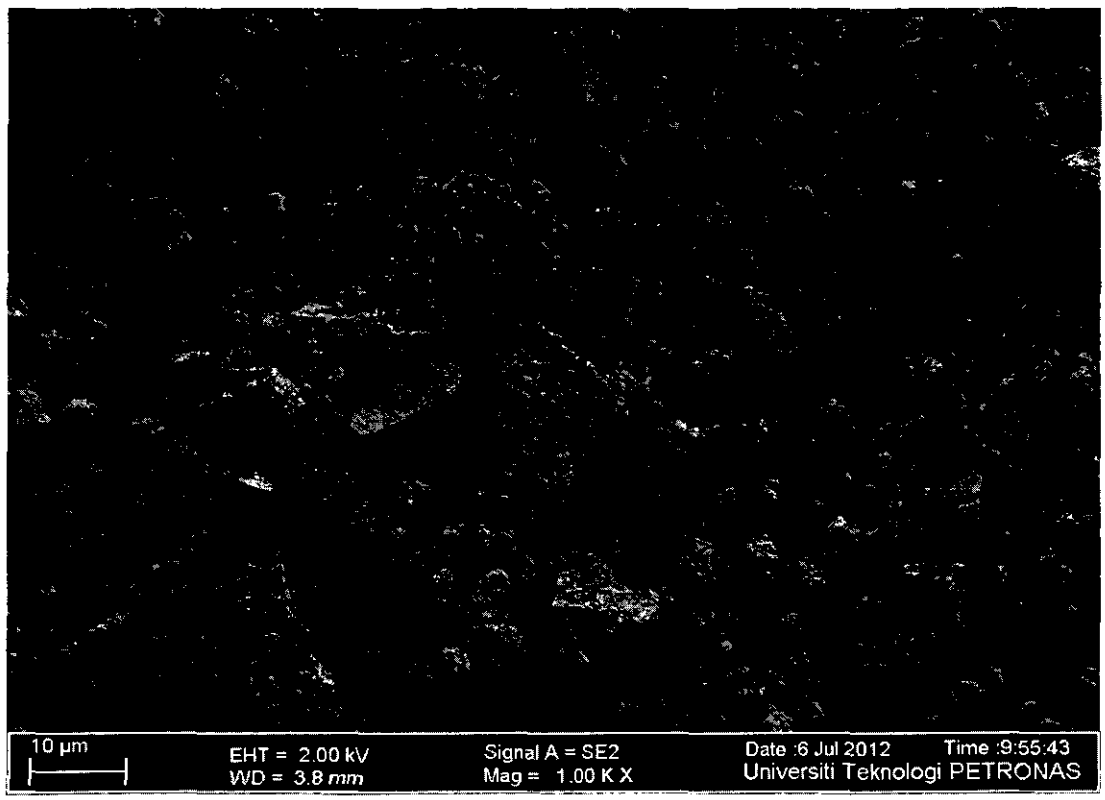

Figure 5.3: FESEM image of the crushed Berea core sample

FESEM images show the topography of the core samples. It can readily be observed that the Berea core sample had a high surface area, and therefore, it had smaller particles, as shown in its FESEM image.

5.6.3 X-Ray Fluorescence (XRF) Spectroscopic Analysis

The composition determined by XRF is shown in Table 5.7. The Berea core contains silica as its major constituent (91.02 %) and alumina (2.97 %). Other components include P_2O_5 (0.015 %), K_2O (0.871 %), MgO (0.6 %) and F_2O_3 (1.33 %). The surface chemistry of the core sample have been defined by these two species.

5.6.4 Point of Zero Charge (PZC)

The point of zero charge for the core has been determined by using the salt addition method, the fast titration method and the potentiometric mass titration (PMT) method. The plots for all three cores determining the PZC by all three methods are presented in Figures 5.4-5.6.

From the plots, it can be observed that the PZC for the Berea core sample was in the vicinity of 7.2 - 8.1 pH units. Any pH value higher than the PZC pH value would make the surface charge predominantly negative.

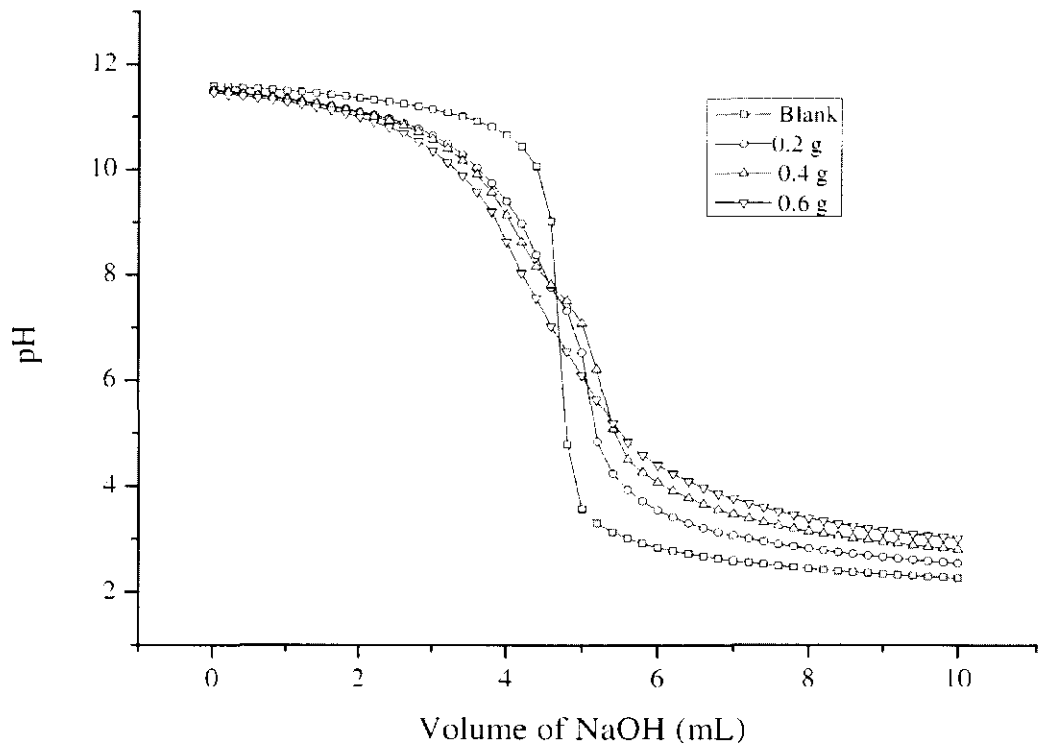

Figure 5.4. PZC determination by using the potentiometric mass titration method

The plot of the PZC determination by using the potentiometric mass titration (PMT) method is shown in Figure 5.3. At the pH value of 8.0, the line for the blank titration cut the lines of the mass titration curves for the 0.2, 0.4 and 0.6 g samples. The pH of 8.0 was termed as the PZC of the core sample.

The plot of the PZC determination by using the salt addition method has been shown in Figure 5.5. It can be observed that at pH 7.8, the value of ΔpH was zero. Therefore, the PZC of the Berea core determined according to the salt addition method was pH 7.8.

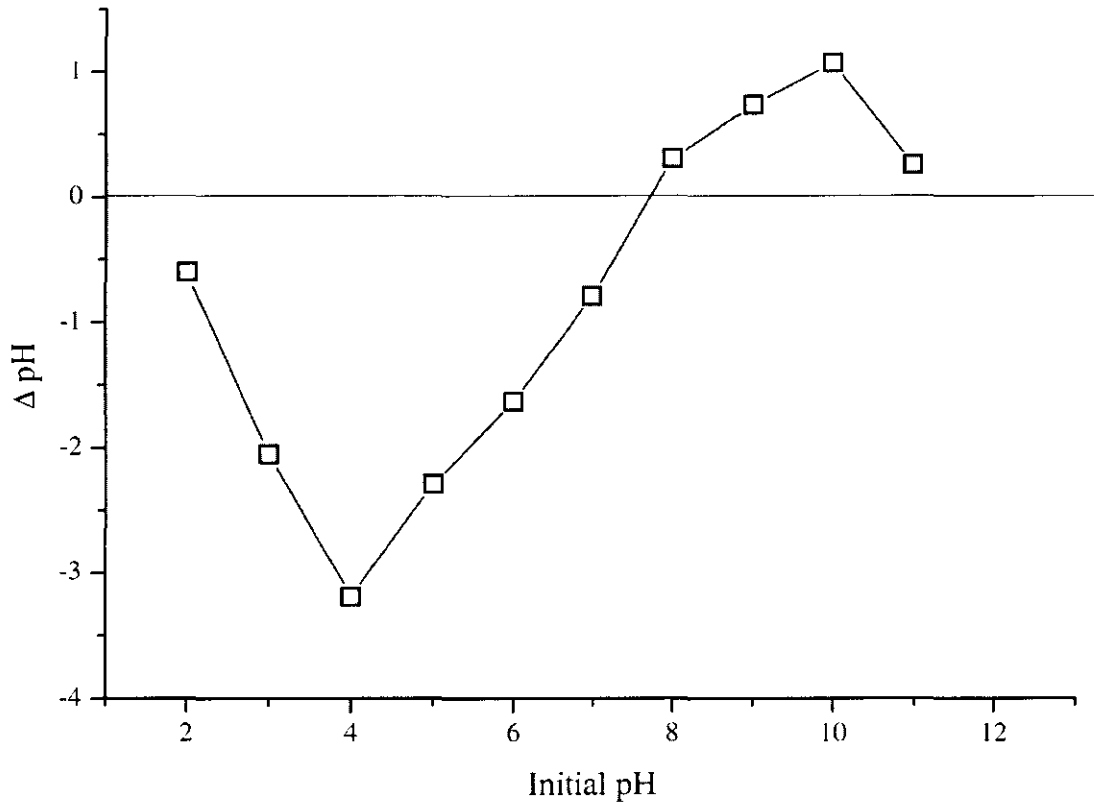

Figure 5.5: PZC determination by using the salt addition method

In Figure 5.6, the plot for the determination of the PZC of the Berea core by using the fast titration method is shown. The surface charge density was zero at pH 8.1, the PZC of the core sample.

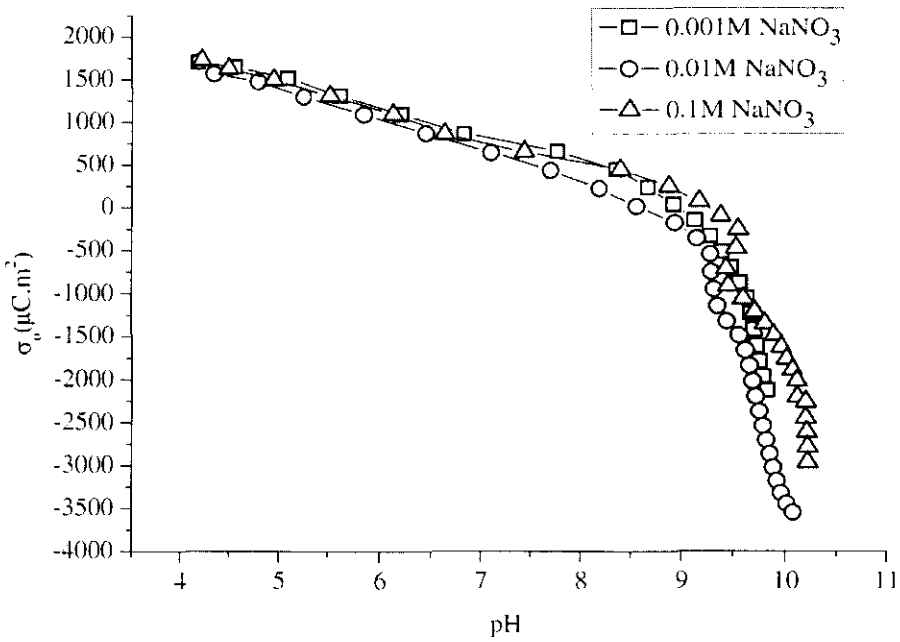

Figure 5.6: PZC determination by using the fast titration method

The PZC determined by using all three methods were 8.0, 7.2 and 8.1 pH units. Therefore, on average, the Berea core PZC was 7.8 pH units. Any pH value of the solution higher that 7.8, would predominantly render the negative charge on the surface.

5.7 Surfactant Adsorption Studies

Four surfactant types, **4f, 4g, 6g** and **6h,** were chosen for the adsorption studies on the Berea core samples.

5.7.1 Adsorption Studies of the 4f Surfactant on the Berea Core Sample

The adsorption isotherm of the **4f** surfactant (9-hexoxy-10-sulfooxy octadecanoic acid methyl ester) is shown in Figure 5.7. The study was conducted at the 60 °C temperature. Two tests were conducted: one without alkali and the other with using alkali to investigate the effect of the alkali (higher pH) on the adsorption of the surfactant.

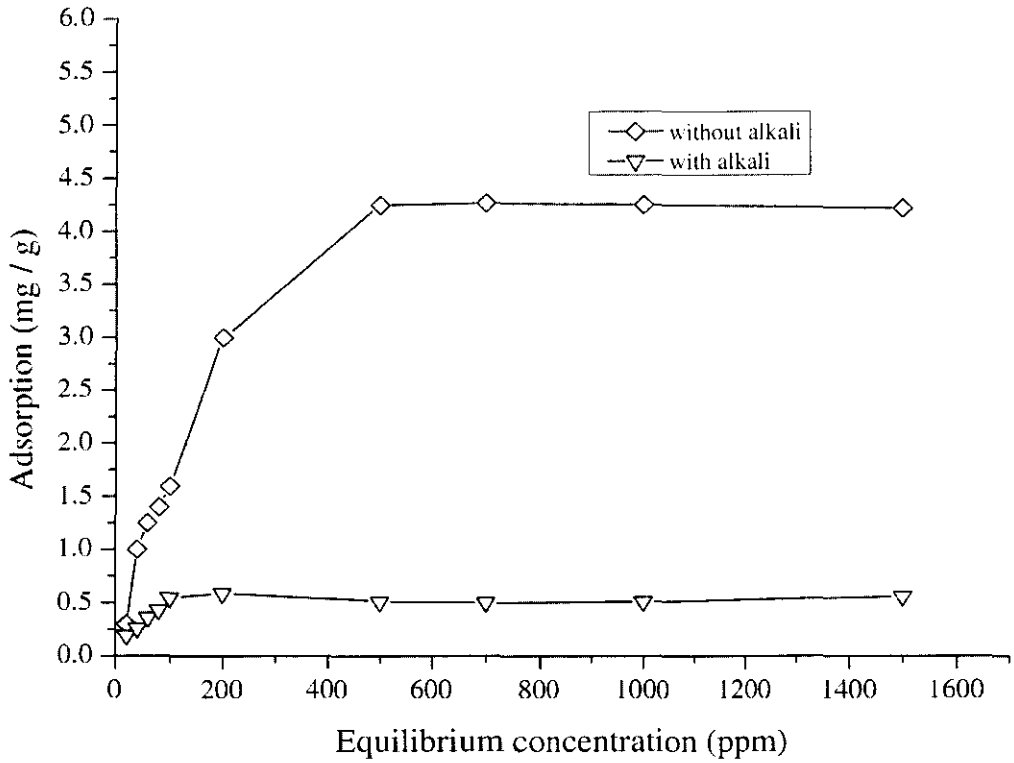

Figure 5.7: Adsorption isotherm of **4f** on the Berea core

The equilibrium adsorption of 4f on the Berea sandstone core was 4.32 mg / g of the core sample. However, in the presence of alkali, this was reduced to 0.54 mg / g of the core sample. The addition of alkali changed the pH from 6.2 to 9.8. The low adsorption was due to the predominantly negative charge on the core surface.

5.7.2 Adsorption Studies of the 4g Surfactant on the Berea Core Sample

The adsorption isotherm for the **4g** surfactant (9-octoxy-10-sulfooxy octadecanoic acid methyl ester) is shown in Figure 5.8. This test was also conducted at 60°C. The equilibrium adsorption found for the **4g** surfactant was 5.14 mg / g of the core sample. The adsorption in the presence of alkali was found to be 0.43 mg / g of the core sample. They relatively higher adsorption of **4g** than **4f** could be attributed to its higher carbon chain bulk. The adsorption was increased with the increasing bulk of the hydrocarbon chain when other factors were the same [236].

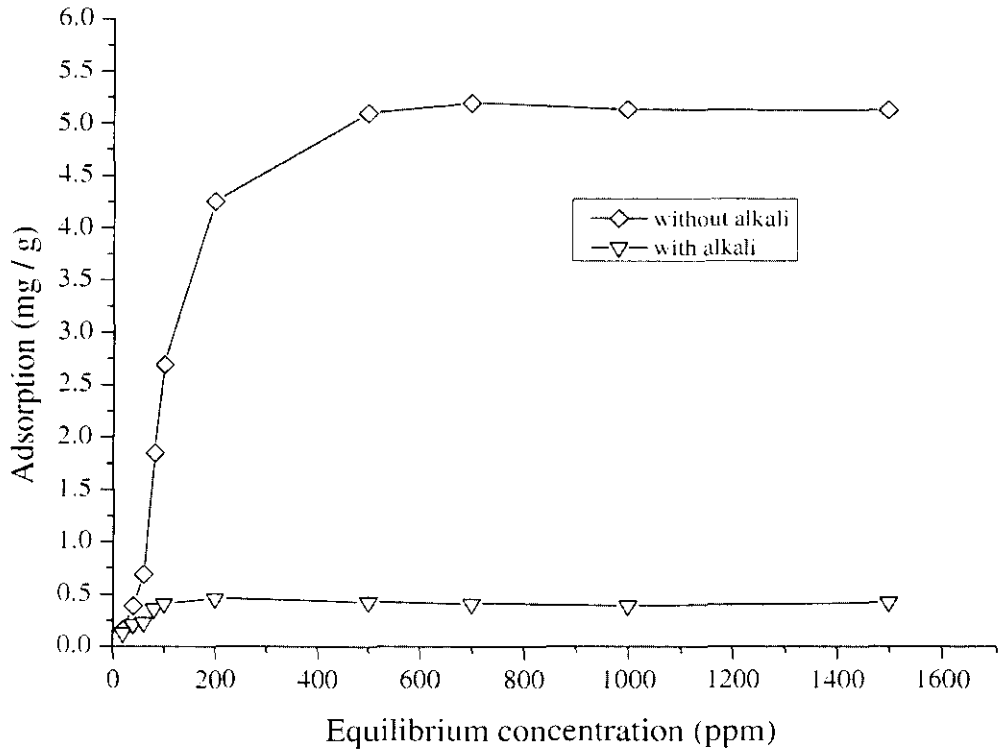

Figure 5.8: Adsorption isotherm of **4g** on the Berea core

5.7.3 Adsorption Studies of the 6g Surfactant on the Berea Core Sample

The **6g** (10-acetoxy-9-octoxy-2-sulfo-octadecanoic acid methyl ester) surfactant is a sulfonate surfactant. Its adsorption isotherm is shown in Figure 5.9. The equilibrium adsorption for 6g was 4.88 mg / g of the core sample. The experiment was conducted at 90 °C. In the presence of alkali, the adsorption was significantly reduced to 0.34 mg / g.

The structure of the hydrocarbon chain for both 6g and 4g was the same. The different amounts of the adsorption on the Berea core sample could be attributed to the experiment temperature. The adsorption test for the 6g sample was conducted at 90 °C, and hence its adsorption was lower as compared to the 4g sample. This fact is in accordance to the literature published by Paria et al. [236].

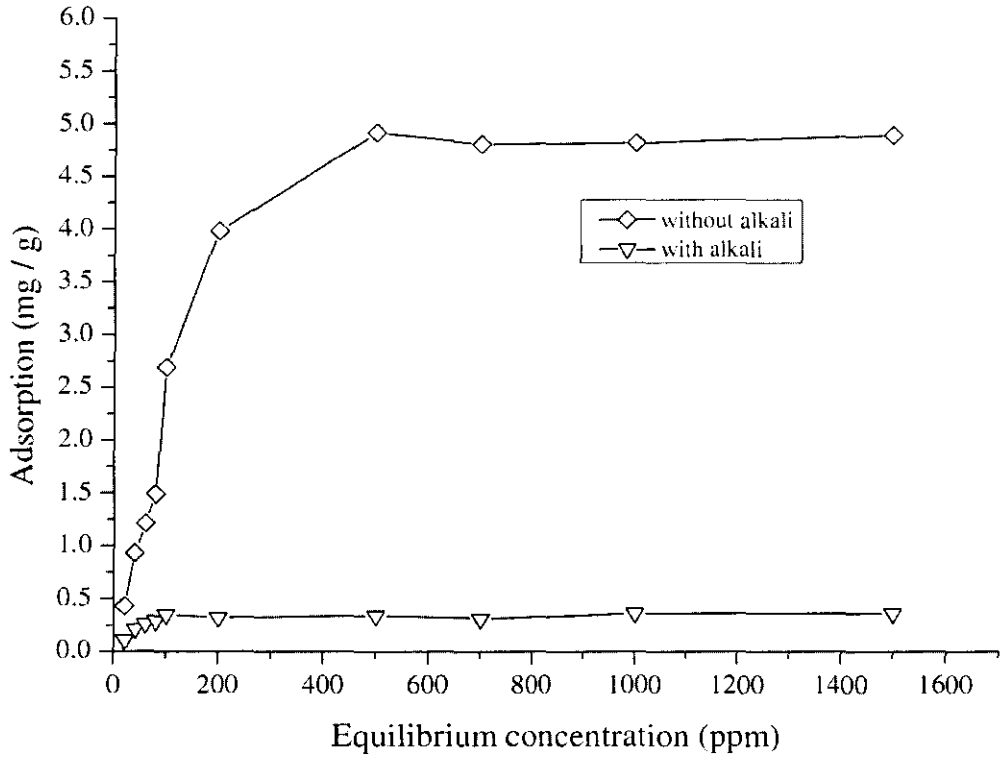

Figure 5.9: Adsorption isotherm of **6g** on the Berea core

5.7.4 Adsorption Studies of the 6h Surfactant on the Berea Core Sample

Sulfonate surfactant **6h** (10-acetoxy-9-decoxy-2-sulfo-octadecanoic acid methyl ester) had the longest hydrocarbon bulk of all four surfactants studied for the adsorption on the Berea core. Its adsorption isotherm is shown in Figure 5.10. The test was conducted at 90°C. The adsorption in the absence of alkali was found to be 4.94 mg / g. In the presence of alkali, the adsorption was found to be low at 0.86 mg / g.

The relatively higher value of adsorption in the case of **6h** was due to a longer hydrocarbon chain. The presence of alkali, however, showed the same effect of reducing the adsorption to 0.86 mg / g.

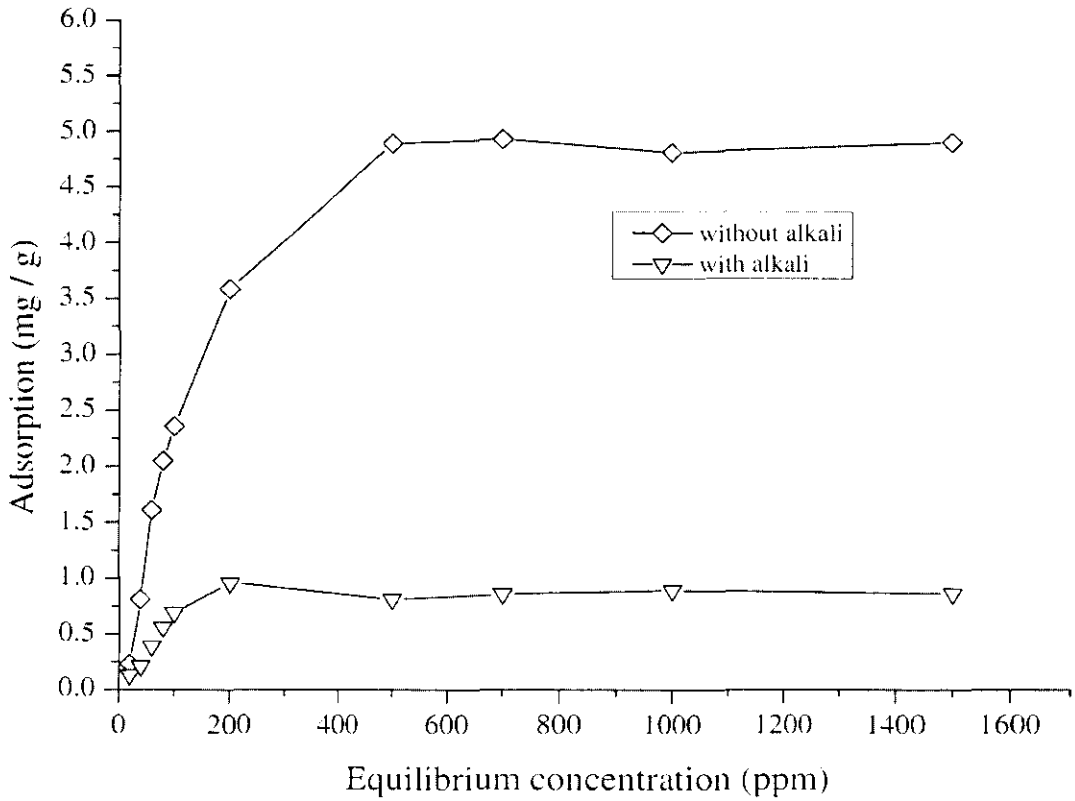

Figure 5.10: Adsorption isotherm of **6h** on the Berea core

5.7.5 Summary of the Adsorption of the Surfactants on the Berea Core Sample

Table 5.7 compiles the results of the adsorption of the surfactants on the Berea core samples. The highest adsorption observed in this study was due to the **4g** surfactant. The sulfonate surfactant with the same and longer hydrocarbon chain length showed relatively lower adsorption on the Berea core sample. The temperature effect in this study was manifested, significantly. The high temperature lowered the adsorption of the surfactants due to more pronounced desorption effects. The molecular movements were also high at higher temperatures and were one of the reasons for the low adsorption as explained earlier.

The low adsorption of all of the surfactants in the presence of alkali (0.34 – 0.86 mg / g) was similar to many commercial surfactants used in different studies [237, 238]. These low values of adsorption make the surfactants suitable for enhanced oil recovery applications.

Table 5.7: Results of the adsorption studies of the surfactants on the Berea core sample

Sample	Temperature (°C)	Adsorption (mg / g)	
		Without Alkali	With Alkali
4f	60	4.32	0.54
4g	60	5.14	0.43
6g	90	4.86	0.34
6h	90	4.94	0.86

5.8 Core Flood Experiments

Four core flood experiments, core flood A, B, C and D, were conducted involving surfactants **4f**, **4g**, **6g** and **6h,** respectively. The core flood studies included the determination of the core plug properties, preparation of the core for the enhanced oil recovery operation (by injecting brine, crude oil and brine in sequence) and then injection of the surfactant solution and polymer solution to evaluate their performance in terms of enhanced oil recovery. This evaluation step is discussed in the following sections.

5.8.1 Brine Floods

Berea sandstone cores were used for the core flood experiments. Core details for all four experiments are presented in Table 5.8. A brine flood with a specific concentration of NaCl as presented in Table 5.10 was conducted after the initial preparation of the core sample by cleaning and then brine saturation. The core was flooded by using three different flow rates of 2 mL / min, 3 mL / min and 5 mL / min. The confining pressure was 1000 psi for all four core flood experiments. The flood

was continued until the steady state conditions were achieved (i.e., the pressure drop across the core became constant). The pressure drop data were used to calculate the brine permeability, k_{brine}. The results are presented in Table 5.9 with other experiment results.

Table 5.8: Berea core properties for the core floods A, B, C and D

Variable	Description			
	Core A	Core B	Core C	Core D
Pore volume (mL)	16.1	16.8	21.5	19.7
Porosity	0.187	0.187	0.246	0.219
Length (cm)	7.69	7.73	7.59	7.76
Diameter (cm)	3.78	3.78	3.83	3.84
Mass (g)	183	184	196	188

5.8.2 Oil Floods

After the brine flood, the oil flood was commenced. The oil flood was performed at a constant injection rate of 2 ft / day at 60 °C and 90 °C. The pressure drop data across the core was noted after the water cut became less than 1 % and the pressure became stabilized. The oil permeability, k_{oil}, was calculated from the pressure drop data. The results are presented in Table 5.9. The initial oil saturation (S_{oi}) for the oil floods were calculated as 0.79, 0.77, 0.80 and 0.82 for oil floods A, B, C and D, respectively.

Table 5.9: Permeability data (mD) for the core floods A, B, C and D

Core Flood	k_{brine}	k_{oil}	k_{ro}	k_{water}	k_{rw}
A	223	182	0.816	41.2	0.184
B	227	180	0.792	46.8	0.206
C	312	260	0.833	53.1	0.170
D	336	286	0.851	50.6	0.150

5.8.3 Water Floods

A water flood with brine (varying NaCl concentrations) was performed after completing the oil flood. The brine was flooded by using two flow rates, 0.3 mL / min and 0.6 mL / min. The pressure drop data for both flow rates were recorded and the water permeability, k_{water}, was calculated. In addition, the initial oil saturation was also calculated. The water relative permeability, k_{rw}, was calculated from these data and the results are presented in Table 5.9.

5.8.4 Chemical Floods

ASP slug was commenced after water flood. All necessary calculations such as end point water and oil permeability values, initial oil saturation and residual water saturation values were performed. The slug consisted of 0.5 % of the surfactant, 1 % alkali, 2 % IBA and varying polymer concentrations. A slug size of 0.3 pore volume was injected at the flow rate of 2 ft / day. After this injection, a polymer drive was injected, until the pressure deferential become constant, with the required concentration of the polymer in the required salinity (NaCl) as shown in Table 5.10

including the type of surfactant used. The estimated shear rate in the porous media (Berea core sample) was 10 s^{-1}.

The differential pressure data were used to calculate the effective oil permeability values (Table 5.9). The oil recovery plots against the injected pore volumes are shown in Figures 5.11 to 5.14 below.

Table 5.10: ASP slug and polymer drive compositions and the cumulative oil recovery data

Flood	Slug / Drive	Surfactant (0.5 %)	Polymer (ppm) **H or L**	Viscosity at 10 s^{-1}	Salinity NaCl ppm	Oil recovery (%)
A	ASP	**4f**	1000	14	26000	90
	Polymer	-	1200	16.5		
B	ASP	**4g**	1000	13	23000	93
	Polymer	-	1200	15		
C	ASP	**6g**	1200	10	25000	94
	Polymer	-	1500	13.2		
D	ASP	**6h**	1200	11.4	24000	96
	Polymer	-	1200	14		

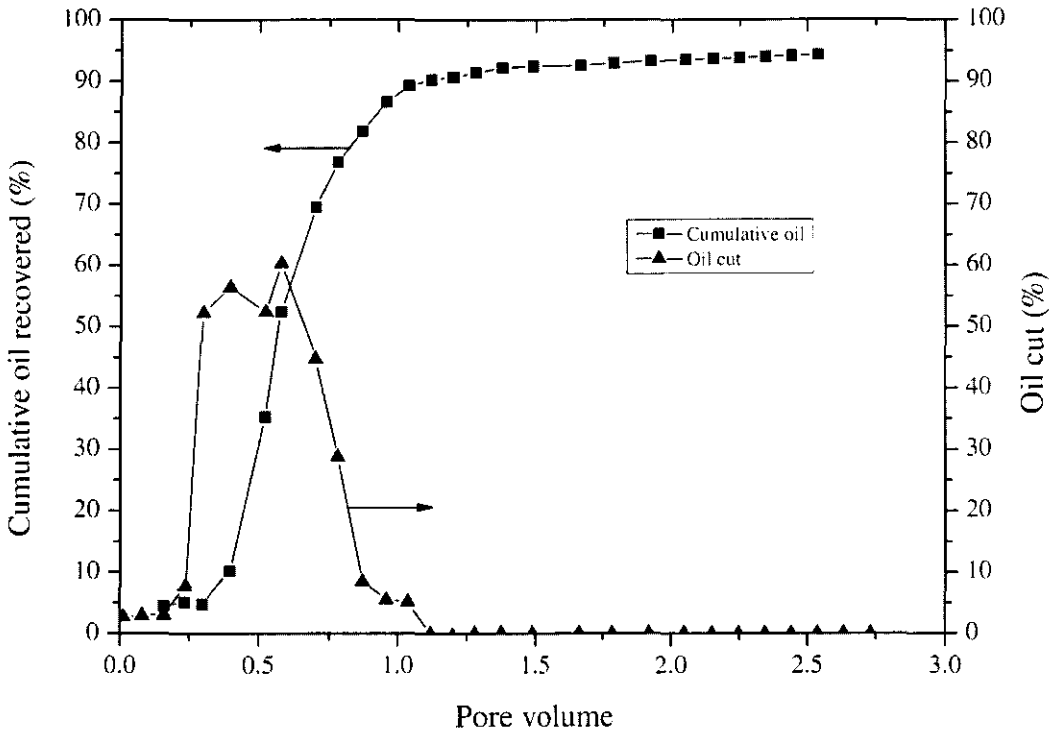

Figure 5.11: Chemical (ASP) core flood A oil recovery

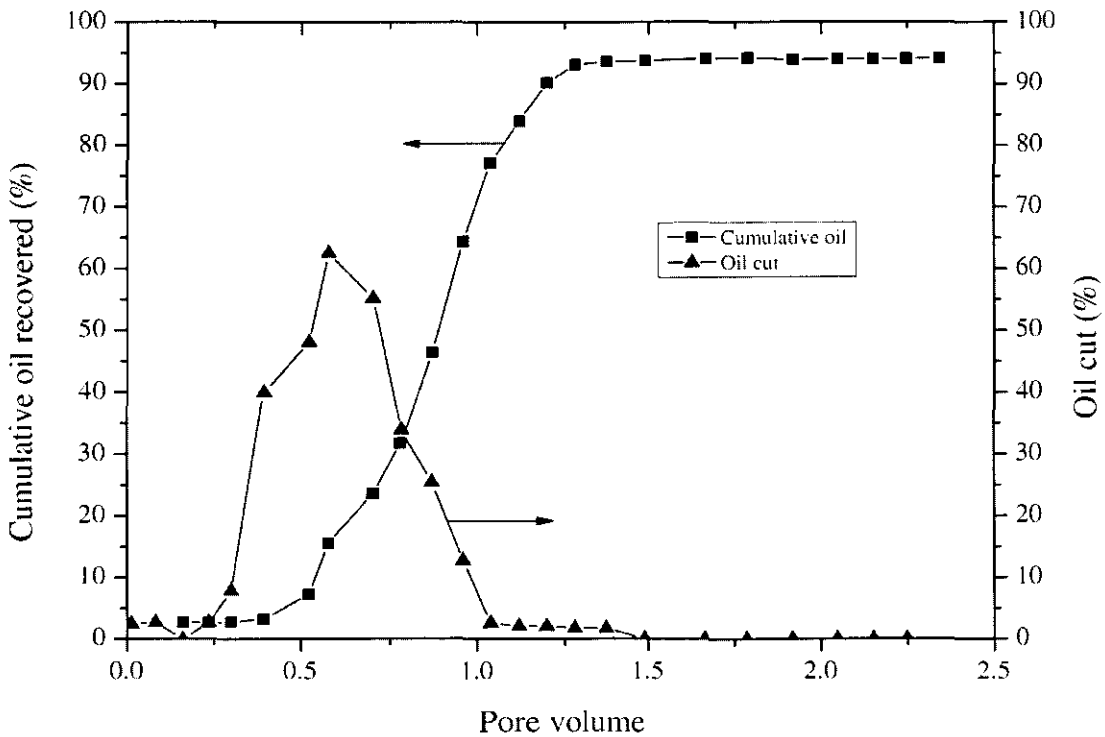

Figure 5.12: Chemical (ASP) core flood B oil recovery

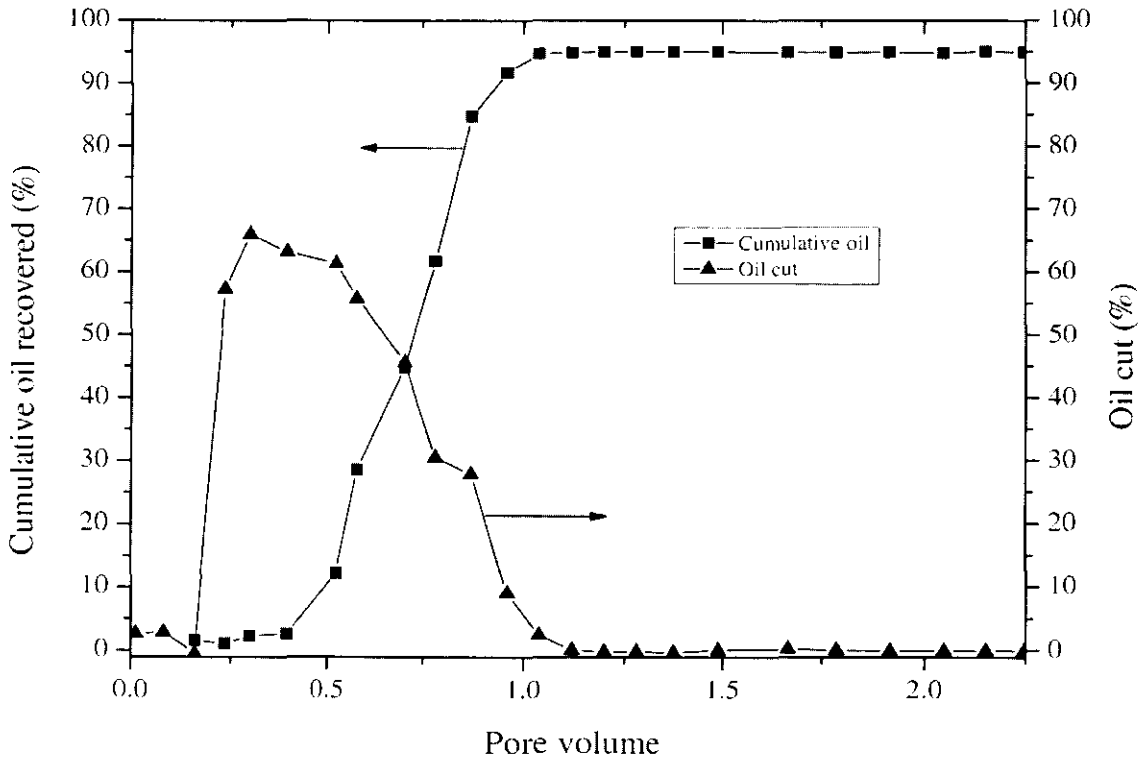

Figure 5.13: Chemical (ASP) core flood C oil recovery

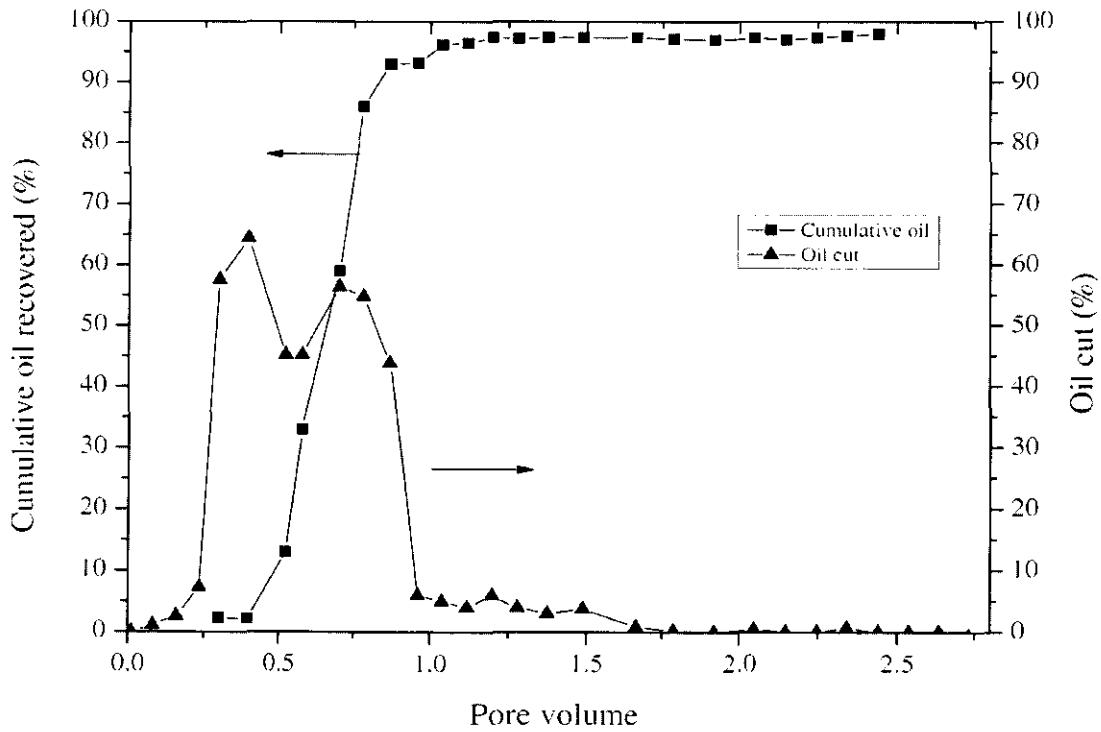

Figure 5.14: Chemical (ASP) core flood D oil recovery

5.8.5 Oil Recovery Performance of the Surfactants

The cumulative oil recovery data are tabulated in Table 5.10. Both the sulfate and sulfonate surfactants were found to be good in performance with the sulfonate being superior to the sulfate counterparts. The sulfate surfactants **4f** and **4g** had side chains of hexoxy and octoxy groups, respectively. The sulfonate surfactants **6g** and **6h** contained octoxy and decoxy side chains. Therefore, both the 4g and 6g surfactants had similar structures with different head groups. If their performance were to be compared, sulfate surfactant (**4g**) recovered 93 % of the oil while sulfonate surfactant (**6g**) recovered 94 % of the oil. The performance of both surfactants was remarkably similar. It is, therefore, concluded that the oil recovery performance of a surfactant is highly dependent on its hydrocarbon structure and its head group is important towards solution issues such as salinity and temperature tolerances.

The exceptionally high performance of **6h** (sulfonate surfactant with decoxy side chain) with an oil recovery of 97 % was due to its long and bulky hydrocarbon chain. The sulfonate group was stable at more than 100 °C making this surfactant a strong candidate for an enhanced oil recovery formulation.

5.9 Chapter Summary

This chapter presented the evaluation of the synthesized surfactants for the EOR applications. The detailed aqueous solubility and stability tests revealed that the sulfate surfactants were more tolerant to salinity than their sulfonate equivalents. The sulfonate surfactants, however, were found more stable at high temperatures. The phase behavior, IFT and core flood tests revealed that the sulfonate surfactant containing the n-hexoxy side chain was the best in the oil recovery performance.

CHAPTER 6

CONCLUSION AND RECOMMENDATION

In this chapter, the conclusions and recommendations for future work are presented.

6.1 Conclusions

In this study, eighteen new surfactants were synthesized from Jatropha oil and high oleic acid methyl ester. Jatropha oil was used due to its inedible nature and no competition for the food and feed market. For the synthesis, Jatropha oil was transesterified with methanol to obtain the fatty acid methyl esters. The hurdle of the high FFA which was preventing the base catalyzed transesterification reaction was solved by developing a new silica based solid catalyst for the FFA esterification. The high FFA value was lowered down to less than 1 % by using the developed catalyst. It was found that the silica sulfuric acid and the silica based BF_3 catalysts were found inferior in performance than their 50:50 weight based mixture, the hybrid catalyst. The unique combination of the SO_3 and BF_3 groups attached to the silica surface acted synergistically to esterify the free fatty acids present in the Jatropha oil. The esterification reaction under the influence of the catalyst was found to obey the first order kinetics with an activation energy of 45.42 kJ mol^{-1}.

The treated Jatropha oil with a low FFA value was transesterified with a base catalyzed transesterification reaction to obtain the fatty acid methyl esters.

The obtained FAME from the Jatropha oil and the HOAME were epoxidized by using formic acid and hydrogen peroxide. The reaction was optimized by using the RSM technique following the Central Composite Rotatable Design. By using this design of

experiment, a new formulation of formic acid and hydrogen peroxide was proposed at a specific reaction temperature. The high yield of the epoxied methyl esters (92.83 %) was obtained in a relatively shorter reaction time than the reported values. In this study, it was concluded that the 3.12 moles of H_2O_2 reacted with 0.96 moles of formic acid at 70.0°C to give the high yield in 4 hours 35 minutes, a reaction time much shorter than the reported 6 hours to 240 hours.

The next step was the attachment of the side chains to the backbone of the epoxidized fatty acid methyl esters thereby forming alkoxy-hydroxy methyl esters. Nine alcohols, namely ethanol, *n*-propanol, iso-propanol, *n*-butanol, iso-butanol, *n*-hexanol, *n*-octanol, *n*-decanol and *n*-dodecanol were successfully attached to the backbone with the ether linkage. BF_3 in the ether was used as the catalysts. The longer chain alcohols were difficult to attach and longer reaction times were required as compared to the short chain alcohols. In addition, alcohols with branches were also hard to attach due to the steric hindrance posed by their branched chains. The leftover alcohols in the product were removed by steam distillation which took a longer time to remove the long chain alcohols.

The alkoxy-hydroxy methyl esters were converted to surfactants by the attachment of the sulfate and sulfonate groups. In this context, nine sulfate surfactants were synthesized by using chlorosulfonic acid as the sulfating agent. The hydroxy group (-OH group) present on the 10^{th} position of the alkoxy-hydroxy methyl ester backbone was sulfated to produce the 9-alkoxy-10-sulfooxy octadecanoic acid methyl ester in high yields ranging from 82 - 91 %. The alkoxy-hydroxy methyl esters with branched side chains and longer side chains yielded low yields depending on the bulk of the side chain. It was concluded that due to the steric hindrance, the longer the side chain was, the lower the yield was.

The sulfonation reaction was used to attach the sulfonic acid group at α- position (2^{nd} position). For the sulfonation reaction, the -OH groups were first protected by the acetylation reaction. The obtained acetoxy-alkoxy methyl esters were used to react with the gaseous SO_3 in a falling film reactor to attach the sulfonate group at the alpha position to obtain the 10-Acetoxy-9-alkoxy-2-sulfo-octadecanoic acid methyl ester. The yield of the sulfonate products was in the range of 81.3 - 87.2 % following the

similar pattern as shown by their sulfate counterparts, i.e., the longer and branched the side chain, the lower the yield will be. This observation was due to two reasons. Firstly, the role of the steric hindrance was there. The reaction was not very efficient in the presence of the longer and branched side chains. The second reason was the high viscosity of the acetoxy-alkoxy methyl esters with the longer side chains. The mass transfer was not efficient at low temperatures due to the high viscosity, and at higher temperatures, the reaction was slow and less efficient due to its exothermic nature.

For the evaluation of the surfactants, the phase behavior and the fluid-fluid compatibility tests were conducted at 60 °C for the sulfate surfactants and at 90°C for the sulfonate surfactants. The temperatures were selected to verify the performance of the obtained surfactants at two temperatures as well as to assess the performance sulfate based surfactants which were not stable at temperatures higher than 60 °C. All sulfate surfactant solutions except for two (9-decoxy-10-sulfooxy octadecanoic acid methyl ester and 9-dodecoxy-10-sulfooxy octadecanoic acid methyl ester) were found to be stable and remained clear in hard brine, 1 % alkali and 0.15 % polymer. On the other hand, at 90 °C, all sulfonate surfactants except for one (10-Acetoxy-9-dodecoxy-2-sulfo-octadecanoic acid methyl ester) were found to be stable. These surfactants were also found compatible with 1 % alkali and 0.15 % polymer solution. The solubility of the surfactants was dependent upon their hydrophobic nature (the tail hydrocarbon bulk). The surfactants with longer side chains were less soluble in water and brine. However, the solubility was improved at a high temperature and this was the reason that sulfonate surfactants were soluble up to10-Acetoxy-9-decoxy-2-sulfo-octadecanoic acid methyl ester while their sulfate complements were found insoluble due to the lower experiment temperature (60 °C against 90 °C).

All of the fifteen stable and soluble surfactants were investigated for the phase behavior test at respective temperatures and at atmospheric pressure with varying amounts of salinity (NaCl %). All sulfate and sulfonate surfactants generated microemulsions which was an indication that these surfactants could be used for the enhanced oil recovery applications. However, due to the large number of surfactants involved, it was decided that the best candidate among the surfactants would be

chosen for the core flood experiments. In this context, it was found that from the sulfate surfactants only **4f** and **4g** (9-hexoxy-10-sulfooxy octadecanoic acid methyl ester and 9-octoxy-10-sulfooxy octadecanoic acid methyl ester) were good, possessing solubilization parameter values of 18 and 22, respectively. The range of solubilization parameter values was 9 – 12 for the sulfate surfactants. The optimum salinity trend was found to be similar with the reported values and the optimum salinity decreased (from 23000 to 39000 ppm NaCl) with an increasing side chain length or carbon chain bulkiness. The optimum salinity for 4f and 4g was 23000 and 26000 ppm NaCl, respectively.

For the sulfonate surfactants, the test was conducted at an elevated (90 °C) temperature. The high temperature enhanced the solubility of the surfactants in brine and, therefore, eight sulfonate surfactants were tried for the phase behavior test as compared to seven from the sulfate surfactants.

The solubilization parameters were found to be similar to those of the sulfate surfactants with equivalent hydrocarbon chains. The range of the solubilization parameter values was 8 to 25. The highest value of 25 was obtained in the case of **6h** (10-Acetoxy-9-decoxy-2-sulfo-octadecanoic acid methyl ester) with an optimum salinity of 24000 ppm NaCl. This surfactant had the largest hydrocarbon tail among all of the sulfate and sulfonate candidates for the phase behavior test. The optimum salinity also reflected the same behavior as was observed for the sulfate surfactants. The range of the optimum salinity was found to be 24000 to 36000 ppm NaCl.

Based on the phase behavior tests, two sulfate surfactants namely **4f**, and **4g**, and three sulfonate surfactants namely **6f**, **6g**, and **6h** were selected for further evaluations by the IFT test and the core flood tests.

The IFT was measured against Dulang crude at the conditions of the maximum solubilization parameters. The lowest IFT (0.008 mN / m) was found for the 6h surfactant. Other surfactants lowered the IFT in the range of 0.008 - 0.025 mN / m.
The synthesized surfactants were also evaluated for their adsorption on Berea sandstone. The effect of alkali was investigated in this context. The adsorption of the **4g** surfactant was the highest at 5.14 mg / g. The sulfonate surfactant with a similar

hydrocarbon chain was less adsorbed, showing a 4.86 mg / g adsorption. The reason for this disparity was the temperature; the sulfonate surfactants were evaluated at 90 °C as compared to 60 °C for the sulfate surfactants. Due to the temperature effect, the adsorption of the **6h** sulfate surfactant was low, 4.49 mg / g despite the fact that it had the longest hydrocarbon chain attachment. The effect of alkali was monumental and in the presence of alkali, the adsorption for all surfactants was less than 0.90 mg / g. The core flood tests were conducted by employing the ASP scheme by injecting the 0.3 pore volumes of ASP as a single slug. Both sulfate surfactants (**4f** and **4g**) recovered 90 and 93 % cumulative oil recovery of the trapped oil, respectively. The performance of the **6g** sulfonate surfactants was slightly better with a 94 % cumulative oil recovery.

The maximum oil recovery (96 %) was obtained with the usage of **6h** (10-Acetoxy-9-decoxy-2-sulfo-octadecanoic acid methyl ester). This surfactant had the largest hydrocarbon bulk and it recovered 96 % of the trapped oil. The performance of sulfate and sulfonate based surfactants (**4g** and **6g**) with similar hydrocarbon chains was found remarkably similar. It is, therefore, concluded that the performance of the surfactants is highly dependent on their hydrocarbon chain structure and bulk. The head groups are mainly responsible for the salinity and temperature tolerance issues. This fact has also been verified by the finding that the **6h** (10-Acetoxy-9-decoxy-2-sulfo-octadecanoic acid methyl ester) surfactant delivered the best performance in terms of the highest cumulative oil recovery of 96 %. This surfactant has the longest hydrocarbon side chain.

6.2 Future Work

The sulfate surfactants were evaluated at 60 °C due to their instability at higher temperatures. However, the sulfate surfactants are reported to be stable at 90 °C by adjusting the pH value between 10 and 11. Therefore, these surfactants can be evaluated at higher temperatures by adjusting the right pH values.

The foaming ability of these surfactants for EOR applications should also be investigated. These surfactants can generate stable foam and are good candidates for foaming agents for mobility control in chemical EOR.

6.3 Chapter Summary

The conclusions drawn from the thesis have been presented in this chapter. Some suggestions for the future work have also been provided.

REFERENCES

[1] http://omrpublic.iea.org, accessed on 19-10-2012.

[2] J.J. Sheng, Modern Chemical Enhanced Oil Recovery, Gulf Professional Publishing, Boston, 2011.

[3] M.K. Hamdan, N.B. Darman, D. Husain, Z.B. Ibrahim, Enhanced Oil Recovery in Malaysia: Making It a Reality, in: SPE Asia Pacific Oil and Gas Conference and Exhibition, Society of Petroleum Engineers, Jakarta, Indonesia, 2005.

[4] A. Manap, M.O. Chong, R.M. Sai, S. Zainal, A.W. Yahaya, M. Othman, Evaluation of Alkali-Surfactant Effectiveness by Single Well Test Pilot in a Malaysian Offshore Field Environment, in: SPE Enhanced Oil Recovery Conference, Society of Petroleum Engineers, Kuala Lumpur, Malaysia, 2011.

[5]http://www.ceresana.com/en/market-studies/chemicals/surfactants/ceresana-research-market-study-surfactants.html, accessed on 26-10-2012.

[6] D. Myers, Surfactant Science and Technology. Third ed. 2006, New Jersey: John Wiley & Sons, Inc.

[7] M. Aoudia, M. Al-Shibli, L. Al-Kasimi, R. Al-Maamari, A. Al-bemani, Novel surfactants for ultralow interfacial tension in a wide range of surfactant concentration and temperature, J. Surfactants Deterg., 9 (2006) 287-293.

[8]http://www.ceresana.com/en/market-studies/chemicals/surfactants/ceresana-research-market-study-surfactants.html, accessed on 26-10-2012.

[9] B.J. Krister Holmberg, Bengt Kronberg, Bjorn Lindman, Surfactants and Polymers in Aqueous Solution, Second ed., John Wiley and Sons Ltd., West Sussex, England, 2003.

[10] R. Narayanan, Interfacial Processes and Molecular Aggregation of Surfactants, in: Advances in Polymer Science Springer-Verlag Berlin Heidelberg, Heidelberg, 2008.

[11] D. Myers, Surfactant Science and Technology, Third ed., John Wiley & Sons, Inc, New Jersey, 2006.

[12] L.L. Schramm, D.G. Marangoni, Surfactants and their Solutions: Basic Principles Cambridge University Press; ISBN No.: 0 521 64067 9; Edited by L.L. Schramm, 2000, 15 pp, in: Surfactants. Fundamentals and Applications in the Petroleum Industry, 2000.

[13] L.L. Schramm, Emulsions, Foams, and Suspensions: Fundamentals and Applications, Wiley-VCH, Weinheim, , Germany, 2005.

[14] J.J. Sheng, Chapter 7 in: Modern Chemical Enhanced Oil Recovery, Gulf Professional Publishing, Boston, 2011, pp. 242.

[15] Thomas, F. Ali, A Realistic Look at Enhanced Oil Recovery, Scientia Iranica, 1 (1994).

[16] L.C. Uren, E.H. Fahmy, Factors influencing the recovery of petroleum from unconsolidated sands by waterflooding, Perrol (1927) Dev. Technol, , Petrol. Div. AIME, 318, (1927).

[17] G.J. Hirasaki, C.A. Miller, M. Puerto, Recent advances in surfactant EOR, in, 2008, pp. 1108-1142.

[18] J.A.D. Jr., S.C. Jones, Displacement Mechanisms of Micellar Solutions, 1968.

[19] I.O.R.b.S.a.P.F. Healy and Reed , A.P. D. O. Shah and R. S. Schecheter. Eds., p. 383-347.

[20] R.N. Healy, R.L. Reed, Immiscible Microemulsion Flooding, (1977).

[21] R.N. Healy, R.L. Reed, C.W. Carpenter Jr., A Laboratory Study of Microemulsion Flooding (includes associated papers 6395 and 6396), 15 (1975).

[22] R.N. Healy, R.L. Reed, D.G. Stenmark, Multiphase Microemulsion Systems, (1976).

[23] J.P. Batychy, F.G. McCaffery, Low Interfacial Tension Displacement Studies, in: Annual Technical Meeting, Calgary, Alberta, 1978.

[24] M.A. Buijse, R.M. Prelicz, J.R. Barnes, C. Cosmo, Application of Internal Olefin Sulfonates and Other Surfactants to EOR. Part 2: The Design and Execution of an ASP Field Test, in: SPE Improved Oil Recovery Symposium, Society of Petroleum Engineers, Tulsa, Oklahoma, USA, 2010.

[25] J.R. Barnes, H. Dirkzwager, J. Smit, J. Smit, A. On, R.C. Navarrete, B. Ellison, M.A. Buijse, Application of Internal Olefin Sulfonates and Other Surfactants to EOR. Part 1: Structure - Performance Relationships for Selection at Different Reservoir Conditions, in: SPE Improved Oil Recovery Symposium, Tulsa, Oklahoma, USA, 2010.

[26] J.R. Barnes, J. Smit, J. Smit, G. Shpakoff, K.H. Raney, M. Puerto, Development of Surfactants for Chemical Flooding at Difficult Reservoir Conditions, in: SPE/DOE Symposium on Improved Oil Recovery, Society of Petroleum Engineers, Tulsa, Oklahoma, USA, 2008.

[27] H.T. Davis, L.E. Scriven, The Origins Of Low Interfacial Tensions For Enhanced Oil Recovery, in: SPE Annual Technical Conference and Exhibition, 1980 Copyright 1980, American Institute of Mining, Metallurgical, and Petroleum Engineers, Inc., Dallas, Texas, 1980.

[28] G.P. Willhite, D.W. Green, D.M. Okoye, M.D. Looney, A Study of Oil Displacement by Microemulsion Systems Mechanisms and Phase Behavior, 20 (1980).

[29] J.O. Amaefule, L.L. Handy, The Effect of Interfacial Tensions on Relative Oil/Water Permeabilities of Consolidated Porous Media, 22 (1982).

[30] C.E. Brown, T.J. Jones, E.L. Neustadter, K.P. Whittingham, The Measurement of Interfacial Forces During Crude Oil/water Immiscible Displacement, 21 (1982).

[31] A. Graciaa, L.N. Fortney, R.S. Schechter, W.H. Wade, S. Yiv, Criteria for Structuring Surfactants To Maximize Solubilization of Oil and Water: Part 1- Commercial Nonionics, (1982).

[32] Y. Barakat, L.N. Fortney, R.S. Schechter, W.H. Wade, S.H. Yiv, A. Graciaa, Criteria for structuring surfactants to maximize solubilization of oil and water: II. Alkyl benzene sodium sulfonates, J. Colloid Interface Sci., 92 (1983) 561-574.

[33] S.J. Salter, Criteria for Surfactant Selection in Micellar Flooding, in: International Meeting on Petroleum Engineering, 1986 Copyright 1986, Society of Petroleum Engineers, Beijing, China, 1986.

[34] R.E. Terry, J.C. Robinson, R.S. Mandel, Characterization of Hydrocarbon-Surfactant Systems by Alcohol-Brine Titration and Hydrocarbon Displacement Experiments, in: SPE Oilfield and Geothermal Chemistry Symposium, Denver, Colorado, 1983.

[35] S.S. Ashrawi, A Study of the Relationship Between Surfactant/Oil/Brine System Phase Behavior and Chemical Flood Recovery in Short Cores, in: SPE Enhanced Oil Recovery Symposium, Tulsa, Oklahoma, 1984.

[36] S.I. Chou, J.H. Bae, Phase-Behavior Correlation for High- Salinity Surfactant Formulations, SPE Reservoir Engineering, 3 (1988).

[37] A. Skauge, O. Palmgren, Phase Behavior and Solution Properties of Ethoxylated Anionic Surfactants, in: SPE International Symposium on Oilfield Chemistry, Houston, Texas, 1989.

[38] A. Witthayapanyanon, E. Acosta, J. Harwell, D. Sabatini, Formulation of ultralow interfacial tension systems using extended surfactants, J. Surfactants Deterg., 9 (2006) 331-339.

[39] P. Zhao, A. Jackson, C. Britton, D.H. Kim, L.N. Britton, D. Levitt, G.A. Pope, Development of High-Performance Surfactants for Difficult Oils, in: SPE/DOE Symposium on Improved Oil Recovery, Society of Petroleum Engineers, Tulsa, Oklahoma, USA, 2008.

[40] H.T. Yang, C. Britton, P.J. Liyanage, S. Solairaj, D.H. Kim, Q.P. Nguyen, U. Weerasooriya, G.A. Pope, Low-Cost, High-Performance Chemicals for Enhanced Oil Recovery, in: SPE Improved Oil Recovery Symposium, Society of Petroleum Engineers, Tulsa, Oklahoma, USA, 2010.

[41] M. Puerto, G.J. Hirasaki, C.A. Miller, J.R. Barnes, Surfactant Systems for EOR in High-Temperature, High-Salinity Environments, SPE Journal, 17 (2012) pp. 11-19.

[42] S. Adkins, G.W.P.P. Arachchilage, S. Solairaj, J. Lu, U. Weerasooriya, G.A. Pope, Development of Thermally and Chemically Stable Large-Hydrophobe Alkoxy

Carboxylate Surfactants, in: SPE Improved Oil Recovery Symposium, Society of Petroleum Engineers, Tulsa, Oklahoma, USA, 2012.

[43] J.R. Barnes, K. Groen, A. On, S.T. Dubey, C. Reznik, M.A. Buijse, A.G. Shepherd, Controlled Hydrophobe Branching To Match Surfactant To Crude Composition For Chemical EOR, in: SPE Improved Oil Recovery Symposium, Society of Petroleum Engineers, Tulsa, Oklahoma, USA, 2012.

[44] J. Drozd, D. Desai, Liquid laundry detergents based on soap and α -sulfo methyl esters, J. Am. Oil Chem. Soc., 68 (1991) 59-62.

[45] K. Raney, P. Shpakoff, D. Passwater, Use of high-active alpha olefin sulfonates in laundry powders, J. Surfactants Deterg., 1 (1998) 361-369.

[46] H.L. Wen, Phase diagram of α-sulfonate methyl esters derived from palm stearin/alcohol/water systems, J. Surfactants Deterg., 7 (2004) 263-270.

[47] Y. Yu, J. Zhao, A.E. Bayly, Development of Surfactants and Builders in Detergent Formulations, Chin. J. Chem. Eng., 16 (2008) 517-527.

[48] E. Maurer, J. Weil, W. Linfield, The biodegradation of esters of α-sulfo fatty acids, J. Am. Oil Chem. Soc., 54 (1977) 582-583.

[49] M. Bavière, B. Bazin, J.-C. Miléo, Physicochemical properties of sulfonated fatty acid esters for oil recovery by surfactant flooding, Colloids Surf., 52 (1991) 301-313.

[50] D.W. Green, Willhite, G.P., 1998. Enhanced Oil Recovery. Society of Petroleum Engineers, Dallas.

[51] L. Schramm Laurier, Petroleum Emulsions, in: Emulsions, American Chemical Society, 1992, pp. 1-49.

[52] R.A. Nasralla, M.A. Bataweel, H.A. Nasr-El-Din, Investigation of Wettability Alteration by Low Salinity Water, in: Offshore Europe, Aberdeen, UK, 2011.

[53] M. Saneifar, H.A. Nasr-El-Din, R.A. Nasralla, M.M. Fahes, D. HIll, Effect of Spent Acids on the Wettability of Sandstones and Carbonates at High Temperature and Pressure, in: SPE European Formation Damage Conference, Noordwijk, The Netherlands, 2011.

[54] W. Anderson, Wettability Literature Survey- Part 2: Wettability Measurement, SPE Journal of Petroleum Technology, (1986).

[55] N.R. Morrow, Wettability and Its Effect on Oil Recovery, SPE Journal of Petroleum Technology, (1990).

[56] C.C. Agbalaka, A.Y. Dandekar, S.L. Patil, S. Khataniar, J. Hemsath, The Effect of Wettability on Oil Recovery: A Review, in: SPE Asia Pacific Oil and Gas Conference and Exhibition, Perth, Australia, 2008.

[57] W.G. Anderson, Wettability Literature Survey- Part 1: Rock/Oil/Brine Interactions and the Effects of Core Handling on Wettability, SPE Journal of Petroleum Technology, (1986).

[58] W.G. Anderson, Wettability Literature Survey- Part 4: Effects of Wettability on Capillary Pressure, SPE Journal of Petroleum Technology, 39 (1987) 1283-1300.

[59] A. Kantzas, B. Nikakhtar, M. Pow, Principles of Three Phase Capillary Pressures, (1998).

[60] Djebbar Tiab , Erle C. Donaldson, E. Petrophysics: theory and practice of measuring reservoir rock and fluid transport properties, New York, 2nd ed, pp102.

[61] http://www.glossary.oilfield.slb.com/Display.cfm?Term=permeability, accessed on 13-10-2011

[62] L.W. Lake,. Enhanced Oil Recovery. 1989, Prentice-Hall.

[63] R.L. Reed, R.N. Healy., Improved Oil Recovery by Surfactant and Polymer Flooding, Academic Press 1977.

[64] I. Fjelde, J. Zuta, I. Hauge, Retention of CO2-foaming agents onto chalk: Effects of surfactant structure, temperature and residual oil saturation, in, 2008, pp. 374-383.

[65] R.V. Zanten, Stabilizing Viscoelastic Surfactants in High Density Brines, in: SPE International Symposium on Oilfield Chemistry, The Woodlands, Texas, USA, 2011.

[66] R.V. Zanten, A.M. Ezzat, Advanced Viscoelastic Surfactant Gels for High-Density Completion Brines, in: SPE European Formation Damage Conference, Noordwijk, The Netherlands, 2011.

[67] G.J. Hirasaki, C.A. Miller, M. Puerto, Recent advances in surfactant EOR, in, 2008, pp. 130-164.

[68] M.H. Sayyouh, A.A. Abdel-Waly, J. George, O.A. Salama, Design of a Microemulsion Slug for Maximizing Tertiary Oil Recovery Efficiency, in, Society of Petroleum Engineers, 1991.

[69] A. Flaaten, Q.P. Nguyen, G.A. Pope, J. Zhang, A Systematic Laboratory Approach to Low-Cost, High-Performance Chemical Flooding, SPE Reservoir Eval. Eng., 12 (2009) pp. 713-723.

[70] P.A. Winsor, Solvent Properties of Amphiphilic Compound, (1985).

[71] R.N. Healy, R.L. Reed, Physicochemical Aspects of Microemulsion Flooding, 14 (1974).

[72] Modern Chemical Enhanced Oil Recovery, Theory and Practice. James J. Sheng, Gulf Professional Publishing, 2011, Chapter 7.

[73] R.N. Healy, R.L. Reed, D.G. Stenmark, Multiphase Microemulsion Systems, 16 (1976).

[74] C. Huh, Interfacial tensions and solubilizing ability of a microemulsion phase that coexists with oil and brine, Journal of Colloid and Interface Science, 71 (1979) 408-426.

[75] G.R. Glinsmann, Surfactant Flooding With Microemulsions Formed In-Situ - Effect Of Oil Characteristics, in: SPE Annual Technical Conference and Exhibition, Las Vegas, Nevada, 1979.

[76] A.K. Flaaten, Q.P. Nguyen, G.A. Pope, J. Zhang, A systematic laboratory approach to low-cost high-performance chemical flooding, SPE Reservoir Evaluation and Engineering, 12 (2009) 713-723.

[77] J.R. Barnes, J. Smit, J. Smit, G. Shpakoff, K.H. Raney, M. Puerto, Phase Behaviour Methods for the Evaluation of Surfactants for Chemical Flooding at Higher Temperature Reservoir Conditions, in: SPE/DOE Symposium on Improved Oil Recovery, Society of Petroleum Engineers, Tulsa, Oklahoma, USA, 2008.

[78] S. Liu, D. Zhang, W. Yan, M. Puerto, G.J. Hirasaki, C.A. Miller, Favorable Attributes of Alkaline-Surfactant-Polymer Flooding, SPE Journal, 13 (2008) pp. 5-16.

[79] G.M. Graham, S.L. Kidd, R. Stalker, R. Wright, Effect of Coreflood Test Methodology on Appropriate Simulation of Field Treatments, in: SPE International Symposium and Exhibition on Formation Damage Control, Society of Petroleum Engineers, Lafayette, Louisiana, USA, 2012.

[80] S. Mustafa, M. Waseem, A. Naeem, K.H. Shah, T. Ahmad, S.Y. Hussain, Selective sorption of cadmium by mixed oxides of iron and silicon, Chem. Eng. J., 157 (2010) 18-24.

[81] S. Solairaj, C. Britton, D.H. Kim, U. Weerasooriya, G.A. Pope, Measurement and Analysis of Surfactant Retention, in: SPE Improved Oil Recovery Symposium, Society of Petroleum Engineers, Tulsa, Oklahoma, USA, 2012.

[82] Z.J. Zhang, C.H. Liang, J. Sui, B. Cheng, Development of petroleum sulfonates for enhanced oil recovery, Xiandai Huagong/Modern Chemical Industry, 23 (2003) 19-22.

[83] F. Curbelo, V. Santanna, E. Neto, T. Dutrajr, T. Dantas, A. Neto, A. Garnica, Adsorption of nonionic surfactants in sandstones, Colloids and Surfaces A: Physicochemical and Engineering Aspects, 293 (2007) 1-4.

[84] A. Tabatabal, M.V. Gonzalez, J.H. Harwell, J.F. Scamehorn, Reducing Surfactant Adsorption in Carbonate Reservoirs, SPE Reservoir Engineering, 8 (1993).

[85] G.J. Hirasaki, C.A. Miller, M. Puerto, Recent Advances in Surfactant EOR, in: SPE Annual Technical Conference and Exhibition, Society of Petroleum Engineers, Denver, Colorado, USA, 2008.

[86] T. Austad, A Review of Retention Mechanisms of Ethoxylated Sulfonates in Reservoir Cores, in: SPE International Symposium on Oilfield Chemistry, 1993 Copyright 1993, Society of Petroleum Engineers, Inc. This paper was prepared for presentation at the SPE International Symposium on Oilfield Chemistry held in New Orleans, Louisiana, U.S.A., March 2-5, New Orleans, Louisiana, 1993.

[87] L.D. Talley, Hydrolytic Stability of Alkylethoxy Sulfates, SPE Reservoir Engineering, (1988).

[88] S. Adkins, P.J. Liyanage, G.W.P.P. Arachchilage, T. Mudiyanselage, U. Weerasooriya, G.A. Pope, A New Process for Manufacturing and Stabilizing High-Performance EOR Surfactants at Low Cost for High-Temperature, High-Salinity Oil Reservoirs, in: SPE Improved Oil Recovery Symposium, Society of Petroleum Engineers, Tulsa, Oklahoma, USA, 2010.

[89] D. Levitt, A. Jackson, C. Heinson, L.N. Britton, T. Malik, V. Dwarakanath, G.A. Pope, Identification and Evaluation of High-Performance EOR Surfactants, SPE Reservoir Eval. Eng., 12 (2009) pp. 243-253.

[90] J.R. Barnes, J.P. Smit, J.R. Smit, P.G. Shpakoff, K.H. Raney, M.C. Puerto, Development of surfactants for chemical flooding at difficult reservoir conditions, in, 2008, pp. 435-452.

[91] E.A. Knaggs, M.L. Nussbaum, J.B. Carlson, R.C. Guenzani, Petroleum Sulfonate Utilization in Enhanced Oil Recovery Systems, in: SPE Annual Fall Technical Conference and Exhibition, New Orleans, Louisiana, 1976.

[92] J. Yang, W. Qiao, Z. Li, L. Cheng, Effects of branching in hexadecylbenzene sulfonate isomers on interfacial tension behavior in oil/alkali systems, Fuel, 84 (2005) 1607-1611.

[93] B.J.B. Shiau, J.H. Harwell, P. Lohateeraparp, A.V. Dinh, B.L. Roberts, T.-P. Hsu, O.I. Anwuri, Designing Alcohol-Free Surfactant Chemical Flood for Oil Recovery, in: SPE EOR Conference at Oil & Gas West Asia, Society of Petroleum Engineers, Muscat, Oman, 2010.

[94] M. Aoudia, W.H. Wade, V. Weerasooriya, Optimum microemulsions formulated with propoxylated guerbet alcohol and propoxylated tridecyl alcohol sodium sulfates, J. Dispersion Sci. Technol., 16 (1995) 115-135.

[95] W.C. Griffin, 1954. Calculation of HLB values of non-ionic surfactants. J. Society of Cosmetic , Chemists 5.

[96] A. Graciaa, J. Lachaise, G. Marion, R.S. Schechter, A study of the required hydrophile-lipophile balance for emulsification, Langmuir, 5 (1989) 1315-1318.

[97] R.C. Pasquali, M.P. Taurozzi, C. Bregni, Some considerations about the hydrophilic–lipophilic balance system, Int. J. Pharm., 356 (2008) 44-51.

[98] J.T. Davies, 1957. A quantitative kinetic theory of emulsion type, I. physical chemistry of the , g.l.a.l.l.i.P.o.t.I. emulsifying agent, Congress of Surface Activity.

[99] P.A. Winsor, 1948. Hydrotropy, solubilization and related emulsification processes, part I. Trans. , Faraday Soc. 44.

[100] M. Bourrel, Schechter, R.S., 1988. Microemulsions and related systems, formulation, solvency, , I. and physical properties. Marcel Dekker.

[101] H.-Z. Wang, Liao, G.-Z., Song, J., 2006b. Combined chemical flooding technologies. In: Shen, , T.D.i.E.O.R.P.I.P. P.P. (Ed.), p. 126–188.

[102] J. Israelachvili, Intermolecular and Surface Forces, Second ed., Academic Press Inc., London, UK., 1992.

[103] A.S. Carlsson, Plant oils as feedstock alternatives to petroleum - A short survey of potential oil crop platforms, Biochimie, 91 (2009) 665-670.

[104] A. Hayyan, M.Z. Alam, M.E. Mirghani, N.A. Kabbashi, N.I. Hakimi, Y.M. Siran, S. Tahiruddin, Sludge palm oil as a renewable raw material for biodiesel production by two-step processes, Bioresour. Technol., (2010).

[105] H.P.S. Makkar, K. Becker, Jatropha curcas, a promising crop for the generation of biodiesel and value-added coproducts, Eur. J. Lipid Sci. Technol., 111 (2009) 773-787.

[106] A. Corma, S. Iborra, A. Velty, Chemical Routes for the Transformation of Biomass into Chemicals, ChemInform, 38 (2007) no-no.

[107] V.V. Goud, S. Dinda, A.V. Patwardhan, N.C. Pradhan, Epoxidation of Jatropha (Jatropha curcas) oil by peroxyacids, Asia-Pac. J. Chem. Eng., 5 (2010) 346-354.

[108] A. Campanella, C. Fontanini, M.A. Baltanás, High yield epoxidation of fatty acid methyl esters with performic acid generated in situ, Chem. Eng. J., 144 (2008) 466-475.

[109] L. Cohen, A. Moreno, J.L. Berna, Two phase titration of anionic surfactants - A new approach, Tenside, Surfactants, Deterg., 34 (1997) 183-185.

[110] Y. Miyake, K. Yokomizo, N. Matsuzaki, Determination of unsaturated fatty acid composition by high-resolution nuclear magnetic resonance spectroscopy, J. Am. Oil Chem. Soc., 75 (1998) 1091-1094.

[111] T. Khlebnikova, Z. Pai, L. Fedoseeva, Y. Mattsat, Catalytic oxidation of fatty acids. II. Epoxidation and oxidative cleavage of unsaturated fatty acid esters containing additional functional groups, React. Kinet. Catal. Lett., 98 (2009) 9-17.

[112] A. Campanella, E. Rustoy, A. Baldessari, M.A. Baltanás, Lubricants from chemically modified vegetable oils, Bioresour. Technol., 101 (2010) 245-254.

[113] L. Daniel, A.R. Ardiyanti, B. Schuur, R. Manurung, A.A. Broekhuis, H.J. Heeres, Synthesis and properties of highly branched Jatropha curcas L. oil derivatives, Eur. J. Lipid Sci. Technol., 113 (2011) 18-30.

[114] B. Hedman, P. Piispanen, E.O. Alami, T. Norin, Synthesis and characterization of surfactants via epoxidation of tall oil fatty acid, J. Surfactants Deterg., 6 (2003) 47-53.

[115] L. Cohen, F. Soto, C. Pratesi, L. Faccetti, Sulfoxidation of fatty acid methyl esters: Conversion and selectivity, J. Surfactants Deterg., 9 (2006) 47-50.

[116] L. Cohen, F. Soto, A. Melgarejo, D. Roberts, Performance of Φ-Sulfo Fatty Methyl Ester Sulfonate Versus Linear Alkylbenzene Sulfonate, Secondary Alkane Sulfonate and α-Sulfo Fatty Methyl Ester Sulfonate, J. Surfactants Deterg., 11 (2008) 181-186.

[117] A. Stirton, a -sulfo fatty acids and derivatives. Synthesis, properties and use, J. Am. Oil Chem. Soc., 39 (1962) 490-496.

[118] F. Smith, A. Stirton, The alpha-sulfonation of alkyl palmitates and stearates, J. Am. Oil Chem. Soc., 44 (1967) 405-406.

[119] R. Bistline, F. Smith, J. Well, A. Stirton, Hexitol and sucrose esters of α-sulfo fatty acids, J. Am. Oil Chem. Soc., 46 (1969) 549-551.

[120] W. Stein, H. Baumann, α-Sulfonated fatty acids and esters: Manufacturing process, properties, and applications, J. Am. Oil Chem. Soc., 52 (1975) 323-329.

[121] B. Kapur, J. Solomon, B. Bluestein, Summary of the technology for the manufacture of higher alpha-sulfo fatty acid esters, J. Am. Oil Chem. Soc., 55 (1978) 549-557.

[122] H. Makkar, J. Maes, W. De Greyt, K. Becker, Removal and degradation of phorbol esters during pre-treatment and transesterification of Jatropha curcas oil, JAOCS, Journal of the American Oil Chemists' Society, 86 (2009) 173-181.

[123] W.M.J. Achten, L. Verchot, Y.J. Franken, E. Mathijs, V.P. Singh, R. Aerts, B. Muys, Jatropha bio-diesel production and use, Biomass Bioenerg., 32 (2008) 1063-1084.

[124] M. Senthil Kumar, A. Ramesh, B. Nagalingam, An experimental comparison of methods to use methanol and Jatropha oil in a compression ignition engine, Biomass Bioenerg., 25 (2003) 309-318.

[125] S. Shah, S. Sharma, M.N. Gupta, Biodiesel preparation by lipase-catalyzed transesterification of Jatropha oil, Energy and Fuels, 18 (2004) 154-159.

[126] M. Mohibbe Azam, A. Waris, N.M. Nahar, Prospects and potential of fatty acid methyl esters of some non-traditional seed oils for use as biodiesel in India, Biomass Bioenerg., 29 (2005) 293-302.

[127] H. Zhou, H. Lu, B. Liang, Solubility of Multicomponent Systems in the Biodiesel Production by Transesterification of Jatropha curcas L. Oil with Methanol, Journal of Chemical & Engineering Data, 51 (2006) 1130-1135.

[128] A. Kumar, S. Sharma, An evaluation of multipurpose oil seed crop for industrial uses (Jatropha curcas L.): A review, Ind. Crop. Prod., 28 (2008) 1-10.

[129] H.J. Berchmans, S. Hirata, Biodiesel production from crude Jatropha curcas L. seed oil with a high content of free fatty acids, Bioresour. Technol., 99 (2008) 1716-1721.

[130] P.D. Patil, S. Deng, Optimization of biodiesel production from edible and non-edible vegetable oils, Fuel, 88 (2009) 1302-1306.

[131] H. Lu, Y. Liu, H. Zhou, Y. Yang, M. Chen, B. Liang, Production of biodiesel from Jatropha curcas L. oil, Computers and Chemical Engineering, 33 (2009) 1091-1096.

[132] P.C. Smith, Y. Ngothai, Q.D. Nguyen, B.K. O'Neill, Alkoxylation of biodiesel and its impact on low-temperature properties, Fuel, 88 (2009) 605-612.

[133] http://www.aocs.org, accessed on 23-7-11

[134] Y. Miyake, K. Yokomizo, N. Matsuzaki, Rapid determination of iodine value by ¹H nuclear magnetic resonance spectroscopy, J. Am. Oil Chem. Soc., 75 (1998) 15-19.

[135] K. Rao, P. Chakrabarti, B. Rao, R. Prasad, Phospholipid Composition of Jatropha curcus Seed Lipids, J. Am. Oil Chem. Soc., 86 (2009) 197-200.

[136] L.C. Meher, D. Vidya Sagar, S.N. Naik, Technical aspects of biodiesel production by transesterification--a review, Renewable and Sustainable Energy Reviews, 10 (2006) 248-268.

[137] A. Murugesan, C. Umarani, T.R. Chinnusamy, M. Krishnan, R. Subramanian, N. Neduzchezhain, Production and analysis of bio-diesel from non-edible oils--A review, Renewable and Sustainable Energy Reviews, 13 (2009) 825-834.

[138] H. Fukuda, A. Kondo, H. Noda, Biodiesel Fuel Production by Transesterification of Oils, The Society for Biotechnology, Japan, 92 (2001) 405-416.

[139] J.K. Satyarthi, D. Srinivas, P. Ratnasamy, Estimation of free fatty acid content in oils, fats, and biodiesel by 1H NMR spectroscopy, Energy and Fuels, 23 (2009) 2273-2277.

[140] AOCS (2009) Official methods and recommended practices of the American oil chemists' society, 6th edn. AOCS Press, Champaign.

[141] I.M. Atadashi, M.K. Aroua, A.R. Abdul Aziz, N.M.N. Sulaiman, Production of biodiesel using high free fatty acid feedstocks, Renewable and Sustainable Energy Reviews, 16 (2012) 3275-3285.

[142] D.Y.C. Leung, Y. Guo, Transesterification of neat and used frying oil: Optimization for biodiesel production, Fuel Process. Technol., 87 (2006) 883-890.

[143] M. Naik, L. Meher, S. Naik, L. Das, Production of biodiesel from high free fatty acid Karanja (Pongamia pinnata) oil, Biomass Bioenerg., 32 (2008) 354-357.

[144] Y. Wang, S.O. Pengzhan Liu, Z. Zhang, Preparation of biodiesel from waste cooking oil via two-step catalyzed process, Energy Conversion and Management, 48 (2007) 184-188.

[145] G. Corro, N. Tellez, E. Ayala, A. Marinez-Ayala, Two-step biodiesel production from Jatropha curcas crude oil using SiO2·HF solid catalyst for FFA esterification step, Fuel, 89 (2010) 2815-2821.

[146] M.E. Borges, L. Díaz, Recent developments on heterogeneous catalysts for biodiesel production by oil esterification and transesterification reactions: A review, Renewable and Sustainable Energy Reviews, 16 (2012) 2839-2849.

[147] M.K. Lam, K.T. Lee, A.R. Mohamed, Homogeneous, heterogeneous and enzymatic catalysis for transesterification of high free fatty acid oil (waste cooking oil) to biodiesel: a review, Biotechnol Adv, 28 (2010) 500-518.

[148] S. Lee, D. Posarac, N. Ellis, An experimental investigation of biodiesel synthesis from waste canola oil using supercritical methanol, Fuel, 91 (2012) 229-237.

[149] X.-R. Chen, Y.-H. Ju, C.-Y. Mou, Direct Synthesis of Mesoporous Sulfated Silica-Zirconia Catalysts with High Catalytic Activity for Biodiesel via Esterification, The Journal of Physical Chemistry C, 111 (2007) 18731-18737.

[150] K.H. Chung, D.R. Chang, B.G. Park, Removal of free fatty acid in waste frying oil by esterification with methanol on zeolite catalysts, Bioresour. Technol., 99 (2008) 7438-7443.

[151] K.H. Chung, B.G. Park, Esterification of oleic acid in soybean oil on zeolite catalysts with different acidity, Journal of Industrial and Engineering Chemistry, 15 (2009) 388-392.

[152] A.A. Kiss, A.C. Dimian, G. Rothenberg, Solid Acid Catalysts for Biodiesel Production —Towards Sustainable Energy, Adv. Synth. Catal., 348 (2006) 75-81.

[153] I.K. Mbaraka, D.R. Radu, V.S.Y. Lin, B.H. Shanks, Organosulfonic acid-functionalized mesoporous silicas for the esterification of fatty acid, J. Catal., 219 (2003) 329-336.

[154] G. Chen, B. Fang, Preparation of solid acid catalyst from glucose-starch mixture for biodiesel production, Bioresour. Technol., 102 (2011) 2635-2640.

[155] K. Wilson, J. H. Clark, Synthesis of a novel supported solid acid BF3 catalyst, Chemical Communications, (1998) 2135-2136.

[156] A. Khalafi-Nezhad, A. Parhami, M.N. Soltani Rad, M.A. Zolfigol, A. Zare, A catalytic method for chemoselective detritylation of 5′-tritylated nucleosides under mild and heterogeneous conditions using silica sulfuric acid as a recyclable catalyst, Tetrahedron Lett., 48 (2007) 5219-5222.

[157] M. Otadi, A. Shahraki, M. Goharrokhi, F. Bandarchian, Reduction of Free Fatty Acids of Waste Oil by Acid-Catalyzed Esterification, Procedia Engineering, 18 (2011) 168-174.

[158] P.C. Smith, B.K. O'Neill, Y. Ngothai, Q.D. Nguyen, Butoxylation of butyl biodiesel: Reaction conditions and cloud point impact, Energy and Fuels, 23 (2009) 3798-3803.

[159] G.J. Suppes, M.J. Goff, S. Lopes, Latent heat characteristics of fatty acid derivatives pursuant phase change material applications, Chemical Engineering Science, 58 (2003) 1751-1763.

[160] F. Seniha Güner, Y. Yagcl, A. Tuncer Erciyes, Polymers from triglyceride oils, Prog. Polym. Sci., 31 (2006) 633-670.

[161] A. Kleinová, P. Fodran, L. Brncalová, J. Cvengros, Substituted esters of stearic acid as potential lubricants, Biomass Bioenerg., 32 (2008) 366-371.

[162] B. Dahlke, S. Hellbardt, M. Paetow, W. Zech, Polyhydroxy fatty acids and their derivatives from plant oils, J. Am. Oil Chem. Soc., 72 (1995) 349-353.

[163] K. Doll, S. Erhan, Synthesis and performance of surfactants based on epoxidized methyl oleate and glycerol, J. Surfactants Deterg., 9 (2006) 377-383.

[164] G. Du, A. Tekin, E. Hammond, L. Wood, Catalytic epoxidation of methyl linoleate, J. Am. Oil Chem. Soc., 81 (2004) 477-480.

[165] R. Mungroo, N.C. Pradhan, V.V. Goud, A.K. Dalai, Epoxidation of canola oil with hydrogen peroxide catalyzed by acidic ion exchange resin, J. Am. Oil Chem. Soc., 85 (2008) 887-896.

[166] L. Gan, S. Goh, K. Ooi, Kinetic studies of epoxidation and oxirane cleavage of palm olein methyl esters, J. Am. Oil Chem. Soc., 69 (1992) 347-351.

[167] A. Campanella, C. Fontanini, M. Baltanas, High yield epoxidation of fatty acid methyl esters with performic acid generated in situ, Chem. Eng. J., 144 (2008) 466-475.

[168] A. Campanella, M.A. Baltanás, Degradation of the oxirane ring of epoxidized vegetable oils in liquid-liquid heterogeneous reaction systems, Chem. Eng. J., 118 (2006) 141-152.

[169] V.V. Goud, A.V. Patwardhan, S. Dinda, N.C. Pradhan, Kinetics of epoxidation of jatropha oil with peroxyacetic and peroxyformic acid catalysed by acidic ion exchange resin, Chem. Eng. Sci., 62 (2007) 4065-4076.

[170] H. Aerts, P. Jacobs, Epoxide yield determination of oils and fatty acid methyl esters using 1H NMR, J. Am. Oil Chem. Soc., 81 (2004) 841-846.

[171] P.C. Smith, Y. Ngothai, Q.D. Nguyen, B.K. O'Neill, The addition of alkoxy side-chains to biodiesel and the impact on flow properties, Fuel, 89 (2010) 3517-3522.

[172] D. Swern, G.N. Billen, J.T. Scanlan, Chemistry of Epoxy Compounds. V.2 Preparation of Some Hydroxy-ethers from 9,10-Epoxystearic Acid and 9,10-Epoxyoctadecanol, J. Am. Chem. Soc., 70 (1948) 1226-1228.

[173] B. Moser, S. Erhan, πSynthesis and evaluation of a series of α-hydroxy ethers derived from isopropyl oleate, J. Am. Oil Chem. Soc., 83 (2006) 959-963.

[174] P. Shao, G. Ji, P. Chen, Gold nanotube membranes: Preparation, characterization and application for enantioseparation, J. Membr. Sci., 255 (2005) 1-11.

[175] B.R. Moser, S.Z. Erhan, Preparation and evaluation of a series of α-hydroxy ethers from 9,10-epoxystearates, Eur. J. Lipid Sci. Technol., 109 (2007) 206-213.

[176] T. Ogoshi, Y. Miyawaki, Soap and related products: Palm and lauric oil, J. Am. Oil Chem. Soc., 62 (1985) 331-335.

[177] P. Sosis, L. Dringoli, Sulfation of synthetic linear primary alcohols with chlorosulfonic acid, J. Am. Oil Chem. Soc., 47 (1970) 229-232.

[178] R. Cremlyn, Chlorosulfonic Acid: A Versatile Reagent, The Royal Society of Chemistry, Cambridge, UK., 2002.

[179] T. Gurkov, D. Dimitrova, K. Marinova, C. Bilkecrause, C. Gerber, I. Ivanov, Ionic surfactants on fluid interfaces: determination of the adsorption; role of the salt and the type of the hydrophobic phase, Colloids and Surfaces A: Physicochemical and Engineering Aspects, 261 (2005) 29-38.

[180] R. Tadmouri, C. Zedde, C. Routaboul, J.-C. Micheau, V.r. Pimienta, Partition and Water/Oil Adsorption of Some Surfactants, The Journal of Physical Chemistry B, 112 (2008) 12318-12325.

[181] J. Gulicovski, L. Cerovic, S. Milonjic, Point of Zero Charge and Isoelectric Point of Alumina, Mater. Manuf. Processes, 23 (2008) 615-619.

[182] www.astm.org. accessed on 03-06-12

[183] http://www.itl.nist.gov/div898/handbook/pri/section1/pri11.htm, accessd on 4-8-12

[184] J.M. Monteagudo, L. Rodríguez, J. Rincón, J. Fuertes, Optimization of the conditions of the fermentation of beet molasses to lactic acid by Lactobacillus delbrueckii, Acta Biotechnologica, 14 (1994) 251-260.

[185] A.L. Larentis, N.S. de Resende, V.M.M. Salim, J.C. Pinto, Modeling and optimization of the combined carbon dioxide reforming and partial oxidation of natural gas, Applied Catalysis A: General, 215 (2001) 211-224.

[186] T.D. Kusworo, A.R. Songip, N.A.S. Amin, Optimization of Partial Oxidation of Methane for Hydrogen Production on NiO-CoO/MgO Catalyst using Design of Experiment, , International Journal of Engineering & Technology IJET-IJENS 10 (2010) 1-8.

[187] D. Wu, Y. Li, Y. Shi, Z. Fang, D. Wu, L. Chang, Effects of the calcination conditions on the mechanical properties of a PCoMo/Al2O3 hydrotreating catalyst, Chemical Engineering Science, 57 (2002) 3495-3504.

[188] S. Sun, X. Ke, L. Cui, G. Yang, Y. Bi, F. Song, X. Xu, Enzymatic epoxidation of Sapindus mukorossi seed oil by perstearic acid optimized using response surface methodology, Ind. Crop. Prod., 33 (2011) 676-682.

[189] F. Naidir, R. Yunus, I. Ramli, T.I. Mohd Ghazi, Response surface methodology for optimization of epoxidized trimethylolpropane ester synthesis from palm oil, Int. J. Chem.React. Eng., 9 (2011).

[190] G.E.P. Box, K.B. Wilson, On the Experimental Attainment of Optimum Conditions (with discussion), Journal of the Royal Statistical Society Series, B13 (1951) 1- 45.

[191] D.C. Montgomery, Design and Analysis of Experiments: Response surface method and designs., John Wiley and Sons, Inc., New Jersey, 2005.

[192] R.O. Kuehl, Design of Experiments: Statistical Principles of Research Design and Analysis, 2nd ed., Brooks/Cole, California 2000.

[193] D.P. Obeng, S. Morrell, T.J. Napier-Munn, Application of central composite rotatable design to modelling the effect of some operating variables on the performance of the three-product cyclone, International Journal of Mineral Processing, 76 (2005) 181-192.

[194] R.D. Crozier, Flotation Theory, Reagents and Ore Testing, Pergamon Press, New York, 1992.

[195] S. Yi, Y. Su, B. Qi, Z. Su, Y. Wan, Application of response surface methodology and central composite rotatable design in optimizing the preparation conditions of vinyltriethoxysilane modified silicalite/polydimethylsiloxane hybrid pervaporation membranes, Separation and Purification Technology, 71 (2010) 252-262.

[196] S. Ghafari, H.A. Aziz, M.H. Isa, A.A. Zinatizadeh, Application of response surface methodology (RSM) to optimize coagulation–flocculation treatment of

leachate using poly-aluminum chloride (PAC) and alum, Journal of Hazardous Materials, 163 (2009) 650-656.

[197] U. Rashid, H.A. Rehman, I. Hussain, M. Ibrahim, M.S. Haider, Muskmelon (Cucumis melo) seed oil: A potential non-food oil source for biodiesel production, Energy, 36 (2011) 5632-5639.

[198] J.J. Ge, G.C. Zhang, P. Jiang, M.Q. Sun, Development of surfactants as chemicals for EOR, Oilfield Chemistry, 24 (2007) 287-292.

[199] M. Roshanfekr, R.T. Johns, Prediction of optimum salinity and solubilization ratio for microemulsion phase behavior with live crude at reservoir pressure, Fluid Phase Equilib., 304 (2011) 52-60.

[200] D.L. Zhang, S. Liu, W. Yan, M. Puerto, G.J. Hirasaki, C.A. Miller, Favorable attributes of alkali-surfactant-polymer flooding, in, 2006, pp. 695-707.

[201] C.A. Miller, P. Neogi, Interfacial Phenomena, Surfactant Science Series,, V. 17, Marcel Dekker, Inc., New York, (1985).

[202] R. Wilson, R. Smith, P. Wilson, M.J. Shepherd, R.A. Riemersma, Quantitative gas chromatography-mass spectrometry isomer-specific measurement of hydroxy fatty acids in biological samples and food as a marker of lipid peroxidation, Anal. Biochem., 248 (1997) 76-85.

[203] S. Mustafa, B. Dilara, K. Nargis, A. Naeem, P. Shahida, Surface properties of the mixed oxides of iron and silica, Colloids and Surfaces A: Physicochemical and Engineering Aspects, 205 (2002) 273-282.

[204] M. Farooq, A. Ramli, D. Subbarao, Physiochemical Properties of γ-Al2O3–MgO and γ-Al2O3–CeO2 Composite Oxides, Journal of Chemical & Engineering Data, (2011).

[205] U. Farooq, M.T. Tweheyo, J. Sjöblom, G. Øye, Surface Characterization of Model, Outcrop, and Reservoir Samples in Low Salinity Aqueous Solutions, J. Dispersion Sci. Technol., 32 (2011) 519-531.

[206] K.S. Rao, P.P. Chakrabarti, B.V.S.K. Rao, R.B.N. Prasad, Phospholipid composition of Jatropha curcus seed lipids, JAOCS, Journal of the American Oil Chemists' Society, 86 (2009) 197-200.

[207] M. Berrios, J. Siles, M. Martin, A. Martin, A kinetic study of the esterification of free fatty acids (FFA) in sunflower oil, Fuel, 86 (2007) 2383-2388.

[208] J. Zhang, L. Jiang, Acid-catalyzed esterification of Zanthoxylum bungeanum seed oil with high free fatty acids for biodiesel production, Bioresour. Technol., 99 (2008) 8995-8998.

[209] P. Nakpong, S. Wootthikanokkhan, High free fatty acid coconut oil as a potential feedstock for biodiesel production in Thailand, Renewable Energy, 35 (2010) 1682-1687.

[210] M. Guillén, N. Cabo, Characterization of edible oils and lard by fourier transform infrared spectroscopy. Relationships between composition and frequency of concrete bands in the fingerprint region, J. Am. Oil Chem. Soc., 74 (1997) 1281-1286.

[211] S.A. Fernandes, A.L. Cardoso, M.J. da Silva, A novel kinetic study of H3PW12O40 - catalyzed oleic acid esterification with methanol via 1H NMR spectroscopy, Fuel Process. Technol., 96 (2012) 98-103.

[212] A. Cardoso, S. Neves, M. Da Silva, Esterification of Oleic Acid for Biodiesel Production Catalyzed by SnCl2: A Kinetic Investigation, Energies, 1 (2008) 79-92.

[213] K.V. Thiruvengadaravi, J. Nandagopal, P. Baskaralingam, V. Sathya Selva Bala, S. Sivanesan, Acid-catalyzed esterification of karanja (Pongamia pinnata) oil with high free fatty acids for biodiesel production, Fuel.

[214] L. Lin, D. Ying, S. Chaitep, S. Vittayapadung, Biodiesel production from crude rice bran oil and properties as fuel, Applied Energy, 86 (2009) 681-688.

[215] D.Y.C. Leung, X. Wu, M.K.H. Leung, A review on biodiesel production using catalyzed transesterification, Applied Energy, 87 (2010) 1083-1095.

[216] G.C.B.a.T.C.M. R. M. Silverstein, Spectrometric Identification of Organic Compounds, 7th Ed., John Wiley & Sons, NJ USA, 2005.

[217] G. Vlahov, Application of NMR to the study of olive oils, Prog. Nucl. Magn. Reson. Spectrosc., 35 (1999) 341-357.

[218] D. Goswami, J.K. Basu, S. De, Optimal hydrolysis of mustard oil to erucic acid: A biocatalytic approach, Chem. Eng. J., 181–182 (2012) 542-548.

[219] V. Goud, N. Pradhan, A. Patwardhan, Epoxidation of karanja (Pongamia glabra) oil by H2O2, J. Am. Oil Chem. Soc., 83 (2006) 635-640.

[220] B. Lin, L. Yang, H. Dai, A. Yi, Kinetic Studies on Oxirane Cleavage of Epoxidized Soybean Oil by Methanol and Characterization of Polyols, J. Am. Oil Chem. Soc., 85 (2008) 113-117.

[221] Z.S. Petrović, A. Zlatanić, C.C. Lava, S. Sinadinović-Fišer, Epoxidation of soybean oil in toluene with peroxoacetic and peroxoformic acids — kinetics and side reactions, Eur. J. Lipid Sci. Technol., 104 (2002) 293-299.

[222] T. Vlček, Z. Petrović, Optimization of the chemoenzymatic epoxidation of soybean oil, J. Am. Oil Chem. Soc., 83 (2006) 247-252.

[223] M.D. Guillén, N. Cabo, Infrared spectroscopy in the study of edible oils and fats, J. Sci. Food Agric., 75 (1997) 1-11.

[224] K. Wadumesthrige, J. Smith, J. Wilson, S. Salley, K. Ng, Investigation of the Parameters Affecting the Cetane Number of Biodiesel, J. Am. Oil Chem. Soc., 85 (2008) 1073-1081.

[225] G. Knothe, Analysis of oxidized biodiesel by 1H-NMR and effect of contact area with air, Eur. J. Lipid Sci. Technol., 108 (2006) 493-500.

[226] G. Knothe, M.O. Bagby, Assignment of ¹³C nuclear magnetic resonance signals in fatty compounds with allylic hydroxy groups, JAOCS, Journal of the American Oil Chemists' Society, 73 (1996) 661-663.

[227] G. Knothe, J.A. Kenar, Determination of the fatty acid profile by 1H-NMR spectroscopy, Eur. J. Lipid Sci. Technol., 106 (2004) 88-96.

[228] Y. Mitei, J. Ngila, S. Yeboah, L. Wessjohann, J. Schmidt, NMR, GC–MS and ESI-FTICR-MS Profiling of Fatty Acids and Triacylglycerols in Some Botswana Seed Oils, J. Am. Oil Chem. Soc., 85 (2008) 1021-1032.

[229] R. Zamora, G. Gómez, M. Dobarganes, F. Hidalgo, Oil fractionation as a preliminary step in the characterization of vegetable oils by high-resolution 13C NMR spectroscopy, J. Am. Oil Chem. Soc., 79 (2002) 261-266.

[230] K. Yamada, S. Matsutani, Analysis of the dark-colored impurities in sulfonated fatty acid methyl ester, J. Am. Oil Chem. Soc., 73 (1996) 121-125.

[231] R. Martinez-Pascual, O. Viñas-Bravo, S. Meza-Reyes, M.A. Iglesias-Arteaga, J. Sandoval-Ramírez, A Fast and Convenient Procedure for the Acetylation of Alcohols, Synth. Commun., 34 (2004) 4591-4596.

[232] B. Stefke, E. Windeisen, M. Schwanninger, B. Hinterstoisser, Determination of the weight percentage gain and of the acetyl group content of acetylated wood by means of different infrared spectroscopic methods, Anal. Chem., 80 (2008) 1272-1279.

[233] M.O. Adebajo, R.L. Frost, Acetylation of raw cotton for oil spill cleanup application: an FTIR and 13C MAS NMR spectroscopic investigation, Spectrochimica Acta Part A: Molecular and Biomolecular Spectroscopy, 60 (2004) 2315-2321.

[234] D. Levitt, A. Jackson, C. Heinson, L.N. Britton, T. Malik, V. Dwarakanath, G.A. Pope, Identification and Evaluation of High-Performance EOR Surfactants, SPE Reservoir Eval. Eng., (2009).

[235] F. Yu, W.Y. Fan, G.Z. Nan, S.P. Li, Y.Z. Duan, Relation between structure and property of fractions of petroleum sulfonate, Shiyou Xuebao, Shiyou Jiagong/Acta Petrolei Sinica (Petroleum Processing Section), 24 (2008) 204-210.

[236] S. Paria, K.C. Khilar, A review on experimental studies of surfactant adsorption at the hydrophilic solid–water interface, Adv. Colloid Interface Sci., 110 (2004) 75-95.

[237] W. Lv, B. Bazin, D. Ma, Q. Liu, D. Han, K. Wu, Static and dynamic adsorption of anionic and amphoteric surfactants with and without the presence of alkali, Journal of Petroleum Science and Engineering, 77 (2011) 209-218.

[238] M.A. Muherei, R. Junin, A.B. Bin Merdhah, Adsorption of sodium dodecyl sulfate, Triton X100 and their mixtures to shale and sandstone: A comparative study, Journal of Petroleum Science and Engineering, 67 (2009) 149-154.

LIST OF PUBLICATIONS

Conference proceedings:

1. Muhammad Mushtaq, I.B. Tan, C. Devi, S. Majidaie, M. Nadeem, S. Lee, *Epoxidation of Fatty Acid Methyl Esters derived from Jatropha oil*, presented in: National Postgraduate Conference (NPC), 2011, pp. 1-4.
2. Muhammad Mushtaq, Isa M. Tan, Muhammad Nadeem, Susan Lee, Saeed Majadai, Rehan Hashmet, Rizwan Azam, *The Determination of Point of Zero Charge (PZC) and Static Adsorption of an Anionic Surfactant On Malaysian Sandstone* , presented in ICIPEG 2012 Kuala Lumpur, Malaysia.
3. Muhammad Mushtaq, Isa M Tan, *Synthesis of Surfactants from Natural Oils,* presented in Advanced Technology Workshop (ATW) on Chemical Flooding EOR, conducted by SPE in Penang Malaysia (2011)
4. Muhammad Hashmet, Isa M. Tan, Saeed Majidaei, Muhammad Mushtaq, *Simultaneous Determination of Capillary Pressure and Relative Permeability* Presented in SPE Annual Technical Symposium and Exhibition Al Khobar, Saudi Arabia 2012.
5. Isa M. Tan, Susan Lee, Muhammad Mushtaq Study of the Cloud Point Behavior of High Oleate Ester-Derived Nonionic Surfactant, Presented in ICFAS 2012, Kuala Lumpur, Malaysia.
6. Saeed Majadai, Muhammad Mushtaq, Isa M. Tan, Birol Demiral, Susa Lee, Non -petrochemical based surfactants for EOR applications, Poster presented at SPE EOR Conference at Oil and Gas West Asia held in Muscat, Oman, 16–18 April 2012.

Journal Papers:

1. Muhammad Mushtaq, I.B. Tan, C. Devi, M. Nadeem, S. Lee, A *Convenient Route for the Alkoxylation of High Oleic Acid Methyl Ester Biodiesel and its Influence on Cold Flow Properties.* Submitted in International Journal of Green Energy, Impact factor 1.188, Published by Taylor & Francis Group
2. Muhammad Mushtaq, I.B. Tan, M. Nadeem, S. Lee, C. Devi, Epoxidation of high oleic acid methyl esters: An optimization study, Accepted for publication in Grasas Y Aceites, Impact factor 1.138, Published by INSTITUTO DE LA GRASA.
3. Muhammad Mushtaq, I.B. Tan, C. Devi, M. Nadeem, S. Lee , *"A novel hybrid catalyst for the esterification of high FFA in Jatropha oil",* Under review in *Jouranl of Industrial and Engineering Chemistry,* Impact factor 1.97, Published by Elsevier Publishing
4. Muhammad Mushtaq, Isa M. Tan, Muhammad Nadeem, Susan Lee, Saeed Majadai, Rehan Hashmet, Rizwan Azam, *The Determination of Point of Zero Charge (PZC) and Static Adsorption of an Anionic Surfactant on Malaysian Sandstone* , Selected for publishing in Petroleum science and technology, Impact factor 0.335, Published by Taylor & Francis Group.

APPENDIX A

AOCS Official Method Te 2a-64, "Determination of Acid Value"

AOCS Official Method Te 2a-64, "Determination of Acid Value"

Procedure:

1. Weigh about 10 g sample in an Erlenmeyer flask and add about 100 mL neutralized solvent (isopropyl alcohol – toluene 50-50 volume ratio) and 1 mL phenolphthalein indicator solution.

2. Swirl till sample dissolved

3. Titrate with standard NaOH solution (0.1 N in methanol) shaking vigorously to the first appearance of permanent pink color which persists for one minute.

4. Calculate acid value, mg KOH per g of sample according to equation A1:

$$\text{Acid value} = \frac{\text{Volume of alkali, mL} \times \text{N} \times 56.1}{\text{mass of sample, g}} \qquad \text{(A1)}$$

Where N is normality of NaOH solution.

APPENDIX B

Tables

Table B 0-1: Full Factorial Central Composite Rotatable Design (CCRD) matrix of four variables in coded and natural units along with the observed and predicted responses (% epoxidation)

		Coded level of variables				Actual level of variables				Epoxidation yield (%)		
Standard order	Point type	X_1	X_2	X_3	X_4	Hydrogen peroxide / C=C mole ratio	Formic acid / C=C mole ratio	Reaction temperature (°C)	Reaction time (min)	Actual value (wt. %)	Predicted value (wt. %)	Residuals
1	Factorial	-1	-1	-1	-1	1.375	0.65	40	112.5	30.45 ± 0.92	31.34	-0.89
2	Factorial	1	-1	-1	-1	3.125	0.65	40	112.5	45.22 ±0.68	44.32	0.90
3	Factorial	-1	1	-1	-1	1.375	1.55	40	112.5	30.43 ±0.93	29.51	0.92
4	Factorial	1	1	-1	-1	3.125	1.55	40	112.5	37.22	39.19	-1.97

										±1.36		
5	Factorial	-1	-1	1	-1	1.375	0.65	70	112.5	35.38 ±0.89	35.28	0.10
6	Factorial	1	-1	1	-1	3.125	0.65	70	112.5	65.69 ±1.83	66.18	-0.49
7	Factorial	-1	1	1	-1	1.375	1.55	70	112.5	37.29 ±1.27	40.01	-2.72
8	Factorial	1	1	1	-1	1.375	1.55	40	277.5	35.14 ±0.68	36.61	-1.47
9	Factorial	-1	-1	-1	1	3.125	1.55	40	277.5	50.45 ±1.06	52.37	-1.92
10	Factorial	1	-1	-1	1	1.375	0.65	70	277.5	56.11 ±0.93	56.10	0.01
11	Factorial	-1	1	-1	1	3.125	0.65	70	277.5	90.34 ±1.83	93.07	-2.73
12	Factorial	1	1	-1	1	1.375	1.55	70	277.5	49.94 ±1.25	52.66	-2.72

13	Factorial	-1	-1	1	1	3.125	1.55	70	277.5	85.27 ±1.46	86.34	-1.07
14	Factorial	1	-1	1	1	0.5	1.1	55	195	30.22 ±0.73	28.56	1.66
15	Factorial	-1	1	1	1	4	1.1	55	195	77.34 ±1.25	75.22	2.12
16	Factorial	1	1	1	1	2.25	0.2	55	195	57.34 ±1.05	57.90	-0.56
17	Axial	-2	0	0	0	2.25	2	55	195	53.67 ±1.31	49.33	4.34
18	Axial	2	0	0	0	1.375	0.65	40	112.5	30.45 ±0.29	31.34	-0.89
19	Axial	0	-2	0	0	3.125	0.65	40	112.5	45.22 ±1.63	44.32	0.90
20	Axial	0	2	0	0	1.375	1.55	40	112.5	30.43 ±1.47	29.51	0.92
21	Axial	0	0	-2	0	2.25	1.1	25	195	33.87 ±1.58	33.76	0.11

22	Axial	0	0	2	0	2.25	1.1	85	195	75.33 ±1.71	71.66	3.67
23	Axial	0	0	0	-2	2.25	1.1	55	30	36.44 ±0.86	35.50	0.94
24	Axial	0	0	0	2	2.25	1.1	55	360	72.34 ±1.22	69.50	2.84
25	Center	0	0	0	0	2.25	1.1	55	195	73.31 ±1.69	72.00	1.32
26	Center	0	0	0	0	2.25	1.1	55	195	71.76 ±1.33	72.00	-0.24
27	Center	0	0	0	0	2.25	1.1	55	195	69.03 ±1.96	72.00	-2.97
28	Center	0	0	0	0	2.25	1.1	55	195	70.87 ±0.92	72.00	-1.13
29	Center	0	0	0	0	2.25	1.1	55	195	74.95 ±1.66	72.00	2.96
30	Center	0	0	0	0	2.25	1.1	55	195	72.05 ±1.57	72.00	0.05

Table B 0-2: NMR spectroscopic data for alkoxylation reaction products

3a: **^{1}H NMR** ($CDCl_3$) δ 0.56-0.58 (-C***H***$_2$ groups)0.89 (-C***H***$_3$), 1.11(-O***H***),1.21(O-CH_2C***H***$_3$) 1.30-1.53 (C***H***$_2$),1.61(C***H***$_2$-CH_2COOCH_3) 2.28-2.32 (C***H***$_2$$COOCH_3$) 3.12,3.14 (***H***-CO-$CH_2CH_3$), 3.51(O-C***H***$_2$$CH_3$) 3.57-3.59(***H***C-OH) 3.62 (C-OO-C***H***$_3$), **^{13}C NMR** ($CDCl_3$) 14.56-16.23 (-***C***H_3), 23.45-34.41 (***C***H_2), 51.52 ($COOCH_3$),63.33 (OCH_2CH_3),72.73 (H***C***-OH),84.65 (H-***C***O-CH_2CH_3), 174.67 (-***C***OO-CH_3).
3b: **^{1}H NMR** ($CDCl_3$) 0.82-0.90 (-C***H***$_2$ groups) 0.98 ($OCH_2CH_2CH_3$), 0.99(-C***H***$_3$) (1.13(-O***H***), 1.33-1.57 (C***H***$_2$),1.60(C***H***$_2$-CH_2COOCH_3) 2.29-2.32 (C***H***$_2$$COOCH_3$) 3.12,3.16 (***H***-CO-$CH_2$ CH_2CH_3), 3.45-3.47 (O-C***H***$_2$$CH_2CH_3$) 3.61(***H***C-OH) 3.79 (C-OO-C***H***$_3$), **^{13}C NMR** ($CDCl_3$) 11.25 (OCH_2CH_2***C***H_3) (14.53 (-***C***H_3), 23.34(O-***C***H_2 CH_2CH_3) 24.31-33.62 (***C***H_2), 51.62 ($COOCH_3$),72.63 ($OCH_2CH_2CH_3$),73.83 (H***C***-OH), 83.65 (H-***C***O-CH_2 CH_2CH_3), 174.17 (-***C***OO-CH_3).
3c: **^{1}H NMR** ($CDCl_3$) 0.84-0.86 (-C***H***$_2$ groups) 0.99(-C***H***$_3$) 1.07(-O***H***),1.27 (OCH (C***H***$_3$)C***H***$_3$) (1.30-1.47 (C***H***$_2$),1.83 (C***H***$_2$-CH_2COOCH_3) 2.29-2.33 (C***H***$_2$$COOCH_3$) 2.99 (***H***-CO-CH ($CH_3$)CH3), 3.58 (OC***H*** ($CH_3$)CH_3) 3.60(***H***C-OH) 3.77 (C-OO-C***H***$_3$), **^{13}C NMR** ($CDCl_3$) 14.63 (-***C***H_3) 22.19(C***H***$_2$-CH_3) 23.55 (OCH(***C***H_3)***C***H_3), 25.21-34.51 (***C***H_2), 51.65 ($COOCH_3$),70.98 (O***C***H (CH_3)CH_3),72.63 (H***C***-OH), 82.17 (H-***C***O-CH(CH_3)CH_3), 174.11 (-***C***OO-CH_3).
3d: ^{1}H NMR ($CDCl_3$) 0.57-0.65 (-C***H***$_2$ groups) 0.99 (terminal C***H***$_3$,butyl C***H***$_3$) 1.07(-O***H***),1.27 (OCH(C***H***$_3$)C***H***$_3$) (1.30-1.47 (C***H***$_2$),1.83 (C***H***$_2$-CH_2COOCH_3) 2.29-2.33 (C***H***$_2$$COOCH_3$) 2.99 (***H***-CO-CH ($CH_3$)CH3), 3.58 (OC***H*** ($CH_3$)CH_3) 3.60(***H***C-OH) 3.77 (C-OO-C***H***$_3$), **^{13}C NMR** ($CDCl_3$) 14.03 (-***C***H_3), 20.1 (O-CH_2-CH_2-***C***H_2-CH_3) 23.1 (***C***H_2-CH_3) 25.93-30.60 (***C***H_2), 32.20 (O-CH_2-***C***H_2-CH_2-CH_3) 33.40 (–***C***H_2-CHOH-CH_2-), 51.89 ($COOCH_3$),70.74 ($OCH_2CH_2CH_2$ CH_3),73.98 (H***C***-OH), 84.78 (H-***C***$OCH_2CH_2CH_2$ CH_3), 174.61 (-***C***OO-CH_3).
3e: **^{1}H NMR** ($CDCl_3$) 0.80-0.87 (-C***H***$_2$ groups) 0.99-1.01 (terminal C***H***$_3$,both butyl C***H***$_3$) (1.33-1.51 (C***H***$_2$), 1.47(-O***H***), ,1.71 (C***H***$_2$-CH_2COOCH_3) 2.29 (C***H***$_2$$COOCH_3$) 3.10 (***H***-CO-$CH_2$CH ($CH_3$)CH3), 3.48 (OC***H***$_2$CH($CH_3$)CH_3) 3.59(***H***C-OH) 3.69 (C-OO-C***H***$_3$), **^{13}C NMR** ($CDCl_3$) 14.03 (-***C***H_3), 19.69 (O-CH_2CH (C***H***$_3$)C***H***$_3$) 23.31-34.19 (***C***H_2), 51.82 ($COOCH_3$), 73.98 (H***C***-OH), 77.94 (O***C***H_2 CH(CH_3)CH_3),84.93 (H***C***OCH_2 CH(CH_3)CH_3)), 174.81 (-***C***OO-CH_3).
3f: **^{1}H NMR** ($CDCl_3$) 0.82-0.84 (-C***H***$_2$ groups) 0.98-1.04 (terminal C***H***$_3$,main chain and hexyl) 1.33-1.43 (C***H***$_2$ main chain and hexyl), 1.41(-O***H***), ,1.72 (C***H***$_2$-CH_2COOCH_3) 2.31 (C***H***$_2$$COOCH_3$) 3.13(***H***-CO-$CH_2$($CH_3$)$_4CH_3$), 3.50 (COC***H***$_2$($CH_3$)$_4CH_3$) 3.57(***H***C-

OH) 3.71 (C-OO-C***H***$_3$), **^{13}C NMR** ($CDCl_3$) 14.06 (-***C***H_3 main chain and hexyl), 19.69 (O-CH_2CH (CH_3)C***H***$_3$) 22.94-31.65 (***C***H_2 main chain and hexyl), 51.92 (COO***C***H_3), 71.03 (O***C***H_2 (CH_3)$_4$$CH_3$), 73.68 (H***C***-OH), 85.02 (H***C***OCH_2 (CH_3)$_4$$CH_3$), 174.63 (-***C***OO-$CH_3$).
3g: **^{1}H NMR** ($CDCl_3$) 0.57-0.98 (-C***H***$_2$ groups) 0.99-1.03 (terminal C***H***$_3$,main chain and octyl) 1.31-1.54 (C***H***$_2$ main chain and octyl), 1.43(-O***H***), 1.84 (C***H***$_2$-$CH_2$$COOCH_3$) 2.43 (C***H***$_2$$COOCH_3$) 3.08 (***H***-CO-$CH_2$($CH_3$)$_6$$CH_3$), 3.58 (COC***H***$_2$($CH_3$)$_6$$CH_3$) 3.63(***H***C-OH) 3.71 (C-OO-C***H***$_3$), **^{13}C NMR** ($CDCl_3$) 14.11 (-***C***H_3 main chain and octyl), 22.33-33.47 (***C***H_2 main chain and octyl), 51.52 (COO***C***H_3), 71.00 (O***C***H_2 (CH_3)$_6$$CH_3$), 73.98 (H***C***-OH), 84.92(H***C***OCH_2(CH_3)$_6$$CH_3$), 174.81 (-***C***OO-$CH_3$).
3h: ^{1}H NMR ($CDCl_3$) 0.83-0.86 (terminal C***H***$_3$,main chain and decyl) 1.30-1.41 (C***H***$_2$ main chain and decyl), 1.69 (C***H***$_2$-$CH_2$$COOCH_3$ 2.33 (C***H***$_2$$COOCH_3$) 2.38(-O***H***), 3.10 (***H***-CO-CH_2(CH_3)$_8$$CH_3$), 3.48 (COC***H***$_2$($CH_3$)$_8$$CH_3$) 3.59(***H***C-OH) 3.69 (C-OO-C***H***$_3$), **^{13}C NMR** ($CDCl_3$) 14.06 (-***C***H_3 main chain and decyl), 22.93-33.51 (***C***H_2 main chain and decyl), 51.82 (COO***C***H_3), 71.10 (O***C***H_2 (CH_3)$_8$$CH_3$), 74.03 (H***C***-OH), 84.78(H***C***OCH_2(CH_3)$_8$$CH_3$), 174.61 (-***C***OO-$CH_3$).
3i: ^{1}H NMR ($CDCl_3$) 0.79-0.80 (-C***H***$_2$ groups),0.91-1.01 (terminal C***H***$_3$,main chain and dodecyl) 1.31-1.47 (C***H***$_2$ main chain and dodecyl), 1.71 (C***H***$_2$-$CH_2$$COOCH_3$ 2.39 (C***H***$_2$$COOCH_3$) 2.41 (-O***H***), 3.13 (***H***-CO-CH_2(CH_3)$_{10}$$CH_3$), 3.45 (COC***H***$_2$($CH_3$)$_{10}$$CH_3$) 3.57(***H***C-OH) 3.71 (C-OO-C***H***$_3$), **^{13}C NMR** ($CDCl_3$) 14.04 (-***C***H_3 main chain and dodecyl), 22.94-33.55 (***C***H_2 main chain and dodecyl), 51.85 (COO***C***H_3), 71.13 (O***C***H_2 (CH_3)$_{10}$$CH_3$), 73.98 (H***C***-OH), 84.79 (H***C***OCH_2(CH_3)$_{10}$$CH_3$), 174.85 (-***C***OO-$CH_3$).

Table B 0-3: FT-IR analysis data for acetylation reaction products

5a: 3462 cm^{-1} (OH stretch), 2925, 2853 (CH_2 stretch), 1741 (carbonyl stretch), 1457 (CH_2 bend), 1437 (C-H asymm and sym bend of CH_3-COO), 1373 (CH vib of acetyl group), 1230 (acetyl CO stretch), 1091 (ether C-O-C asymm stretch), 831, 875 (ether C-O-C symm. stretch), 721 (CH_2 rocking).
5b: 3464 cm^{-1} (OH stretch), 2924, 2852 (CH_2 stretch), 1742 (carbonyl stretch), 1457 (CH_2 bend), 1438 (C-H asymm and sym bend of CH_3-COO), 1372 (CH vib of acetyl group), 1231 (acetyl CO stretch), 1092 (ester C-O-C asymm stretch), 832, 874 (ether C-O-C symm. stretch), 722 (CH_2 rocking).
5c: 3461 cm^{-1} (OH stretch), 2921, 2853 (CH_2 stretch), 1742 (carbonyl stretch), 1458 (CH_2 bend), 1436 (C-H asymm and sym bend of CH_3-COO), 1374 (CH vib of acetyl group), 1228 (acetyl CO stretch), 1091 (ether C-O-C asymm stretch), 831, 874 (ether C-O-C symm. stretch), 721 (CH_2 rocking).
5d: 3458 cm^{-1} (OH stretch), 2924, 2854 (CH_2 stretch), 1742 (carbonyl stretch), 1456 (CH_2 bend), 1437 (C-H asymm and sym bend of CH_3-COO), 1372 (CH_3 sym bend), 1229 (acetyl CO stretch), 1090 (ether C-O-C asymm stretch), 830, 875 (ether C-O-C symm. stretch), 722 (CH_2 rocking).
5e: 3460 cm^{-1} (OH stretch), 2923, 2853 (CH_2 stretch), 1741 (carbonyl stretch), 1460 (CH_2 bend), 1435 (C-H asymm and sym bend of CH_3-COO), 1372 (CH vib of acetyl group), 1230 (acetyl CO stretch), 1092 (ether C-O-C asymm stretch), 831, 876 (ether C-O-C symm. stretch), 721 (CH_2 rocking).
5f: 3461 cm^{-1} (OH stretch), 2922, 2855 (CH_2 stretch), 1742 (carbonyl stretch), 1462 (CH_2 bend), 1435 (C-H asymm and sym bend of CH_3-COO), 1371 (CH vib of acetyl group), 1230 (acetyl CO stretch), 1093 (ether C-O-C asymm stretch), 829, 874 (ether C-O-C symm. stretch), 723 (CH_2 rocking).
5g: 3463 cm^{-1} (OH stretch), 2923, 2852 (CH_2 stretch), 1743 (carbonyl stretch), 1461 (CH_2 bend), 1436 (C-H asymm and sym bend of CH_3-COO), 1372 (CH vib of acetyl group), 1230 (acetyl CO stretch), 1091 (ether C-O-C asymm stretch), 831, 875 (ether C-O-C symm. stretch), 721 (CH_2 rocking).
5h: 3463 cm^{-1} (OH stretch), 2924, 2855 (CH_2 stretch), 1742 (carbonyl stretch), 1463 (CH_2 bend), 1437 (C-H asymm and sym bend of CH_3-COO), 1373 (CH vib of acetyl group), 1231 (acetyl CO stretch), 1093 (ether C-O-C asymm stretch), 831, 876 (ether C-

O-C symm. stretch), 722 (CH_2 rocking).
5i: 3464 cm^{-1} (OH stretch), 2923, 2856 (CH_2 stretch), 1743 (carbonyl stretch), 1462 (CH_2 bend), 1437 (C-H asymm and sym bend of CH_3-COO), 1374 (CH vib of acetyl group), 1230 (acetyl CO stretch), 1090 (ether C-O-C asymm stretch), 829, 874 (ether C-O-C symm. stretch), 721 (CH_2 rocking).

APPENDIX C

Figures

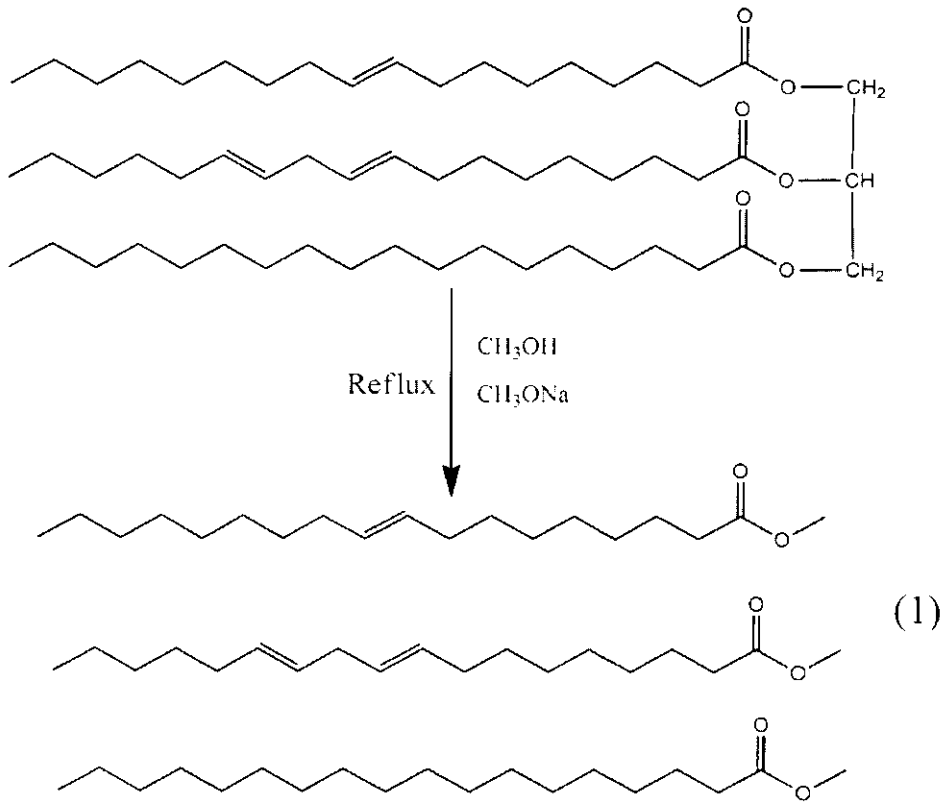

Figure C 1: Transesterification reaction for the synthesis of methyl esters

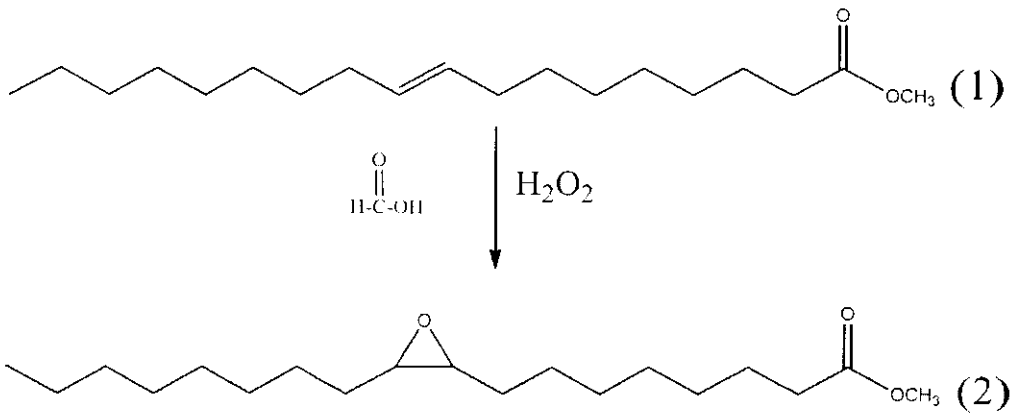

Figure C 2: Epoxidation reaction for the synthesis of epoxidized methyl esters

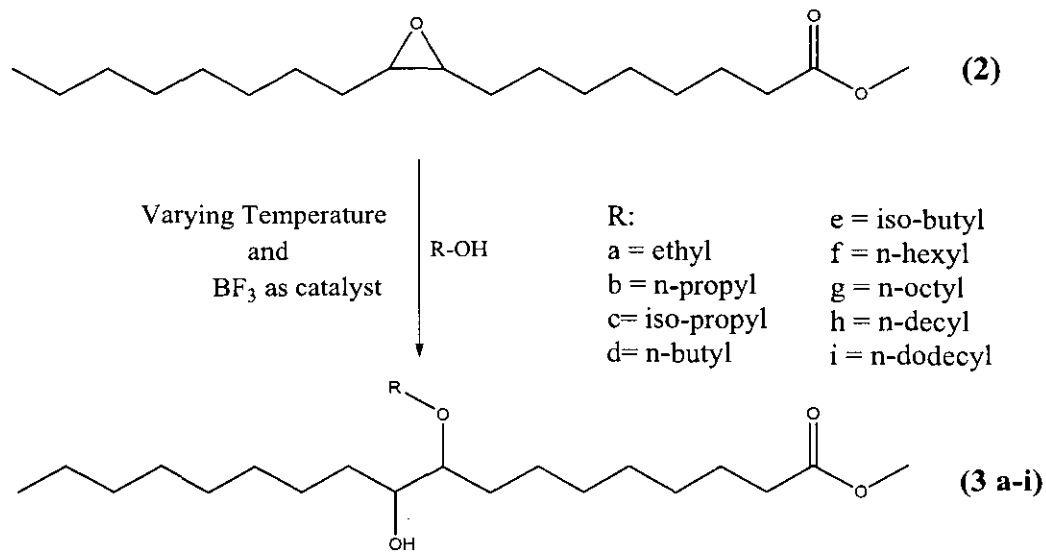

Figure C 3: Alkoxylation reaction for the synthesis of alkoxy-hydroxy methyl esters

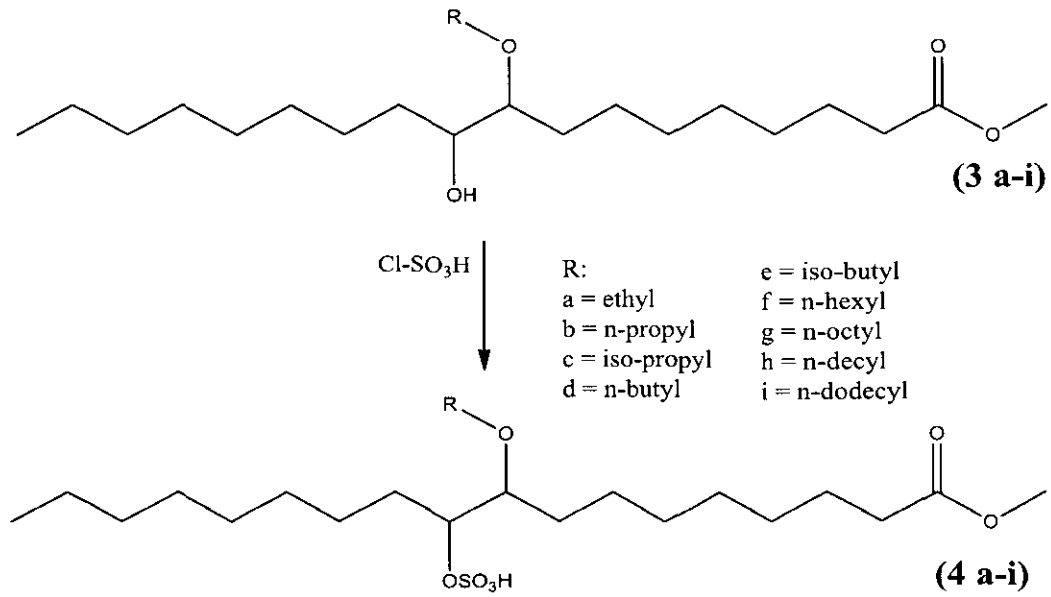

Figure C 4: Sulfation reaction for the synthesis of sulfate surfactants

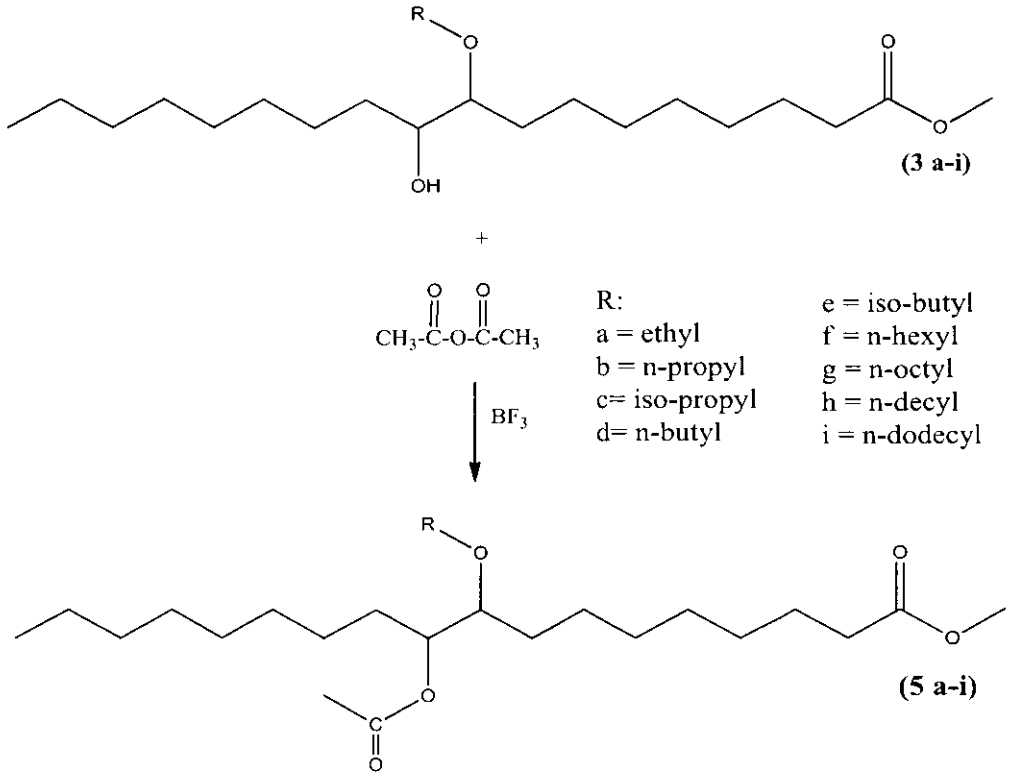

Figure C 5 : Acetylation reaction for the protection of -OH groups

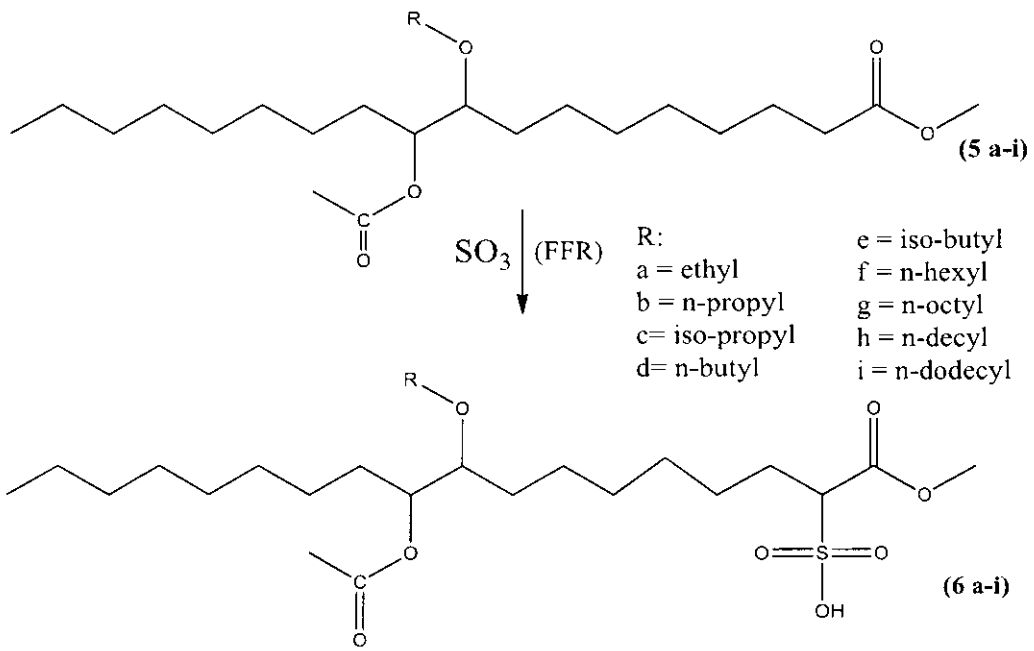

Figure C 6: Sulfonation reaction for the synthesis of sulfonate surfactants

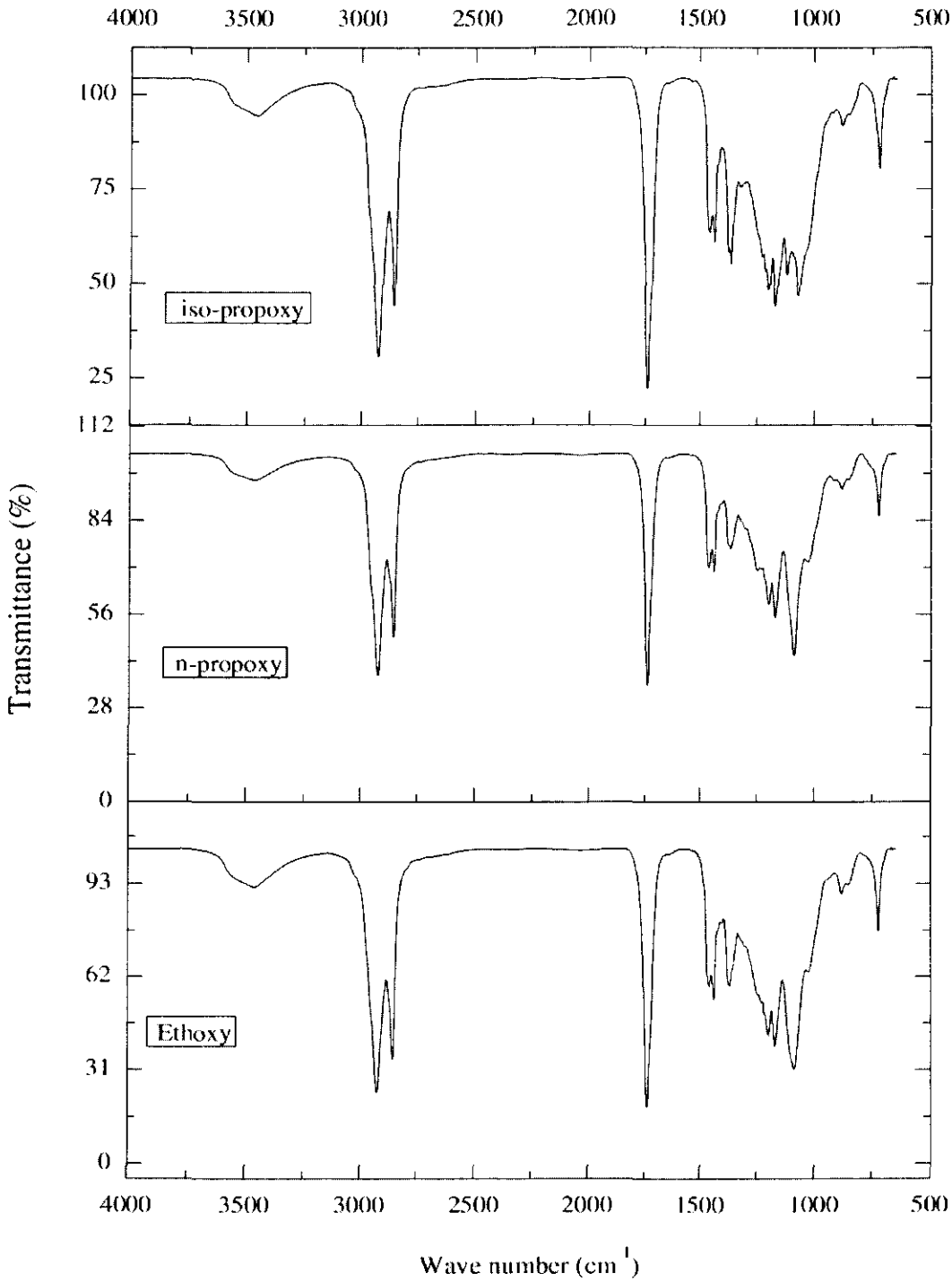

Figure C 7: FT-IR spectra of alkoxylated products from ethanol, n-propanol and iso-propanol

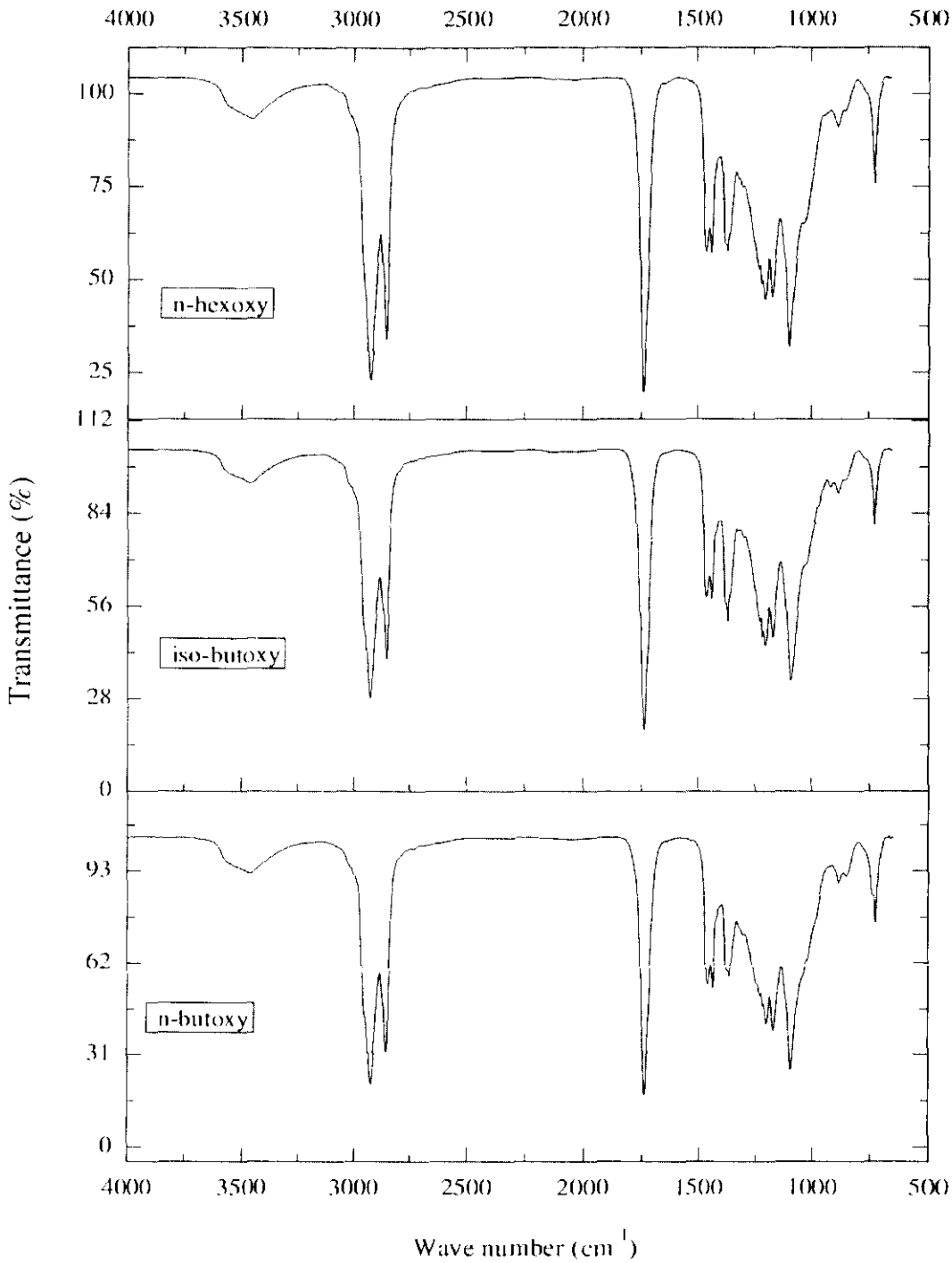

Figure C 8: FT-IR spectra of alkoxylated products from n-butanol, iso-butanol and n-hexanol

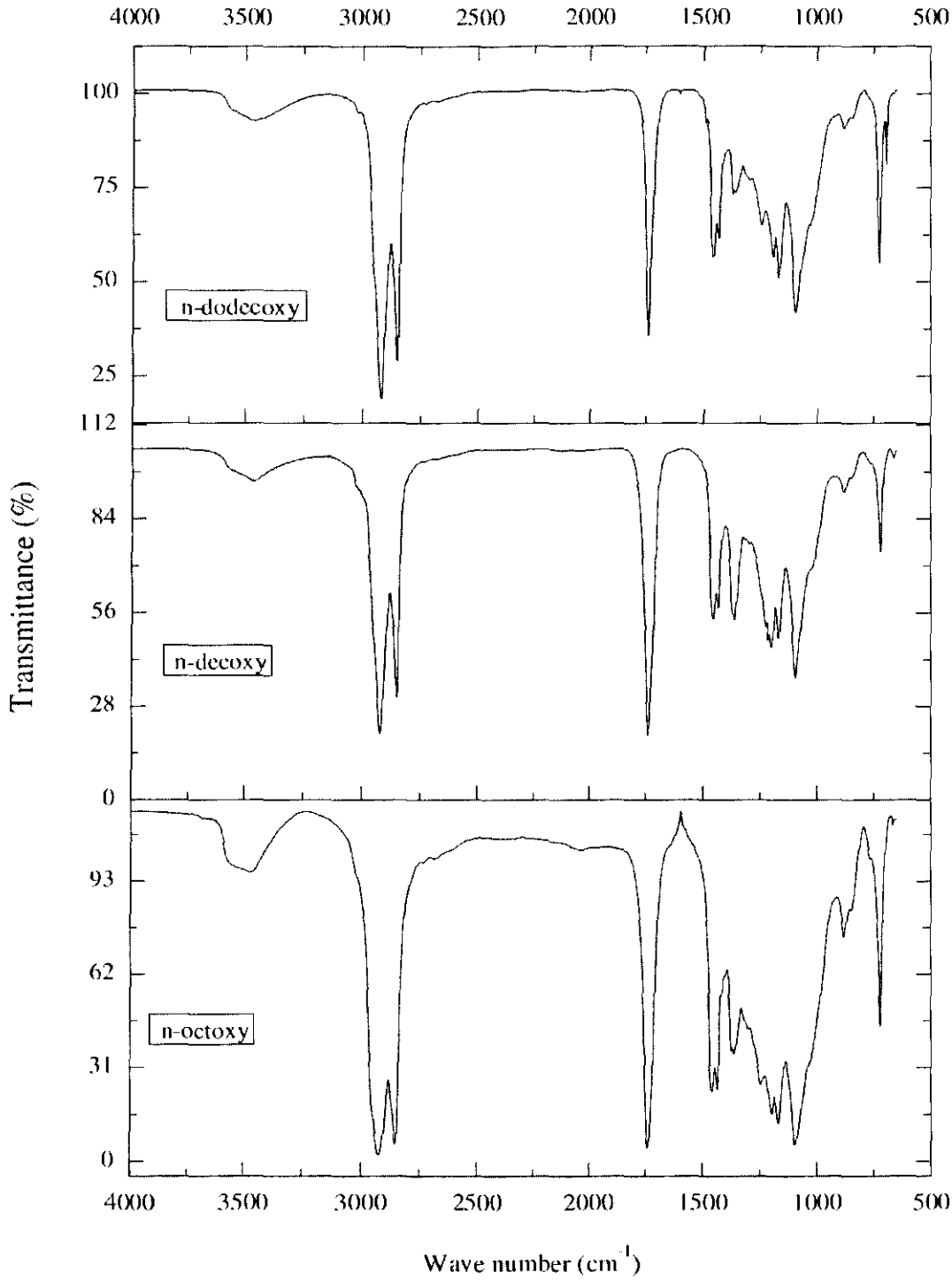

Figure C 9: FT-IR spectra of alkoxylated products from n-octanol, n-decanol and n-dodecanol

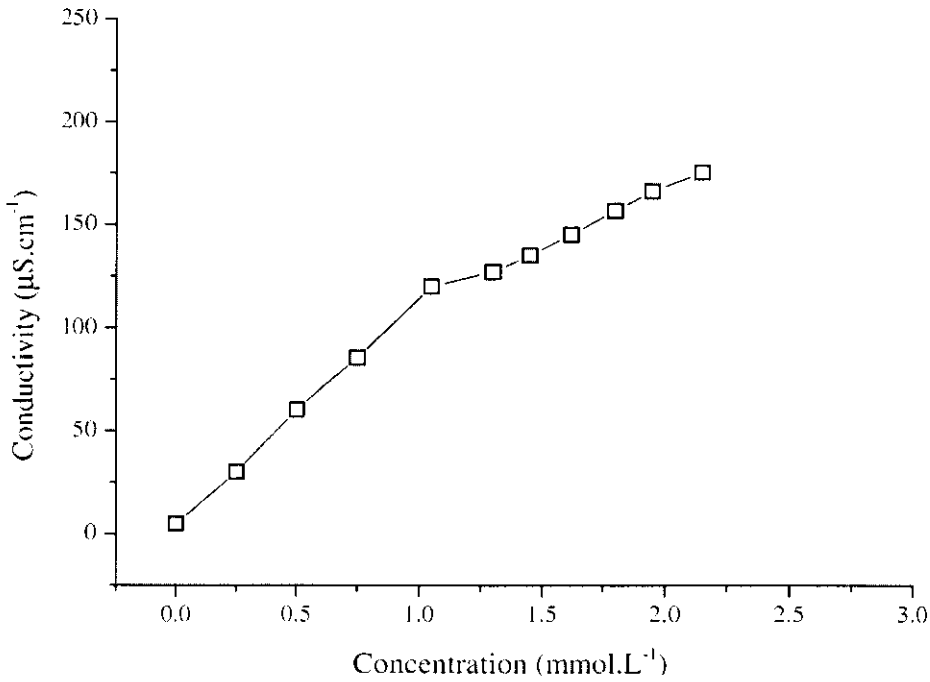

Figure C 10: CMC plot for surfactant 4a

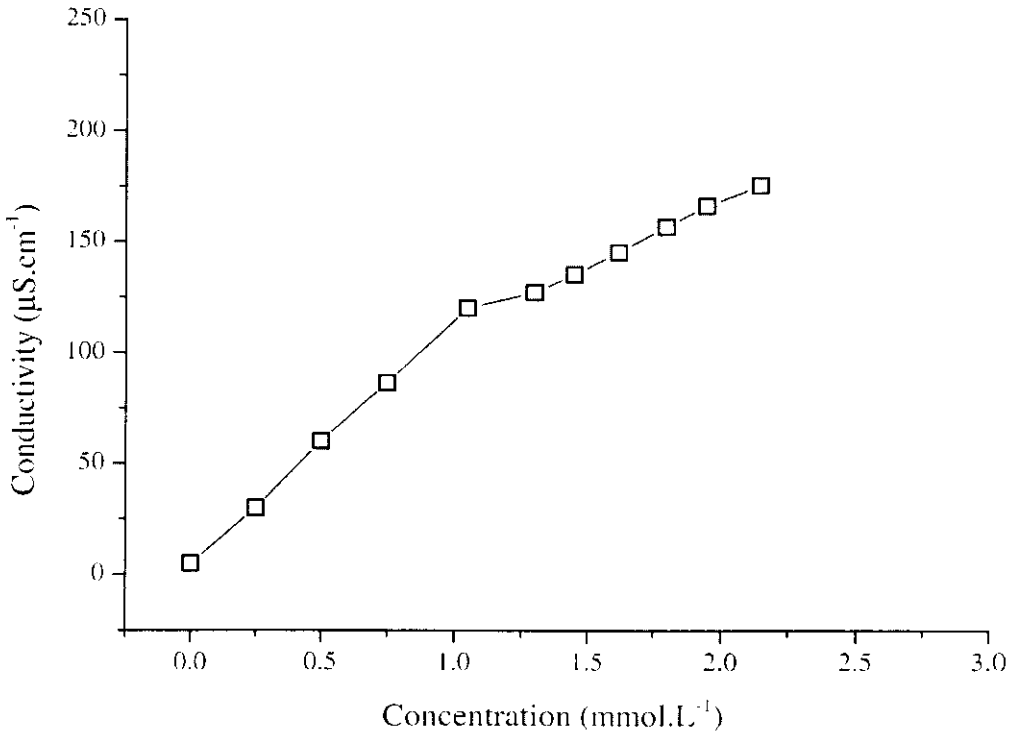

Figure C 11: CMC plot for surfactant 4b

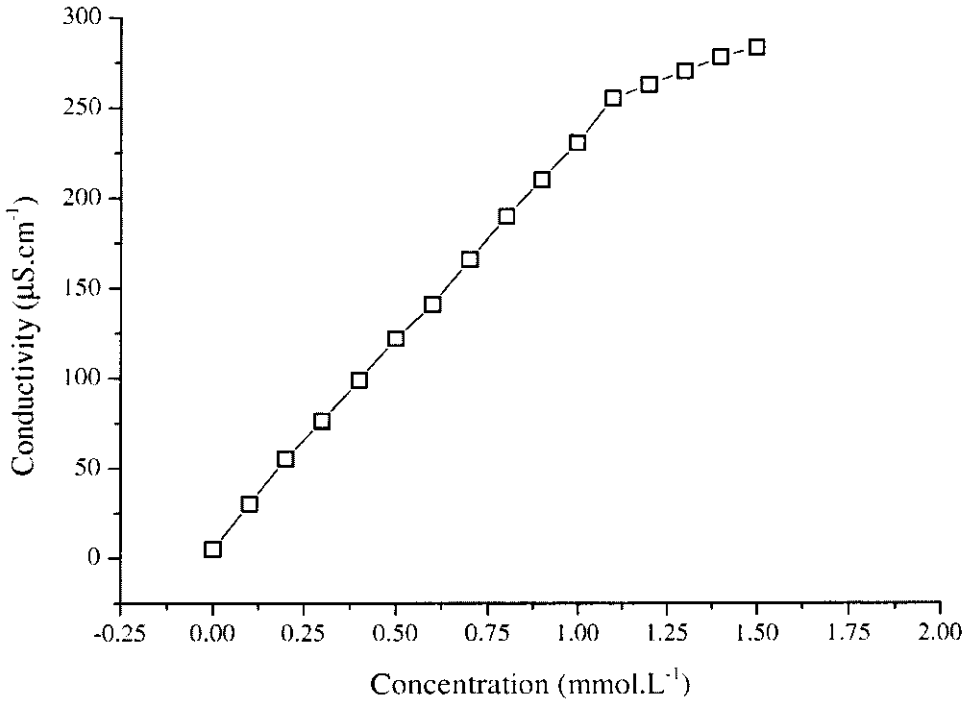

Figure C 12: CMC plot for surfactant 4c

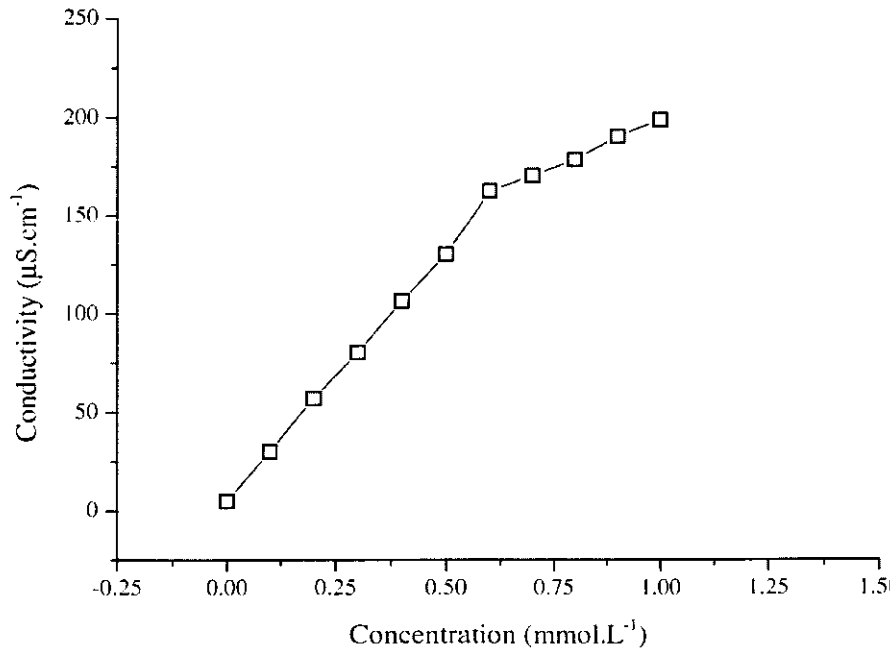

Figure C 13: CMC plot for surfactant 4d

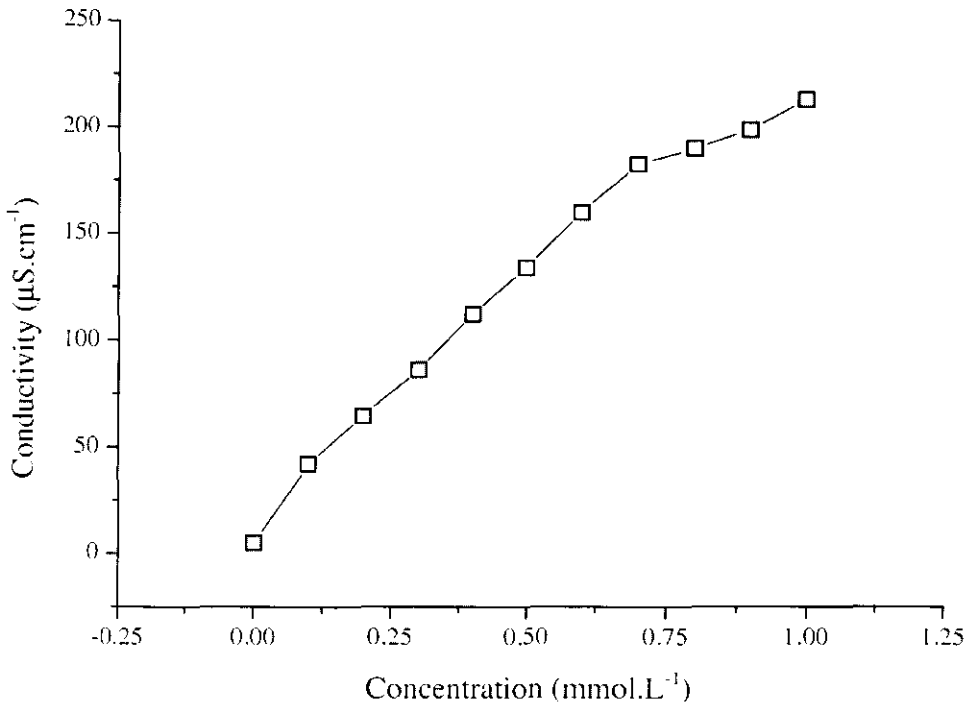

Figure C 14: CMC plot for surfactant 4e

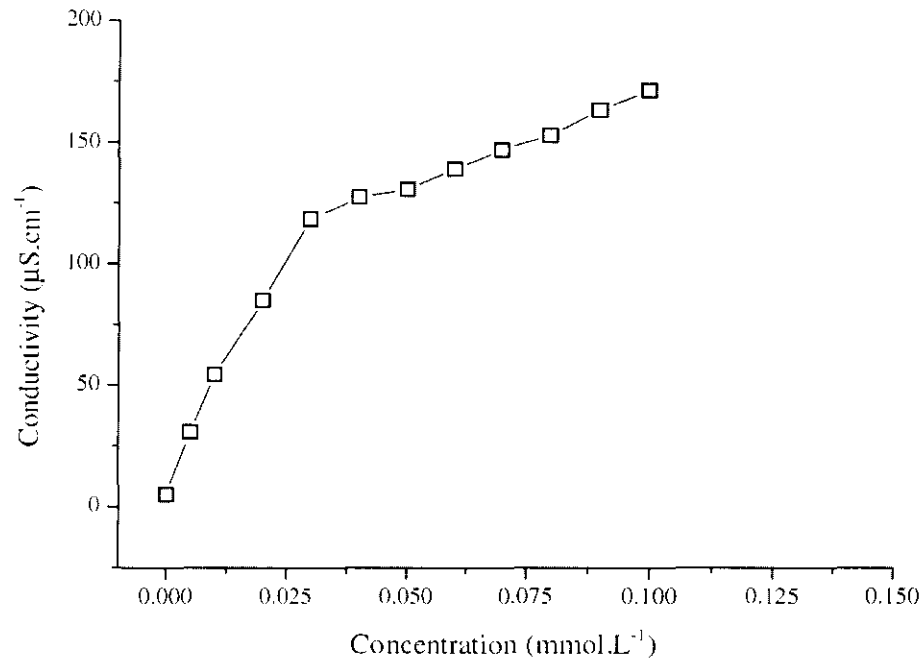

Figure C 15: CMC plot for surfactant 4f

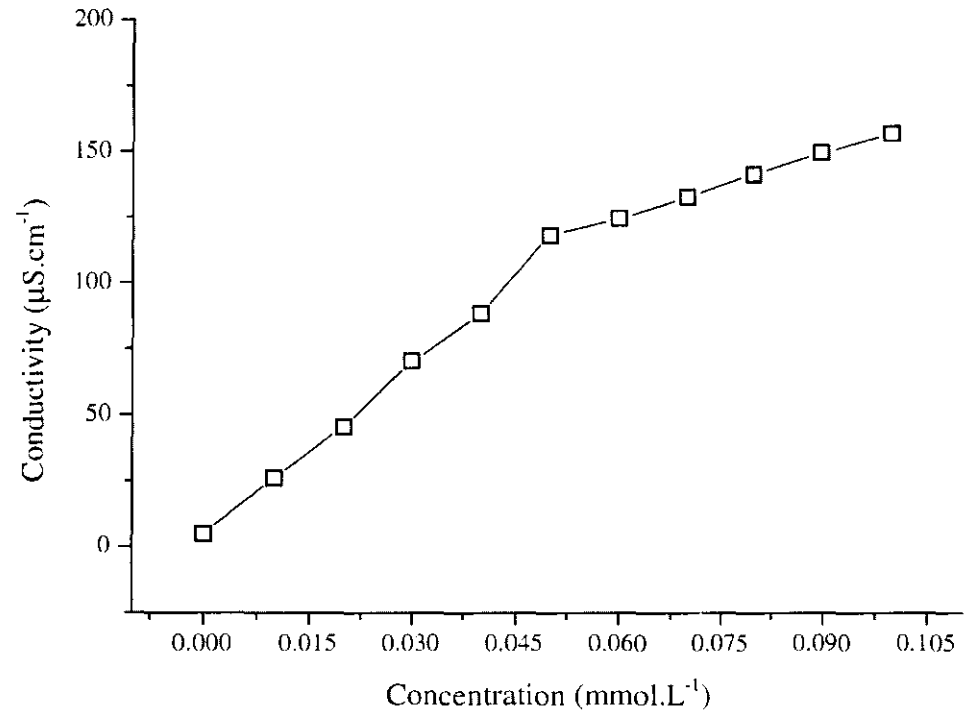

Figure C 16: CMC plot for surfactant 4g

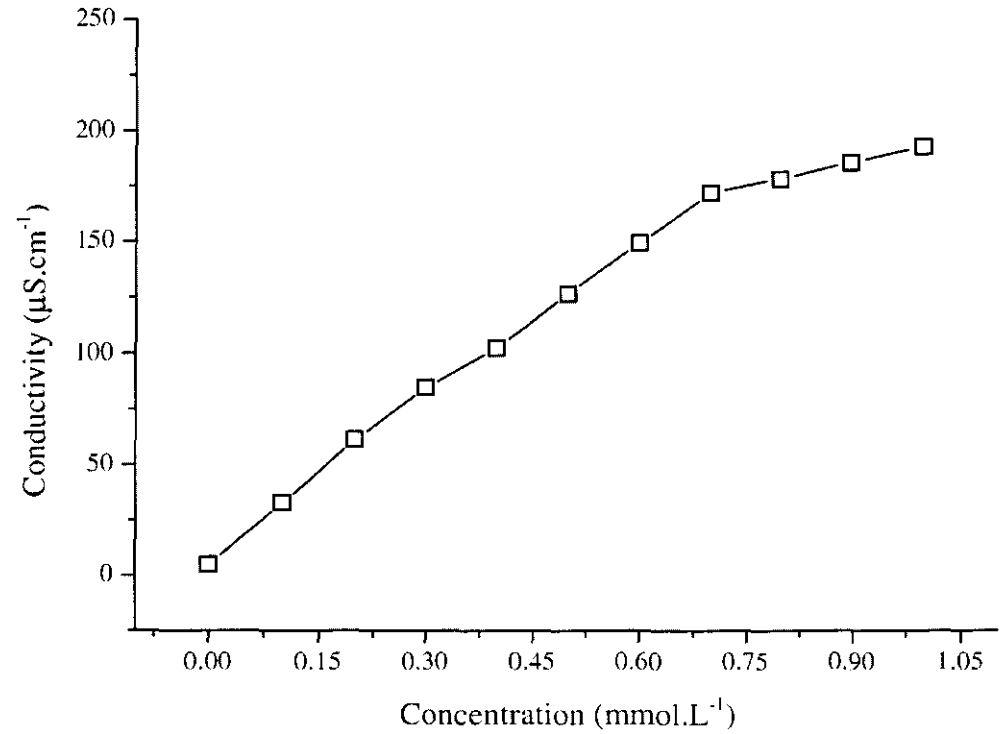

Figure C 17: CMC plot for surfactant 6a

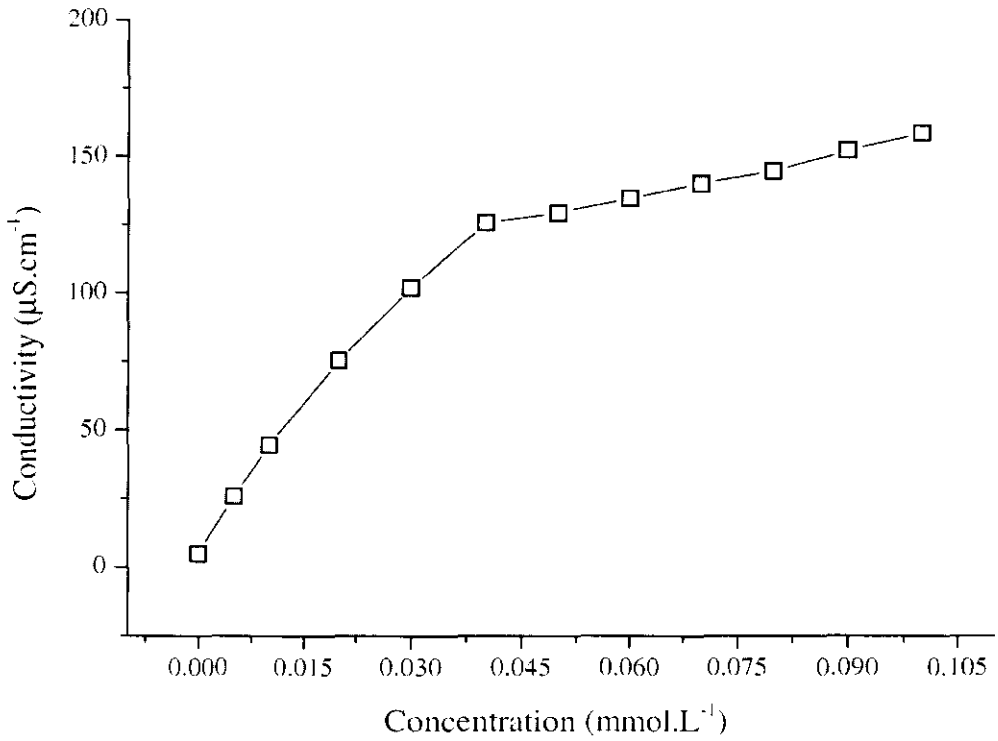

Figure C 18: CMC plot for surfactant 6b

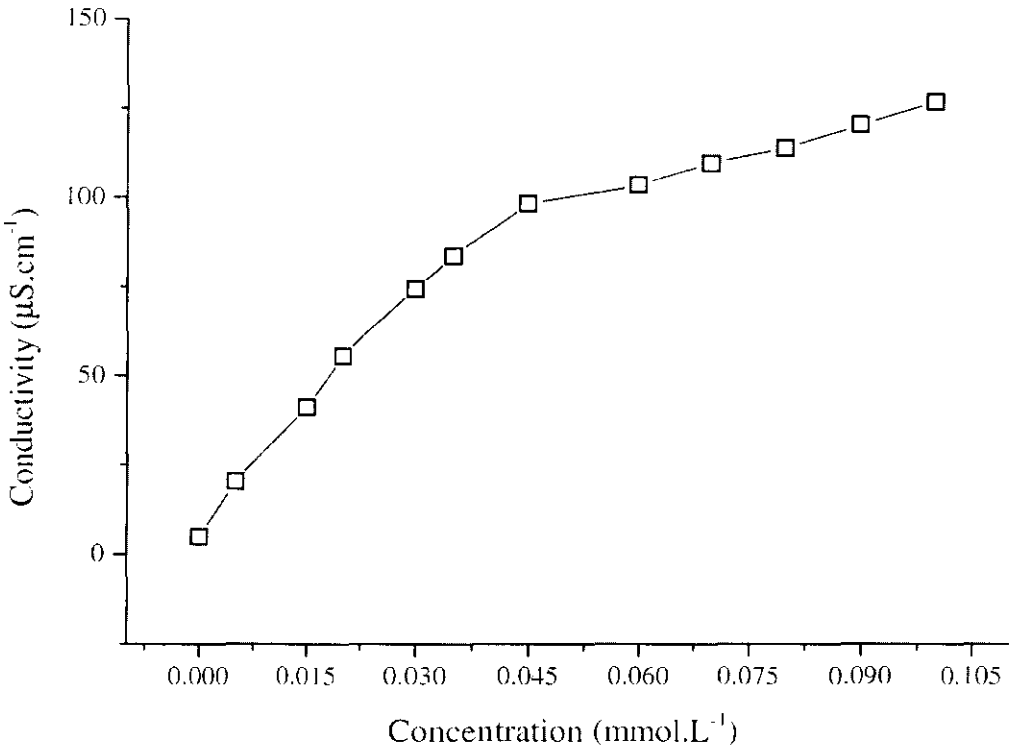

Figure C 19: CMC plot for surfactant 6c

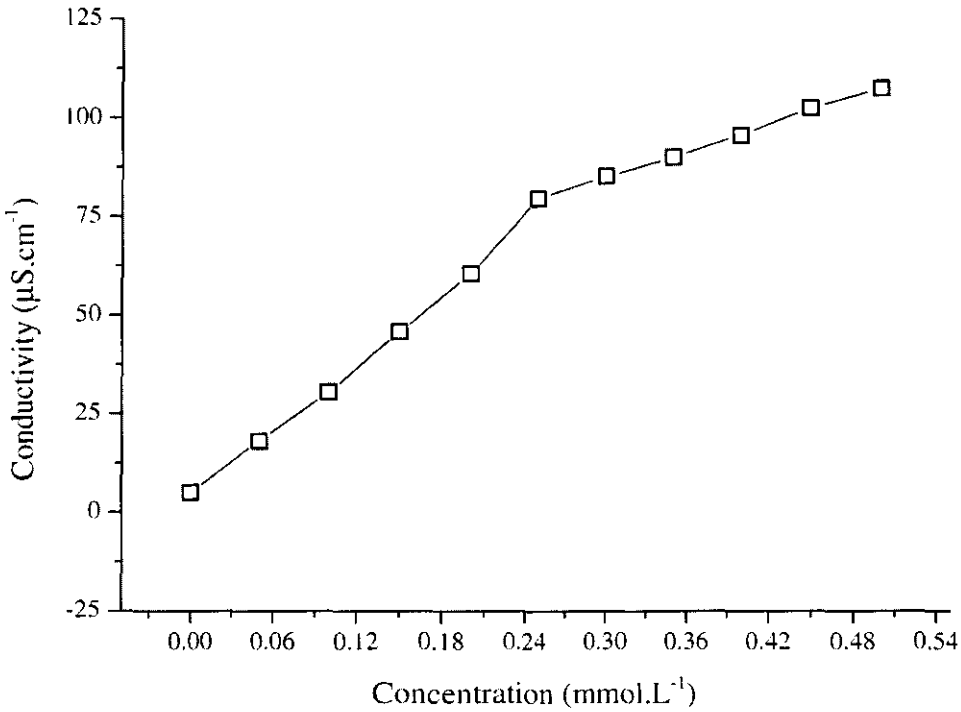

Figure C 20: CMC plot for surfactant 6d

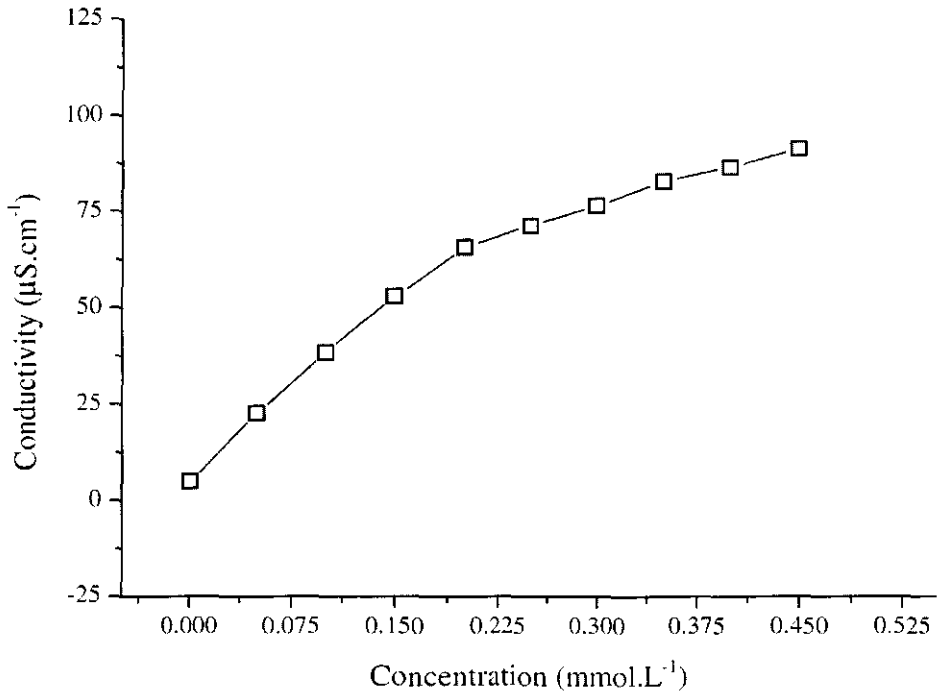

Figure C 21: CMC plot for surfactant 6e

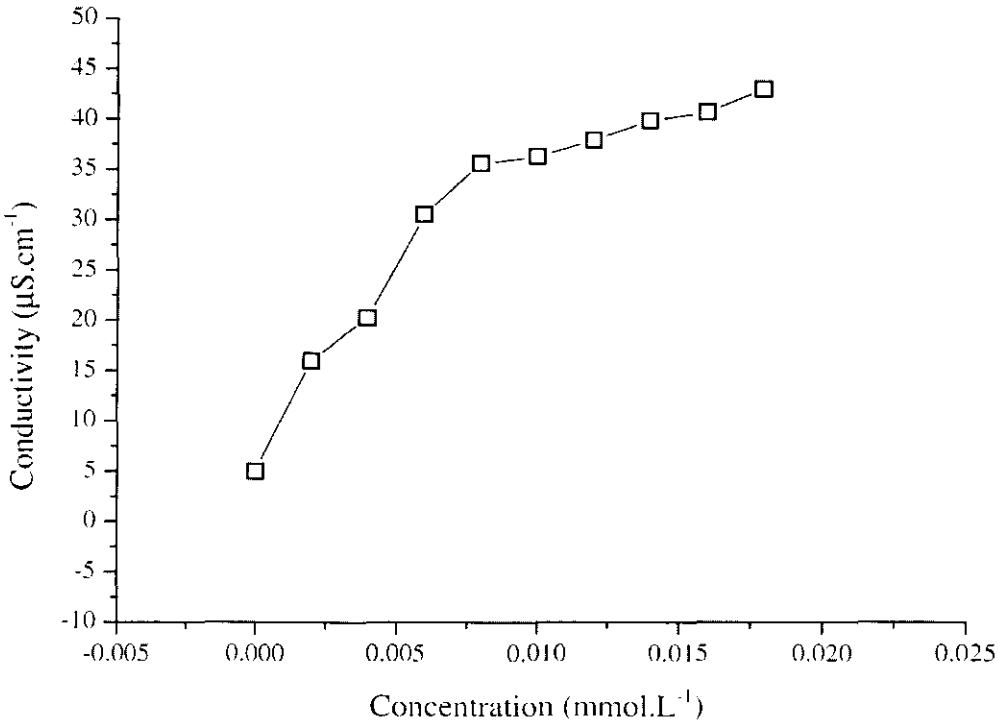

Figure C 22: CMC plot for surfactant 6f

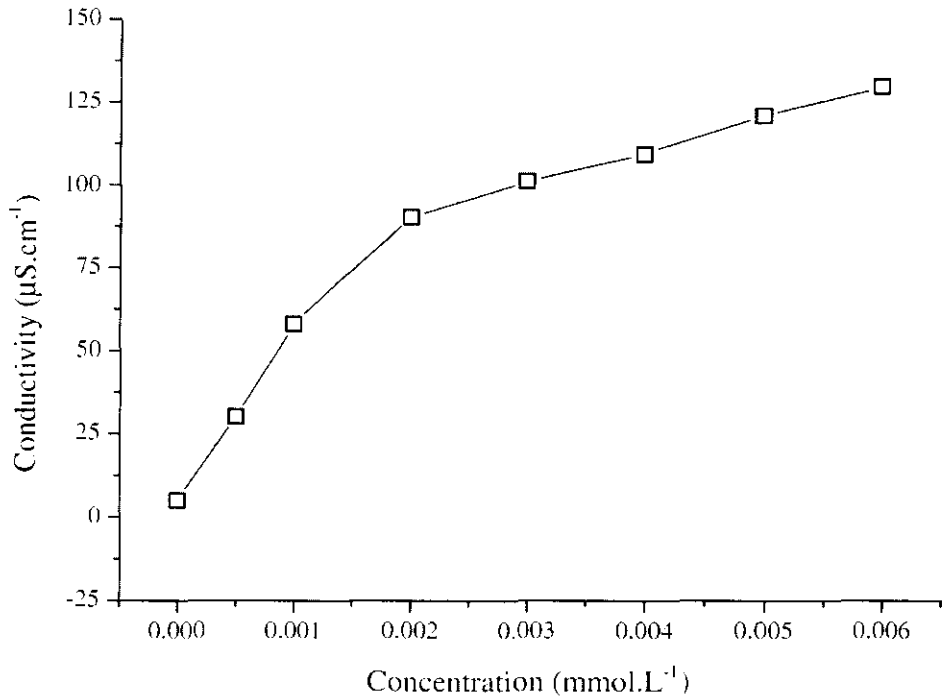

Figure C 23: CMC plot for surfactant 6g

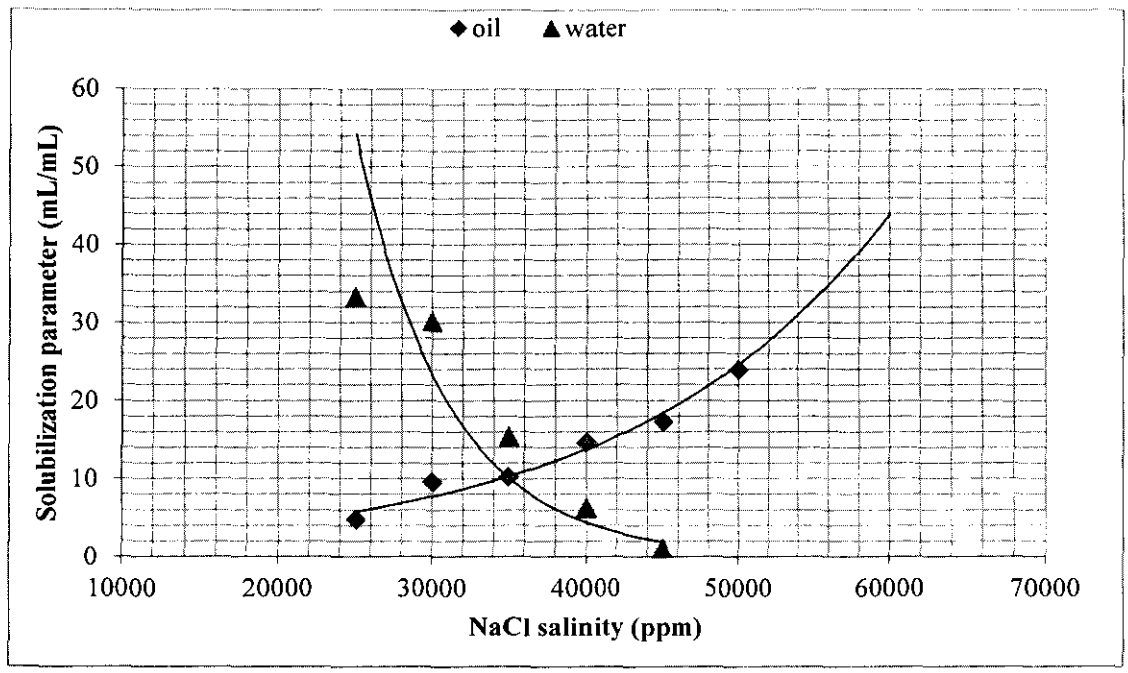

Figure C 24: Solubilization plot of phase behavior for surfactant 4a

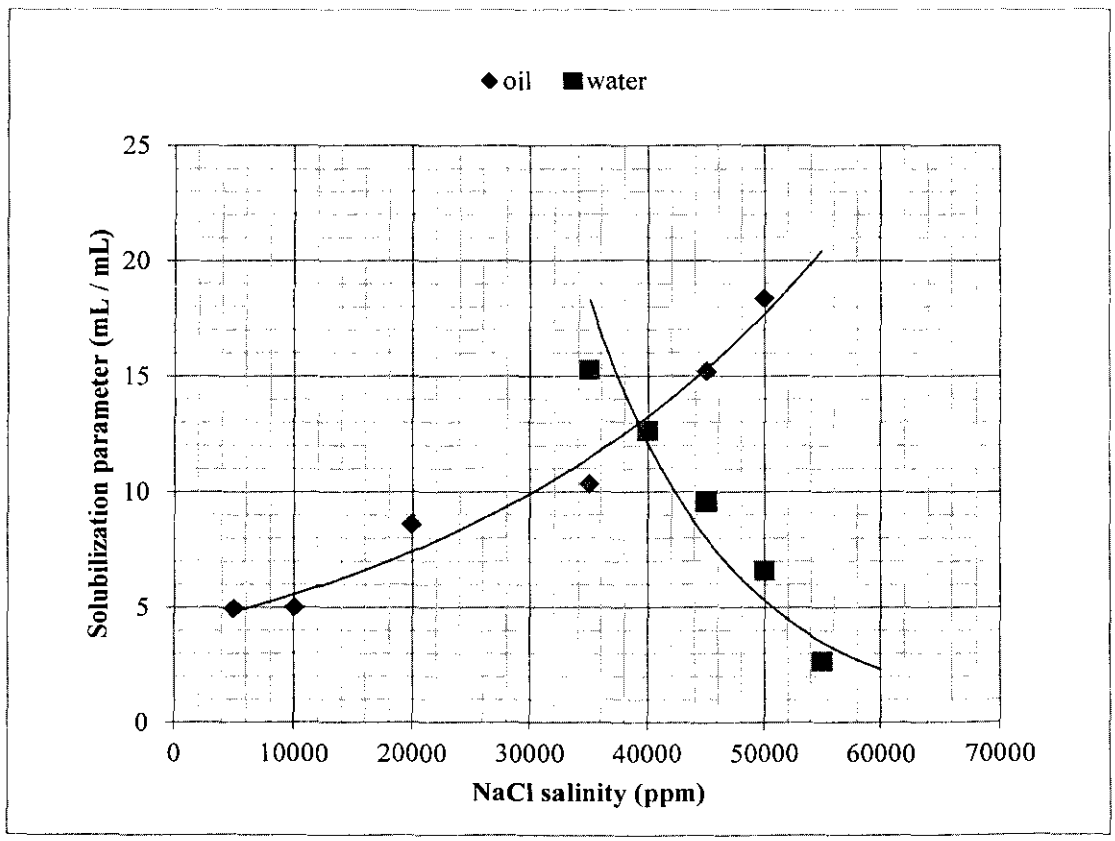

Figure C 25: Solubilization plot of phase behavior for surfactant 4b

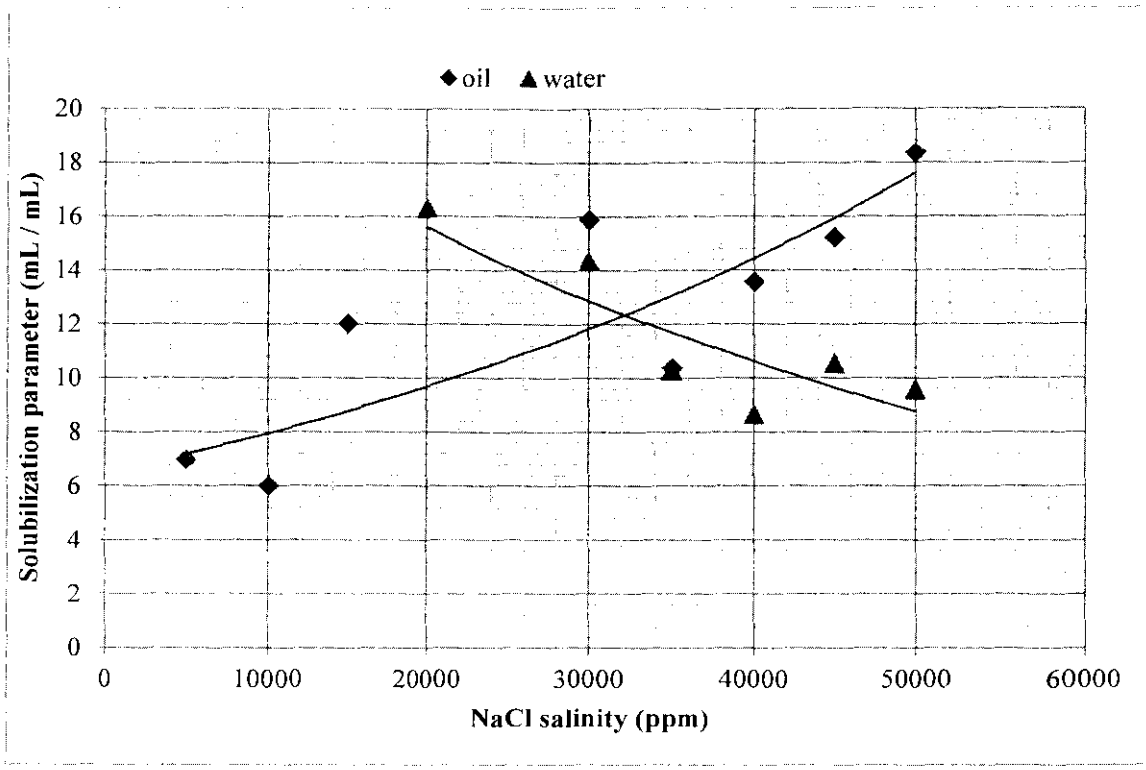

Figure C 26: Solubilization plot of phase behavior for surfactant 4c

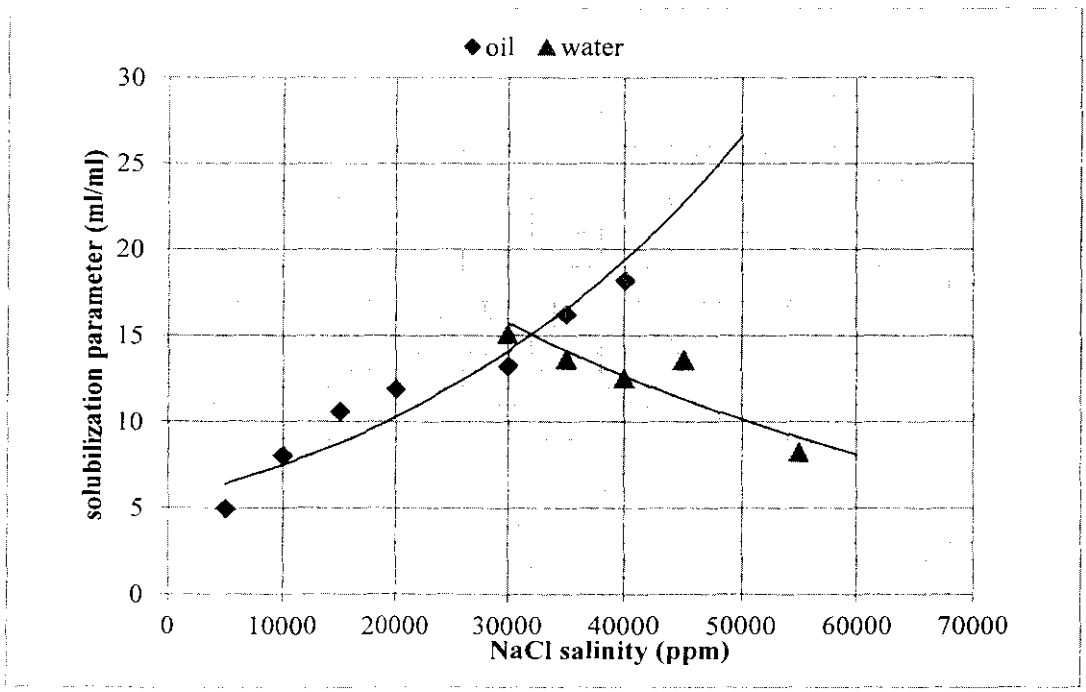

Figure C 27: Solubilization plot of phase behavior for surfactant 4d

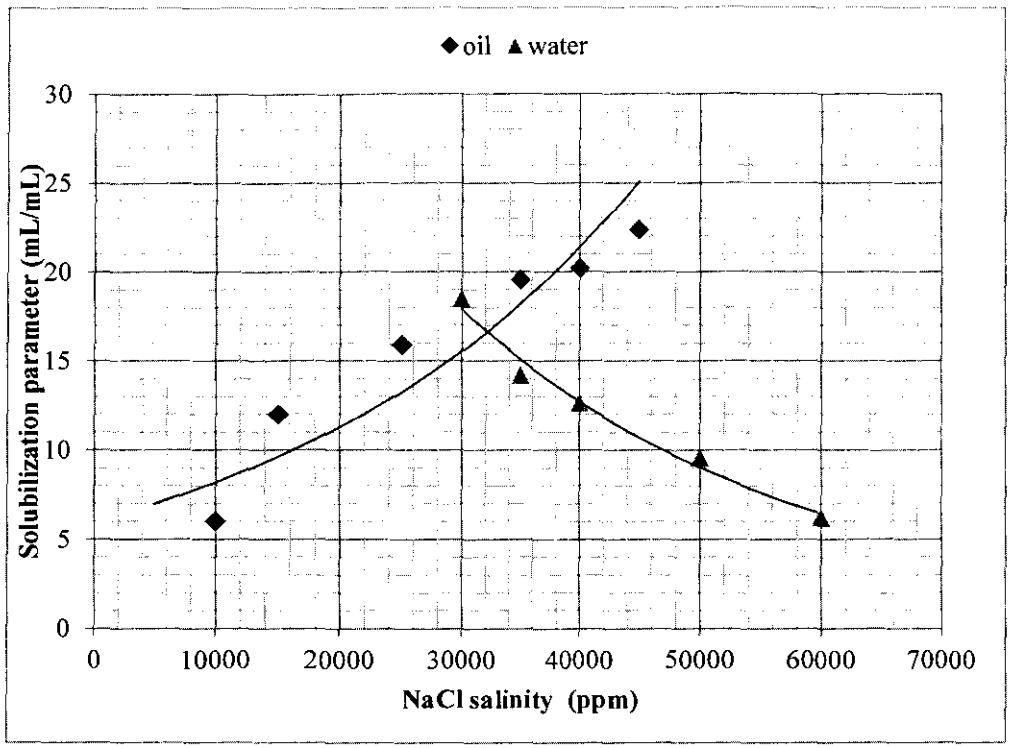

Figure C 28: Solubilization plot of phase behavior for surfactant 4e

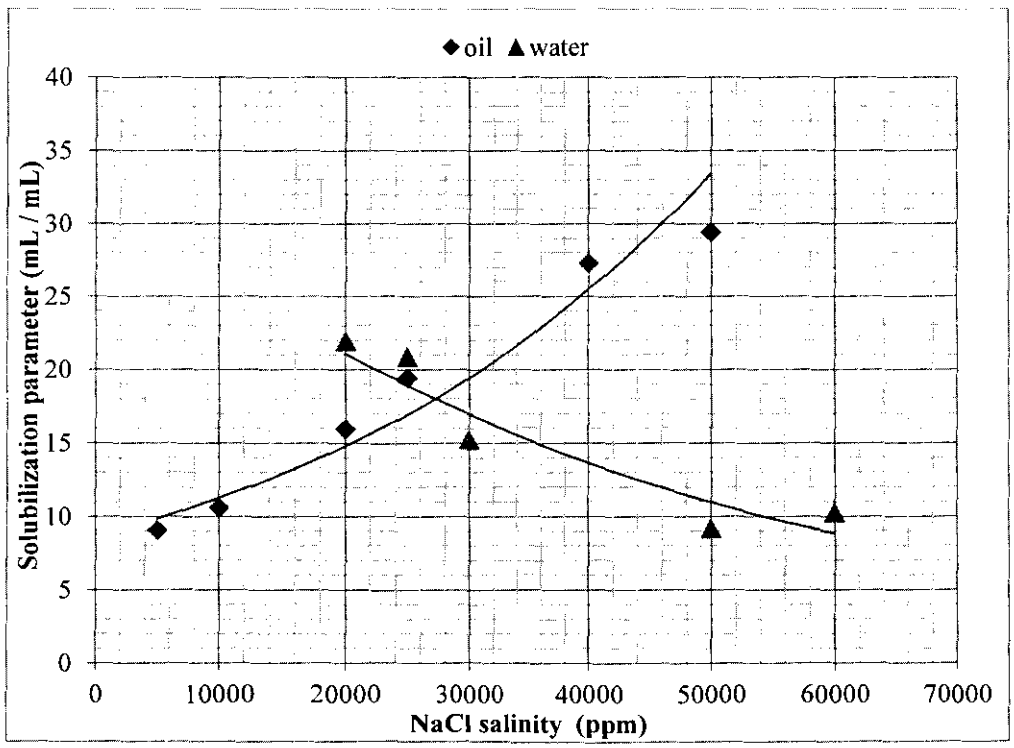

Figure C 29: Solubilization plot of phase behavior for surfactant 4f

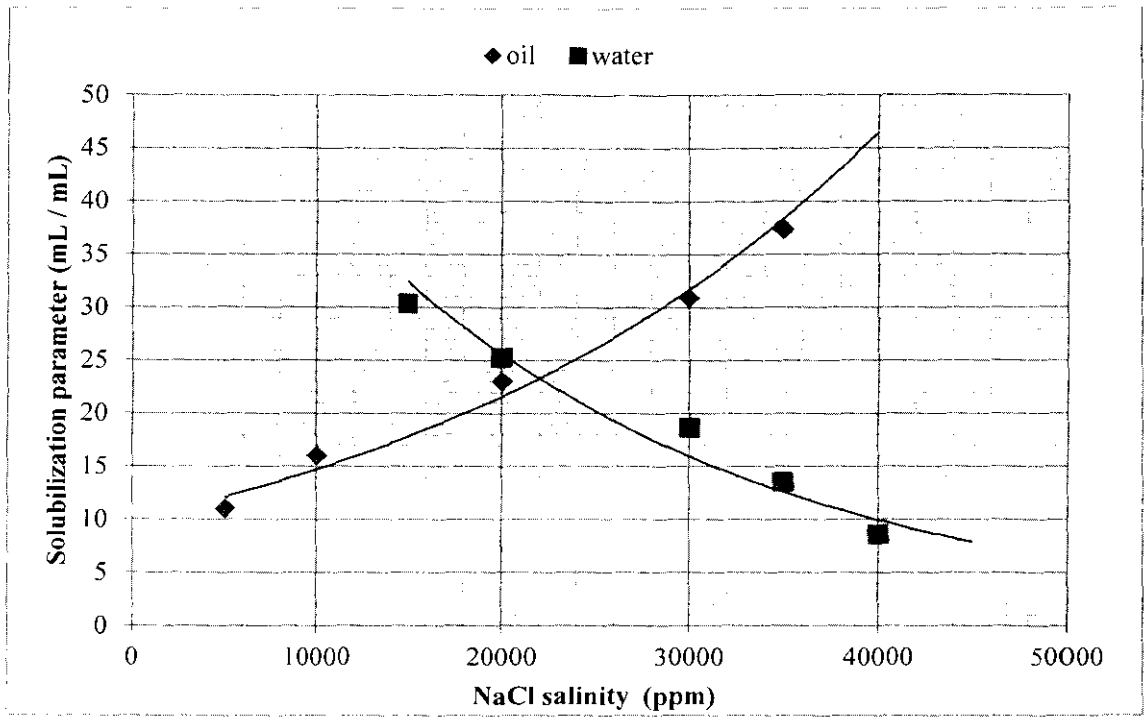

Figure C 30: Solubilization plot of phase behavior for surfactant 4g

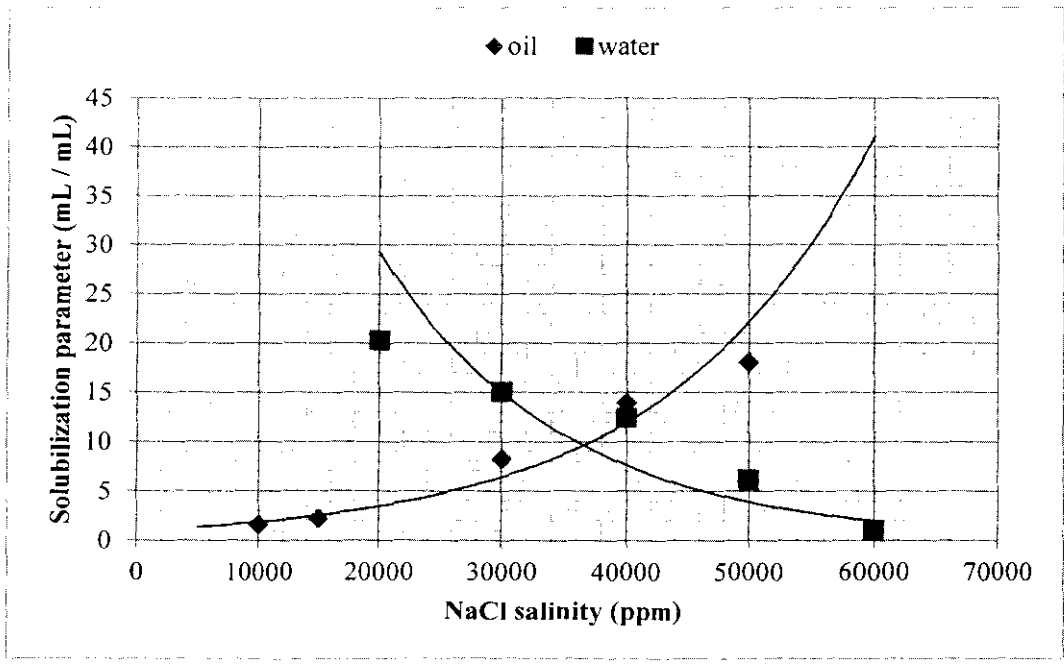

Figure C 31: Solubilization plot of phase behavior for surfactant 6a

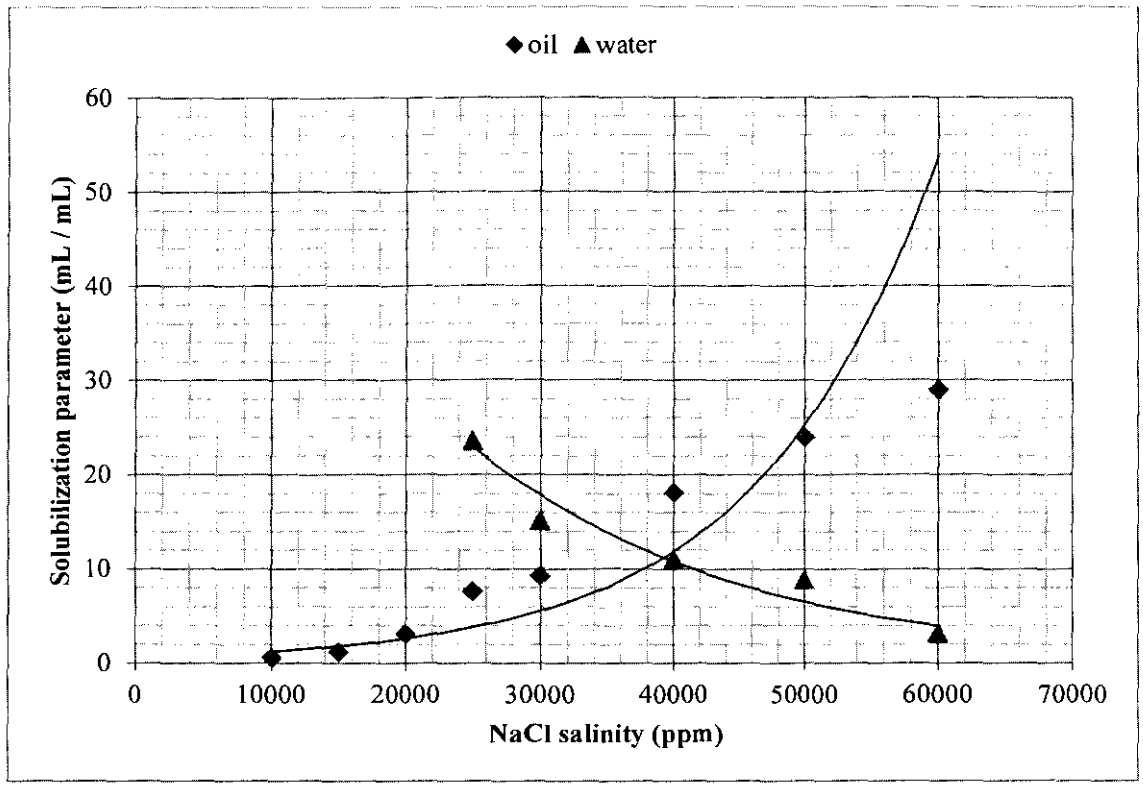

Figure C 32: Solubilization plot of phase behavior for surfactant 6b

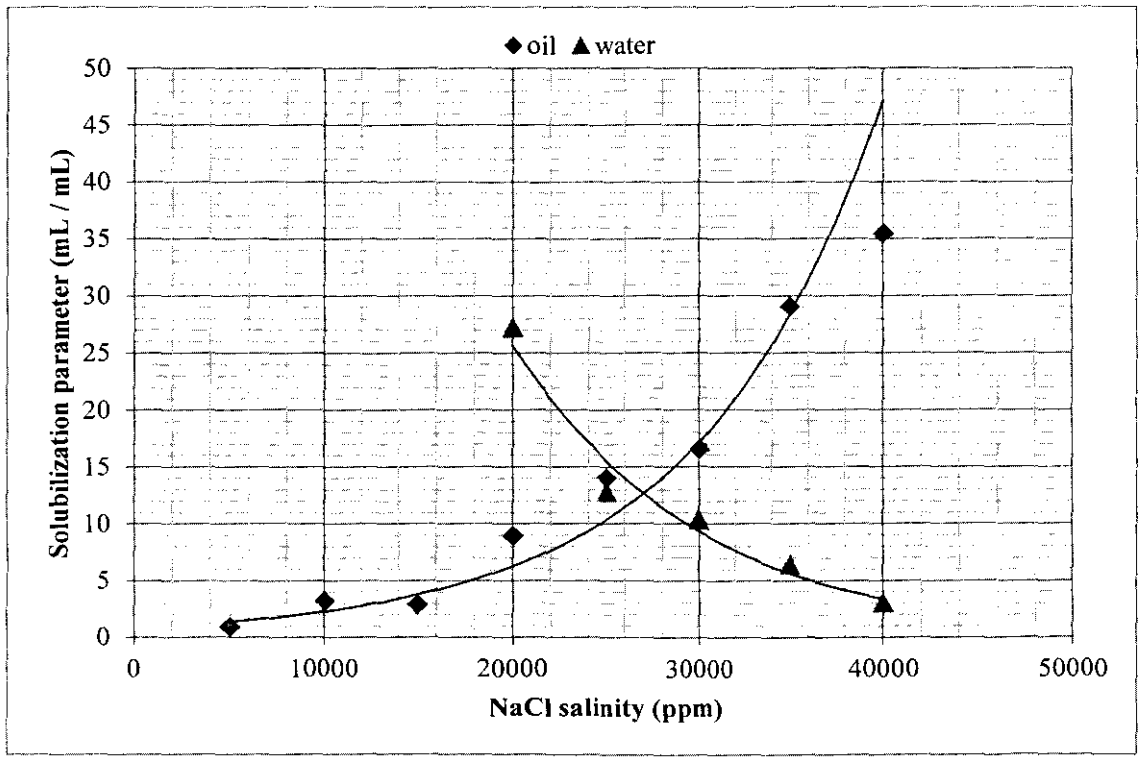

Figure C 33: Solubilization plot of phase behavior for surfactant 6c

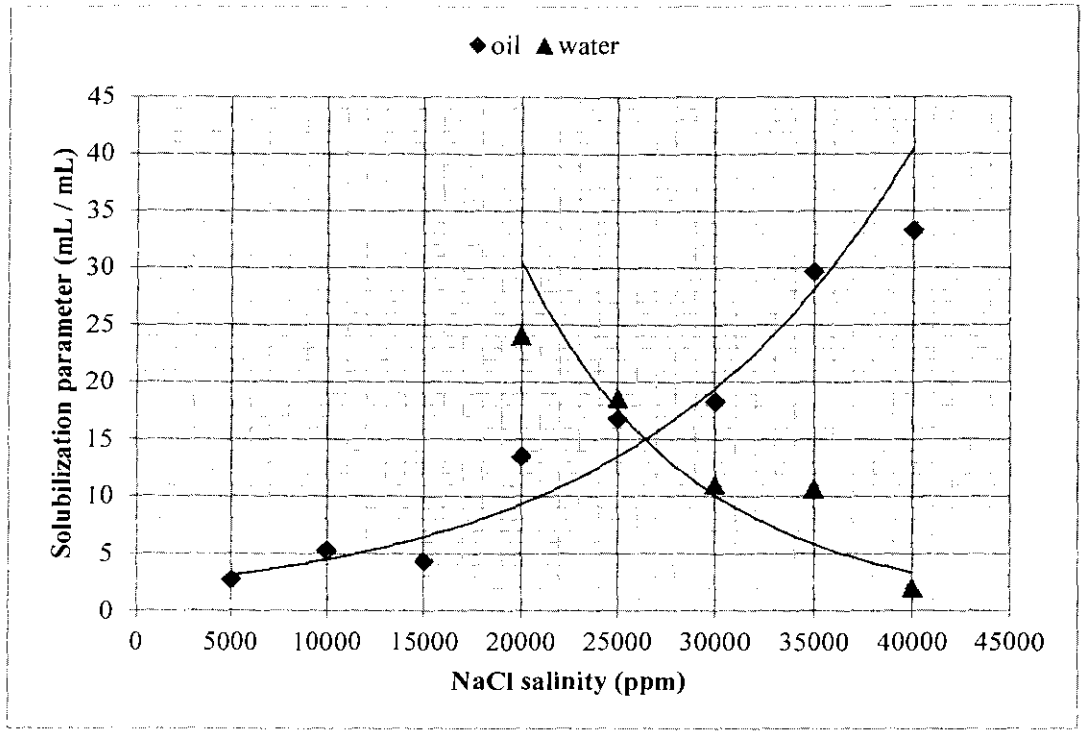

Figure C 34: Solubilization plot of phase behavior for surfactant 6d

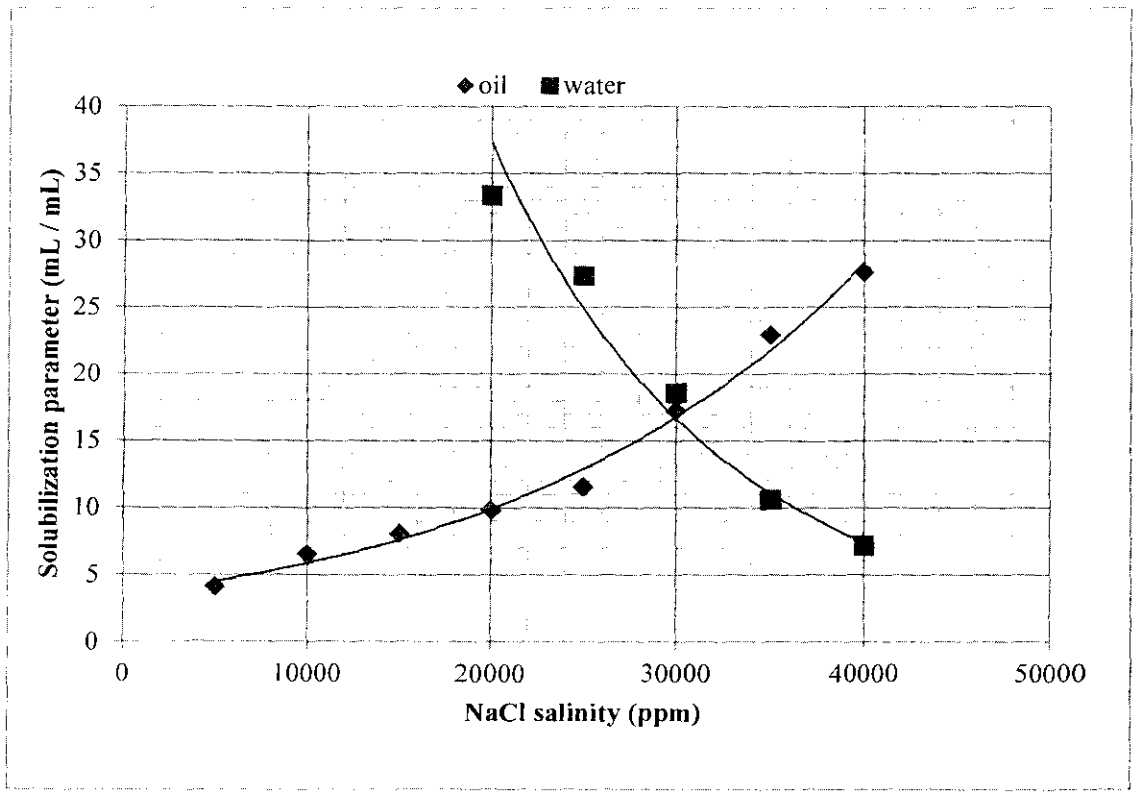

Figure C 35: Solubilization plot of phase behavior for surfactant 6e

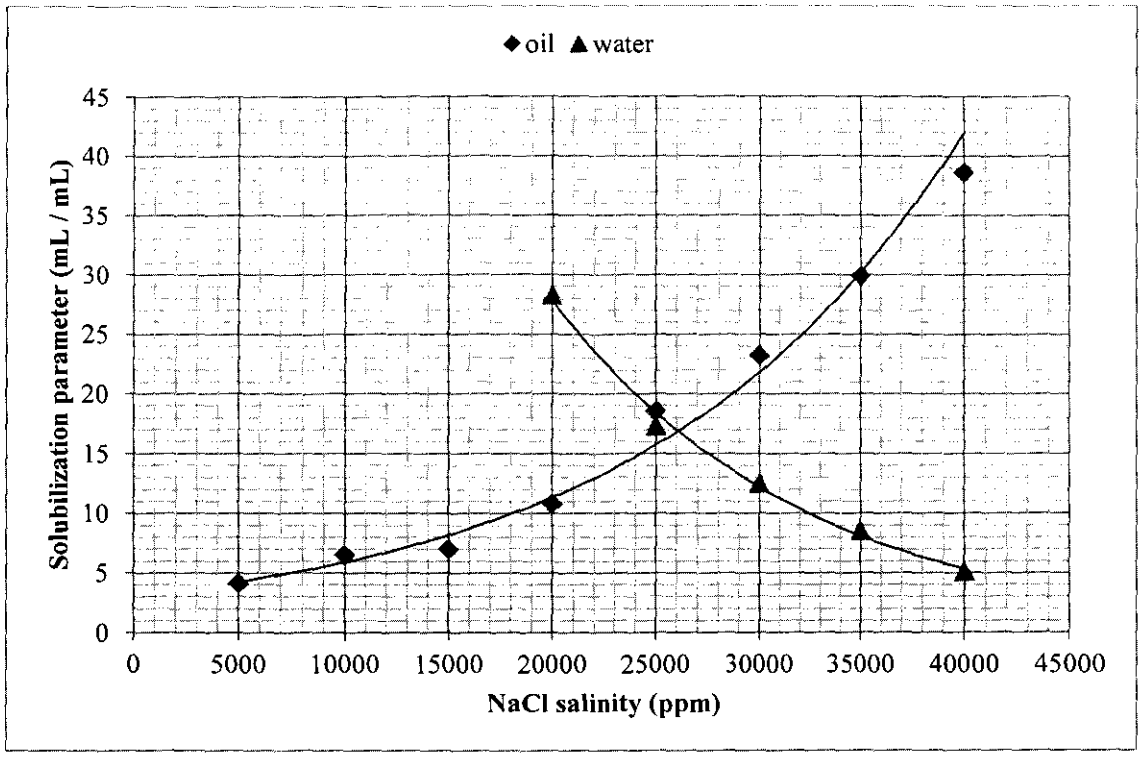

Figure C 36: Solubilization plot of phase behavior for surfactant 6f

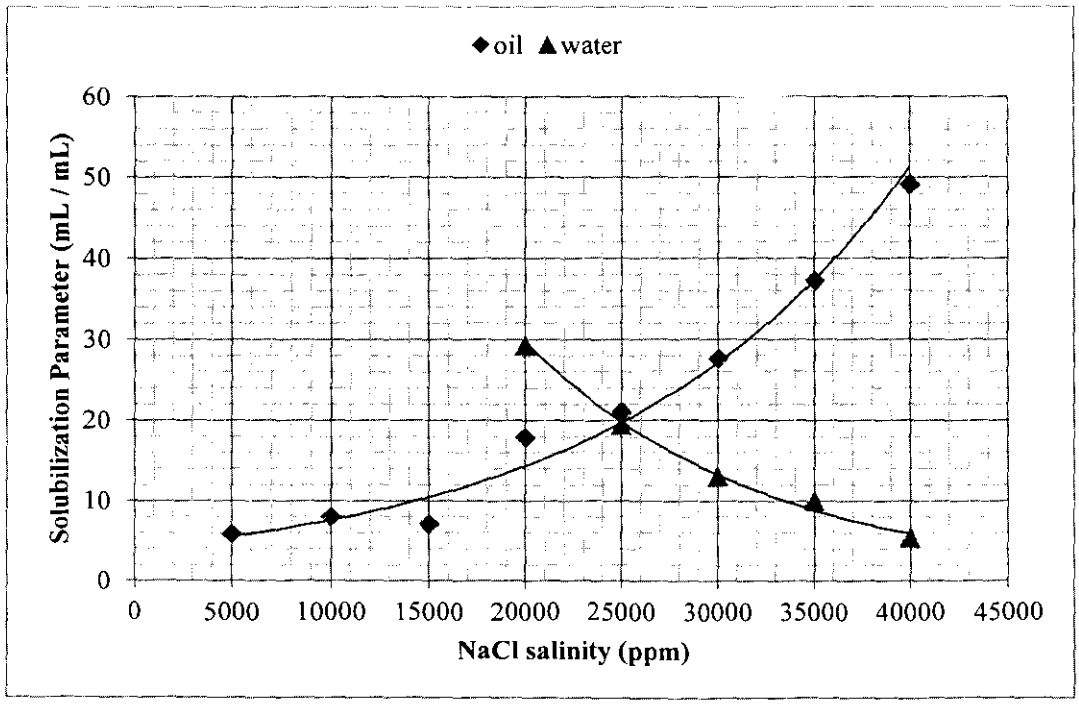

Figure C 37: Solubilization plot of phase behavior for surfactant 6f

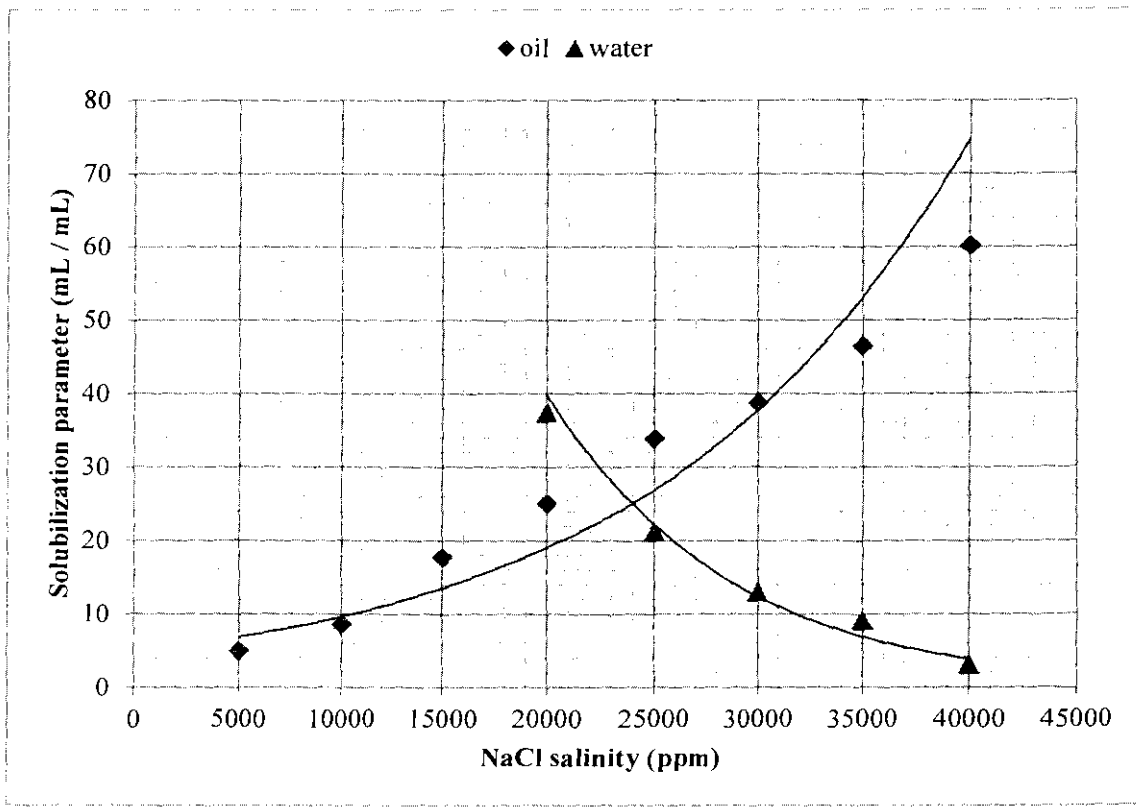

Figure C 38: Solubilization plot of phase behavior for surfactant 6h